



UNIVERSITAT
POLITÈCNICA
DE VALÈNCIA

ORIGIN & EVOLUTION OF THE C3HDZ-ACL5-SACL REGULATORY MODULE IN LAND PLANTS

PhD in Biotechnology

• Anna Solé-Gil •

Advisors:

Dr. Miguel Ángel Blázquez Rodríguez

Dr. Javier Agustí Felíu

Valencia, July 2023



UNIVERSITAT
POLITÈCNICA
DE VALÈNCIA

PhD in Biotechnology

**ORIGIN AND EVOLUTION OF THE C3HDZ-ACL5-SACL
REGULATORY MODULE IN LAND PLANTS**

Anna Solé Gil

Advisors:

Dr. Miguel Ángel Blázquez Rodríguez

Dr. Javier Agustí Feliu

Valencia, July 2023



**A les meves àvies, Carmeta i Maria,
i als meus avis, Jaume i Narcís**

SUMMARY

The correct development of vascular tissues depends on the precise adjustment between vascular cell proliferation and cell differentiation. In *Arabidopsis thaliana*, vascular cell proliferation in the cambium is enhanced by cytokinin, whose synthesis is promoted by the auxin-dependent activity of a transcription factor (TF) heterodimer formed by LONESOME HIGHWAY (LHW) and TARGET OF MONOPTEROS 5 (TMO5). As a safety mechanism, auxin also deploys a negative feedforward regulatory module which involves the precise induction of the Thermospermine (Tspm) synthase ACAULIS5 (ACL5) in proliferating vascular cells by the joint action of auxin and the class-III HD-ZIP (C3HDZ) AtHB8 TF. Tspm then allows the cell-autonomous translation of the SACL proteins, which impair the activity of LHW.

However, the observation that these elements are present in the genomes of all land plants -and not only vascular plants- poses two questions from an evolutionary perspective: (i) what is the function of these genes in non-vascular land plants? and (ii) when was the full regulatory module assembled? In this Thesis, through the combination of phylogenetic, cellular, and molecular genetic analyses with the liverwort *Marchantia polymorpha*, we propose that auxin and C3HDZ are ancestral regulators of *ACL5* expression, and that this connection is maintained in extant tracheophytes and bryophytes. On the contrary, thermospermine-dependent translation of SACL seems to be specific of tracheophytes, based on the appearance of a conserved uORF in the 5' leader sequence of *SACL* transcripts and on experimental evidence using transient assays for SACL translation. In agreement with these observations, the functions of MpACL5 and MpSACL are different in *M. polymorpha*. MpACL5 is expressed in apical notches and modulates meristem bifurcation. On the other hand, MpSACL expression is mostly excluded from apical notches and its activity negatively affects gemmae and rhizoid production through the interaction with MpRSL1. Finally, *in situ* RNA hybridization of *C3HDZ*, *ACL5* and *SACL* orthologs in the gymnosperm *Ginkgo biloba*, the fern *Ceratopteris richardi* and the lycophyte *Selaginella kraussiana* indicates that the expression of the three genes overlaps in vascular tissues. Our results suggest that the function of C3HDZ, ACL5



and SACL followed divergent evolutionary trajectories in bryophytes and tracheophytes, to ultimately control different lineage-specific functions. Only in tracheophytes was the regulatory module assembled and associated with the restriction of vascular cell proliferation.



RESUM

El correcte desenvolupament dels teixits vasculars depèn del precís ajust entre la proliferació de cèl·lules vasculars i la diferenciació cel·lular. En *Arabidopsis thaliana*, la proliferació de cèl·lules vasculars al càmbium és potenciada per la citoquinina, la síntesi de la qual està promoguda per l'activitat dependent d'auxina d'un heterodímer de factors de transcripció (TF) format per LONESOME HIGHWAY (LHW) i TARGET OF MONOPTEROS 5 (TMO5). Com a mecanisme de seguretat, l'auxina també activa un mòdul inhibidor que implica la inducció precisa de la Termospermina (Tspm) sintasa ACAULIS5 (ACL5) en cèl·lules vasculars proliferants per l'acció conjunta de l'auxina i del TF Class III HD-ZIP (C3HDZ) AtHB8. Llavors, la Tspm permet la traducció de les proteïnes SACL de forma autònoma cel·lular, que perjudiquen l'activitat de LHW.

Tanmateix, l'observació de que aquests elements estan presents en els genomes de totes les plantes terrestres – i no només de les plantes vasculars – planteja dues preguntes des d'una perspectiva evolutiva: (i) quina és la funció d'aquests gens en les plantes terrestres no vasculars? i (ii) quan es va crear el mòdul regulador complet? En aquesta Tesi, mitjançant la combinació d'anàlisis filogenètics, cel·lulars i moleculars amb la hepàtica *Marchantia polymorpha*, proposem que l'auxina i C3HDZ són reguladors ancestrals de l'expressió d'ACL5, i que aquesta connexió es mantén en els traqueòfits i briòfits existents. Per contra, la traducció depenent de Tspm de SACL sembla ser específica dels traqueòfits, basat en l'aparició d'un uORF conservat a la seqüència 5' líder dels transcrits de SACL i en evidència experimental basada en assajos transitoris per a la traducció de SACL. D'acord amb aquestes observacions, les funcions de MpACL5 i MpSACL són diferents a *M. polymorpha*. MpACL5 s'expressa en "notch" apicals i modula la bifurcació dels meristems. D'altra banda, l'expressió de MpSACL està majoritàriament exclosa dels "notch" apicals i la seva activitat afecta negativament la producció de gemmes i rizoids mitjançant la interacció amb MprSL1. Finalment, la hibridació d'ARN *in situ* d'ortòlegs de C3HDZ, ACL5 i SACL a la gimnosperma *Ginkgo biloba*, la falguera *Ceratopteris richardii* i el licòfit *Selaginella kraussiana* indica que l'expressió dels tres



gens es solapa als teixits vasculars. Els nostres resultats suggereixen que la funció de C3HDZ, ACL5 i SACL va seguir trajectòries evolutives divergents en briòfits i traqueòfits, per controlar, finalment, diferents funcions específiques dins de cada llinatge. Només en els traqueòfits es va formar el mòdul regulador i es va associar amb la restricció de la proliferació de cèl·lules vasculars.

RESUMEN

El correcto desarrollo de tejidos vasculares depende del ajuste preciso entre la proliferación de células vasculares y la diferenciación celular. En *Arabidopsis thaliana*, la proliferación de células vasculares en el cambium es potenciada por la citoquinina, la síntesis de la cual está promovida por la actividad dependiente de auxina de un heterodímero de factores de transcripción (TF) formado por LONESOME HIGHWAY (LHW) y por TARGET OF MONOPTEROS 5 (TMO5). Como mecanismo de seguridad, las auxinas también activan un módulo inhibitorio que implica la inducción precisa de la Termostermina (Tspm) sintasa ACAULIS5 (ACL5) en células vasculares proliferantes por acción conjunta de las auxinas y del TF Class III HD-ZIP (C3HDZ) AtHB8. Entonces, la Tspm permite la traducción de las proteínas SACL de forma celular autónoma, que perjudican la actividad de LHW.

Sin embargo, la observación de que estos elementos están presentes en los genomas de todas las plantas terrestres – y no sólo de las plantas vasculares – plantea dos preguntas desde una perspectiva evolutiva: (i) ¿cuál es la función de estos genes en las plantas terrestres no vasculares? y (ii) ¿cuándo se creó el módulo regulador concreto? En esta Tesis, mediante la combinación de análisis filogenéticos, celulares y moleculares con la hepática *Marchantia polymorpha*, proponemos que la auxina y C3HDZ son reguladores ancestrales de la expresión de *ACL5*, y que esta conexión se mantiene en las traqueófitas y las briófitas existentes. Por el contrario, la traducción dependiente de Tspm de *SACL* parece ser específica de las traqueófitas, basado en la aparición de un uORF conservado en la secuencia 5' líder de los transcritos de *SACL* y en evidencia experimental basada en ensayos transitorios para la traducción de *SACL*. De acuerdo con estas observaciones, las funciones de MpACL5 y MpSACL son diferentes en *M. polymorpha*. MpACL5 se expresa en "notches" apicales y modula la bifurcación de los meristemos. Por otro lado, la expresión de MpSACL está mayoritariamente excluida de los "notches" apicales y su actividad afecta negativamente la producción de gemas y rizoides mediante la interacción con MpRSL1. Finalmente, la hibridación de ARN *in situ* de ortólogos de C3HDZ, ACL5 y SACL en la gimnosperma *Ginkgo biloba*, el helecho *Ceratopteris richardii* y la licófito



Selaginella kraussiana indican que la expresión de los tres genes se solapa en los tejidos vasculares. Nuestros resultados sugieren que la función de C3HDZ, ACL5 y SACL ha seguido trayectorias evolutivas divergentes en briófitas y traqueófitas, para controlar, finalmente, diferentes funciones específicas dentro de cada linaje. Sólo en las traqueófitas se formó el módulo regulador y se asoció con la restricción de la proliferación de células vasculares.



ACKNOWLEDGEMENTS / AGRAÏMENTS / AGRADECIMIENTOS

En primer lugar, quiero mencionar a mis directores de tesis, Javi y Miguel, sin los cuales no habría podido llevar a cabo esta tesis doctoral. Creedme que ha sido un honor aprender de vosotros y me llena de orgullo poder decir que vuestra sabiduría (tanto a nivel científico como personal) me ha guiado durante todo el doctorado, y probablemente lo seguirá haciendo durante el resto de mi vida. No habría podido tener unos mejores directores de tesis, y por eso tenéis mi absoluto respeto y cariño.

I would also like to thank Dr. François Parcy and Dr. Maite Sanmartín Artiñano for their participation as international PhD committee, for their kind help and scientific feedback; and Dr. Cristina Ferrándiz Maestre for facilitating my scientific exchange through the RISE scholarship.

Aviso al lector de que los agradecimientos que siguen serán probablemente lacrimógenos, pero no puedo evitar ponerme así cuando hablo de personas tan importantes y que han dejado tanta huella en mí. A todas las personas con las que he compartido laboratorio, coffees, cenas, cervezas, tardes de juegos de mesa y fiestas, y que en general me han acompañado siempre en mi viaje, quiero que sepáis me habéis hecho muy feliz y que os echaré de menos con todo mi corazón. Especial mención a Yaiza, mi "gemela" que entró en el laboratorio por las mismas fechas y hemos vivido todo el doctorado junto con Alberto y Laura, que entraron poco después, y rápidamente construimos nuestro grupo, nuestro apoyo incondicional; hemos compartido infinitas risas, pero también lágrimas, y hemos vivido muchísimas cosas juntos. A mis amigos Paula y Borja, que siempre se han prestado a ayudarme personal y científicamente y que hasta me ofrecieron su casa en tiempos de necesidad. Same goes for Cynthia, the main artist behind the covers and chapter titles of this thesis, you are a wonderful friend and an amazing scientist. Maca, gracias por siempre confiar en mi criterio (se me ha quedado grabado tu "Anna..." y siempre me sale una sonrisa cuando lo pienso), por tu amistad (y dramas), y por tu ayuda siempre. A Cris Úrbez, por ser ese "ser de luz" lleno de bondad, paciencia y sabiduría, nuestro



ángel de la guarda (y del pesebre). Y al resto de gente que ha participado en mi experiencia por el IBMCP de alguna forma u otra, Alabadí, Carlos, Juanma, Jaime, Joan, Antonio, Anselmo, Anselm, Ceci, Fede, Santi, Mariana, Shurong, Fiona, Asier, Alberto, Julián, Jorge, Pepi, Noel, Brumós, Eugene... gracias. Por encima de todo, ha sido muy divertido.

Bruno, you deserve a paragraph entirely for you. What first started as a "workout" by the river, and I use quotation marks because we quickly realized how we enjoyed talking way more than the running itself, and it soon became an excuse to just hang out and spend wonderful times with you. I am very grateful for your unconditional help, for your love for science and evo devo that inspired me when I needed it the most. I am glad to take your friendship with me everywhere we go.

ブランカさんとフランさんに、"ありがとうございます" と言いたい。あなた達は素晴らしい友達で、愛しています！ PD: 私が結婚するとき、ブランカさんとフランさんが私の一番ゲストです。

To the amazing scientists that I met during my stay in Kobe and New York, especially Dr. Ishizaki Kimitsune and Dr. Sakai Yuuki, from whom I learnt so much about *Marchantia* and Japanese culture, and Dr. Barbara Ambrose, for her kind help and contribution to my thesis. I would also like to thank the people from New York, especially Nelson and Chiara, for their friendship and so many memorable moments that I will treasure forever.

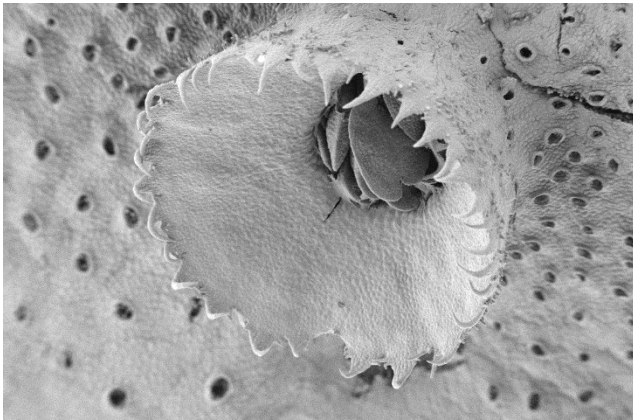
Per l'Alberto, que sempre ha estat aquí, recolzant-me, fent-me notar les coses bones quan ho veia massa fosc, i amb qui he compartit riures, plors, somnis i pors, felicitat i amor. I per tot el que ha vingut amb ell, la seva família; la Lúdia, el Jesús, l'Alberto i la Laura, per acollir-me i recolzar-me durant aquesta època de la meva vida.

A la Marta i a la Rut, que hem crescut juntes i que no em puc imaginar una vida sense elles. Gràcies per les vostres converses i per treure'm de casa, agafar aire, i recordar-me que "respirar" també és una part de "treballar". A la Cris, Meri, Anna, i Mariona, les de tota la vida, moltes gràcies per estar aquí sempre.

I finalment, als meus pares i al meu germà, per acompanyar-me i fer que aquest temps d'escriptura sigui agradable (i no tirar-me els plats pel cap quan estava insuportable). Sense vosaltres, la vostra confiança i els vostres ànims, no hagués arribat mai tan lluny. Us estimo moltíssim.

La realización de esta Tesis Doctoral ha sido posible gracias a una Ayuda para Contratos Predoctorales para la Formación de Doctores FPI (BES-2017-080387), una ayuda europea EMBO Scientific Exchange (9534), y la financiación MSCA H2020 RISE (NR. 101007738). Así mismo, el trabajo experimental ha sido financiado por los proyectos [EVOLITE] del Ministerio de Ciencia e Innovación AEI-MICINN (PID2019-110717GB-I00), [HUBFUN] del Ministerio de Economía y Competitividad (BFU2016-80621-P); [GEN-VIRON] del Ministerio de Ciencia e Innovación (PID2019-108084RB-I00), [CAMBI-ATORS] del Ministerio de Economía y Competitividad (BIO2016-79147-R). [BIODRO] del Ministerio de Ciencia e Innovación (PID2021-125829OB-I00), y de una beca Ramón y Cajal del Ministerio de Economía y Competitividad (RYC-2014-15752) durante el período 2017-2023.

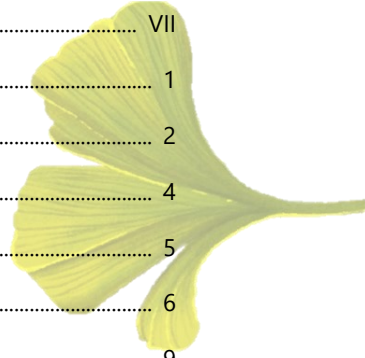




Marchantia polymorpha gemma cup (original: personal Cryo-FESEM archive)

TABLE OF CONTENTS

Summary.....	I
Acknowledgements	VII
Table of Contents	1
List of Figures	2
List of Tables	4
Abbreviations.....	5
Glossary.....	6
Introduction	9
Objectives	43
Chapter 1	47
Origin and genetic regulation of <i>C3HDZ</i>, <i>ACL5</i> and <i>SACL</i> genes in land plants	
Chapter 2	89
The role of <i>C3HDZ</i>, <i>ACL5</i> and <i>SACL</i> genes in <i>M. polymorpha</i>	
Chapter 3	139
Spatial analyses of <i>C3HDZ</i>, <i>ACL5</i> and <i>SACL</i> expression in extant tracheophyte lineages	
General Discussion	183
Conclusions	197
Annexes.....	201



LIST OF FIGURES

Introduction

Figure 1. Overview of the plant taxonomy within green plants and example species.....	11
Figure 2. Schematic representation of cell division types occurring within the (pro)cambial stem cells to produce xylem and phloem initials, and overview of xylem and phloem cells maturation	15
Figure 3. Anatomical overview and molecular mechanisms controlling vascular cell proliferation in <i>A. thaliana</i>	17
Figure 4. Polyamine biosynthesis route.....	19
Figure 5. Overview of <i>M. polymorpha</i> gametophyte development.....	26

Chapter 1

Figure 1. Phylogenetic analysis and inferred history of C3HDZ in Streptophyta.....	50
Figure 2. Phylogenetic analysis and inferred history of polyamine aminopropyl transferases with emphasis on Archaeplastida lineages.....	54
Figure 3. Alternative models for TSPMS activity origin and evolution in plants.....	55
Figure 4. Phylogenetic analysis and inferred history of ACL5 in Archaeplastida	57
Figure 5. Polyamine quantifications from yeast extracts	60
Figure 6. Detection of <i>ACL5</i> transcripts in cDNA from <i>A. thaliana</i> , <i>P. abies</i> , <i>P. patens</i> , <i>M. polymorpha</i> and <i>C. reinhardtii</i> with semi quantitative PCR	62
Figure 7. <i>ACL5</i> promoters from different streptophyte lineages have conserved C3HDZ bs.....	63
Figure 8. Phylogenetic analysis and inferred history of SACL in land plants	65
Figure 9. Overview of conserved domains in SACL proteins.....	67
Figure 10. Description of 5' leader sequences in SACL transcripts and tracheophyte-specific uORFs.....	69
Figure 11. Bubble plot representing the tracheophyte-specific uORF length (bp) versus the intercistronic space (bp) in 5' leader sequences.....	
Figure 12. The 5' leaders containing the uORF are sensitive to Tspm	72
Figure 13. Tspm-dependent translation is lost when the uORF is not translated.....	73
Figure 14. Alignment of the tracheophyte-specific uORF and the Marchantiophyta-specific uORF.....	74
Figure 15. LUC base expression in 5' leader sequences of <i>A. thaliana</i> , <i>C. richardii</i> , <i>S. kraussiana</i> and <i>M. polymorpha</i>	75

Chapter 2

Figure 1. <i>MpC3HDZ</i> promoter is active in apical notches in adult plants.....	91
Figure 2. <i>MpACL5</i> promoter is active in apical notches, midribs and base of gemma cups.	92
Figure 3. <i>MpACL5</i> localizes in developing gemmae and shifts towards apical notches in mature dormant gemmae.	94
Figure 4. <i>MpSACL</i> promoter is active in epidermal tissues and developing gemma cups, but it is excluded from the apical region	95
Figure 5. Analysis of <i>MpC3HDZ</i> , <i>MpACL5</i> and <i>MpSACL</i> transcript abundances in <i>M. polymorpha</i> gametophyte tissues: apical notch, thallus, and intermediate zones.....	95
Figure 6. Genetic characterization of <i>MpC3HDZ</i> loss and gain of function mutations... 97	
Figure 7. <i>MpC3HDZ</i> regulates meristem identity and dorsoventral patterning.	98



Figure 8. <i>Mpc3hdz</i> phenotype is alleviated by conditional constitutive expression of <i>MpC3HDZ</i>	99
Figure 9. Characterization of <i>Mpac15</i> loss of function mutants.....	101
Figure 10. <i>MpACL5</i> regulates plastochron length and correlates with <i>Tspm</i> levels in <i>M. polymorpha</i>	102
Figure 11. <i>Tspm</i> is the only polyamine that influences plastochron length.....	104
Figure 12. <i>MpACL5</i> promotes meristem growth.....	105
Figure 13. <i>MpACL5</i> influences thallus thickness and cell divisions in adult thalli.	106
Figure 14. <i>Tspm</i> is a positive regulator of cell size during gemma development.....	107
Figure 15. Molecular characterization of <i>Mpsacl</i> loss of function mutants.....	108
Figure 16. <i>MpSACL</i> is a negative regulator of rhizoid development.....	109
Figure 17. <i>MpSACL</i> is a negative regulator of gemma and mucilage cell development	110
Figure 18. Characterization of <i>Mprsl1</i> loss-of-function mutants.....	112
Figure 19. <i>MpRSL1</i> is epistatic to <i>MpSACL</i>	113
Figure 20. <i>MpSACL</i> does not regulate <i>MpRSL1</i> expression during early stages of gemma development	114
Figure 21. <i>MpSACL</i> interacts with <i>MpRSL1</i> in Yeast-two hybrid (Y2H) assays.....	115
Figure 22. <i>MpRSL1</i> can interact with <i>MpSACL</i> in a BiFC.....	116
Figure 23. <i>MpC3HDZ</i> and <i>MpARF1</i> are transcriptional activators of <i>MpACL5</i>	119
Figure 24. <i>MpC3HDZ</i> regulates <i>MpACL5</i> transcription in vivo.....	120
Figure 25. <i>MpACL5</i> is induced in auxin treatments.....	121
Figure 26. Ectopic <i>MpC3HDZ</i> or IAA treatments are not sufficient to drive ectopic <i>MpACL5</i> expression	122
Figure 27. Overview of <i>MpC3HDZ</i> , <i>MpACL5</i> and <i>MpSACL</i> roles in <i>M. polymorpha</i> and their functional connections.....	123
Chapter 3	
Figure 1. Anatomy overview of <i>G. biloba</i> , <i>C. richardii</i> , and <i>S. kraussiana</i>	141
Figure 2. Anatomy of the SAM and primary root of <i>G. biloba</i> in cross sections after toluidine blue staining	142
Figure 3. Anatomy of the primary root of <i>C. richardii</i>	144
Figure 4. Anatomy of the SAM and rhizophore of <i>S. kraussiana</i>	145
Figure 5. C3HDZ, ACL5 and SACL orthologs from <i>G. biloba</i> , <i>C. richardii</i> and <i>S. kraussiana</i>	148
Figure 6. <i>SACL</i> transcripts from <i>G. biloba</i> , <i>C. richardii</i> and <i>S. kraussiana</i> contain the tracheophyte-specific uORF	149
Figure 7. Expression of <i>GbiC3HDZ.1</i> , <i>GbiC3HDZ.2</i> and <i>GbiACL5.1</i> in <i>G. biloba</i> shoots and roots.	151
Figure 8. Expression of <i>GbiACL5.2</i> , <i>GbiSACL.1</i> and <i>GbiSACL.2</i> from <i>G. biloba</i> shoots and roots.	152
Figure 9. Expression of C3HDZ, ACL5 and SACL orthologs in <i>C. richardii</i> root.....	153
Figure 10. Expression of C3HDZ, ACL5 and SACL orthologs in <i>S. kraussiana</i>	155
Figure 11. Summary of interactions in Yeast-2-Hybrid and Bimolecular Fluorescence Complementation assays between SACL, LHW and RSL class I orthologs.....	159
Figure 12. Reciprocate Yeast 2 Hybrid assays between <i>MpSACL</i> , LHW and RSL class I orthologs.....	160



Figure 13. Reciprocate Yeast 2 Hybrid assays between AtSAC51, LHW and RSL class I orthologs.....	161
Figure 14. Reciprocate Yeast 2 Hybrid assays between AtSACL3, LHW and RSL class I orthologs.....	162
Figure 15. BiFC assay on <i>N. benthamiana</i> leaves between MpSACL, LHW and RSL class I orthologs.	163
Figure 16. BiFC assay on <i>N. benthamiana</i> leaves between AtSAC51, LHW and RSL class I orthologs.	164
Figure 17. BiFC assay on <i>N. benthamiana</i> leaves between AtSACL3, LHW and RSL class I orthologs.	165
Figure 18. AtSACL3 does not share downstream regulation with MpSACL.....	167
Supplemental Figure 1. <i>In situ</i> hybridizations with sense probes in <i>G. biloba</i> tissues.	180
Supplemental Figure 2. <i>In situ</i> hybridization with sense probes in <i>Ceratopteris richardii</i> root.....	181
Supplemental Figure 3. <i>In situ</i> hybridizations with sense probes in <i>S. kraussiana</i> tissues.	182
General Discussion	
Figure 1. Hypothetical model of C3HDZ, ACL5 and SACL evolutionary trajectory in land plants.....	186

LIST OF TABLES

Chapter 1

Table 1. Summary of polyamine quantifications in plant tissues from key species.....	63
Table 2. Analysis of the 5' leader sequences in representative tracheophyte and bryophyte species.....	77
Table 3. Primers used for PCR analyses	81
Table 4. Primers used for cloning and expression in yeast.	82
Table 5. Primers used for Tspm-dependent translation assays in <i>N. benthamiana</i> leaves.....	84

Supplementary File S1 (Link to Frontiers, Data Sheet 1)

Chapter 2

Table 1. Primers used for PCR analyses.....	126
Table 2. Primers used for transgenic line construction, Y2H and BiFC assays.....	127

Chapter 3

Table 1. List of C3HDZ, ACL5 and SACL orthologs in <i>G. biloba</i> , <i>C. richardii</i> and <i>S. kraussiana</i>	149
Table 2. List of primers used for the synthesis of <i>in situ</i> hybridization sense and antisense probes.....	173
Table 3. List of primers used for the generation of entry clones for Y2H and BiFC.....	174
Table 4. List of primers used for RT-qPCR in <i>M. polymorpha</i>	175



ABBREVIATIONS

35S	Cauliflower Mosaic Virus 35S promoter	PAO	POLYAMINE OXIDASE
3AT	3-aminotriazole	Pax6	Paired box 6
ABA	Abscisic acid	PCD	Programmed cell death
ACL5	ACAULIS5	PHB	PHABULOSA
ANT	AINTEGUMENTA	PHV	PHAVOLUTA
ARF	AUXIN RESPONSE FACTOR	PHY	PHYTOCHROME PHOTORECEPTOR
ARF5/MP	ARF 5 / MONOPTEROS	PIF	PHYTOCHROME-INTERACTING FACTOR
ATG	Methionine, Start Codon	PMT	PUTRESCINE METHYL TRANSFERASE
AtHB8	ARABIDOPSIS THALIANA HOMEBOX 8	PRI	Pale Rhizoid Initials
bHLH	Basic Helix-Loop-Helix	Put	Putrescine
BIFC	Bimolecular Fluorescence Complementation	RAM	Root Apical Meristem
BLAST	Basic Local Alignment Search tool	REV	REVOLUTA
BLASTP	Basic Local Alignment Search for Proteins	RHD6	ROOT HAIR DEFECTIVE 6
bp	base pairs	ROS	Reactive Oxygen Species
bs	Binding site	RSL1	ROOT HAIR DEFECTIVE SIX-LIKE 1
C3HDZ	Class III Homeodomain-Leucine Zipper	RT-qPCR	Retro-Transcribed Quantitative Real Time PCR
CDS	coding sequence	SAC51	SUPPRESSOR OF ACAULIS 51
Cit	Citrine	SACL	SUPPRESSOR OF ACAULIS51-LIKE
CNA	CORONA	SACL1-3	SUPPRESSOR OF ACAULIS51-LIKE 1-3
CRE	Cis-regulatory element(s)	SAM	Shoot Apical Meristem
dcSAM	decarboxylated S-adenosylmethionine	SAMDC	S-ADENOSYLMETHIONINE DECARBOXILASE
Dex	Dexamethasone	SH aLRT	Shimodaira-Hasegawa-like approximate likelihood ratio test
EdU	5-ethynyl-2'-deoxyuridine	Spd	Spermidine
EF1	ELONGATION FACTOR1	SPDS	SPERMIDINE SYNTHASE
EIF5A	Elongation factor 5A	Spm	Spermine
Ey	Eyeless	SPMS	SPERMINE SYNTHASE
FCC	Food-conducting cells	SSAT	SPERMIDINE/SPERMINE N- ACETYLTRANSFERASE
GAIA4	GIBBERELLIN A INSENSITIVE DEL. 4	START	Steroidogenic acute regulatory protein (StAR)-related lipid transfer domain
GR	Glucocorticoid receptor	STM	SHOOTMERISTEMLESS
GUS	β -GLUCURONIDASE	Tak-1	Takaragaike-1 (male wild type)
HD	Homeodomain	TBLASTN	Translated Nucleotide Basic Local Alignment Search tool
IAA	Auxin, Indole-3-acetic acid	TdTomato	Modified red fluorescent protein
INDEL	Insertions and/or deletions	TE	Tracheary element
KNOX	Class I Knotted-like Homeobox	TF	Transcription factor
LECA	Last Eukaryotic Common Ancestor	TM05	TARGET OF MONOPTEROS 5
LFY	LEAFY	Tspm	Thermospermine
LHW	LONESOME HIGHWAY	TSPMS	THERMOSPERMINE SYNTHASE
LUC	Firefly LUCIFERASE	TSS	Transcription Start Site
LUCA	Last Universal Common Ancestor	uORF	upstream Open Reading Frame
ML	Maximum Likelihood	WCC	Water-conducting cells
mORF	main Open Reading Frame	WGD	Whole Genome Duplications
MpFRH	MpFEW RHIZOIDS	Y2H	Yeast-two Hybrid
MpKAR	MpKARAPPO	YFP	Yellow Fluorescent Protein
MpYUC2	MpYUCCA2		
mRNA	messenger RNA		
NLS	Nuclear Localization Sequence		
NMD	Nonsense Mediated Decay		



GLOSSARY

Aerenchyma	Parenchymatic tissue with large intercellular spaces forming air channels.
Analogy/analogous structures	The result of convergent evolution, structures that do not share a common origin but are similar (usually because of natural selection).
Apical notch	Concave structures that contain the apical meristematic cells responsible for growth.
Chromista	A taxonomic kingdom inside Eukarya, that includes diatoms, cryptophytes, and brown algae (which are not plants)
Clade	Each of the ramifications of a phylogenetic tree that contains a common ancestor and all its descendants.
Convergent evolution	The result of an independent evolution of similar structures that do not share a common ancestor, like the wings of insects and birds. Convergent evolution generates analogous structures.
Co-option	A process in which a gene, or regulatory module, acquires new functions as a result of recruitment.
Dichotomous branching	A typical growth where the stem or apical meristem divides into two (usually) equal branches.
Extant	A group of organisms that are non-extinct and can be found in the nature.
Gametophyte	A haploid life phase (n), derived from an asexual haploid spore.
Heteroblasty	The change of development or function of a structure that occurs during the lifespan of a plant. For example, leaf shapes in juvenile or adult plants of the same species. In <i>C. richardii</i> , the first three roots do not produce lateral roots, whereas the subsequently developed roots do.
Holomycota	A clade within the Opisthokonta, that includes the Fungi kingdom and Cristidiscoidea.
Homology/homolog	When two structures (or genes) share a common ancestor. For example, animal limbs.
Leptosporangiate ferns	The largest group of ferns that have one layer of cells in the sporangium, versus the multiple cell layers in eusporangiate ferns.
Meristele	A stele, in organizations that include more than one vascular bundle.
Merophyte	A group of daughter cells that derive from a meristematic cell.
Midrib	The central part of the thallus in <i>M. polymorpha</i> that contains the highest accumulation of vascular cells in the



ventral part (or pegged rhizoids) and gemma cups and seta in the dorsal part.

Monophyly/monophyletic	When all organisms in a group derive from a common ancestor.
Neofunctionalization	The result of genetic divergence, that derives in a new genetic function not shared with the ancestor.
Oil body	Specialized <i>M. polymorpha</i> cells that accumulate secondary metabolites.
Orthology/ortholog	A group of genes that derive from a common ancestor and are present in several organisms from different species.
Outgroup	The gene that is the most distantly related to a group of genes and is used as a reference to calculate the evolutionary divergence within this group.
Paralogy/paralog	A group of genes that derive from a unique ancestor, usually a result of a single or multiple gene duplications.
Plastochron	The time interval between dichotomous bifurcations of the thallus (or shoots).
Polycistronic mRNA	A messenger RNA that has multiple open reading frames.
Protostele	Typical vascular arrangement in plants that develop vascular tissues at the center of the shoots or roots.
Provascular tissues	Tissues that will differentiate into mature vascular tissues, like xylem or phloem.
Setaphyta	A clade inside the bryophytes that includes liverworts and mosses, but not hornworts. They all produce a "seta", a stalk that elevates a single sporangium for sexual reproduction.
S-phase cells	Cells in synthesis phase, also considered a "growth" state, where DNA replication happens before a cell division.
Sporophyte	A diploid life phase (2n), usually pluricellular, derived from the fertilization of sexual gametes.
Stele	Also called vascular bundle or ground tissue, refers to the combination of vascular tissues that have a shared origin: xylem, phloem, and procambium; but also the pericycle, that is not considered a conductive tissue.
Vegetative development	Non-reproductive growth.





GENERAL INTRODUCTION





The origin and diversification of land plants

The Archaeplastida lineage, or the plant kingdom, originated around 1558 MYA after a eukaryotic cell phagocytized a photosynthetic cyanobacterium that ultimately became the chloroplast by primary endosymbiosis (Ponce-Toledo et al., 2017; Yoon et al., 2004). The subsequent diversification of a unicellular ancestor gave rise to the Glaucophyta, Rhodophyta (red algae), and the Viridiplantae lineages (green plants) (Yoon et al., 2004). Green plants are classified in two main monophyletic lineages (see Glossary) (**Figure 1**): (i) the Chlorophyta, a group of marine, freshwater, and terrestrial algae that were the first group to diverge from the Viridiplantae; and (ii) the Streptophyta, that include the Charophyta, a freshwater and

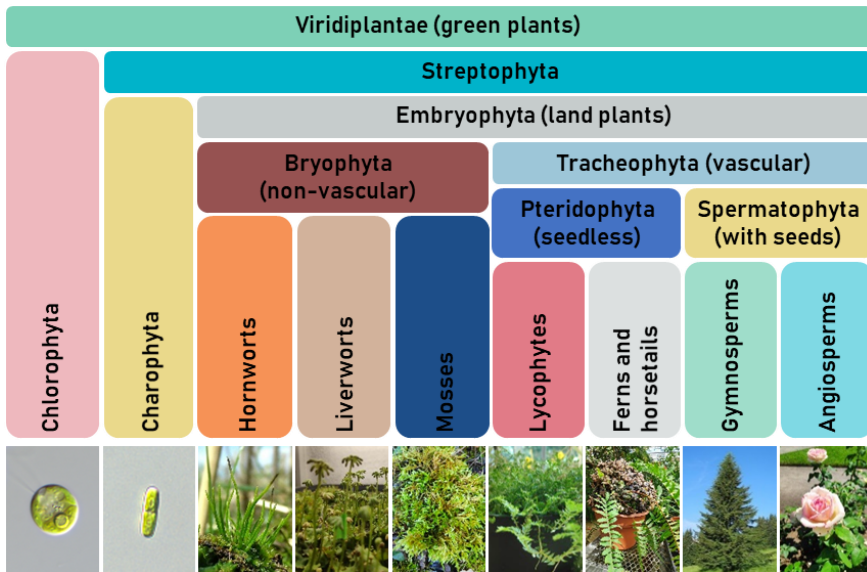


Figure 1. Overview of the plant taxonomy within green plants and example species.

Chlorophyta: *Chlamydomonas reinhardtii* (obtained from Phytozome: <https://phytozome-next.jgi.doe.gov/>); Charophyta: *Mesotaenium endlicherianum* (courtesy of Dr. Bruno Catarino); Hornworts: *Anthoceros agrestis* (obtained from the University of Zurich: <https://www.hornworts.uzh.ch/en.html>); Liverworts: *Marchantia polymorpha*; Mosses: *Pleurozium schreberi*; Lycophytes: *Selaginella kraussiana*; Ferns and horsetails: *Lecanopteris crustacea*; Gymnosperms: *Picea abies* (obtained from Plaza Gymnosperms: <https://bioinformatics.psb.ugent.be/>); Angiosperms: *Rosa chinensis*



terrestrial algae, and the Embryophyta, or land plants. Embryophytes evolved from a carophycean common ancestor around 450 MYA and gave rise to all extant (see Glossary) plant species living on land (Bowman et al., 2017; Delwiche & Cooper, 2015; Lemieux et al., 2007; Lewis & McCourt, 2004; Wellman et al., 2003; Bowman, 2022).

Extant land plants are classified in two principal monophyletic lineages (**Figure 1**): the bryophytes (mosses, hornworts, and liverworts) and the tracheophytes (pteridophytes and seed plants), whose evolutionary trajectories have led to very different body plans and lineage-specific morphological innovations (Graham et al., 2000; Harris et al., 2020, 2022; Puttick et al., 2018). For instance, the ability to produce seeds defines the seedless plants “pteridophytes” (lycophytes, ferns, and horsetails) which use spores for reproduction; and the “spermatophytes”, that are able to develop seeds as a result of sexual reproduction (**Figure 1**). Other innovations include the development of leaves and roots in tracheophytes, that have many independent origins in pteridophytes and spermatophytes (Aragón-Raygoza et al., 2020; Hetherington & Dolan, 2017, 2018, 2019; Kenrick & Strullu-Derrien, 2014). Among the morphological innovations that characterize the divergence of the bryophyte and tracheophyte body plan, is the dominance of the gametophyte (asexual) or the sporophyte (sexual) life phases (see Glossary). Bryophytes possess a dominant gametophyte with a sporophyte that totally depends on the gametophyte for survival, while tracheophytes have a dominant sporophyte and a reduced gametophyte (Kenrick, 1994). However, the main morphological innovation that is used to classify these lineages is the presence of lignified vascular tissues, that are an innovation at the tracheophyte common ancestor, and therefore one that bryophytes do not possess (**Figure 1**).

The innovation of lignified vascular tissues

Vascular tissues are specialized in the transport of water by water-conducting cells (WCC); and carbohydrates and signaling molecules by the food-conducting cells (FCC). These tissue types appear in both bryophytes and tracheophytes and share some similarities, like the loss of cytoplasmic contents for WCC, secondary cell walls in some cases, and programmed cell death (PCD) for WCC;



however, they are not homologous structures (see Glossary) and are likely a result of convergent evolution (see Glossary) (Kenrick & Crane, 1997; Ligrone et al., 2000; Xu et al., 2014). Nevertheless, only tracheophytes are considered true vascular plants, since they have developed an advanced lignified vascular system (Agustí & Blázquez, 2020; de Rybel et al., 2016; Keener et al., 1990). In tracheophytes, the tissue containing WCC is termed “xylem”, and the FCC-containing tissue is referred to as “phloem” (Esau, 1960). Bryophytes are able to produce lignin-like polymers too; however, they do not have the same mechanical properties nor appear in vascular cell types, and therefore support the independent origins of vascular tissues in bryophytes and tracheophytes (Españeira et al., 2011; Ligrone et al., 2008). The establishment of lignified vascular tissues provided extra rigidity and structural support to the vascular plant, which allowed to endure a higher hydraulic pressure and a greater apical growth. In other words, it allowed vascular plants to grow taller and deeper in the soil, allowing the survival in dryer climates and without the need of moist habitats, and supposed one of the most important hallmarks in land plant evolution.

The vascular tissues in tracheophytes are produced by a lateral meristem called “procambium” or “vascular cambium”. Usually, the procambium produces a limited number of vascular cells—a process known as “primary vascular development” and is common to all tracheophytes—and then differentiates into parenchymatic tissue (Spicer & Groover, 2010). As an innovation within some tracheophyte lineages, such as gymnosperms and angiosperms, the procambium can give rise to the vascular cambium, which bifacially produces secondary xylem and secondary phloem indefinitely, in a process that is known as “secondary vascular development” (Agustí & Blázquez, 2020; Smetana et al., 2019; Spicer & Groover, 2010). Given their common origin, function, and for the sake of clarity, these meristems are often referred to as the (pro)cambium and are treated as the same meristem.

According to the axis on which the new cell is formed, cell divisions from the (pro)cambium can be classified as (i) periclinal cell divisions, where the axis of division is parallel to the surface of the organ; and (ii) radial, which are parallel to the plant body axis (**Figure 2A**). To create new xylem and phloem initials, the (pro)cambium divides in a periclinal manner, whereas radial cell divisions are used to



increase the number of cambial cells and enlarge the circumference of the (pro)cambium (**Figure 2**).

The newly formed xylem and phloem initials can mature into different cell types. In xylem, there are two types of mature cells (**Figure 2B**): (i) the tracheary elements (TE), that can be classified as vessel elements (or tracheids, that originally gave the name to the “tracheophytes”) and fibers, and (ii) parenchyma. Mature vessel elements and fibers are devoid of cytoplasmic contents, have a lignified secondary cell wall and have undergone programmed plant cell death (Courtois-Moreau et al., 2009; Escamez & Tuominen, 2014). Their differences rely on cell size and connections with other cells of their kind. On one hand, vessel elements have a considerably wider diameter and are shorter than any of the other cell types; they are connected to other vessel elements through perforated terminal ends. On the other hand, fibers are long and narrow cells that are not interconnected. In consequence, besides providing structural support, vessel elements are the only TE that is used for long-distance water transport. Xylem parenchyma cells are live cells that do not have a lignified secondary cell wall but maintain all organelles, and are involved in many different processes such as storage and lignification of the vessel elements.

There are three types of phloem mature cells: (i) the sieve elements, (ii) the companion cells, and (iii) phloem fibers (**Figure 2B**). Sieve elements are the equivalent of xylem vessel elements since they are the main cell type for long-distance transport of carbohydrates and other elements. They are interconnected with other sieve elements through the sieve plates; however, they are considerably smaller than vessel elements and do not have a lignified secondary cell wall, nor a nucleus. Nonetheless, sieve elements are live cells, as opposed to vessel elements. Companion cells are found next to the sieve elements, to whom they are connected via plasmodesmata. Their role is to assist sieve elements since the latter lack most of their cytoplasmic contents. Like xylem fibers, phloem fibers are also long and narrow cells that provide physical strength to the phloem structure.



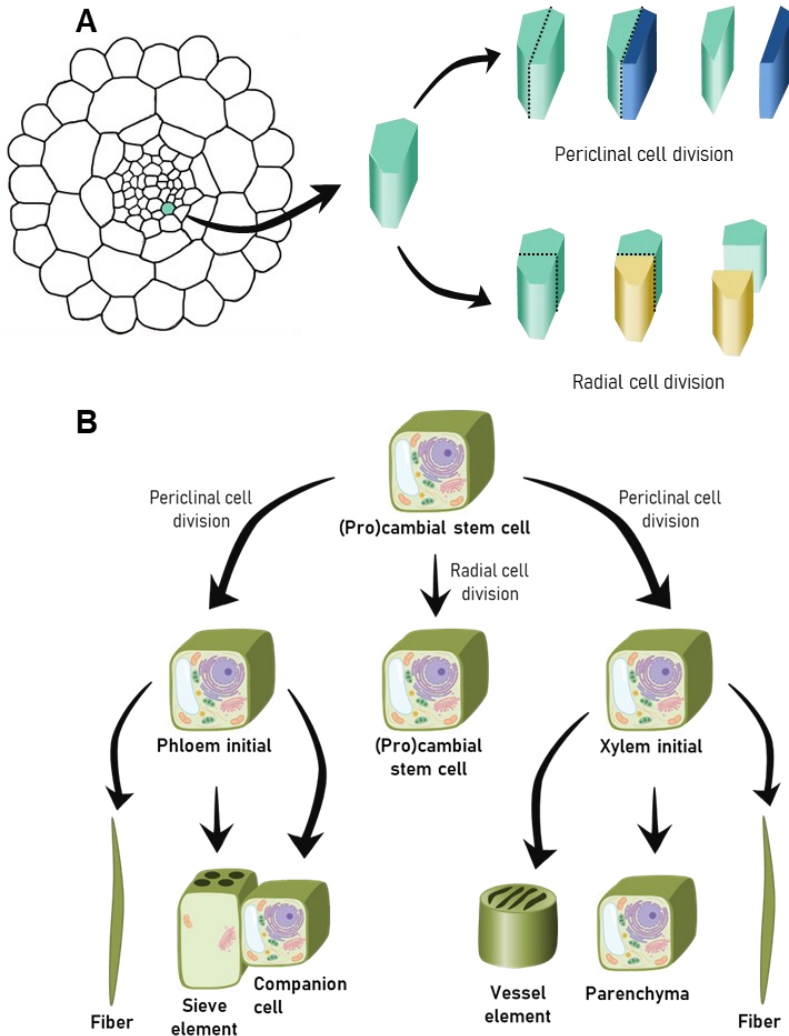


Figure 2. Schematic representation of cell division types occurring within the (pro)cambial stem cells to produce xylem and phloem initials, and overview of xylem and phloem cells maturation. A, Procambial stem cells divide in a periclinal manner to create phloem and xylem initials, and radially to create more (pro)cambial stem cells. Root diagram is adapted from Janes et al. (2018). **B,** phloem initials differentiate into mature sieve elements, companion cells, and fibers; xylem initials differentiate into mature TE (vessel elements and fibers) and parenchyma. Reconstructed from Schuetz et al., 2013. Images of alive cells were modified from Biorender (<https://biorender.com/>).



Vascular development in *A. thaliana*, an angiosperm

Vascular patterning of the A. thaliana root

The stele (see Glossary) in the primary root of *A. thaliana* (**Figure 3A**) is diarch and has bilateral symmetry (Baum et al., 2002; Campbell et al., 2017; Dolan et al., 1993) with two xylem poles and two phloem poles that develop at opposite flanks of the root, surrounded by the procambium. The xylem poles are the first xylem cells to undergo differentiation towards vessel elements and are termed “protoxylem”. They are located at both ends of the future xylem axis. Then, three to five more vessel elements (the “metaxylem”) will differentiate to vessel elements and join both protoxylem cells forming the primary xylem axis. The two phloem poles are composed of a pair of sieve elements and a pair of companion cells. Another layer of cells, the “pericycle”, is found surrounding the phloem, xylem, and procambial tissues, and provides cell protection to the vascular bundle and is responsible for the formation of lateral roots and cork (**Figure 3**) (Dolan et al., 1993).

During secondary development (**Figure 3B**), the vascular cambium, which is found creating a circumference in between xylem and phloem tissues, arises from the procambium and pericycle and produces vascular initials massively. Xylem initials will develop into secondary xylem at the center of the root, which will differentiate mostly into TE (Chaffey et al., 2002). Phloem initials, in turn, will form secondary phloem and are found surrounding the vascular cambium. The xylem, cambium, and phloem tissues are also surrounded by many layers of cells, the phelloderm, that derive from the phellogen, which arises from pericycle cells (**Figure 3B**).

The heterodimer TMO5-LHW is responsible for new vascular cell formation

The regulation of periclinal cell divisions from the vascular cambium is strictly regulated through an interplay between auxin and cytokinin during primary and secondary vascular development of *A. thaliana* (**Figure 3C**) (Mellor et al., 2017). Auxin is continuously transported from the procambial cells towards the xylem domain. In developing xylem cells, the AUXIN RESPONSE FACTOR 5, also called MONOPTEROS (ARF5/MP) induces the expression of TMO5, a basic Helix-Loop-Helix



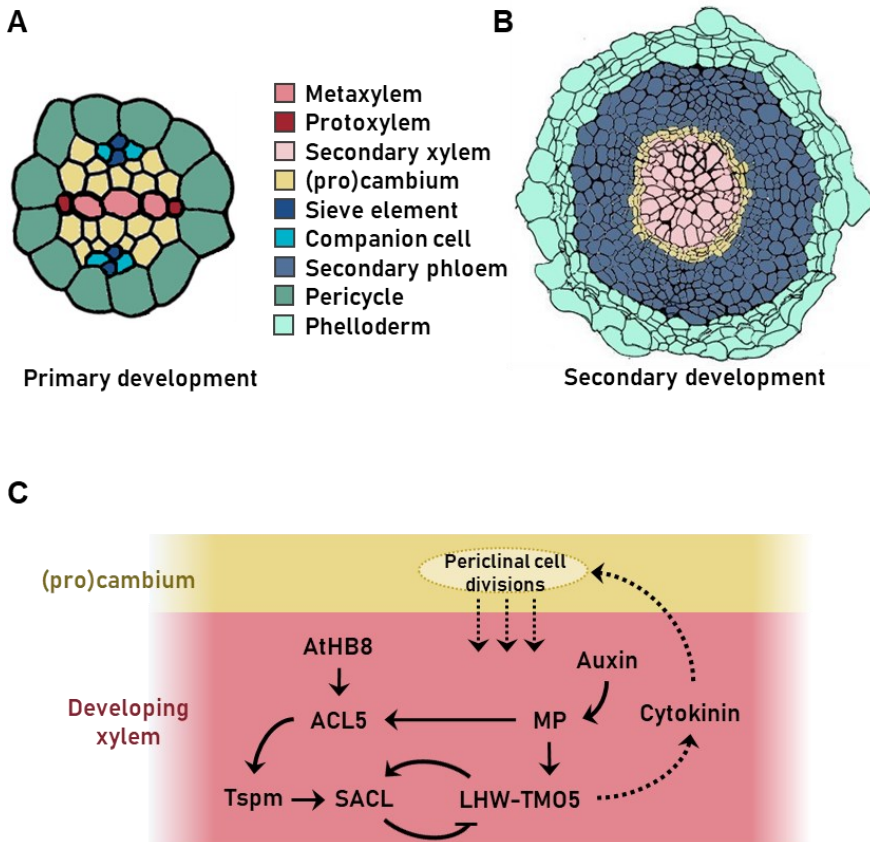


Figure 3. Anatomical overview and molecular mechanisms controlling vascular cell proliferation in *A. thaliana*. **A**, primary root showing the procambium and first differentiated vascular elements in the stele; **B**, secondary root depicting secondary xylem, phloem, and the vascular cambium. **C**, molecular mechanisms regulating periclinal cell divisions from the (pro)cambium. Developing xylem cells accumulate auxin, which results in the induction of MP and its target, TMO5. The heterodimer TMO5/LHW activates cytokinin biosynthesis genes, that will promote cell proliferation in the vascular cambium. The AtHB8/ACL5/SACL module is activated by TMO5/LHW and auxin, and restricts the activity of TMO5/LHW to avoid an over-proliferation of vascular cells. Illustrations of *A. thaliana* root under primary and secondary development are modified from Smetana et al. (2019) and Ye, et al. (2021).



(bHLH) TF. TMO5 heterodimerizes in these cells with LHW, another bHLH TF, and together induce the expression of cytokinin biosynthesis genes. This leads to an increase in periclinal cell divisions in the (pro)cambium (Berleth & Jurgens, 1993; Busse & Evert, 1999; Caño-Delgado et al., 2010; Hardtke & Berleth, 1998; Mayer et al., 1991; Ruonala et al., 2017; Wenzel et al., 2007). This mechanism ensures that the (pro)cambium continuously provides new xylem and phloem initials; however, its activity must be regulated by a safety mechanism to avoid over-proliferation: this is the role of the AtHB8, ACL5 and SACL module.

The AtHB8/ACL5/SACL module restricts vascular proliferation

In the developing vessel elements during primary and secondary development, the Tspm synthase ACL5 is upregulated by auxin/MP and ARABIDOPSIS HOMEODOMAIN 8 (AtHB8) (**Figure 3C**) (Baima et al., 2014; Knott, 2009; Knott et al., 2007).

AtHB8, together with other four paralogs (see Glossary) in *A. thaliana*, PHABULOSA (PHB), PHAVOLUTA (PHV), REVOLUTA (REV) and CORONA (CNA) are C3HDZ and are members of the homeodomain (HD) superfamily. Their HD domains are characterized by a chain of 60 amino acid residues that allow DNA binding and are very conserved among eukaryotes (Bürglin & Affolter, 2016). The rest of the subfamily is classified according to the presence of other conserved domains. C3HDZ contain four more conserved domains: the leucine zipper domain, consistent of six heptad repeats of aliphatic amino acid residues for homo and heterodimerization and DNA binding (Ariel et al., 2007; Brandt et al., 2014), a Steroidogenic acute regulatory protein (StAR)-related lipid transfer (START/SAD) domain for TF activity (Ponting & Aravind, 1999; Schrick et al., 2004), a MEKHLA/PAS domain for binding to palindromic DNA sequences (Franco-Zorrilla et al., 2014; Mukherjee & Bürglin, 2006; O'Malley et al., 2016; Palena et al., 2001), and a miRNA 165/166 target sequence for degradation (Floyd & Bowman, 2004; Reinhart et al., 2002). AtHB8 is an inducer of cambial activity and participates in xylem development; in addition, AtHB8 is the main inducer of AtACL5 expression in xylem vessels, and therefore of Tspm biosynthesis during vascular development (Baima et al., 2014).



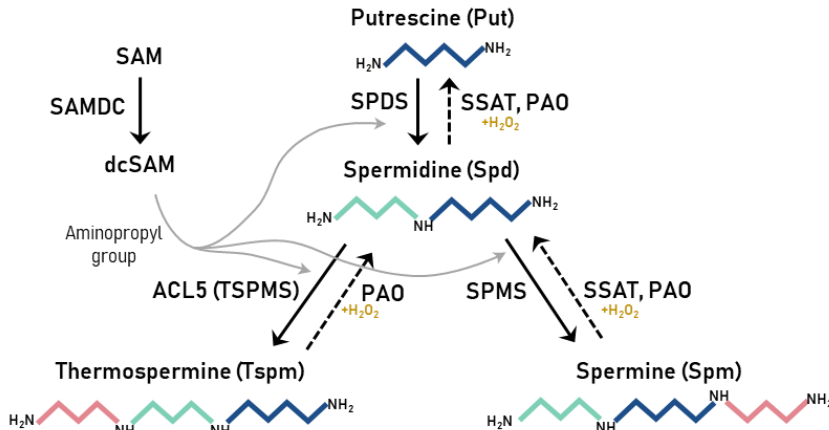


Figure 4. Polyamine biosynthesis route. The diamine Put is converted to Spd by the addition of an aminopropyl group through the Spermidine synthase enzyme (SPDS). Spm and Tspm are synthesized by the addition of an aminopropyl group to Spd by the SPMS and TSPMS or ACL5, respectively. The donor of aminopropyl groups is a decarboxylated SAM by a SAM decarboxylase (SAMDC). Polyamine catabolism is performed with the joint activity of N-acetyltransferase SPERMINE/SPERMIDINE ACETYL TRANSFERASE (SSAT) and the POLYAMINE OXIDASE genes (PAOs) generating hydrogen peroxide (H₂O₂) as a byproduct

Tspm is a tetraamine synthesized with the addition of an extra aminopropyl group to the triamine Spermidine (Spd) and is an isomer of the tetraamine Spermine (Spm) (**Figure 4**) (Knott et al., 2007; Michael, 2016; Minguet et al., 2008; Takano et al., 2012; Vera-Sirera et al., 2010). Tspm has two necessary functions: (i) the correct maturation of xylem vessel elements, maintaining differentiating cells alive until lignin has been fully deposited on their walls (Clay & Nelson, 2005; Muñoz et al., 2008; Tiburcio et al., 2014); and (ii) the restriction of vascular cell proliferation (Katayama et al., 2015b; Vera-Sirera et al., 2010, 2015). It has been proposed that the first function could be achieved via Tspm-dependent catabolism generating hydrogen peroxide (H₂O₂) as a byproduct (Salvi & Tavladoraki, 2020; Tavladoraki et al., 2012) (**Figure 4**). This, in turn, contributes to generate reactive oxygen species (ROS), which play important roles during plant cell death and cell wall deposition in xylem tracheids.



However, the second function has been more extensively studied and the mechanism involves the promotion, by Tspm, of the translation of the atypical bHLH TF SUPPRESSOR OF ACAULIS5 1 (SAC51) and its paralogs SAC51-LIKE (SACL1 to 3) (Katayama et al., 2015b; Vera-Sirera et al., 2010, 2015). The 5' leader sequences of AtSACLs contain an inhibitory regulatory *cis* element (CRE), an upstream open reading frame (uORF), that represses the translation of the main ORF. The precise mechanism of this translational regulation has not been solved yet, but it might be due to a stalling sequence at the end of the uORF, which is present in all *A. thaliana* SACLs 5' leaders (Ishitsuka et al., 2019). In the presence of Tspm, the inhibitory effect of the uORF is bypassed and SACL proteins can be translated (**Figure 3C**) (Imai et al., 2006; Katayama et al., 2015b; Vera-Sirera et al., 2015).

SACLs are bHLH TF (Pires & Dolan, 2010a). The signature domain of bHLH proteins, the bHLH, usually contains two functionally distinct regions: a basic domain (b) at the N-terminal end, which is required for DNA binding; and the HLH domain at the C-terminal end, that forms two α -helices separated by a loop sequence for homo- and heterodimerization activity (Ferré-D'Amaré et al., 1993; Murre et al., 1989). SACLs, however, belong to the XIV subfamily that lack the basic domain for DNA binding (Pires & Dolan, 2010a; Toledo-Ortiz et al., 2003), and therefore their activity relies on other interaction with other DNA-binding partners.

SACL paralogs have redundant functions in *A. thaliana*: they compete with TMO5 for dimerization with LHW, which limits cytokinin biosynthesis, thereby restricting the cell proliferation of the vascular cambium (**Figure 3C**) (Cai et al., 2016; Kakehi et al., 2008; Katayama et al., 2015b; Vera-Sirera et al., 2015). Accordingly, *Atacl5* mutants, in which SACL translation is limited due to impaired Tspm synthesis, are characterized by an over-proliferation of xylem cells and subsequent stunted growth (Kakehi et al., 2008; Muñiz et al., 2008). This is explained through the unrestricted activity of the TMO5-LHW heterodimer. Strikingly, SACL paralog expression is upregulated by the TMO5/LHW heterodimer, most probably through direct interaction with their promoters (**Figure 3C**) (Katayama et al., 2015b; Vera-Sirera et al., 2015). Hence, the same factors that induce cell proliferation in *A. thaliana* (in this case, auxin, and the heterodimer TMO5-LHW), also participate in the induction



of the AtHB8-ACL5-SACL module, creating an incoherent feedforward loop to regulate the pace for initial vascular cell formation and allow the maturation of the developing vascular cells.

Occurrence of C3HDZ, ACL5 and SACL in land plants

C3HDZ have multiple roles in land plants

The five paralogs of the C3HDZ family of TF in *A. thaliana* have distinct, overlapping, and antagonistic functions in addition to their role in vascular development (Baima et al., 1995, 2001; Prigge et al., 2005; Ramachandran et al., 2017; Roodbarkelari & Groot, 2017). For instance, they are regulators of leaf dorsoventral polarity (Emery et al., 2003; McConnell et al., 2001; Merelo et al., 2016; Prigge et al., 2005), and are shoot apical meristem (SAM) and axillary meristem initiators (Emery et al., 2003; Green et al., 2005; Otsuga et al., 2001; Prigge et al., 2005; Talbert et al., 1995). Because of such important roles in *A. thaliana*, they have gained the interest of the evo-devo field, and it has been established that this family originated before the divergence of land plants. Most remarkably, they are suggested to be part of the “ancestral toolkits” for the regulation of the land plant body plan (Catarino et al., 2016; Floyd et al., 2006; Floyd & Bowman, 2007; Prigge & Clark, 2006a). Their role in vascular development, leaf development, and apical growth has been subsequently extrapolated to all tracheophyte lineages based on expression domain analysis (Floyd et al., 2006; Prigge & Clark, 2006a; Vasco et al., 2016; Zumajo-Cardona et al., 2021). Nevertheless, there is no functional characterization of the tracheophyte C3HDZ family outside of the angiosperm lineage. Strikingly, although their roles in phyllid development in the mosses *P. patens* or *D. superba* indicate a conservation of the “leaf-development” function in the bryophyte lineage, their function in apical growth is not conserved (Yip et al., 2016). No information is available at this point about the functions of C3HDZ in other bryophytes.

Polyamines have conserved roles in stress and translation in eukaryotes

The diamine putrescine (Put) and the triamine Spd are the most commonly found polyamines in eukaryotes, while the tetra-amine spermine (Spm) is found in



yeasts, most animals, seed plants and some bacteria (Pegg & Michael, 2010; Michael, 2016). The tetra-amine Tspm has been detected in archaea, diatoms, and plants, but not in animals or bacteria (Michael, 2016).

Triamines and tetra-amines are mainly synthesized by a set of evolutionarily related aminopropyl transferases, which add an extra aminopropyl group to a pre-existing di- or triamine from a donor, a decarboxylated S-adenosylmethionine (dcSAM). dcSAM, in turn, is facilitated by a SAM decarboxylase (SAMDC) (**Figure 4**). Polyamines are catabolized through an initial step of N-acetylation by a SPERMIDINE/SPERMINE ACETYL TRANSFERASE (SSAT) followed by oxidation by polyamine oxidases (PAO), which are ancient, conserved enzymes that back convert polyamines (Salvi & Tavladoraki, 2020; Tavladoraki et al., 2012) generating hydrogen peroxide (H_2O_2) as a byproduct (**Figure 4**). The ability to synthesize specific polyamines is clade-specific and is mainly the result of evolutionary adjustments in the polyamine biosynthesis pathway, reflected in the presence or absence of specific polyamine biosynthetic enzymes in given clades (see Glossary). It has been proposed that while Spm synthase (SPMS) genes in fungi and plants have likely emerged independently after duplication and neofunctionalization (see Glossary) of spermidine synthase (SPDS) genes, the thermospermine synthase (TSPMS) gene in plants was probably acquired through endosymbiosis of a cyanobacterium (Minguet et al., 2008). However, it is arguable whether such gene originally encoded a TSPMS or an agmatine aminopropyl transferase (Pegg & Michael, 2010; Michael, 2016). Considering everything, the capacity to synthesize different polyamines in a given species is defined by (i) the presence or absence of specific polyamine biosynthetic enzymes and (ii) the degree of specificity of the polyamine biosynthesis enzymes towards their substrates. For instance, it has been reported that an aminopropyl transferase from the archaea *Pyrobaculum aerophilum* displays its highest specificity *in vitro* towards norspermidine, resulting in norspermine biosynthesis, but it is also able to synthesize Tspm from Spd (Knott, 2009). Similarly, the gymnosperm *Pinus sylvestris* lacks a specific SPMS gene, but the aminopropyl transferase encoded by PsSPDS efficiently converts Put to Spd, as well as Spd to Spm (Vuosku et al., 2018).

While the diamine Put and the triamine Spd are essential for life (Imai et al., 2004), all polyamines participate in stress responses and development in tracheophytes (Chen et al., 2019; Tiburcio et al., 2014; Vera-Sirera et al., 2010). Their role can be explained through their chemical features or the products of their catabolism. In line with this, polyamine homeostasis and the H₂O₂ produced in polyamine catabolism can contribute to ROS production in response to mechanical damage (Gonzalez et al., 2011; Yoda et al., 2003) or participate in abscisic acid (ABA) signaling, which regulates stress responses (An et al., 2008; Petřivalský et al., 2007; Xue et al., 2009). Tetra-amines like Spm and Tspm have also been linked with biotic stress responses to infection by *Pseudomonas viridiflava* (Gonzalez et al., 2011; Marina et al., 2013). Also, given their nature, polyamines are thought to interact with negatively charged macromolecules, such as RNA and DNA. In fact, Spd and Put are most commonly found in RNA complexes (Watanabe et al., 1991), and can stimulate translation efficiency in eukaryotic and prokaryotic cell-free systems by binding to ribosomes (Igarashi et al., 1974, 1982). Probably as a direct implication of their interaction with RNA and ribosomes, polyamines can influence the nonsense mediated decay (NMD) of mRNA, which is induced by – but not limited to – premature stop codons in the 5' leaders (Poidevin et al., 2019).

In bryophytes, some studies have analyzed the senescent effect of exogenously applied polyamines (Stanislaus & Maravolo, 1994); however, very little is known about the roles of polyamines on development or stress, since most studies have focused on the quantification of polyamines or the characterization of polyamine biosynthetic genes rather than functional experimentation (Fuell et al., 2010; Hamana & Matsuzaki, 1982, 1985; Minguet et al., 2008).

The only known role of SACL proteins is the regulation of vascular development in A. thaliana

The function of SACL proteins has never been characterized outside *A. thaliana* (Katayama et al., 2015; Milhinhos et al., 2020; Ohashi-Ito et al., 2014; Vera-Sirera et al., 2015). The expression of one ortholog (see Glossary) of SACL has also been examined in *Populus trichocarpa* (Milhinhos et al., 2020) and the presence of



the inhibitory uORF has been suggested to be conserved in angiosperms, since it has been found in the orthologs of several other species of this lineage (Ishitsuka et al., 2019). Additionally, the sequence of the uORF has been found in the genomes of some species of gymnosperms and ferns (Hayden & Jorgensen, 2007); however, it was based on Basic Local Alignment Search for Proteins (BLASTP) searches using only the aminoacidic sequence of the uORF and it is unknown whether they belonged to the 5' leader of *SACL* orthologs in these species, their connection with *Tspm*, or whether they have a relevant role in vascular development. Interestingly, bryophytes have been recently shown to contain *SACL* genes (Catarino et al., 2016), whose function remains to be characterized in this lineage as well.

The use of phylogenetically distant model organisms for evo devo studies

As the number of sequenced plant genomes increases, so is the realization that this information is an essential tool to infer the evolutionary events that shaped fundamental biological processes (Delaux et al., 2019). The recent advances in genetic and genomic tools in *M. polymorpha*, a liverwort (Bowman et al., 2017; Ishizaki et al., 2008; Nishihama et al., 2016; Suzuki et al., 2020), as well as in *P. patens*, a moss (Hohe et al., 2004; Rensing et al., 2008; D. Schaefer et al., 1991; D. G. Schaefer, 2002) has revealed synapomorphies (see Glossary) and shared developmental programs within the land plant lineage.

For instance, evo devo studies have shed light on the evolution of plant adaptation to changing environments through the study of DELLA proteins in *M. polymorpha*, *P. patens*, *S. moellendorffii*, *S. lycopersicum* and *A. thaliana* (Briones-Moreno et al., 2017, 2023; Hernández-García et al., 2019, 2021), or the conservation of the auxin transcriptional machinery shaping the body plan of land plants (Ashton et al., 1979; Cooke et al., 2002; Eklund et al., 2015; Flores-Sandoval et al., 2015, 2018; Ishizaki et al., 2012; Kato et al., 2015, 2017). Hence, the use of phylogenetically distant model organisms, such as *M. polymorpha*, but also species from other plant lineages, such as pteridophytes and spermatophytes, is key for evo-devo studies to infer the evolutionary history of a character and the developmental pathways behind morphological innovations.



Vegetative development and molecular regulation of M. polymorpha

M. polymorpha has a gametophyte-dominant life cycle, typical in bryophytes, characterized by an alternation of generations between the haploid gametophyte (n) and the diploid sporophyte (2n). Vegetative development (see Glossary) starts with the germination of a haploid spore, which will develop into thalloid gametophyte through the activity of an apical cell (Shimamura, 2016). A typical *M. polymorpha* gametophytic thallus harbors several unique and specialized structures that contribute to its vegetative development, among which are apical notches, gemma cups, air pore complexes, rhizoids, and ventral scales (**Figure 5**).

Apical notches are located in concave structures at the apical ends of the thallus or gemma and contain a cuneate apical cell, responsible for the formation of daughter cells at the dorsal, ventral, and lateral surfaces (**Figure 5**). These cells are termed merophytes (see Glossary) and will further generate the rest of the tissues of the thallus in an organized manner (Kohchi et al., 2021; Suzuki et al., 2020). How this process is regulated at the genetic level is still an open question. Recently, some studies have shown that the mechanisms supporting *A. thaliana* apical meristem development are conserved in *M. polymorpha*. For instance, auxin is a positive regulator of meristem size and apical notch activity through the AUXIN RESPONSE FACTOR 1 (MpARF1) (Flores-Sandoval et al., 2015; Kato et al., 2017), and several genetic pathways might be also required for meristem growth, like the CLE-family of peptide hormones and their receptors (Bowman et al., 2017; Cammarata & Scanlon, 2020; Hirakawa et al., 2020).

Apical notches branch dichotomously (see Glossary) in regular intervals during vegetative growth (Solly et al., 2017) but, so far, the only exogenous cue characterized that influences dichotomous branching in *M. polymorpha* is light and shade (Streubel et al., 2022). Light and shade response involves the orthologues of phytochrome photoreceptors (PHY) and PHYTOCHROME INTERACTING FACTORS (PIF) in *M. polymorpha* (MpPHY and MpPIF), that positively regulate meristem dormancy in shade conditions.



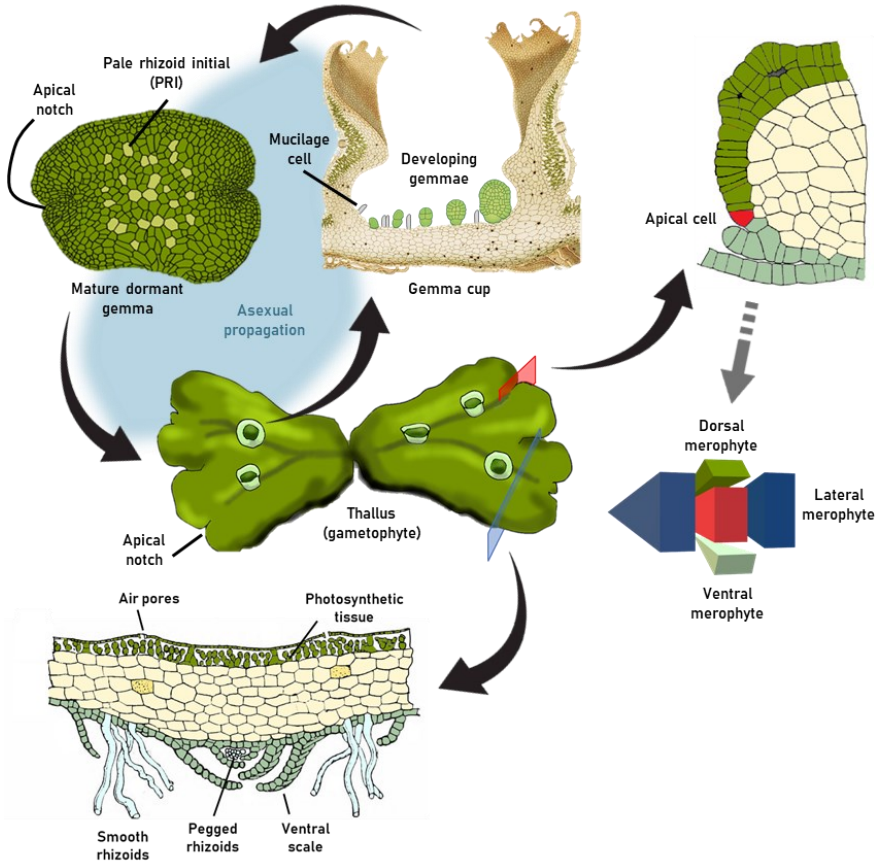


Figure 5. Overview of *M. polymorpha* gametophyte development. Schematic illustration of a thallus and unique structures typical from this species: the gemma cup, where gemmae development takes place and the gemma, the asexual propagule with specified pale rhizoid initials, contribute to the asexual propagation of the gametophyte. The apical cell (in red) is found in apical notches, concave structures at the end of the thallus. The apical cell divides in four planes (dorsal, ventral, right and left – lateral) to create dorsal, ventral and lateral merophytes, respectively. Other structures in the dorsal face of the thallus are the air chambers, which contain photosynthetic tissue and permit gas exchange through the air pores. In the ventral face of the thallus, ventral scales, smooth rhizoids and pegged rhizoids are developed. Illustration adapted from J.F. Schreider Eslingin Edit. (Botanical illustration); Suzuki et al., (2020); Kato et al., (2020); and Shimamura et al., (2016)

Gemma cups are specialized organs for asexual propagation (**Figure 5**). They are cup-shaped structures that derive from dorsal and lateral merophytes (Suzuki et al., 2020) and produce the gemmae, a clonal asexual propagule, and mucilage cells (Shimamura, 2016). Both gemmae and mucilage cells derive from gemma cup basal cells termed “initials”, that have acquired a differential specification. These cells then protrude from the epidermis and develop into fully mature gemmae. During gemmae development, the elongated cell divides transversally to create the multipotent gemma primordium and the stalk, which maintains the gemma attached to the base of the gemma cup. The final gemma is developed from subsequent asymmetric cell divisions of the gemma primordium. The molecular regulation of gemma development is achieved through several genetic pathways. For instance, auxin regulation mediated by MpARF1 has been shown to positively regulate gemma development (Eklund et al., 2015; Flores-Sandoval et al., 2015; Ishizaki et al., 2012; Kato et al., 2015), where *Mparf1* mutants are defective in gemmae final cell arrangement (Kato et al., 2017). MpKARAPPO (MpKAR), which means “empty” in Japanese due to the empty gemma cups in *Mpkar* mutants, is a small Rho-GTPase that is required for the protrusion of the gemma and mucilage initials (Hiwatashi et al., 2019). Similarly, the only ROOTHAIR DEFECTIVE SIX-LIKE (RSL) class I ortholog in *M. polymorpha*, MpRSL1, is also required for gemmae development, and loss of function *Mprsl1* as well as an overexpression of *FEW RHIZOIDS* (MpFRH), a microRNA targeting *MpRSL1* mRNA, is characterized by having empty gemma cups (Honkanen et al., 2018; Proust et al., 2016; Thamm et al., 2020).

Rhizoids and scales are found at the ventral face of the thallus (**Figure 5**). Ventral scales are pluricellular leaf-like tissues that protect rhizoid bundles (Kohchi et al., 2021; Shimamura, 2016). Rhizoids are unicellular structures with a rooting function that develop from the ventral epidermis or scales. They provide anchorage and act as WCC. In *M. polymorpha* these two functions are separated in two types of rhizoids: smooth rhizoids, which grow into the media and provide anchorage, and pegged (or tuberculate) rhizoids, that function as a water conducting system and are found parallel to the ventral surface of the thallus (Duckett et al., 2014; Kohchi et al., 2021; Shimamura, 2016). In mature gemmae, smooth rhizoids are developed from pre-



specified pale rhizoid initials (PRI) (**Figure 5**). Rhizoid specification is regulated by lateral inhibition through the interplay of MpRSL1 and MpFRH: MpFRH is induced in rhizoid initials and moves towards the neighboring cells, where MpRSL1 mRNA, required for rhizoid specification, is then inhibited. This mechanism ensures that no over-proliferation of rhizoid cells occurs (Honkanen et al., 2018; Proust et al., 2016; Thamm et al., 2020).

REFERENCES

- Agustí, J., & Blázquez, M. A.** (2020). Plant vascular development: mechanisms and environmental regulation. *Cellular and Molecular Life Sciences*, 77(19), 3711–3728. <https://doi.org/10.1007/s00018-020-03496-w>
- An, Z., Jing, W., Liu, Y., & Zhang, W.** (2008). Hydrogen peroxide generated by copper amine oxidase is involved in abscisic acid-induced stomatal closure in *Vicia faba*. *Journal of Experimental Botany*, 59(4). <https://doi.org/10.1093/jxb/erm370>
- Aragón-Raygoza, A., Vasco, A., Blilou, I., Herrera-Estrella, L., & Cruz-Ramírez, A.** (2020). Development and cell cycle activity of the root apical meristem in the fern *Ceratopteris richardii*. *Genes*, 11(12). <https://doi.org/10.3390/genes11121455>
- Ariel, F. D., Manavella, P. A., Dezar, C. A., & Chan, R. L.** (2007). The true story of the HD-Zip family. In *Trends in Plant Science* (Vol. 12, Issue 9). <https://doi.org/10.1016/j.tplants.2007.08.003>
- Ashton, N. W., Grimsley, N. H., & Cove, D. J.** (1979). Analysis of gametophytic development in the moss, *Physcomitrella patens*, using auxin and cytokinin resistant mutants. *Planta*, 144(5). <https://doi.org/10.1007/BF00380118>
- Baima, S., Forte, V., Possenti, M., Peñalosa, A., Leoni, G., Salvi, S., Felici, B., Ruberti, I., & Morelli, G.** (2014). Negative feedback regulation of auxin signaling by ATHB8/ACL5-BUD2 transcription module. *Molecular Plant*, 7(6). <https://doi.org/10.1093/mp/ssu051>
- Baima, S., Nobili, F., Sessa, G., Lucchetti, S., Ruberti, I., & Morelli, G.** (1995). The expression of the Athb-8 homeobox gene is restricted to provascular cells in *Arabidopsis thaliana*. *Development*, 121(12). <https://doi.org/10.1242/dev.121.12.4171>
- Baima, S., Possenti, M., Matteucci, A., Wisman, E., Altamura, M. M., Ruberti, I., & Morelli, G.** (2001). The 28 kDa ATHB-8 HD-zip protein acts as a differentiation-



- promoting transcription factor of the vascular meristems. *Plant Physiology*, 126(2). <https://doi.org/10.1104/pp.126.2.643>
- Baum, S. F., Dubrovsky, J. G., & Rost, T. L.** (2002). Apical organization and maturation of the cortex and vascular cylinder in *Arabidopsis thaliana* (Brassicaceae) roots. *American Journal of Botany*, 89(6). <https://doi.org/10.3732/ajb.89.6.908>
- Berleth, T., & Jurgens, G.** (1993). The role of the *monopteros* gene in the basal body region of the *Arabidopsis* embryo. *Development*, 118(2). <https://doi.org/10.1242/dev.118.2.575>
- Bowman, J. L., Kohchi, T., Yamato, K. T., Jenkins, J., Shu, S., Ishizaki, K., Yamaoka, S., Nishihama, R., Nakamura, Y., Berger, F., Adam, C., Aki, S. S., Althoff, F., Araki, T., Arteaga-Vazquez, M. A., Balasubramanian, S., Barry, K., Bauer, D., Boehm, C. R., ... Schmutz, J.** (2017). Insights into Land Plant Evolution Garnered from the *Marchantia polymorpha* Genome. *Cell*, 171(2), 287-304.e15. <https://doi.org/10.1016/j.cell.2017.09.030>
- Brandt, R., Cabedo, M., Xie, Y., & Wenkel, S.** (2014). Homeodomain leucine-zipper proteins and their role in synchronizing growth and development with the environment. *Journal of Integrative Plant Biology*, 56(6). <https://doi.org/10.1111/jipb.12185>
- Briones-Moreno, A., Hernández-García, J., Vargas-Chávez, C., Blanco-Touriñán, N., Phokas, A., Úrbez, C., Cerdán, P. D., Coates, J. C., Alabadi, D., & Blázquez, M. A.** (2023). DELLA functions evolved by rewiring of associated transcriptional networks. *Nature Plants*. <https://doi.org/10.1038/s41477-023-01372-6>
- Briones-Moreno, A., Hernández-García, J., Vargas-Chávez, C., Romero-Campero, F. J., Romero, J. M., Valverde, F., & Blázquez, M. A.** (2017). Evolutionary analysis of DELLA-associated transcriptional networks. *Frontiers in Plant Science*, 8. <https://doi.org/10.3389/fpls.2017.00626>
- Bürglin, T. R., & Affolter, M.** (2016). Homeodomain proteins: an update. In *Chromosoma* (Vol. 125, Issue 3). <https://doi.org/10.1007/s00412-015-0543-8>
- Busse, J. S., & Evert, R. F.** (1999). Pattern of differentiation of the first vascular elements in the embryo and seedling of *Arabidopsis thaliana*. *International Journal of Plant Sciences*, 160(1). <https://doi.org/10.1086/314098>
- Cai, Q., Fukushima, H., Yamamoto, M., Ishii, N., Sakamoto, T., Kurata, T., Motose, H., & Takahashi, T.** (2016). The SAC51 family plays a central role in thermospermine responses in *Arabidopsis thaliana*. *Plant and Cell Physiology*, 57(8). <https://doi.org/10.1093/pcp/pcw113>



- Cammarata, J., & Scanlon, M. J.** (2020). A functionally informed evolutionary framework for the study of LRR-RLKs during stem cell maintenance. *Journal of Plant Research*, 133(3). <https://doi.org/10.1007/s10265-020-01197-w>
- Campbell, L., Turner, S., & Etchells, P.** (2017). Regulation of vascular cell division. In *Journal of Experimental Botany* (Vol. 68, Issue 1). <https://doi.org/10.1093/jxb/erw448>
- Caño-Delgado, A., Lee, J. Y., & Demura, T.** (2010). Regulatory mechanisms for specification and patterning of plant vascular tissues. In *Annual Review of Cell and Developmental Biology* (Vol. 26). <https://doi.org/10.1146/annurev-cellbio-100109-104107>
- Catarino, B., Hetherington, A. J., Emms, D. M., Kelly, S., & Dolan, L.** (2016). The Stepwise Increase in the Number of Transcription Factor Families in the Precambrian Predated the Diversification of Plants on Land. *Molecular Biology and Evolution*, 33(11). <https://doi.org/10.1093/molbev/msw155>
- Chaffey, N., Cholewa, E., Regan, S., & Sundberg, B.** (2002). Secondary xylem development in *Arabidopsis*: A model for wood formation. *Physiologia Plantarum*, 114(4). <https://doi.org/10.1034/j.1399-3054.2002.1140413.x>
- Chen, D., Shao, Q., Yin, L., Younis, A., & Zheng, B.** (2019). Polyamine function in plants: Metabolism, regulation on development, and roles in abiotic stress responses. In *Frontiers in Plant Science* (Vol. 9). <https://doi.org/10.3389/fpls.2018.01945>
- Clay, N. K., & Nelson, T.** (2005). *Arabidopsis* thickvein mutation affects vein thickness and organ vascularization, and resides in a provascular cell-specific spermine synthase involved in vein definition and in polar auxin transport. In *Plant Physiology* (Vol. 138, Issue 2). <https://doi.org/10.1104/pp.104.055756>
- Cooke, T. J., Poli, D. B., Sztein, A. E., & Cohen, J. D.** (2002). Evolutionary patterns in auxin action. *Plant Molecular Biology*, 49(3–4). <https://doi.org/10.1023/A:1015242627321>
- Courtois-Moreau, C. L., Pesquet, E., Sjödin, A., Muñiz, L., Bollhöner, B., Kaneda, M., Samuels, L., Jansson, S., & Tuominen, H.** (2009). A unique program for cell death in xylem fibers of *Populus* stem. *Plant Journal*, 58(2). <https://doi.org/10.1111/j.1365-313X.2008.03777.x>
- de Rybel, B., Mähönen, A. P., Helariutta, Y., & Weijers, D.** (2016). Plant vascular development: from early specification to differentiation. *Nature Reviews Molecular Cell Biology*, 17(1), 30–40. <https://doi.org/10.1038/nrm.2015.6>
- Delaux, P. M., Hetherington, A. J., Coudert, Y., Delwiche, C., Dunand, C., Gould, S., Kenrick, P., Li, F. W., Philippe, H., Rensing, S. A., Rich, M., Strullu-Derrien, C., & de Vries,**



- J. (2019). Reconstructing trait evolution in plant evo–devo studies. In *Current Biology* (Vol. 29, Issue 21). <https://doi.org/10.1016/j.cub.2019.09.044>
- Delwiche, C. F., & Cooper, E. D.** (2015). The evolutionary origin of a terrestrial flora. In *Current Biology* (Vol. 25, Issue 19). <https://doi.org/10.1016/j.cub.2015.08.029>
- Dolan, L., Janmaat, K., Willemsen, V., Linstead, P., Poethig, S., Roberts, K., & Scheres, B.** (1993). Cellular 31 relevant 31 is 31 of the *Arabidopsis thaliana* root. *Development*, 119(1). <https://doi.org/10.1242/dev.119.1.71>
- Duckett, J. G., Ligrone, R., Renzaglia, K. S., & Pressel, S.** (2014). Pegged and smooth rhizoids in complex thalloid liverworts (Marchantiopsida): Structure, function and evolution. *Botanical Journal of the Linnean Society*, 174(1). <https://doi.org/10.1111/boj.12121>
- Eklund, D. M., Ishizaki, K., Flores-Sandoval, E., Kikuchi, S., Takebayashi, Y., Tsukamoto, S., Hirakawa, Y., Nonomura, M., Kato, H., Kouno, M., Bhalerao, R. P., Lagercrantz, U., Kasahara, H., Kohchi, T., & Bowman, J. L.** (2015). Auxin Produced by the Indole-3-Pyruvic Acid Pathway Regulates Development and Gemmae Dormancy in the Liverwort *Marchantia polymorpha*. *The Plant Cell*, 27(6), 1650–1669. <https://doi.org/10.1105/TPC.15.00065>
- Emery, J. F., Floyd, S. K., Alvarez, J., Eshed, Y., Hawker, N. P., Izhaki, A., Baum, S. F., & Bowman, J. L.** (2003). Radial Patterning of *Arabidopsis* Shoots by Class III HD-ZIP and KANADI Genes. *Current Biology*, 13(20). <https://doi.org/10.1016/j.cub.2003.09.035>
- Esau, K.** (1960). *Anatomy of Seed Plants*. *Soil Science*, 90(2). <https://doi.org/10.1097/00010694-196008000-00031>
- Escamez, S., & Tuominen, H.** (2014). Programmes of cell death and autolysis in tracheary elements: When a suicidal cell arranges its own corpse removal. In *Journal of Experimental Botany* (Vol. 65, Issue 5). <https://doi.org/10.1093/jxb/eru057>
- Espiñeira, J. M., Novo Uzal, E., Gómez Ros, L. v., Carrión, J. S., Merino, F., Ros Barceló, A., & Pomar, F.** (2011). Distribution of lignin monomers and the evolution of lignification among lower plants. *Plant Biology*, 13(1). <https://doi.org/10.1111/j.1438-8677.2010.00345.x>
- Ferré-D'Amaré, A. R., Prendergast, G. C., Ziff, E. B., & Burley, S. K.** (1993). Recognition by Max of its cognate DNA through a dimeric b/HLH/Z domain. *Nature*, 363(6424). <https://doi.org/10.1038/363038a0>
- Flores-Sandoval, E., Eklund, D. M., & Bowman, J. L.** (2015). A Simple Auxin Transcriptional Response System Regulates Multiple Morphogenetic Processes in the Liverwort



- Marchantia polymorpha. PloS Genetics, 11(5).
<https://doi.org/10.1371/journal.pgen.1005207>
- Flores-Sandoval, E., Romani, F., & Bowman, J. L.** (2018). Co-expression and transcriptome analysis of 32 relevant 32i polymorpha transcription factors supports class c arfs as independent actors of an ancient auxin regulatory module. *Frontiers in Plant Science*, 9. <https://doi.org/10.3389/fpls.2018.01345>
- Floyd, S. K., & Bowman, J. L.** (2004). Gene regulation: ancient microRNA target sequences in plants. *Nature*, 428(6982).
- Floyd, S. K., & Bowman, J. L.** (2007). The ancestral developmental tool kit of land plants. *International Journal of Plant Sciences*, 168(1), 1–35. <https://doi.org/10.1086/509079/ASSET/IMAGES/LARGE/FG12.JPEG>
- Floyd, S. K., Zalewski, C. S., & Bowman, J. L.** (2006). Evolution of class III homeodomain-leucine zipper genes in streptophytes. *Genetics*, 173(1). <https://doi.org/10.1534/genetics.105.054239>
- Franco-Zorrilla, J. M., López-Vidriero, I., Carrasco, J. L., Godoy, M., Vera, P., & Solano, R.** (2014). DNA-binding specificities of plant transcription factors and their potential to define target genes. *Proceedings of the National Academy of Sciences of the United States of America*, 111(6). <https://doi.org/10.1073/pnas.1316278111>
- Fuell, C., Elliott, K. A., Hanfrey, C. C., Franceschetti, M., & Michael, A. J.** (2010). Polyamine biosynthetic diversity in plants and algae. *Plant Physiology and Biochemistry*, 48(7). <https://doi.org/10.1016/j.plaphy.2010.02.008>
- Gonzalez, M. E., Marco, F., Minguet, E. G., Carrasco-Sorli, P., Blázquez, M. A., Carbonell, J., Ruiz, O. A., & Pieckenstain, F. L.** (2011). Perturbation of spermine synthase gene expression and transcript profiling provide new insights on the role of the tetraamine spermine in *Arabidopsis* defense against *Pseudomonas viridiflava*. *Plant Physiology*, 156(4). <https://doi.org/10.1104/pp.110.171413>
- Graham, L. E., Cook, M. E., & Busse, J. S.** (2000). The origin of plants: Body plan changes contributing to a major evolutionary radiation. In *Proceedings of the National Academy of Sciences of the United States of America* (Vol. 97, Issue 9). <https://doi.org/10.1073/pnas.97.9.4535>
- Green, K. A., Prigge, M. J., Katzman, R. B., & Clark, S. E.** (2005). Corona, a member of the class III homeodomain leucine zipper gene family in *Arabidopsis*, regulates stem cell specification and organogenesis. *Plant Cell*, 17(3). <https://doi.org/10.1105/tpc.104.026179>



- Hamana, K., & Matsuzaki, S.** (1982). Widespread occurrence of norspermidine and norspermine in eukaryotic algae. *Journal of Biochemistry*, 91(4). <https://doi.org/10.1093/oxfordjournals.jbchem.a133818>
- Hamana, K., & Matsuzaki, S.** (1985). Distinct difference in the polyamine compositions of bryophyta and 33 relevant 33 is 33 . *Journal of Biochemistry*, 97(6). <https://doi.org/10.1093/oxfordjournals.jbchem.a135216>
- Hardtke, C. S., & Berleth, T.** (1998). The Arabidopsis gene MONOPTEROS encodes a transcription factor mediating embryo axis formation and vascular development. *EMBO Journal*, 17(5). <https://doi.org/10.1093/emboj/17.5.1405>
- Harris, B. J., Clark, J. W., Schrepf, D., Szöllösi, G. J., Donoghue, P. C. J., Hetherington, A. M., & Williams, T. A.** (2022). Divergent evolutionary trajectories of bryophytes and tracheophytes from a complex common ancestor of land plants. *Nature Ecology and Evolution*, 6(11). <https://doi.org/10.1038/s41559-022-01885-x>
- Harris, B. J., Harrison, C. J., Hetherington, A. M., & Williams, T. A.** (2020). Phylogenomic Evidence for the Monophyly of Bryophytes and the Reductive Evolution of Stomata. *Current Biology*, 30(11). <https://doi.org/10.1016/j.cub.2020.03.048>
- Hayden, C. A., & Jorgensen, R. A.** (2007). Identification of novel conserved peptide uORF homology groups in Arabidopsis and rice reveals ancient eukaryotic origin of select groups and preferential association with transcription factor-encoding genes. *BMC Biology*, 5(1), 32. <https://doi.org/10.1186/1741-7007-5-32>
- Hernández-García, J., Briones-Moreno, A., Dumas, R., & Blázquez, M. A.** (2019). Origin of Gibberellin-Dependent Transcriptional Regulation by Molecular Exploitation of a Transactivation Domain in DELLA Proteins. *Molecular Biology and Evolution*, 36(5). <https://doi.org/10.1093/molbev/msz009>
- Hernández-García, J., Sun, R., Serrano-Mislata, A., Inoue, K., Vargas-Chávez, C., Esteve-Bruna, D., Arbona, V., Yamaoka, S., Nishihama, R., Kohchi, T., & Blázquez, M. A.** (2021). Coordination between growth and stress responses by DELLA in the liverwort *Marchantia polymorpha*. *Current Biology*, 31(16). <https://doi.org/10.1016/j.cub.2021.06.010>
- Hetherington, A. J., & Dolan, L.** (2017). The evolution of lycopsid rooting structures: conservatism and disparity. In *New Phytologist* (Vol. 215, Issue 2). <https://doi.org/10.1111/nph.14324>
- Hetherington, A. J., & Dolan, L.** (2018). Stepwise and independent origins of roots among land plants. *Nature*, 561(7722), 235–238. <https://doi.org/10.1038/s41586-018-0445-z>



- Hetherington, A. J., & Dolan, L.** (2019). Rhynie chert fossils demonstrate the independent origin and gradual evolution of lycophyte roots. In *Current Opinion in Plant Biology* (Vol. 47). <https://doi.org/10.1016/j.pbi.2018.12.001>
- Hirakawa, Y., Fujimoto, T., Ishida, S., Uchida, N., Sawa, S., Kiyosue, T., Ishizaki, K., Nishihama, R., Kohchi, T., & Bowman, J. L.** (2020). Induction of Multichotomous Branching by CLAVATA Peptide in *Marchantia polymorpha*. *Current Biology*, 30(19), 3833-3840.e4. <https://doi.org/10.1016/j.cub.2020.07.016>
- Hiwatashi, T., Goh, H., Yasui, Y., Koh, L. Q., Takami, H., Kajikawa, M., Kirita, H., Kanazawa, T., Minamino, N., Togawa, T., Sato, M., Wakazaki, M., Yamaguchi, K., Shigenobu, S., Fukaki, H., Mimura, T., Toyooka, K., Sawa, S., Yamato, K. T., ... Ishizaki, K.** (2019). The RopGEF KARAPPO Is Essential for the Initiation of Vegetative Reproduction in *Marchantia polymorpha*. *Current Biology*, 29(20). <https://doi.org/10.1016/j.cub.2019.08.071>
- Hohe, A., Egener, T., Lucht, J. M., Holtorf, H., Reinhard, C., Schween, G., & Reski, R.** (2004). An improved and highly relevant transformation procedure allows efficient production of single and multiple targeted gene-knockouts in a moss, *Physcomitrella patens*. *Current Genetics*, 44(6). <https://doi.org/10.1007/s00294-003-0458-4>
- Honkanen, S., Thamm, A., Arteaga-Vazquez, M. A., & Dolan, L.** (2018). Negative regulation of conserved RSL class I bHLH transcription factors evolved independently among land plants. *Elife*, 7. <https://doi.org/10.7554/eLife.38529>
- Igarashi, K., Hashimoto, S., Miyake, A., Kashiwagi, K., & Hirose, S.** (1982). Increase of Fidelity of Polypeptide Synthesis by Spermidine in Eukaryotic Cell-Free Systems. *European Journal of Biochemistry*, 128(2-3). <https://doi.org/10.1111/j.1432-1033.1982.tb07006.x>
- Igarashi, K., Sugawara, K., Izumi, I., Nagayama, C., & Hirose, S.** (1974). Effect of Polyamines on Polyphenylalanine Synthesis by *Escherichia coli* and Rat-Liver Ribosomes. *European Journal of Biochemistry*, 48(2). <https://doi.org/10.1111/j.1432-1033.1974.tb03790.x>
- Imai, A., Hanzawa, Y., Komura, M., Yamamoto, K. T., Komeda, Y., & Takahashi, T.** (2006). The dwarf phenotype of the *Arabidopsis* ac15 mutant is suppressed by a mutation in an upstream ORF of a bHLH gene. *Development*, 133(18). <https://doi.org/10.1242/dev.02535>
- Imai, A., Matsuyama, T., Hanzawa, Y., Akiyama, T., Tamaoki, M., Saji, H., Shirano, Y., Kato, T., Hayashi, H., Shibata, D., Tabata, S., Komeda, Y., & Takahashi, T.** (2004).

- Spermidine synthase genes are essential for survival of 35 relevant 35 is. *Plant Physiology*, 135(3). <https://doi.org/10.1104/pp.104.041699>
- Ishitsuka, S., Yamamoto, M., Miyamoto, M., Kuwashiro, Y., Imai, A., Motose, H., & Takahashi, T.** (2019). Complexity and Conservation of Thermospermine-Responsive uORFs of SAC51 Family Genes in Angiosperms. *Frontiers in Plant Science*, 10. <https://doi.org/10.3389/FPLS.2019.00564>
- Ishizaki, K., Chiyoda, S., Yamato, K. T., & Kohchi, T.** (2008). Agrobacterium-mediated transformation of the haploid liverwort *Marchantia polymorpha* L., an emerging model for plant biology. *Plant and Cell Physiology*, 49(7). <https://doi.org/10.1093/pccp/pcn085>
- Ishizaki, K., Nonomura, M., Kato, H., Yamato, K. T., & Kohchi, T.** (2012). Visualization of auxin-mediated transcriptional activation using a common auxin-responsive reporter system in the liverwort *Marchantia polymorpha*. *Journal of Plant Research*, 125(5). <https://doi.org/10.1007/s10265-012-0477-7>
- Takehi, J. I., Kuwashiro, Y., Niitsu, M., & Takahashi, T.** (2008). Thermospermine is Required for Stem Elongation in *Arabidopsis thaliana*. *Plant and Cell Physiology*, 49(9). <https://doi.org/10.1093/pccp/pcn109>
- Katayama, H., Iwamoto, K., Kariya, Y., Asakawa, T., Kan, T., Fukuda, H., & Ohashi-Ito, K.** (2015). A Negative Feedback Loop Controlling bHLH Complexes Is Involved in Vascular Cell Division and Differentiation in the Root Apical Meristem. *Current Biology*, 25(23), 3144–3150. <https://doi.org/10.1016/j.cub.2015.10.051>
- Kato, H., Ishizaki, K., Kouno, M., Shirakawa, M., Bowman, J. L., Nishihama, R., & Kohchi, T.** (2015). Auxin-Mediated Transcriptional System with a Minimal Set of Components Is Critical for Morphogenesis through the Life Cycle in *Marchantia polymorpha*. *PLoS Genetics*, 11(5). <https://doi.org/10.1371/journal.pgen.1005084>
- Kato, H., Kouno, M., Takeda, M., Suzuki, H., Ishizaki, K., Nishihama, R., & Kohchi, T.** (2017). The roles of the sole activator-type auxin response factor in pattern formation of 35 relevant 35 i *polymorpha*. *Plant and Cell Physiology*, 58(10). <https://doi.org/10.1093/pccp/pcx095>
- Keener, C. S., Gifford, E. M., & Foster, A. S.** (1990). Morphology and Evolution of Vascular Plants. *Systematic Botany*, 15(2), 348. <https://doi.org/10.2307/2419189>
- Kenrick, P.** (1994). Alternation of generations in land plants: New phylogenetic and palaeobotanical evidence. *Biological Reviews of the Cambridge Philosophical Society*, 69(3). <https://doi.org/10.1111/j.1469-185x.1994.tb01273.x>



- Kenrick, P., & Crane, P. R.** (1997). The origin and early evolution of plants on land. *Nature* 1997 389:6646, 389(6646), 33–39. <https://doi.org/10.1038/37918>
- Kenrick, P., & Strullu-Derrien, C.** (2014). The origin and early evolution of roots. *Plant Physiology*, 166(2). <https://doi.org/10.1104/pp.114.244517>
- Knott, J. M.** (2009). Biosynthesis of long-chain polyamines by crenarchaeal polyamine synthases from *Hyperthermus butylicus* and *Pyrobaculum aerophilum*. *FEBS Letters*, 583(21). <https://doi.org/10.1016/j.febslet.2009.10.014>
- Knott, J. M., Römer, P., & Sumper, M.** (2007). Putative spermine synthases from *Thalassiosira pseudonana* and *Arabidopsis thaliana* synthesize thermospermine rather than spermine. *FEBS Letters*, 581(16). <https://doi.org/10.1016/j.febslet.2007.05.074>
- Kohchi, T., Yamato, K. T., Ishizaki, K., Yamaoka, S., & Nishihama, R.** (2021). Development and Molecular Genetics of *Marchantia polymorpha*. <https://doi.org/10.1146/Annurev-Arplant-082520-094256>, 72, 677–702. <https://doi.org/10.1146/ANNUREV-ARPLANT-082520-094256>
- Lemieux, C., Otis, C., & Turmel, M.** (2007). A clade uniting the green algae *Mesostigma viride* and *Chlorokybus atmophyticus* represents the deepest branch of the Streptophyta in chloroplast genome-based phylogenies. *BMC Biology*, 5. <https://doi.org/10.1186/1741-7007-5-2>
- Lewis, L. A., & McCourt, R. M.** (2004). Green algae and the origin of land plants. In *American Journal of Botany* (Vol. 91, Issue 10). <https://doi.org/10.3732/ajb.91.10.1535>
- Ligrone, R., Carafa, A., Duckett, J. G., Renzaglia, K. S., & Ruel, K.** (2008). Immunocytochemical detection of lignin-related epitopes in cell walls in bryophytes and the charalean alga *Nitella*. *Plant Systematics and Evolution*, 270(3–4). <https://doi.org/10.1007/s00606-007-0617-z>
- Ligrone, R., Duckett, J. G., & Renzaglia, K. S.** (2000). Conducting tissues and phyletic relationships of bryophytes. *Philosophical Transactions of the Royal Society B: Biological Sciences*, 355(1398). <https://doi.org/10.1098/rstb.2000.0616>
- Marina, M., Sirera, F. V., Rambla, J. L., Gonzalez, M. E., Blázquez, M. A., Carbonell, J., Pieckenstein, F. L., & Ruiz, O. A.** (2013). Thermospermine catabolism increases *Arabidopsis thaliana* resistance to *Pseudomonas viridiflava*. *Journal of Experimental Botany*, 64(5). <https://doi.org/10.1093/jxb/ert012>
- Mayer, U., Ruiz, R. A. T., Berleth, T., Miseéra, S., & Jürgens, G.** (1991). Mutations affecting body organization in the *Arabidopsis* embryo. *Nature*, 353(6343). <https://doi.org/10.1038/353402a0>



- McConnell, J. R., Emery, J., Eshed, Y., Bao, N., Bowman, J., & Barton, M. K.** (2001). Role of PHABULOSA and PHAVOLUTA in determining radial patterning in shoots. *Nature*, 411(6838). <https://doi.org/10.1038/35079635>
- Mellor, N., Adibi, M., El-Showk, S., de Rybel, B., King, J., Mähönen, A. P., Weijers, D., Bishopp, A., & Etchells, P.** (2017). Theoretical approaches to understanding root vascular patterning: A consensus between recent models. In *Journal of Experimental Botany* (Vol. 68, Issue 1). <https://doi.org/10.1093/jxb/erw410>
- Merele, P., Ram, H., Caggiano, M. P., Ohno, C., Ott, F., Straub, D., Graeff, M., Cho, S. K., Yang, S. W., Wenkel, S., & Heisler, M. G.** (2016). Regulation of MIR165/166 by class II and class III homeodomain leucine zipper proteins establishes leaf polarity. *Proceedings of the National Academy of Sciences of the United States of America*, 113(42). <https://doi.org/10.1073/pnas.1516110113>
- Michael, A. J.** (2016). Polyamines in eukaryotes, bacteria, and archaea. In *Journal of Biological Chemistry* (Vol. 291, Issue 29). <https://doi.org/10.1074/jbc.R116.734780>
- Milhinhos, A., Bollhöner, B., Blázquez, M. A., Novák, O., Miguel, C. M., & Tuominen, H.** (2020). ACAULIS5 Is Required for Cytokinin Accumulation and Function During Secondary Growth of Populus Trees. *Frontiers in Plant Science*, 11. <https://doi.org/10.3389/fpls.2020.601858>
- Minguet, E. G., Vera-Sirera, F., Marina, A., Carbonell, J., & Blázquez, M. A.** (2008). Evolutionary diversification in polyamine biosynthesis. *Molecular Biology and Evolution*, 25(10). <https://doi.org/10.1093/molbev/msn161>
- Mukherjee, K., & Bürglin, T. R.** (2006). MEKHLA, a novel domain with similarity to PAS domains, is fused to plant homeodomain-leucine zipper III proteins. *Plant Physiology*, 140(4). <https://doi.org/10.1104/pp.105.073833>
- Muñiz, L., Minguet, E. G., Singh, S. K., Pesquet, E., Vera-Sirera, F., Moreau-Courtois, C. L., Carbonell, J., Blázquez, M. A., & Tuominen, H.** (2008). ACAULIS5 controls Arabidopsis xylem specification through the prevention of premature cell death. *Development*, 135(15), 2573–2582. <https://doi.org/10.1242/dev.019349>
- Murre, C., McCaw, P. S., & Baltimore, D.** (1989). A new DNA binding and dimerization motif in immunoglobulin enhancer binding, daughterless, MyoD, and myc proteins. *Cell*, 56(5). [https://doi.org/10.1016/0092-8674\(89\)90682-X](https://doi.org/10.1016/0092-8674(89)90682-X)
- Nishihama, R., Ishida, S., Urawa, H., Kamei, Y., & Kohchi, T.** (2016). Conditional gene expression/deletion systems for *Marchantia polymorpha* using its own heat-shock



- promoter and cre/loxP-mediated site-specific recombination. *Plant and Cell Physiology*, 57(2). <https://doi.org/10.1093/pcp/pcv102>
- Ohashi-Ito, K., Saegusa, M., Iwamoto, K., Oda, Y., Katayama, H., Kojima, M., Sakakibara, H., & Fukuda, H.** (2014). A bHLH Complex Activates Vascular Cell Division via Cytokinin Action in Root Apical Meristem. *Current Biology*, 24(17), 2053–2058. <https://doi.org/10.1016/J.CUB.2014.07.050>
- O'Malley, R. C., Huang, S. S. C., Song, L., Lewsey, M. G., Bartlett, A., Nery, J. R., Galli, M., Gallavotti, A., & Ecker, J. R.** (2016). Cistrome and Epicistrome Features Shape the Regulatory DNA Landscape. *Cell*, 165(5). <https://doi.org/10.1016/j.cell.2016.04.038>
- Otsuga, D., DeGuzman, B., Prigge, M. J., Drews, G. N., & Clark, S. E.** (2001). REVOLUTA regulates meristem initiation at lateral positions. *Plant Journal*, 25(2). <https://doi.org/10.1046/j.1365-313X.2001.00959.x>
- Palena, C. M., Tron, A. E., Bertoncini, C. W., Gonzalez, D. H., & Chan, R. L.** (2001). Positively charged residues at the N-terminal arm of the homeodomain are required for efficient DNA binding by homeodomain-leucine zipper proteins. *Journal of Molecular Biology*, 308(1). <https://doi.org/10.1006/jmbi.2001.4563>
- Petřiválský, M., Brauner, F., Luhová, L., Gagneul, D., & Šebela, M.** (2007). Aminoaldehyde dehydrogenase activity during wound healing of mechanically injured pea seedlings. *Journal of Plant Physiology*, 164(11). <https://doi.org/10.1016/j.jplph.2007.01.018>
- Pires, N., & Dolan, L.** (2010). Origin and diversification of basic-helix-loop-helix proteins in plants. *Molecular Biology and Evolution*, 27(4), 862–874. <https://doi.org/10.1093/MOLBEV/MSP288>
- Poidevin, L., Unal, D., Belda-Palazón, B., & Ferrando, A.** (2019). Polyamines as Quality Control Metabolites Operating at the Post-Transcriptional Level. *Plants*, 8(4), 109. <https://doi.org/10.3390/plants8040109>
- Ponce-Toledo, R. I., Deschamps, P., López-García, P., Zivanovic, Y., Benzerara, K., & Moreira, D.** (2017). An Early-Branching Freshwater Cyanobacterium at the Origin of Plastids. *Current Biology*, 27(3). <https://doi.org/10.1016/j.cub.2016.11.056>
- Ponting, C. P., & Aravind, L.** (1999). START: A lipid-binding domain in StAR, HD-ZIP and signalling proteins. *Trends in Biochemical Sciences*, 24(4). [https://doi.org/10.1016/S0968-0004\(99\)01362-6](https://doi.org/10.1016/S0968-0004(99)01362-6)
- Prigge, M. J., & Clark, S. E.** (2006). Evolution of the class III HD-Zip gene family in land plants. *Evolution Development*, 8(4), 350–361. <https://doi.org/10.1111/j.1525-142X.2006.00107.x>

- Prigge, M. J., Otsuga, D., Alonso, J. M., Ecker, J. R., Drews, G. N., & Clark, S. E.** (2005). Class III homeodomain-leucine zipper gene family members have overlapping, antagonistic, and distinct roles in Arabidopsis development. *Plant Cell*, 17(1). <https://doi.org/10.1105/tpc.104.026161>
- Proust, H., Honkanen, S., Jones, V. A. S., Morieri, G., Prescott, H., Kelly, S., Ishizaki, K., Kohchi, T., & Dolan, L.** (2016). RSL Class I Genes Controlled the Development of Epidermal Structures in the Common Ancestor of Land Plants. *Current Biology*, 26(1). <https://doi.org/10.1016/j.cub.2015.11.042>
- Puttick, M. N., Morris, J. L., Williams, T. A., Cox, C. J., Edwards, D., Kenrick, P., Pressel, S., Wellman, C. H., Schneider, H., Pisani, D., & Donoghue, P. C. J.** (2018). The Interrelationships of Land Plants and the Nature of the Ancestral Embryophyte. *Current Biology*, 28(5), 733-745.e2. <https://doi.org/10.1016/j.cub.2018.01.063>
- Ramachandran, P., Carlsbecker, A., Etchells, J. P., & Turner, S.** (2017). Class III HD-ZIPs govern vascular cell fate: An HD view on patterning and differentiation. In *Journal of Experimental Botany* (Vol. 68, Issue 1). <https://doi.org/10.1093/jxb/erw370>
- Reinhart, B. J., Weinstein, E. G., Rhoades, M. W., Bartel, B., & Bartel, D. P.** (2002). MicroRNAs in plants. *Genes and Development*, 16(13). <https://doi.org/10.1101/gad.1004402>
- Rensing, S. A., Lang, D., Zimmer, A. D., Terry, A., Salamov, A., Shapiro, H., Nishiyama, T., Perroud, P. F., Lindquist, E. A., Kamisugi, Y., Tanahashi, T., Sakakibara, K., Fujita, T., Oishi, K., Shin-I, T., Kuroki, Y., Toyoda, A., Suzuki, Y., Hashimoto, S. I., ... Boore, J. L.** (2008). The Physcomitrella genome reveals evolutionary insights into the conquest of land by plants. *Science*, 319(5859). <https://doi.org/10.1126/science.1150646>
- Roodbarkelari, F., & Groot, E. P.** (2017). Regulatory function of homeodomain-leucine zipper (HD-ZIP) family proteins during embryogenesis. In *New Phytologist* (Vol. 213, Issue 1). <https://doi.org/10.1111/nph.14132>
- Ruonala, R., Ko, D., & Helariutta, Y.** (2017). Genetic Networks in Plant Vascular Development. In *Annual Review of Genetics* (Vol. 51). <https://doi.org/10.1146/annurev-genet-120116-024525>
- Salvi, D., & Tavladoraki, P.** (2020). The tree of life of polyamine oxidases. *Scientific Reports*, 10(1). <https://doi.org/10.1038/s41598-020-74708-3>
- Schaefer, D. G.** (2002). A new moss genetics: Targeted mutagenesis in *Physcomitrella patens*. In *Annual Review of Plant Biology* (Vol. 53). <https://doi.org/10.1146/annurev.arplant.53.100301.135202>



- Schaefer, D., Zryd, J. P., Knight, C. D., & Cove, D. J.** (1991). Stable transformation of the moss *Physcomitrella patens*. *MGG Molecular & General Genetics*, 226(3). <https://doi.org/10.1007/BF00260654>
- Schrack, K., Nguyen, D., Karlowski, W. M., & Mayer, K. F. X.** (2004). START lipid/sterol-binding domains are amplified in plants and are predominantly associated with homeodomain transcription factors. *Genome Biology*, 5(6). <https://doi.org/10.1186/gb-2004-5-6-r41>
- Shimamura, M.** (2016). *Marchantia polymorpha*: Taxonomy, Phylogeny and Morphology of a Model System. *Plant and Cell Physiology*, 57(2), 230–256. <https://doi.org/10.1093/PCP/PCV192>
- Smetana, O., Mäkilä, R., Lyu, M., Amiryousefi, A., Sánchez Rodríguez, F., Wu, M. F., Solé-Gil, A., Leal Gavarrón, M., Siligato, R., Miyashima, S., Roszak, P., Blomster, T., Reed, J. W., Broholm, S., & Mähönen, A. P.** (2019). High levels of auxin signalling define the stem-cell organizer of the vascular cambium. *Nature*, 565(7740). <https://doi.org/10.1038/s41586-018-0837-0>
- Solly, J. E., Cunniffe, N. J., & Harrison, C. J.** (2017). Regional Growth Rate Differences Specified by Apical Notch Activities Regulate Liverwort Thallus Shape. *Current Biology*, 27(1). <https://doi.org/10.1016/j.cub.2016.10.056>
- Spicer, R., & Groover, A.** (2010). Evolution of development of vascular cambia and secondary growth. In *New Phytologist* (Vol. 186, Issue 3). <https://doi.org/10.1111/j.1469-8137.2010.03236.x>
- Stanislaus, R. C., & Maravolo, N. C.** (1994). The influence of polyamines on senescence in *Marchantia polymorpha*. *Bryologist*, 97(2). <https://doi.org/10.2307/3243753>
- Suzuki, H., Harrison, C. J., Shimamura, M., Kohchi, T., & Nishihama, R.** (2020). Positional cues regulate dorsal organ formation in the liverwort *Marchantia polymorpha*. *Journal of Plant Research*, 133(3). <https://doi.org/10.1007/s10265-020-01180-5>
- Takano, A., Kakehi, J. I., & Takahashi, T.** (2012). Thermospermine is not a minor polyamine in the plant kingdom. In *Plant and Cell Physiology* (Vol. 53, Issue 4). <https://doi.org/10.1093/pcp/pcs019>
- Talbert, P. B., Adler, H. T., Parks, D. W., & Comai, L.** (1995). The REVOLUTA gene is necessary for apical meristem development and for limiting cell divisions in the leaves and stems of *Arabidopsis thaliana*. *Development*, 121(9). <https://doi.org/10.1242/dev.121.9.2723>
- Tavladoraki, P., Cona, A., Federico, R., Tempera, G., Viceconte, N., Saccoccio, S., Battaglia, V., Toninello, A., & Agostinelli, E.** (2012). Polyamine catabolism: Target for



- antiproliferative therapies in animals and stress tolerance strategies in plants. In *Amino Acids* (Vol. 42, Issues 2–3). <https://doi.org/10.1007/s00726-011-1012-1>
- Thamm, A., Saunders, T. E., & Dolan, L.** (2020). MpFEW RHIZOIDS1 miRNA-Mediated Lateral Inhibition Controls Rhizoid Cell Patterning in *Marchantia polymorpha*. *Current Biology*, 30(10). <https://doi.org/10.1016/j.cub.2020.03.032>
- Tiburcio, A. F., Altabella, T., Bitrián, M., & Alcázar, R.** (2014). The roles of polyamines during the lifespan of plants: From development to stress. *Planta*, 240(1), 1–18. <https://doi.org/10.1007/S00425-014-2055-9/FIGURES/3>
- Toledo-Ortiz, G., Huq, E., & Quail, P. H.** (2003). The Arabidopsis Basic/Helix-Loop-Helix Transcription Factor Family[W]. *The Plant Cell*, 15(8), 1749–1770. <https://doi.org/10.1105/tpc.013839>
- Vasco, A., Smalls, T. L., Graham, S. W., Cooper, E. D., Wong, G. K. S., Stevenson, D. W., Moran, R. C., & Ambrose, B. A.** (2016). Challenging the paradigms of leaf evolution: Class III HD-Zips in ferns and lycophytes. *New Phytologist*, 212(3). <https://doi.org/10.1111/nph.14075>
- Vera-Sirera, F., De Rybel, B., Úrbez, C., Kouklas, E., Pesquera, M., Álvarez-Mahecha, J. C., Minguet, E. G., Tuominen, H., Carbonell, J., Borst, J. W., Weijers, D., & Blázquez, M. A.** (2015). A bHLH-Based Feedback Loop Restricts Vascular Cell Proliferation in Plants. *Developmental Cell*, 35(4), 432–443. <https://doi.org/10.1016/j.devcel.2015.10.022>
- Vera-Sirera, F., Minguet, E. G., Singh, S. K., Ljung, K., Tuominen, H., Blázquez, M. A., & Carbonell, J.** (2010). Role of polyamines in plant vascular development. *Plant Physiology and Biochemistry*, 48(7), 534–539. <https://doi.org/10.1016/J.PLAPHY.2010.01.011>
- Vuosku, J., Karppinen, K., Muilu-Mäkelä, R., Kusano, T., Sagor, G. H. M., Avia, K., Alakärppä, E., Kestilä, J., Suokas, M., Nickolov, K., Hamberg, L., Savolainen, O., Häggman, H., & Sarjala, T.** (2018). Scots pine aminopropyltransferases shed new light on evolution of the polyamine biosynthesis pathway in seed plants. *Annals of Botany*, 121(6). <https://doi.org/10.1093/aob/mcy012>
- Watanabe, S. I., Kusama-Eguchi, K., Kobayashi, H., & Igarashi, K.** (1991). Estimation of polyamine binding to macromolecules and ATP in bovine lymphocytes and rat liver. *Journal of Biological Chemistry*, 266(31). [https://doi.org/10.1016/s0021-9258\(18\)54780-3](https://doi.org/10.1016/s0021-9258(18)54780-3)



- Wellman, C. H., Osterloff, P. L., & Mohiuddin, U.** (2003). Fragments of the earliest land plants. *Nature*, 425(6955). <https://doi.org/10.1038/nature01884>
- Wenzel, C. L., Schuetz, M., Yu, Q., & Mattsson, J.** (2007). Dynamics of MONOPTEROS and PIN-FORMED1 expression during leaf vein pattern formation in *Arabidopsis thaliana*. *Plant Journal*, 49(3). <https://doi.org/10.1111/j.1365-313X.2006.02977.x>
- Xu, B., Ohtani, M., Yamaguchi, M., Toyooka, K., Wakazaki, M., Sato, M., Kubo, M., Nakano, Y., Sano, R., Hiwatashi, Y., Murata, T., Kurata, T., Yoneda, A., Kato, K., Hasebe, M., & Demura, T.** (2014). Contribution of NAC Transcription Factors to Plant Adaptation to Land. *Science*, 343(6178), 1505–1508. <https://doi.org/10.1126/science.1248417>
- Xue, B., Zhang, A., & Jiang, M.** (2009). Involvement of polyamine oxidase in abscisic acid-induced cytosolic antioxidant defense in leaves of maize. *Journal of Integrative Plant Biology*, 51(3). <https://doi.org/10.1111/j.1744-7909.2008.00766.x>
- Yip, H. K., Floyd, S. K., Sakakibara, K., & Bowman, J. L.** (2016). Class III HD-Zip activity coordinates leaf development in *Physcomitrella patens*. *Developmental Biology*, 419(1). <https://doi.org/10.1016/j.ydbio.2016.01.012>
- Yoda, H., Yamaguchi, Y., & Sano, H.** (2003). Induction of hypersensitive cell death by hydrogen peroxide produced through polyamine degradation in tobacco plants. *Plant Physiology*, 132(4). <https://doi.org/10.1104/pp.103.024737>
- Yoon, H. S., Hackett, J. D., Ciniglia, C., Pinto, G., & Bhattacharya, D.** (2004). A Molecular Timeline for the Origin of Photosynthetic Eukaryotes. *Molecular Biology and Evolution*, 21(5), 809–818. <https://doi.org/10.1093/MOLBEV/MSH075>
- Zumajo-Cardona, C., Little, D. P., Stevenson, D., & Ambrose, B. A.** (2021). Expression analyses in *Ginkgo biloba* provide new insights into the evolution and development of the seed. *Scientific Reports*, 11(1), 21995. <https://doi.org/10.1038/s41598-021-01483-0>



OBJECTIVES



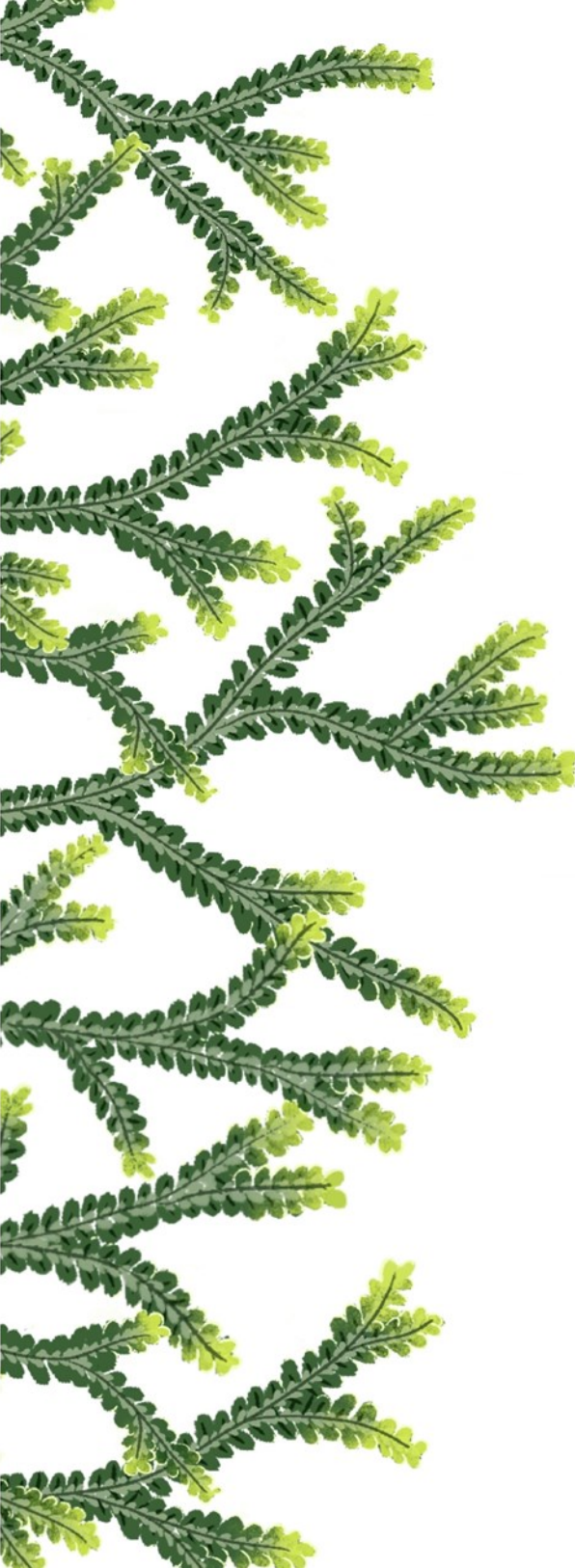


As shown above, vascular cell divisions are promoted in *A. thaliana* by high CK levels through the TMO5-LHW heterodimer. Excessive cell proliferation is prevented through a regulatory module by which auxin and the C3HDZ TF AtHB8, ensure the ACL5/Tspm-dependent translation of the SACL transcriptional regulators, which inhibit the activity of TMO5-LHW. The three elements of this regulatory module are present in all (vascular or non-vascular) land plants. But despite the importance of this regulatory circuit, several aspects are still unsolved: when did this circuit originate in evolution? Does this circuit operate in non-vascular plants? Is this the only mechanism to prevent overproliferation of vascular cells? Our working hypothesis is that the C3HDZ-ACL5/Tspm-SACL module was assembled in the last tracheophyte common ancestor, while the three elements perform different roles in bryophytes. To infer the evolutionary trajectory of this module in land plants and the events that led to the regulation of vascular development we have focused on three objectives:

1. **To reconstruct the evolutionary history of C3HDZ, ACL5 and SACL proteins and the genetic regulation underlying their conformation as a module.** This goal contemplates a thorough phylogenetic analysis of these proteins combined with the exploration of CRE responsible for their putative regulation, to infer the conformational state of the module in extant land plants.
2. **To analyze the function of C3HDZ, ACL5 and SACL orthologs in the bryophyte *M. polymorpha*.** By exploring the role of these genes and their putative connections as a module in a non-vascular plant, we expect to generate insight of their implication in biological processes other than vascular development in divergent land plant lineages.
3. **To establish a timeline for the recruitment of C3HDZ, ACL5, and SACL to vascular tissues.** As we explore the association of these genes with vascular tissues in representative species of extant tracheophyte lineages, we can infer the origin of the module within tracheophytes.

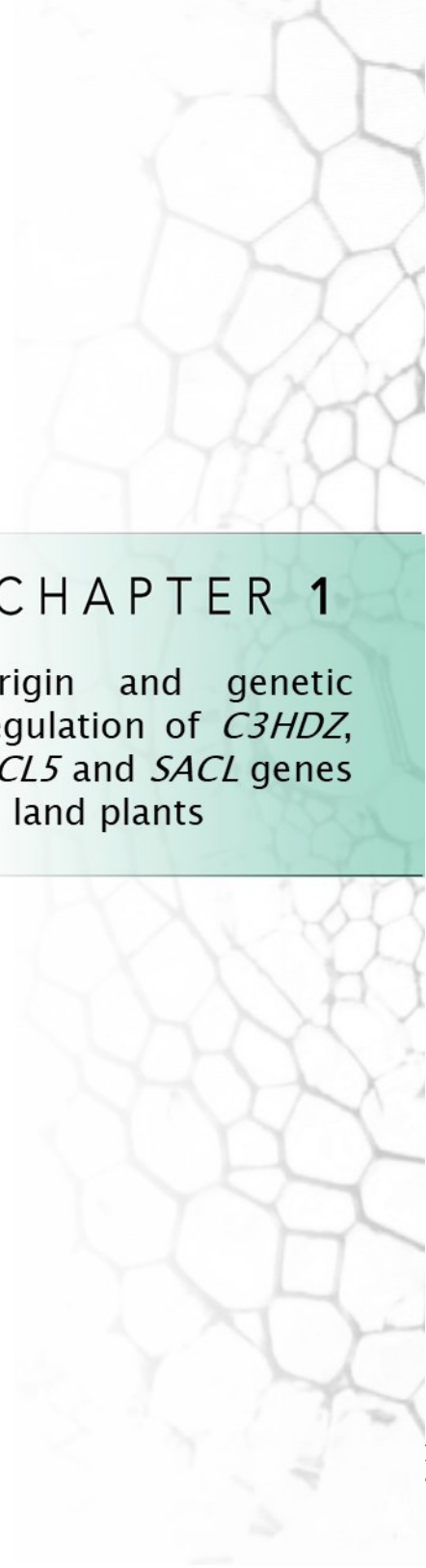






CHAPTER 1

Origin and genetic regulation of *C3HDZ*, *ACL5* and *SACL* genes in land plants



It is widely accepted that C3HDZ, ACL5 and SACL are present in land plants (Catarino et al., 2016; Floyd et al., 2006; Minguet et al., 2008; Prigge & Clark, 2006; Takano et al., 2012). However, previous studies are limited due to (i) the low number of available sequenced bryophyte and tracheophyte species and (ii) the biased use of representative species, especially for the bryophyte lineages and ACL5 and SACL proteins. In this chapter, thanks to projects like Earth BioGenome or OneKP (Exposito-Alonso et al., 2020; Leebens-Mack et al., 2019), we will perform a thorough phylogenetic analysis of C3HDZ, ACL5 and SACL proteins in an unbiased number of land plant species, which will allow to fill missing land plant lineages and update the distribution of C3HDZ, ACL5, and SACL orthologs in extant land plants.

We will also confirm that the biochemical properties of ACL5 in extant land plants are conserved, by testing ACL5 enzymatic activity and the expression of *ACL5* genes coupled with Tspm quantifications in several land plant tissues. Lastly, we will analyze the conservation of the CRE required for molecular regulation of C3HDZ, ACL5 and SACL as a putative module, such as C3HDZ binding sites (bs) in ACL5 promoters, and the Tspm-sensitive uORF in *SACL* transcripts.

RESULTS AND DISCUSSION

C3HDZ is distributed across all land plant lineages

In order to retrieve the putative *C3HDZ* sequences from the widest range of plant species, we screened by Translated Nucleotide Basic Local Alignment Search tool (TBLASTN) the Phytozome, OneKP and NCBI databases using as a query the aminoacidic sequence of the five *C3HDZ* proteins encoded in the *A. thaliana* genome (AtHB8, AtCNA, AtREV, AtPHB, and AtPHV). Given that the HD is a distinctive feature common to all classes of HDZ, we constructed an initial tree including representative class one to class four HDZ sequences from *A. thaliana* and *S. lepidophylla* to unambiguously identify the sequences solely belonging to the *C3HDZ* clade. Sequences with a partial or missing HD were removed from the final alignment to ensure a better-supported phylogenetic tree. This final alignment included 649 *C3HDZ* sequences covering every major plant lineage, which was used to construct a maximum likelihood (ML) phylogenetic tree (**Figure 1A**). In agreement with the idea that *C3HDZ* originated in the last streptophyte common ancestor (Catarino et al., 2016; Floyd & Bowman, 2006; Prigge & Clark, 2006b; Romani et al., 2018), we found *C3HDZ* sequences only in Streptophyta species.

Several monophyletic groups could be observed in the *C3HDZ* tree (**Figure 1A**). Charophytes were used as an outgroup (see Glossary) and formed a monophyletic lineage, and the rest of the sequences were classified into two clear monophyletic groups. The first group consisted of sequences of lycophytes, hornworts, liverworts, and mosses; the second monophyletic group comprised solely sequences from spermatophytes (angiosperms and gymnosperms). Fern sequences, however, were contained in a paraphyletic group sister to spermatophyte sequences. More than 99,5% of the *C3HDZ* sequences were coherent with the phylogenetic relationships of plant lineages, with the only exceptions of three gymnosperm *C3HDZ* sequences (*Ginkgo biloba C3HDZ.4*, *C3HDZ.5*, and *Saxegothaea conspicua C3HDZ.1*) that grouped unequivocally within the fern lineage. Interestingly, this is the first time that the monophyly of spermatophyte *C3HDZ* sequences has been evidenced.



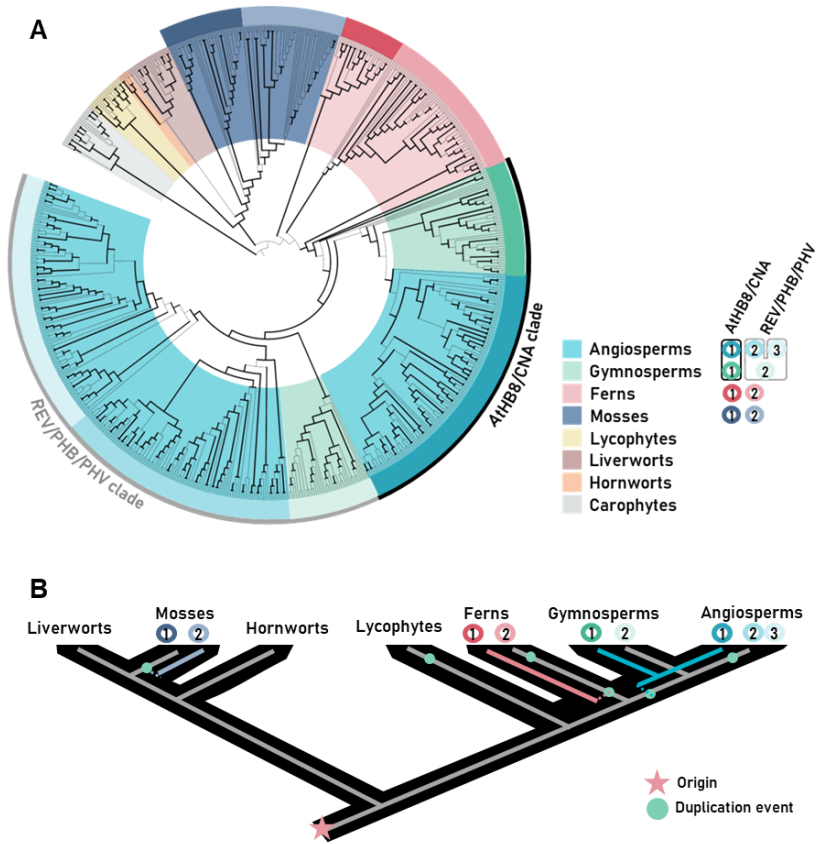


Figure 1. Phylogenetic analysis and inferred history of C3HDZ in Streptophyta. A. C3HDZ ML phylogenetic tree. Branch support values are based on SH-like aLRT, and values over 0.8 are marked with wider black branches. Charophyta sequences are used as the outgroup. Wider background-colored groups mark the different plant lineages, while color outer circles are used to differentiate C3HDZ phylogenetic groups inside each lineage. Black and grey outer circles represent the AtHB8/CNA and the REV/PHB/PHV clades, respectively. **B.** Schematic depiction of the inferred history of C3HDZ and the six major duplication events. Phylogenetic relationships are represented in grey line; duplications that led to gene diversification are marked in light blue (for mosses), pink (for ferns), and cyan (for angiosperms and gymnosperms). Plant phylogenetic relationships are based on the work of Harris et al. (2020). Origin of C3HDZ sequences is marked with a pink star, while major duplication events are marked with turquoise blue circles. *AtHB8*, *ARABIDOPSIS THALIANA HOMEBOX8*, *CNA*: *CORONA*; *REV*: *REVOLUTA*; *PHB*: *PHABULOSA*; *PHV*: *PHAVOLUTA*.



Previous studies were unable to fully demonstrate the separation between fern and spermatophyte sequences (Floyd et al., 2006; Prigge & Clark, 2006; Vasco et al., 2016). Comparing our phylogenetic analysis with these previous studies, this is probably a consequence of their preferential use of *G. biloba* as a gymnosperm representative, which led to clade misinterpretations due to their resemblance with fern sequences. Similarly, the low number of available non-vascular or lycophyte genomes also reflected a biased interpretation of lycophyte and bryophyte clades, which were considered as paraphyletic to the rest of the spermatophytes (Floyd et al., 2006; Prigge & Clark, 2006a; Vasco et al., 2016). In this regard, the clustering of lycophyte and bryophyte sequences in a monophyletic group underlines the evolutionary distance of the lycophytes to other vascular lineages, which are thought to be the first to diverge (Harris et al., 2020, 2022). Hence, a more balanced phylogenetic analysis using a representative number of sequences from each plant clade has allowed to update the evolution and origins of the C3HDZ sequences in the plant lineage and within each plant clade, which will provide a base for future functional interpretation of C3HDZ roles in land plants.

Then, we focused on clade specific duplications to infer the evolutionary history of C3HDZ in land plants. Generally, non-vascular lineages like charophytes, hornworts and liverworts harbor only one copy of *C3HDZ*, which we confirmed in the fully sequenced *Klebsormidium nitens* (a charophyte), *Marchantia polymorpha* (a liverwort), *Anthoceros agrestis* and *Anthoceros punctatus* (hornworts). Mosses, however, have undergone a genetic duplication that led to the diversification of two differentiated C3HDZ clades: Mosses 1 and 2. These results are consistent with previous studies that examined C3HDZ evolution in non-vascular lineages and found no other gene duplications except in the moss lineage (Catarino et al., 2016; Floyd & Bowman, 2006; Prigge & Clark, 2006b). Given that most of the examined moss species had – at least – one C3HDZ copy in each of the two moss clades, the gene duplication can be inferred in the common ancestor of mosses (**Figure 1B**).

This analysis also pointed at multiple duplications inside the tracheophyte lineage. Most lycophyte species carry two C3HDZ paralogs, although they do not form two phylogenetic clades, suggesting that the lycophyte *C3HDZ* genes evolution



occurred in parallel to the species diversification. Fern sequences are divided into Ferns 1 and 2, both with a monophyletic origin. Supporting our observations, *Ceratopteris richardii*, a fully sequenced fern, has three C3HDZ paralogs (CriC3HDZ.1 to 3) that are distributed between Ferns 1 and 2. This is an evidence of an internal duplication event in the fern lineage, which is an idea also suggested by other authors (Vasco et al., 2016). Spermatophyte C3HDZ, in turn, are distributed between the AtHB8/CNA clade and the REV/PHB/PHV clade, which suggests a gene duplication at the common ancestor of the spermatophytes (**Figure 1B**). However, angiosperms harbor one to four paralogs, pointing to species-specific gene loss and one or various internal duplications giving rise to the AtHB8, CNA, REV, PHB, and PHV independent families mostly in eudicots (**Figure 1B**). *Ginkgo biloba*, in contrast, contains five C3HDZ paralogs that were also identified in previous studies and suggests an additional internal duplication inside the Ginkgoaceae (Floyd et al., 2014; Floyd & Bowman, 2006; Prigge & Clark, 2006b).

In summary, we revisited the origin of C3HDZ in land plants, which was set to the common ancestor of streptophytes (Catarino et al., 2016; Floyd & Bowman, 2006; Prigge & Clark, 2006b; Romani et al., 2018). We also provided an updated evolutionary history of these TF in land plants. We have inferred six gene duplication events that correlate well with reported whole genome duplications (WGD) in land plants (Jiao et al., 2011; Li et al., 2015; Wood et al., 2009): (i) in the common ancestor of mosses; (ii) in the common ancestor of lycophytes; (iii) in the common ancestor of ferns followed by (iv) additional duplication(s) inside the fern lineage; (v) in the common ancestor of the spermatophytes, and (vi) internal duplication(s) inside the angiosperm lineage, which gave rise to the AtHB8, CNA, REV, PHB, and PHV families (**Figure 1B**).

ACL5 are present in all Archaeplastida

Polyamine biosynthesis enzymes display high degree of similarity (Hashimoto et al., 1998; Panicot et al., 2002; Teuber et al., 2007). Therefore, to guarantee accurate identification of putative *ACL5* orthologs, we screened the Phytozome and OneKP databases using as baits the Arabidopsis *ACL5* sequence, and



also the sequences of the two *Arabidopsis* genes encoding SPDS, and the single gene for SPMS (see Materials for details). We obtained 549 sequences covering every major plant lineage and included members of representative bacteria, archaea, and other non-plant eukaryotic groups, which were aligned and used for the construction of a phylogenetic tree (**Figure 2A**). This is the most extensive phylogenetic study of plant polyamine aminopropyl transferases done to date, and it not only confirms some of the previous evolutionary models (Hashimoto et al., 1998; Minguet et al., 2008; Panicot et al., 2002; Teuber et al., 2007) but also provides new details on certain key events.

First, our analysis expands the presence of *ACL5* homologs and *SPDS* genes to all plant lineages not previously studied, like charophytes and chlorophytes. Second, the exclusive origin of *SPMS* genes in angiosperms, previously proposed based only on a few sequences (Minguet et al., 2008), is now set in the common ancestor of all spermatophytes with more sequences from gymnosperms and their absence in multiple genomes of other land plants. And third, we find indications for a possible transfer of an additional SPDS of Holomycota origin to Setophyta (see Glossary), based on the presence of extra copies in the genomes of the bryophyte *Sphagnum* and of several liverworts that unequivocally cluster with some sequences of that class (**Supplementary File S1**).

Regarding TSPMS sequences, our more extensive research still identified *ACL5* orthologs only in plants, red algae, diatoms, archaea and bacteria, as proposed in previous analyses (Minguet et al., 2008; Takano et al., 2012). The new data are compatible with the proposed model that TSPMS activity in Archaeplastida has a prokaryotic origin, while the common root with the Archaea *Sulfolobus* and *Pyrobaculum*, of two additional copies of *ACL5* orthologs in *Thalassiosira pseudonana* suggests a possible second event of horizontal gene transfer to Chromista (see Glossary) (**Figure 2B**). It has been proposed that TSPMS had appeared in plants by endosymbiosis of a cyanobacterium (Minguet et al., 2008). Our data are compatible with three alternative hypotheses in this respect (**Figure 3**). The most parsimonious one is that TSPMS was already present before Eubacteria and Archaea and was lost in the major eukaryotic branch (**Figure 3C**). A second loss would have occurred



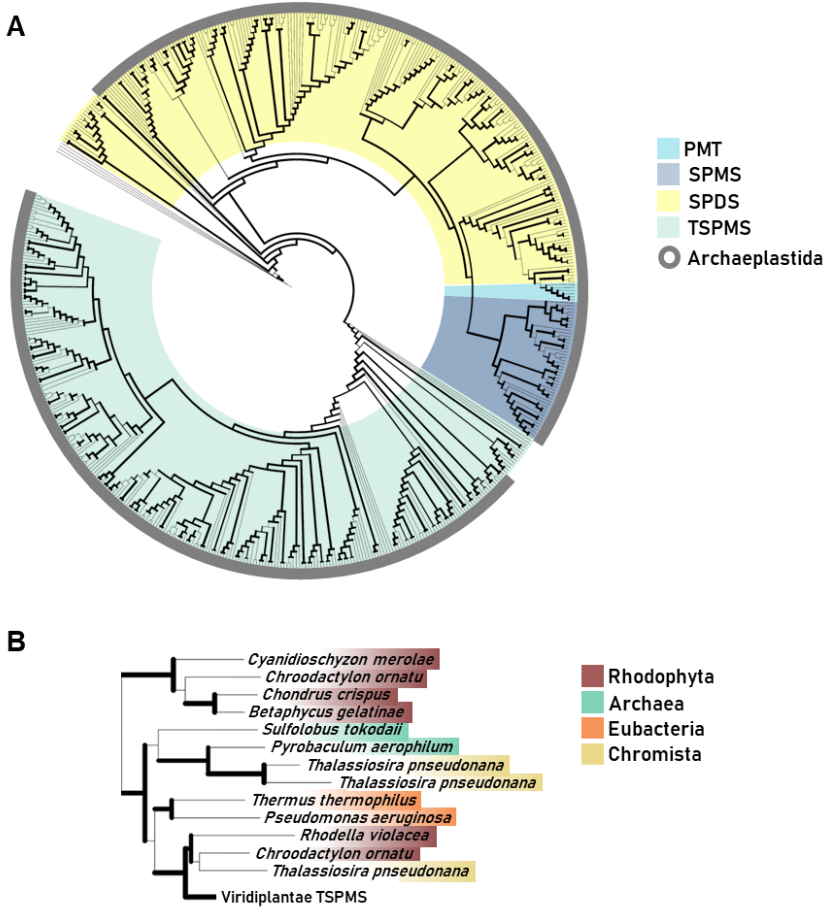


Figure 2. Phylogenetic analysis and inferred history of polyamine aminopropyl transferases with emphasis on Archaeplastida lineages. **A.** Polyamine aminopropyl transferases ML phylogenetic tree. Branch support values are based on SH-like aLRT, and values over 0.75 are marked with wider black branches. Animal SPDS sequences are used as the outgroup (*Homo sapiens*, *Danio rerio*). Wider background-colored groups mark the different clades based on polyamine synthase activities, while dark grey outer circles are used to differentiate Archaeplastida sequences. **B.** Rhodophyta (marked in brown), Archaea (turquoise), Eubacteria (orange) and Chromista sequences (yellow) at the base of the TSPMS clade. Values over 0.75 of bootstrap are marked with thicker black branches. Viridiplantae TSPMS are collapsed to ease visualization. PMT, Putrescine methyl transferase; SPMS, Spermine synthase; SPDS, Spermidine synthase; TSPMS, Thermospermine synthase.



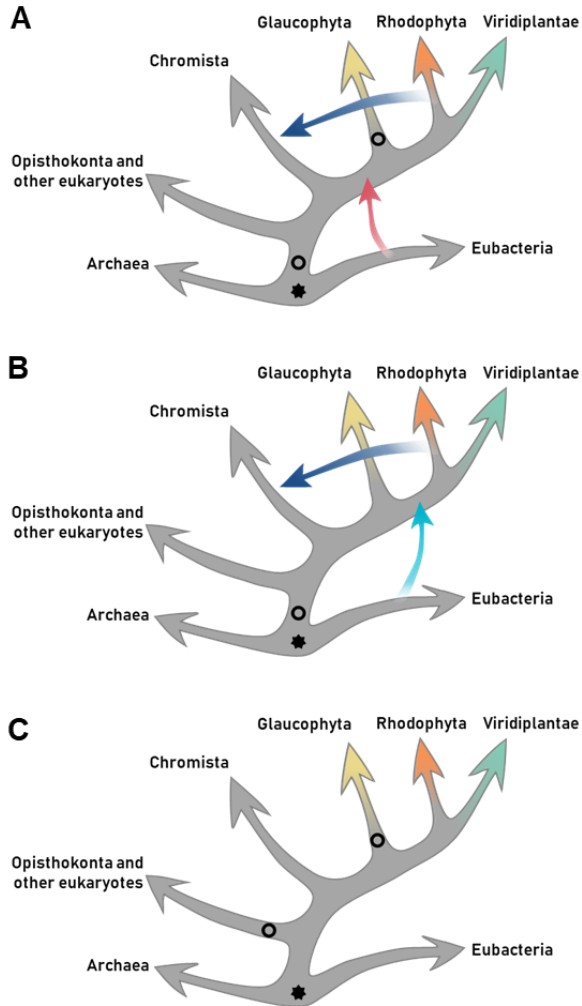


Figure 3. Alternative models for TSPMS activity origin and evolution in plants. The three models are ordered by increasing parsimony. **A**, the ancestor of TSPMS activity in the Last Universal Common Ancestor (LUCA) (possibly with a different activity) is lost in LECA; then it is acquired by Archaeplastida via HGT and lost again in Glaucophyta. Chromista acquire it through secondary endosymbiosis. **B**, Like the previous one, but Archaeplastida acquire the *ACL5* ortholog after divergence of Glaucophyta. **C**, the ancestor of TSPMS activity in LUCA is lost early in major eukaryotic clades, after the divergence of the green lineage, followed by an additional loss in Glaucophyta. Stars represent genetic origin, while hollow circles represent genetic loss.



during the divergence of Glaucophyta, explaining the absence in such branch and the presence in the Chromista, Rhodophyta and Viridiplantae branches. A less parsimonious, but plausible possibility is that TSPMS was lost in the last eukaryotic common ancestor (LECA) and that it then was transferred either from Eubacteria or from Archaea (i) to Archaeplastida after Glaucophyta had diverged and (ii) to Chromista (**Figure 3B**). A third, less parsimonious hypothesis would postulate that TSPMS was lost in LECA and transferred either from Eubacteria or from Archaea to the early lineage of Archaeplastida and to Chromista (**Figure 3A**). TSPMS would have been lost again in Glaucophyta. However, phylogenetic positioning of TSPMS points to the horizontal transfer of TSPMS genes from Rhodophyta to diatoms (and possibly other algal groups originated during secondary chloroplast acquisition), thus excluding this latter hypothesis, which is also based in a very low sampling among Chromista representatives. Given that it is almost practically impossible to differentiate between the two remaining models, the hypothesis that contemplates only one loss and two reported horizontal transfers seems the most likely one (**Figure 3B**).

To have a better insight on the diversification of ACL5 in plants, we constructed a phylogenetic tree of TSPMS sequences from Archaeplastida (**Figure 4A**). In general, the sequences grouped according to the phylogenetic relationships between plant lineages and were distributed into four monophyletic groups. The most divergent group belonged to Rhodophyta ACL5 and was used as an outgroup for the rest of Archaeplastida lineages. Chlorophytes conformed the second monophyletic group. The third group was formed by non-vascular species (charophytes, mosses, liverworts, and hornworts) and the vascular lineage of lycophytes, which appeared paraphyletic to the rest of the bryophytes. Lastly, the fourth group contained the sequences for the vascular lineages of ferns and spermatophytes.

Characterization of the intra-clade specific duplications allowed to infer the evolutionary history of ACL5 in land plants. This analysis revealed that algal species, as well as hornworts and liverworts, harbor only one copy of ACL5; this was further confirmed in the fully sequenced genomes of *Volvox carteri* and *Chlamydomonas*

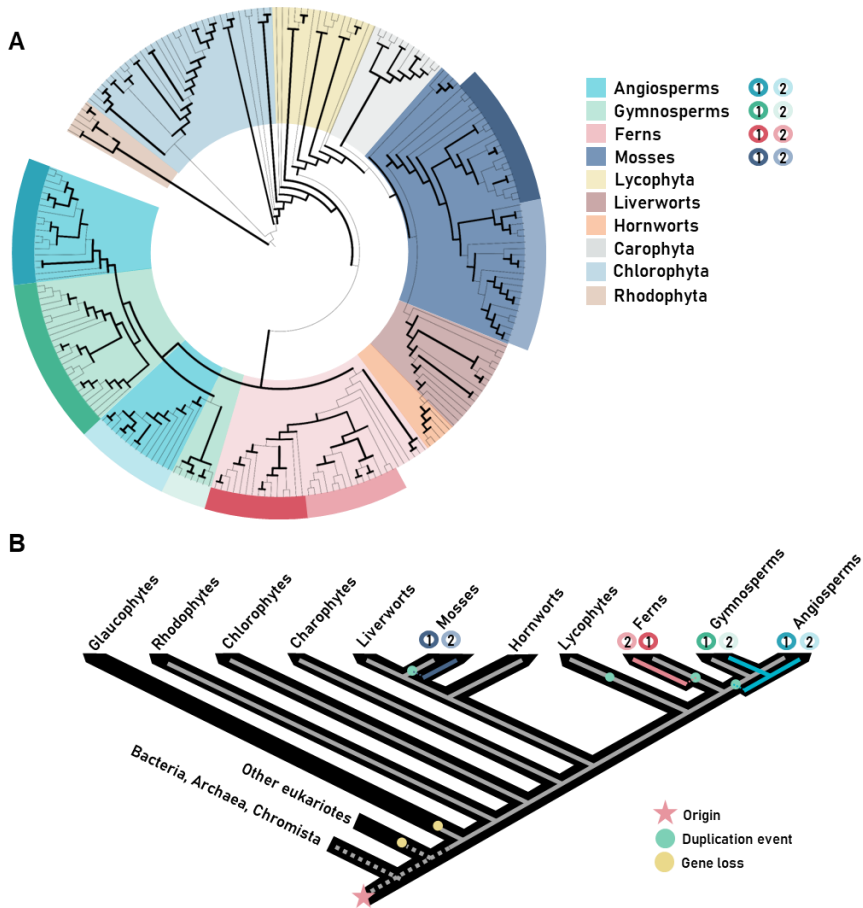


Figure 4. Phylogenetic analysis and inferred history of *ACL5* in Archaeplastida. A. *ACL5* ML phylogenetic tree. Branch support values are based on SH-like aLRT, and values over 0.75 are marked with wider black branches. Rhodophyta sequences are used as the outgroup. Wider background-colored groups mark the different plant lineages, while color outer circles are used to differentiate *ACL5* monophyletic groups inside each lineage. **B.** Schematic depiction of the inferred history of *ACL5* and the 5 major duplication events and gene losses with especial emphasis on Archaeplastida. Phylogenetic relationships are represented in grey line. Plant phylogenetic relationships are based on the work of Harris et al. (2020) Origin of *ACL5* sequences is marked with a pink star, major duplication events are marked with turquoise blue circles and gene loss events are marked with yellow circles.



reinhardtii (chlorophytes), *Klebsormidium nitens* (a charophyte), *Anthoceros agrestis* and *Anthoceros punctatus* (hornworts) and *Marchantia polymorpha* (a liverwort). Mosses were the only non-vascular lineage that underwent gene duplication, with two phylogenetic clades: Mosses 1 and 2. Among the moss sequenced genomes, *Physcomitrium patens*, inside Bryopsida, contains three ACL5 orthologs that belong to Mosses 1 (PpaACL5.2 and 3) and to Mosses 2 (PpaACL5.1); and *Sphagnum fallax*, from the Sphagnaceae family, harbors one copy of ACL5 for each moss phylogenetic clades. Together, this indicates an early ACL5 duplication within the moss lineage (**Figure 4B**).

Tracheophyte lineages generally harbor two ACL5 copies, although only fern, gymnosperm and angiosperm duplicates are classified into two phylogenetic clades (**Figure 4A**). In this regard, fern ACL5 sequences are distributed into Ferns 1 and 2, and most fern families harbor one ACL5 in each phylogenetic group, pointing to an early duplication in the fern common ancestor (**Figure 4B**). In contrast with the rest of the fern species, the recently sequenced fern *Ceratopteris richardii* only contains an ACL5 ortholog, suggesting a possible species-specific gene loss. Spermatophyte sequences, in turn, belonged to two monophyletic groups containing both angiosperm and gymnosperm sequences (**Figure 4A**), that indicates a duplication of ACL5 at the spermatophyte common ancestor (**Figure 4B**). There is evidence of multiple family-specific duplications or gene losses in some families of sequenced angiosperms, like *A. thaliana* with only one ACL5 copy, or *Medicago truncatula* with three ACL5 copies. Most gymnosperm species, in contrast, have lost one of the ACL5 copies, except for *Ginkgo biloba*, the sequenced *Picea abies*, and *Callitris macleyana*, that have two ACL5 orthologs distributed into the two spermatophyte monophyletic groups.

Taken together, these data suggest four independent events of duplication that led to ACL5 diversification in land plants (**Figure 4B**): (i) at the common ancestor of mosses; (ii) at the common ancestor of lycophytes, (iii) at the common ancestor of ferns; and (iv) at the common ancestor of spermatophytes. Interestingly, the similar ACL5 and C3HDZ distribution in land plants suggest a possible parallel evolution of both genes in land plants, although this could be only due to a deep correlation with



previously documented WGD in plants (Jiao et al., 2011; Li et al., 2015; Wood et al., 2009).

Tspm is synthesized across all plant lineages

Our phylogenetic analyses identified at least one putative *ACL5* ortholog in all studied non-vascular plant species (**Figure 4A**). Since the only confirmed function for Tspm in plants is the regulation of xylem maturation dynamics (which, by definition, does not occur in non-vascular plants), we wondered whether the identified sequences encode enzymes displaying actual TSPMS activity. Therefore, we expressed the *ACL5* homologs of representative plant lineages in yeast, an organism that can synthesize all polyamines but is unable to produce Tspm. Among the non-vascular plants, we tested the *ACL5* homologs of a chlorophyte (*Chlamydomonas reinhardtii*), a liverwort (*Marchantia polymorpha*) and a moss (*Physcomitrella patens*). As representative vascular plants we chose one lycophyte (*Selaginella lepidophylla*), and one gymnosperm (*Picea abies*), with the angiosperm *Arabidopsis thaliana* as a control (see Materials for details). An HPLC analysis showed the presence of Put, Spd and Spm, but not Tspm, in the extracts of a wild-type yeast strain transformed with an empty plasmid (**Figure 5A**). In contrast, all the tested *ACL5* homologs allowed the production of Tspm in yeast (**Figure 5 B-G**) demonstrating that these genes encode enzymes with TSPMS activity. This is in accordance with the previously reported partial complementation of the *Arabidopsis acl5* mutant by one of the moss Ppa*ACL5* orthologs (Takahashi & Kakehi, 2010). The observed differences in Tspm production between the different *ACL5* genes suggest either species-specific variation in TSPMS activity kinetic parameters or in the variable capacity of yeast to express the different heterologous genes.

To check whether the presence of *ACL5* orthologs with TSPMS activity correlated with the ability of these species to synthesize Tspm *in vivo*, we examined the polyamine levels in samples of these plants grown in standard conditions (see Materials for details). As expected, all vascular and non-vascular species accumulated Put and Spd to different levels (**Table 1**). For instance, Put levels in the chlorophyte *C. reinhardtii* were between one and three orders of magnitude higher than in the



examined land plants, while Spd levels were generally higher in the land plants than in *C. reinhardtii*, except for *P. patens*. On the other hand, Spm was detectable in *A. thaliana* and *P. abies*, in agreement with previous reports for the occurrence of this

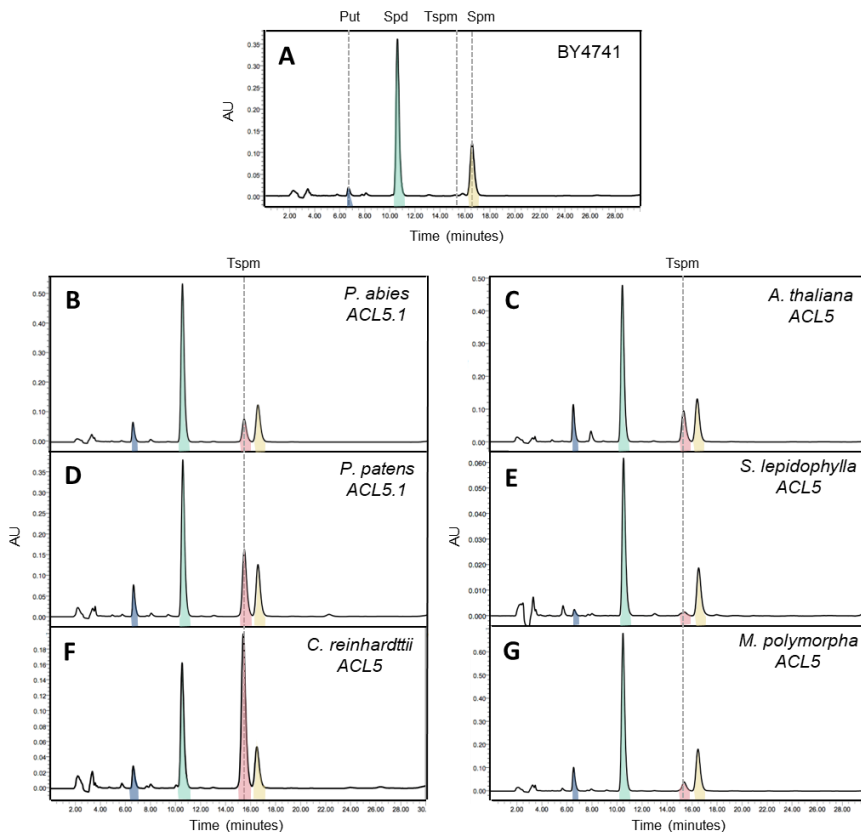


Figure 5. Polyamine quantifications from yeast extracts. TSPMS activity was measured in yeast strain BY4741 that was transformed with an empty vector (**A**) or *ACL5* homologues from different plant species: *Picea abies* (**B**), *Arabidopsis thaliana* (**C**), *Physcomitrium patens* (**D**), *Selaginella lepidophylla* (**E**), *Chlamydomonas reinhardtii* (**F**), *Marchantia polymorpha* (**G**). Put, Putrescine; Spd, Spermidine; Tspm, Thermospermine; Spm, Spermine. AU, absorbance units.

tetraamine in seed plants (Gonzalez et al., 2011; Vuosku et al., 2018) and the presence of SPMS orthologs in this clade (**Figure 2A**). The detection of Spm in *S. lepidophylla* despite the absence of SPMS orthologs in lycophytes indicates that this tetra-amine might be synthesized by a less strict SPDS, as already suggested for *P. sylvestris* (Vuosku et al., 2018). With respect to Tspm, all the species tested were able to synthesize this polyamine at different levels, which varied between 1.13 nM/g (fresh weight) in *C. reinhardtii* and 154 nM/g in *P. abies*.

nM/g FW, nanomoles per gram of fresh weight; n.d., not detected; *A. thaliana*, *Arabidopsis thaliana*; *P. abies*, *Picea abies*; *S. lepidophylla*, *Selaginella lepidophylla*; *P. patens*, *Physcomitrium patens*; *M. polymorpha*, *Marchantia polymorpha*; *C. reinhardtii*, *Chlamydomonas reinhardtii*.

	Putrescine (nM/g FW ± SE)	Spermidine (nM/g FW ± SE)	Spermine (nM/g FW ± SE)	Thermospermine (nM/g FW ± SE)
<i>A. thaliana</i>	10.76 ± 3.19	52.34 ± 15.48	2.14 ± 0.35	4.69 ± 1.77
<i>P. abies</i>	37.74 ± 5.31	131.09 ± 20.99	42.84 ± 12.39	154.06 ± 19.52
<i>S. lepidophylla</i>	77.59 ± 12.17	123.59 ± 24.80	1.21 ± 0.27	17.27 ± 3.75
<i>P. patens</i>	2.58 ± 0.54	19.87 ± 2.42	n.d.	10.7 ± 3.01
<i>M. polymorpha</i>	15.26 ± 5.06	53.88 ± 13.32	n.d.	1.37 ± 0.19
<i>C. reinhardtii</i>	1032.51 ± 16.62	27.44 ± 1.18	n.d.	1.13 ± 0.15

Table 1. Summary of polyamine quantifications in plant tissues from key species.

It is worth noting that, while previous reports show that Tspm tends to accumulate less than Spm in *Arabidopsis* (Rambla et al., 2010), in the species, tissues and conditions analyzed here, the two polyamines showed comparable levels. Although this result does not demonstrate that the *ACL5* orthologs identified in all the selected species are responsible for the Tspm synthesis shown here, this possibility is further supported by the observation that these genes are expressed in the same growth conditions as the ones used for Tspm quantification (**Figure 6**).

In sum, we have confirmed that Tspm is found in all plant lineages examined, which correlates with TSPMS enzymatic activity and *ACL5* expression *in vivo*. Given that *ACL5* function is deeply linked with vascular development, our observations



clearly argue in favor of possible functions other than in xylem development in non-vascular plants, which will be examined in *M. polymorpha* in **Chapter 2**.

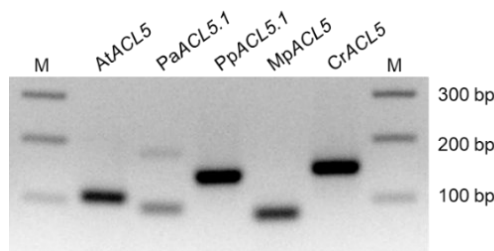


Figure 6. Detection of *ACL5* transcripts in cDNA from *A. thaliana*, *P. abies*, *P. patens*, *M. polymorpha* and *C. reinhardtii* with semi quantitative PCR. The tissues used for RNA extraction were the same used for HPLC quantification. bp, base pairs; M, loading marker.

Land plant *ACL5* promoters contain conserved CRE for C3HDZ binding

To gain further evidence of the conservation in the tracheophyte lineage of the molecular connection between *C3HDZ* and *ACL5* observed in angiosperms (Baima et al., 2014), we analyzed the sequence of *ACL5* promoters amongst the land plant lineages. We retrieved the *ACL5* promoters from four mosses (*Ceratodon purpureus*, *Physcomitrium patens*, *Sphagnum magellanicum* and *Sphagnum fallax*), two lycophytes (*Selaginella moellendorffii* and *Diphasiastrum complanatum*), one fern (*Ceratopteris richardii*), and three gymnosperms (*Pinus taeda*, *Picea abies* and *Thuja plicata*) from the Phytozome (Goodstein et al., 2012) and the Gymnosperm Plaza (Proost et al., 2015) databases. We then scanned them for the presence of putative C3HDZ bs with the Morpheus score tool (Minguet et al., 2015) using the AtCNA binding matrix as the standard C3HDZ *cis* element (see Materials for details). All analyzed promoters contained C3HDZ bs (**Figure 7**), suggesting that the C3HDZ and *ACL5* connection might be conserved in land plants. [Further experimental evidence supporting the relevance of this connection is shown in the upcoming chapters: in **Chapter 2**, a functional description of C3HDZ and *ACL5* is provided for the non-vascular plant *M. polymorpha*; and in **Chapter 3** we provide information supporting the co-expression of *C3HDZ* and *ACL5* in a few tracheophyte species].



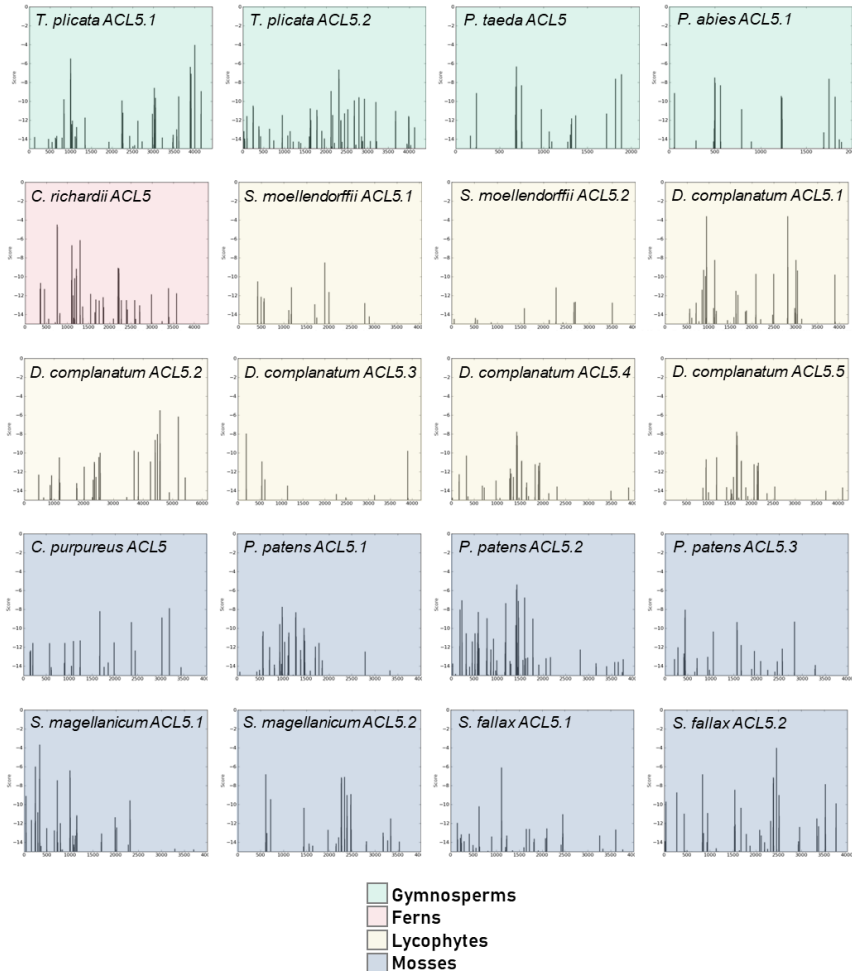


Figure 7. ACL5 promoters from different streptophyte lineages have conserved C3HDZ bs. *In silico* binding site analysis using the binding matrix of AtCNA in promoters of *Thuja plicata* ACL5.1 and ACL5.2, *Pinus taeda* ACL5 and *Picea abies* ACL5.1, as gymnosperms; *Ceratopteris richardii* ACL5 as a fern, *Selaginella moellendorffii* ACL5.1 and ACL5.2 and *Diphasiastrum complanatum* ACL5.1 to ACL5.5 as lycophytes. As bryophytes, *Ceratodon purpureus* ACL5, *Physcomitrium patens* ACL5.1 to ACL5.3, *Sphagnum magellanicum* ACL5.1 and ACL5.2, and *Sphagnum fallax* ACL5.1 and ACL5.2. Peaks correspond to a high binding score after MORPHEUS scan. All scanned promoters are 4Kb long except for *Picea abies* and *Pinus taeda*, that are 2Kb long.



SACL is present in embryophytes and was lost in mosses

bHLH TF have a highly conserved bHLH domain, usually 60 amino acids long (Ferré-D'Amaré et al., 1993). Small changes in the bHLH sequence explain most of the subfamily classification (Carretero-Paulet et al., 2010; Catarino et al., 2016). In consequence, performing a TBLASTN using the bHLH domains of *A. thaliana* SACLs (SAC51 and SACL1-3) as baits retrieved sequences from all subfamilies of bHLH in the target phylum or class. However, a TBLASTN using the entire aminoacidic sequence of *A. thaliana* SACLs as bait resulted in low E-value matches, which is probably due to a phylum- or class-specific divergent domains in SACL proteins. To bypass this limitation, we used the bHLH domain of *A. thaliana* SAC51 as bait in the Phytozome database to retrieve the putative bHLH genes from *M. polymorpha*. Then, we constructed a phylogenetic tree with representative sequences of bHLH from other groups from *A. thaliana* (I-XVIII) and identified the *M. polymorpha* SACL ortholog, MpSACL. As an additional support for our results, this gene was also previously identified as a member of the XIV subfamily of bHLH (Catarino et al., 2016). We then performed iterative searches in the OneKP, NCBI and Phytozome databases using whole SACL aminoacidic sequences from different taxa to ensure that SACL orthologs from all plant lineages were identified. We obtained 765 sequences that were used for alignment and final ML tree construction (**Figure 8A**).

We did not find bHLH sequences of subfamily XIV in chlorophycean and charophycean algae species, which indicates that this particular subfamily originated in the last common ancestor of land plants. In addition, the observation that mosses do not possess SACL sequences suggests an early loss of SACL in this lineage. Our results are consistent with previous reports on the evolution of bHLH TF in plants (Catarino et al., 2016; Pires & Dolan, 2010a) and provide further detail of the evolutionary events within the SACL subfamily.

According to our phylogenetic analysis, SACL genes in land plants are grouped in three monophyletic clades: (i) the SACL3 clade, that contains the SACL orthologs from all land plant clades; (ii) the SAC51 clade, which is specific for

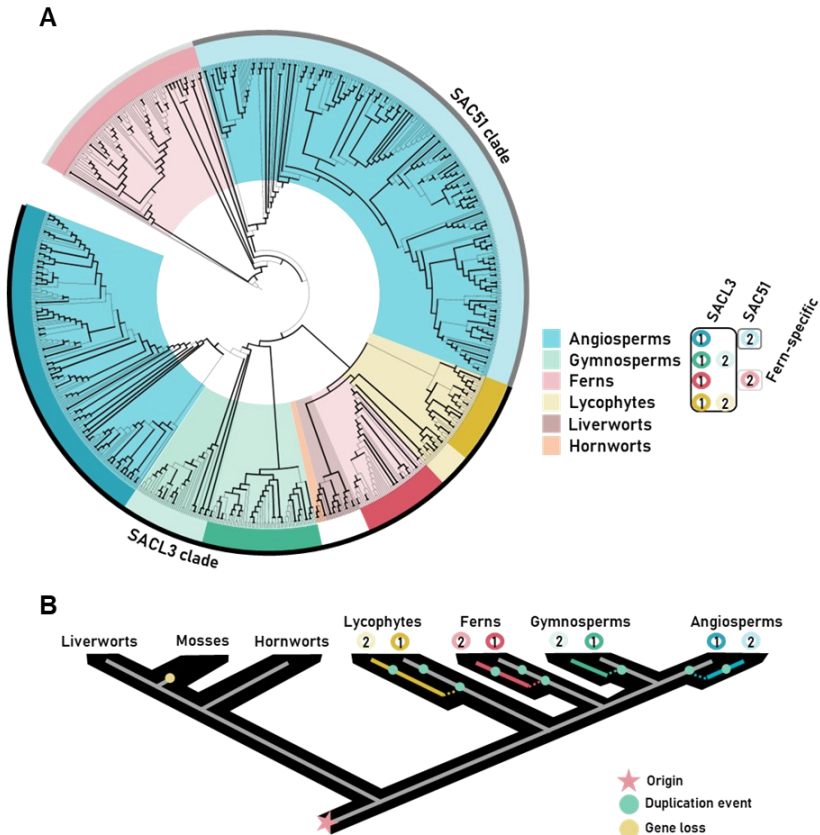


Figure 8. Phylogenetic analysis and inferred history of *SACL* in land plants. A. *SACL* ML phylogenetic tree. Branch support values are based on SH-like aLRT, and values over 0.75 are marked with wider black branches. bHLH XVII sequence is used as the outgroup. Wider background-colored groups mark the different plant lineages, while color outer circles are used to differentiate *SACL* phylogenetic groups inside each lineage. Black, grey and light grey outer circles represent the *SACL3*, *SAC51* and the Fern-specific clades, respectively. **B.** Schematic depiction of the inferred history of *SACL* and the duplication events in each plant lineage. Phylogenetic relationships are represented with grey lines (*SACL3* clade) and internal duplications that lead to gene diversifications are marked in yellow (lycophytes), dark pink (ferns), green (gymnosperms) and cyan (angiosperms). Plant phylogenetic relationships are based on the work of Harris et al. (2020). Origin of *SACL* sequences is marked with a pink star, major duplication events are marked with turquoise blue circles and gene loss is marked with light yellow circles. *SAC51*, *SUPPRESSOR OF ACAULIS51*; *SACL3*: *SAC51-LIKE3*



angiosperms, and (iii) a fern-specific clade (**Figure 8A**). In general, the sequences cluster according to the species relationships and the topology is well-supported. Hence, we proceeded to characterize the clade specific duplications to infer the evolutionary history of SACL in land plants.

Except for liverworts and hornworts, most lineages have undergone early gene duplications (**Figure 8B**). Lycophytes harbor two to six SACL paralogs that are divided into two monophyletic groups (Lycophytes 1 and 2) and have undergone family-specific duplications. Ferns, in turn, have undergone an internal duplication at its common ancestor that gave rise to two monophyletic groups: Ferns 1 (inside the SACL3 clade) and Ferns 2. It is therefore clear that the HLH domain of Ferns 2 (the fern-specific clade), which has been used for this phylogenetic analysis, has diversified from the rest of the SACL clades and has been accompanied also by divergent protein domains between Ferns 1 and 2 (**Figure 9**). Most fern families contain one to four SACL orthologs inside Ferns 1 and 2, which is also indicative of successive family-specific duplications in ferns. Most gymnosperm families have one copy of *SACL*, except for the sister clades Taxaceae, Cupressaceae, and Ginkgoaceae, that underwent a family-specific duplication and harbor two SACL paralogs. Angiosperm sequences cluster in two monophyletic groups, the SACL3 clade (Angiosperms 1) and SAC51 clade, that has diversified from the SACL3 clade (Angiosperms 2). Most angiosperm families have paralogs inside both SACL3 and SAC51 clade. For example, *A. thaliana* contains one copy inside SACL3 clade (*AtSACL3*) and three copies inside SAC51 clade (*AtSAC51*, *AtSACL1* and *AtSACL2*). It is interesting to note that some angiosperm families have lost the copy inside SACL3 clade (Asteraceae, Convolvulaceae, Primulaceae and Orchidaceae) or the SAC51 clade copies (Papaveraceae and Portulacaceae).

After a thorough domain analysis of SACL proteins we could infer the degree of conservation of other SACL domains among land plants. We identified three other conserved domains in tracheophytes (1 to 3), in addition to the HLH domain (4), which is the only conserved domain in all land plant clades (**Figure 9**). While the first domain is only specific for tracheophytes, liverworts contain part of the second and the entire third domains. Hornworts, in turn, do not share any other domain other



than the HLH with other plant clades. In addition, we found clade-specific domain innovations in gymnosperms, ferns, liverworts, and hornworts (**Figure 9**). Taken together, this indicates that (i) the domain 1 was acquired at the tracheophyte common ancestor; and (ii) the domains 2 and 3 and the HLH domain are conserved in land plants, and therefore were probably common domains in the ancestor SACL ortholog. Considering that SACL vascular role in *A. thaliana* is specifically through their interaction with other bHLHs (Katayama et al., 2015a; Vera-Sirera et al., 2015), and that some SACL protein domains – except for the HLH – are divergent in land plants, it remains to be elucidated whether it will affect SACL interactions with other proteins or their roles in other plant lineages. In **Chapter 2** and **3** we will functionally characterize SACL orthologs in non-vascular plants, as well as assess and compare SACL interaction partners in a non-vascular plant, *M. polymorpha*, and an angiosperm, *A. thaliana*.

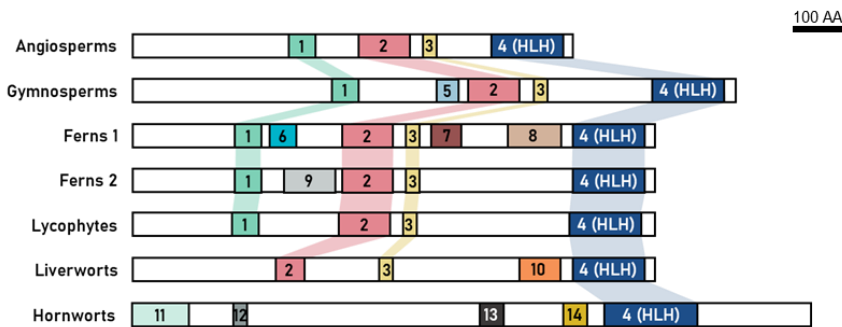


Figure 9. Overview of conserved domains in SACL proteins. Protein lengths are based on clade-specific averages.

As a summary, we revisited the SACL origin in embryophytes, and identified SACL orthologs in all embryophytes except for mosses, which indicates an early gene loss in this lineage. We have inferred at least six events of duplication (**Figure 8B**), which are also in agreement with documented WGD in plants (Jiao et al., 2011; Li et al., 2015; Wood et al., 2009): (i) inside lycophytes, family-specific duplication(s); (ii) at the common ancestor of ferns and (iii) family-specific internal duplications in ferns; (iv) at the last common ancestor of Cupressaceae, Taxaceae and Ginkgoaceae families,



inside gymnosperms; (v), at the common ancestor of angiosperms giving rise to the SACL3 clade and the SAC51 clade, and (vi) further family-specific internal duplications in angiosperms.

The uORF is absent in bryophytes

In *Arabidopsis*, *SACL* transcripts are under Tspm-dependent post-translational regulation through an uORF in their 5' leaders (Cai et al., 2016; Imai et al., 2006; Ishitsuka et al., 2019; Vera-Sirera et al., 2015; Yamamoto & Takahashi, 2017). This sequence is highly conserved, especially at the C-terminus end of the peptide (Cai et al., 2016; Vera-Sirera et al., 2015). In other tracheophytes, like ferns and gymnosperms, this uORF is also present (Hayden & Jorgensen, 2007) but its dependency on Tspm regulation or link with *SACL* transcripts remains unexplored. Thus, we decided to investigate the degree of conservation of this uORF in *SACL* transcripts in embryophytes.

An examination of the 5' leader sequence in *SACL* transcripts described above showed that the uORF was absent in bryophytes and expanded the conservation of the uORF to all previously unexplored tracheophyte lineages, like lycophytes (**Figure 10**). In addition, tracheophyte *SACL* transcripts did not contain any conserved uORFs other than the previously identified that is responsible for Tspm regulation. Hence, from now on we will use the generic term "uORF" to refer specifically to the conserved tracheophyte uORF. As expected, all tracheophyte uORFs displayed a high conservation degree at the C-terminus end (**Figure 10A**), which agrees with previous observations that point mutations altering specifically this peptide sequence abolish the translational regulation of the *SACL* transcripts in *A. thaliana* (Cai et al., 2016; Vera-Sirera et al., 2015). In an alternative approach, we used the *A. thaliana* AtSACL3 and AtSAC51 uORF aminoacidic sequences as baits in a TBLASTN search against the available plant transcriptomes, and only retrieved tracheophyte *SACL* orthologs, indicating that this uORF is only associated to this subfamily of bHLH TFs. We then retrieved all available tracheophyte-specific uORF sequences and performed a ML phylogenetic tree (**Figure 10B**). In general, the sequences clustered according to the species phylogenetic relationships, as it had



also been observed for the main ORF of *SACL* genes. This suggests that the evolution of the uORF and the main ORF has occurred in parallel.

All things considered, the absence of the uORF in bryophytes and the conservation of the uORF sequence in tracheophyte *SACL* transcripts suggests two possible hypotheses: (i) the uORF sequence was present in the land plant common

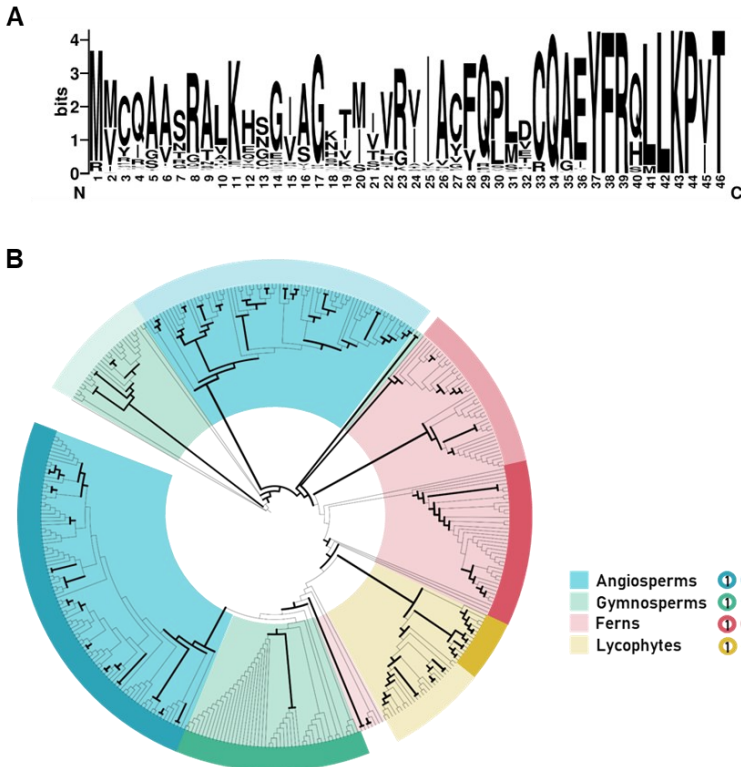


Figure 10. Description of 5' leader sequences in *SACL* transcripts and tracheophyte-specific uORFs. **A.** Conservation of the amino acid sequence of tracheophyte-specific uORF represented by sequence logo (www.weblogo.berkeley.edu). **B.** uORF ML phylogenetic tree. Branch support values are based on SH-like aLRT, and values over 0.75 are marked with wider black branches. Gymnosperm 2 sequences are used as the outgroup. Wider background-colored groups mark the different plant lineages, while color outer circles are used to differentiate uORF phylogenetic groups inside each lineage.



ancestor and was lost in bryophytes; or (ii) the uORF was acquired *de novo* in the tracheophyte lineage. Given that other families of bHLH do not contain this specific uORF, the most parsimonious scenario is that the uORF was an acquisition inside the tracheophyte lineage. In any case, it appears that the regulation of SACL translation by Tspm might have been intimately linked to vascular development during evolution.

Tspm regulation operates through the uORF

The presence of the uORF in tracheophyte *SACL* transcripts suggests that, as it is the case in *A. thaliana* and other angiosperms, their translation may be regulated by Tspm (Cai et al., 2016; Imai et al., 2006; Ishitsuka et al., 2019; Vera-Sirera et al., 2015; Yamamoto & Takahashi, 2017). However, the absence of the uORF in bryophytes transcripts does not rule out that Tspm also participates in the regulation of *SACL* translation through a different mechanism. Hence, we proceeded to analyze the factors that might influence the uORF inhibitory effect on translation. In addition, we also considered the 5' leader of a *SACL* ortholog from a non-vascular plant, *M. polymorpha* (Mp*SACL*) to see if these criteria could also be met by a different uORF.

Other studies have established the general criteria for optimal translational regulation (Fuütterer & Hohn, 1992; Kozak, 1987): the length of the uORF should be approximately 150 base pairs (bp), and the distance from the main ORF should exceed 79 bp in length. To check if these criteria are generally met by the tracheophyte uORFs, we determined the uORF length and intercistronic space in all the available *SACL* transcripts of tracheophytes (**Figure 11**). In general, the average uORF length was 159 bp and was similar in all phylogenetic groups, except for Ferns 2 (the fern-specific clade), which was significantly higher with an average of 253 bp. In this regard, longer uORFs are correlated with a more negative effect on translation (Fuütterer & Hohn, 1992), pointing Ferns 2 uORF as a possibly stronger inhibitor than other uORFs. Regarding intercistronic space, most angiosperm, gymnosperm, and fern sequences had an average distance of 260 bp, except for Angiosperms 2 (*SAC57* clade) whose distance was 100 bp shorter but still within the optimal intercistronic range. Lycophyte sequences were the most divergent in intercistronic space with an average of 484 bp for Lycophytes 1 and 385 for Lycophytes 2. Interestingly, Mp*SACL*



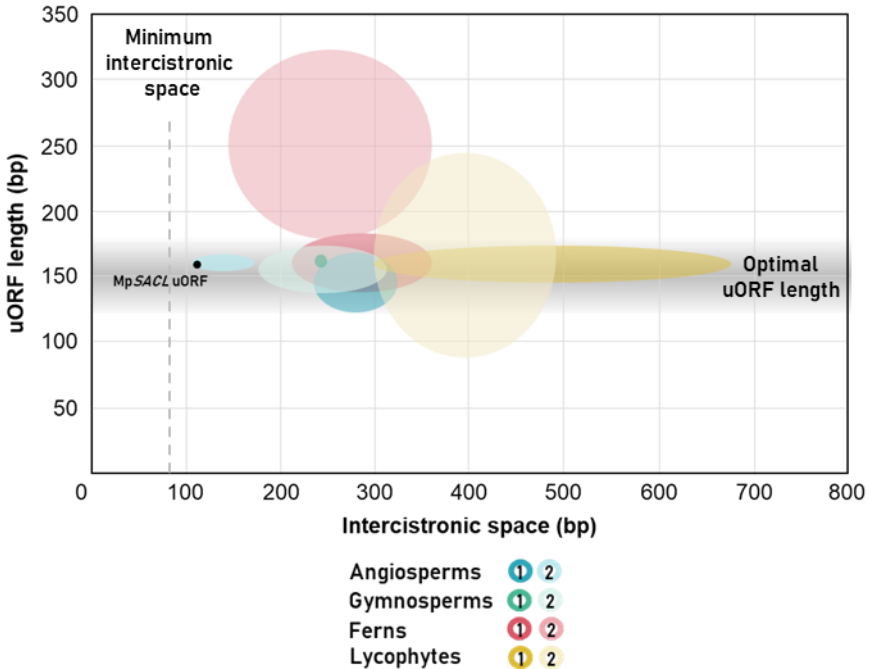


Figure 11. Bubble plot representing the tracheophyte-specific uORF length (bp) versus the intergenic space (bp) in 5' leader sequences. Bubble sizes are used to depict the standard deviation in uORF lengths (height) and intergenic space measures (length). Dashed line delimits the minimum intergenic space required for mORF regulation, and grey box marks the optimal uORF length. Both criteria are based on Fuütterer & Hohn (1992) and Kozak (1987) research. uORF: upstream open reading frame; bp, base pairs.

5' leader contained a uORF that could also meet these criteria for translational regulation (**Figure 11**). To test whether the uORF is relevant for Tspm-mediated translation of *SACL* transcripts in the different plant clades, we selected sequences from tracheophytes for which we had good quality full length 5' leaders, as well as the *M. polymorpha* MpSACL 5' leader. We found a total of 90 sequences for ferns and 30 sequences for lycophytes that harbored a putative functional uORF. Among these species, we chose four representatives of each clade: for ferns, *Ligodium japonicum*, *Cibotium glaucum*, *Polypodium hesperium* and *Ceratopteris richardii*. For lycophytes, we chose *Isoetes tegetiformans*, *Diphasiastrum digitatum*, *Lycopodium deuterodensum*



and *Selaginella kraussiana*. Furthermore, we used the 5' leader region from *Arabidopsis thaliana* *AtSACL3* as a positive control for Tspm-dependent translation (Cai et al., 2016; Vera-Sirera et al., 2015). We then transiently expressed these 5' leaders fused to the *Firefly* luciferase gene (LUC) in *N. benthamiana* leaves and performed Tspm treatments to detect changes in LUC translation (see Materials for details).

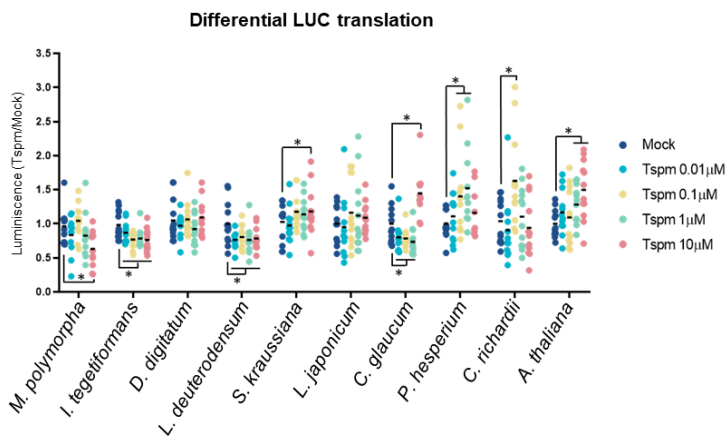


Figure 12. The 5' leaders containing the uORF are sensitive to Tspm. Tspm-dependent translation after 0.01, 0.1, 1, and 10 μM Tspm treatments in the 5' leader sequences of the liverwort *M. polymorpha*, the lycophytes *I. tegetiformans*, *D. digitatum*, and *S. kraussiana*, the ferns *L. japonicum*, *C. glaucum*, *P. hesperium* and *C. richardii*, and the angiosperm and positive control *A. thaliana*. From these species, Tspm induces mORF translation in one lycophyte (*S. kraussiana*), three out of four ferns (*C. glaucum*, *P. hesperium* and *C. richardii*) and the angiosperm *A. thaliana*. The non-vascular plant *M. polymorpha* does not have Tspm-dependent regulation. the tracheophyte-specific uORF (*S. kraussiana*, *C. richardii*, *A. thaliana*) LUC values were normalized with *Renilla* luciferase. Differential translation is calculated with the ratio of Tspm treatments over Mock conditions. Statistical analyses were performed with T-student tests with $N = 12$ and $\alpha = 0.05$. P-values ≤ 0.05 are marked with an asterisk (*).

Transcripts from all tracheophyte clades showed Tspm-dependent translation, although the Tspm response, measured through the differential LUC luminescence, was variable among all inspected 5' leaders. We observed a positive



effect of Tspm on translation of the *SACL* transcripts in the angiosperm *A. thaliana*, one of the lycophyte species, *S. kraussiana*, and in three fern species, *C. richardii*, *P. hesperium* and *C. glaucum*. In contrast, the non-vascular *M. polymorpha* did not show any Tspm-dependent translation (**Figure 12**). It is to be considered, however, that the lack of Tspm response in *M. polymorpha* 5' leader could also be derived from the heterologous luciferase system.

To test the hypothesis that only the tracheophyte uORF confers Tspm sensitivity, we substituted every Met codon to Lys codon from the tracheophyte uORFs and the *M. polymorpha* uORF and confirmed that, under those circumstances, Tspm-dependent translation was lost in tracheophyte *SACLs* (**Figure 13**). Likewise, other studies performed on *A. thaliana* *SACL* transcripts showed that Tspm sensitivity was lost after eliminating the conserved uORF (Ishitsuka et al., 2019; Vera-Sirera et al., 2015), supporting our initial hypothesis.

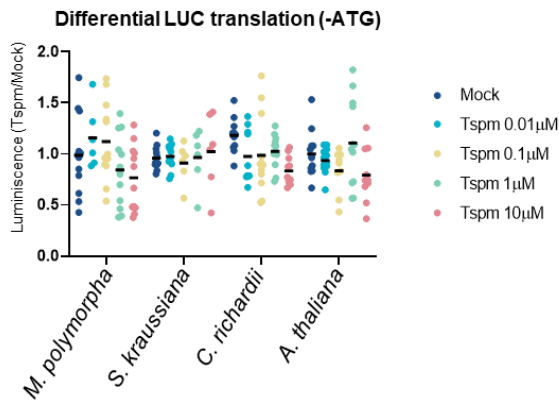


Figure 13. Tspm-dependent translation is lost when the uORF is not translated. Tspm-dependent translation after substitution of the Met codons for Lys codons from the Marchantiophyta-specific uORF (*M. polymorpha*) and the tracheophyte-specific uORF (*S. kraussiana*, *C. richardii*, *A. thaliana*) and after Tspm treatments (0.01, 0.1, 1 and 10 μM). Tspm-dependent translation is lost after removing the AUG codons from the tracheophyte lineage; there is no change in *M. polymorpha*. LUC values were normalized with *Renilla* luciferase. Differential translation is calculated with the ratio of Tspm treatments over Mock conditions. Statistical analyses were performed with T-student tests with $N=12$ and $\alpha=0.05$. P-values ≤ 0.05 are marked with an asterisk (*).



The observed differences in Tspm sensitivity in vascular species might be influenced by various factors such as variability in uORF sequence or presence of other CRE that may interfere with translation. Previous research has identified the key amino acid positions for Tspm regulation, which correspond to the 8th, 5th, and 3rd–1st amino acids from the stop codon (Vera-Sirera et al., 2015). All fern species contain the conserved key amino acids, though lycophytes only contain four out of the five conserved key positions (**Figure 14**). Supporting this idea, one of the most divergent uORFs belonged to *I. tegetiformans*, whose 5' leader did not show Tspm-dependent translation and only contains two out of the five key amino acids (**Figure 14**). This suggests that Tspm sensitivity is tightly linked with the C-terminus of the uORF sequence.

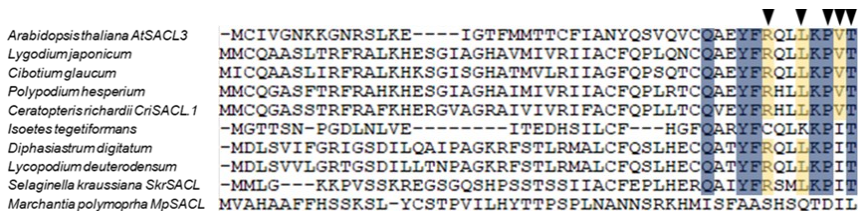


Figure 14. Alignment of the tracheophyte-specific uORF and the Marchantiophyta-specific uORF. The 3' region of the tracheophyte-specific uORF is the most conserved. The tracheophyte-conserved amino acid positions are marked with dark blue, whereas partially conserved amino acid positions are marked in yellow. Arrowheads mark the key amino acids for Tspm sensitivity.

Interestingly, we also observed a negative effect on LUC translation, of increasing number of other uORFs in 5' leader sequences (**Table 2**). Similarly, basal translation was increased by two-fold after the substitution of Met codons to Lys codons in the tracheophyte-specific uORFs in mock and Tspm treatments (**Figure 15**). This is in accordance with the negative effect of an increasing number of uORFs in the translation of the main Open Reading Frame (mORF) in polycistronic mRNAs (see Glossary) (Kozak, 1987, 2002), and confirms that this uORF has a negative effect on translation, independently of the Tspm content.



	uORF n°	LUC base translation
<i>Arabidopsis thaliana</i>	8	0.91
<i>Lygodium japonicum</i>	9	0.03
<i>Cibotium glaucum</i>	14	0.05
<i>Polypodium hesperium</i>	20	0.05
<i>Ceratopteris richardii</i>	20	0.04
<i>Isoetes tegetiformans</i>	7	3.39
<i>Diphasiastrum digitatum</i>	14	1.60
<i>Lycopodium deuterodensum</i>	22	0.03
<i>Selaginella kraussiana</i>	18	0.26
<i>Marchantia polymorpha</i>	8	1.30

Table 2. Analysis of the 5' leader sequences in representative tracheophyte and bryophyte species. Darker turquoise represents a higher value and white represents the lower values for better visual observation. Number of uORFs was quantified independently of the sense or antisense direction inside the 5' leader sequence. LUC base translation represents the normalized value of the LUC luminescence with the *Renilla* luciferase luminescence.

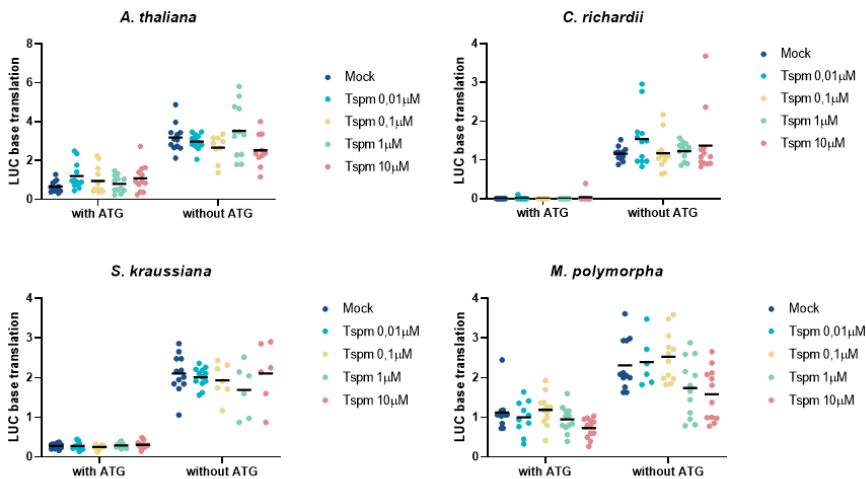


Figure 15. LUC base expression in 5' leader sequences of *A. thaliana*, *C. richardii*, *S. kraussiana* and *M. polymorpha*. Comparison between 5' leader sequences containing uORF with ATG or without ATG, treated with mock, uORF with uORF with ATG or without ATG, treated with mock, 0.01, 0.1, 1, and 10µM Tspm. The sequences without ATG show a clear increase of LUC base translation. Tspm, thermospermine; µM, micromolar; LUC, luciferase



Altogether, our results demonstrate that Tspm-dependent translation in *SACL* transcripts occurs in all vascular lineages, and the only CRE responsible for Tspm sensitivity is the conserved uORF. Thus, although we have tested the 5' leader sequence from only one bryophyte, the absence of conserved uORFs in any of the *SACL* transcripts from bryophytes makes it very unlikely that Tspm has any role in *SACL* translation in this lineage.

MATERIALS

Plant material and growth conditions

Plant samples for polyamine extraction and RNA extraction were collected simultaneously for both experiments. *Arabidopsis thaliana* ecotype Col-0 seeds were surface sterilized and grown on MS medium (Murashige and Skoog basal medium 4.33g/L, sucrose 1%, Plant Propagation Agar PPA 1%) under long-day conditions at 22°C in a growth chamber for 15 days. *Picea abies* shoots were collected from adult trees. *Selaginella lepidophylla* was hydrated for 24 hours prior to being transplanted into potting soil containing 25% perlite on long day conditions with 16 hours light at 22°C in a growth chamber. *Physcomitrium patens* was obtained from Jesús Vicente Carbajosa's Lab (CBGP-Madrid, Spain) and gametophytes were grown in BCD medium supplemented with 1 mM Ca²⁺ (Cove et al., 2009) for 10 days under continuous light conditions at 22°C in a growth chamber. *Marchantia polymorpha* Tak-1 accession was grown on 1/2 strength Gamborg's B5 medium (Gamborg's B5 medium 1.58g/L, MES monohydrate 0.5g/L, Plant Propagation Agar PPA 10g/L) at pH 5.7 under continuous light in a growth chamber. *Chlamydomonas reinhardtii* genetic and plant material was provided by Federico Valverde's lab (IBVF-Sevilla, Spain).

Phylogenetic analysis

The sequences used in this chapter were obtained by extensive TBLASTN analysis in every plant family found in the Phytozome (<http://www.phytozome.net/>), NCBI (<http://www.ncbi.nlm.nih.gov/>) and OneKP databases



(<http://db.cngb.org/onekp/>). Sequences were managed using the Benchling tool (<https://benchling.com>). In order to identify the C3HDZ orthologs in the plant lineage, the five Arabidopsis C3HDZ were used as baits. These are: *AtHB8* (At4G32880), *AtCNA* (At1G52150), *AtREV* (At5G60690), *AtPHB* (At2G34710) and *AtPHV* (At1G30490). The aminoacidic sequences of the genes in the transcripts were extracted manually and used for a preliminary maximum-likelihood (PhyML) phylogenetic tree with representative members of C1HDZ, C2HDZ, C3HDZ and C4HDZ of *A. thaliana*, *O. sativa*, *S. moellendorffii*, *P. patens*, *M. polymorpha* and *K. flaccidum* (Catarino et al., 2016) using NGPhylogeny.fr webtool (Lemoine et al., 2019). Only the sequences that fell into the C3HDZ clade were used for the final C3HDZ phylogenetic analysis. Sequences with a partial or missing HD were removed from the final alignment to ensure a better-supported phylogenetic tree.

The identification of polyamine aminopropyl transferases and TSPMS orthologs was performed using the Arabidopsis SPDS genes (*SPDS1*-At1G23820, *SPDS2*-At1G70310), Spermine synthase (*SPMS*-At5G53120) and Thermospermine synthase (*ACL5*-At5G19530) as baits. Regarding SACL orthologs, the bHLH domains of the Arabidopsis *SAC51* (At5g64340), *SACL1* (At5G09460), *SACL2* (At5g50010), and *SACL3* (At1G29950) were used as baits to initially identify the *M. polymorpha* *MpSACL* (Mp5g09710) in the Phytozome database, which was confirmed with an initial ML analysis with representative sequences of bHLH from other groups from *A. thaliana* (I-XVIII). We then performed iterative searches in the OneKP, NCBI and Phytozome databases using whole SACL aminoacidic sequences from *A. thaliana*, *O. sativa*, *S. moellendorffii*, *P. patens*, and *K. flaccidum* (Catarino et al., 2016) to ensure that SACL orthologs from all plant lineages were identified. In addition, previous to the available *Ceratopteris richardii* genome in Phytozome, *SACL* transcript sequences were kindly provided by the Cheng laboratory (University of Iowa, USA). The uORF sequences in SACL 5' prime leaders, as well as the distance from the main ORF, were retrieved from the available *SACL* transcript sequences used for the phylogenetic analysis of SACL orthologs.

The orthologs of C3HDZ, polyamine aminopropyl transferases, SACL, and the uORFs present at the *SACLs* 5'leader were aligned separately in MEGA X (Kumar



et al., 2018) using MAFFT ver. 7 in default parameters (Kato & Standley, 2013) and manually curated to ensure the presence of the conserved domains in C3HDZ (HD), in ACL5, in SACL (bHLH domain) and in the uORFs. ML trees were produced with PhyML in NGPhylogeny.fr (Goodstein et al., 2012). Statistical significance was evaluated by a Shimodaira-Hasegawa-like approximate likelihood ratio test (SH-like aLRT). Phylogenetic tree graphical representations were generated using the webtool Interactive Tree of Life (iTOL) version 6.5.8 (<https://itol.embl.de/>) and final Figures were edited manually.

RNA Extraction and PCR Analysis

For *A. thaliana* and *M. polymorpha*, total RNA was isolated using the NucleoSpin™ RNA Plant Kit from Macherey-Nagel following the manufacturer's instructions. The trizol-chloroform method was used as described (Siebers et al., 2017) to extract RNA from *C. reinhardtii*, *P. patens*, and *S. lepidophylla*. For *P. abies*, total plant RNA was extracted using a modified protocol from RNA extraction in pineapple, which is optimal for tissues with excessive starch or secondary metabolite production. Tissue was grinded with mortar and pestle using liquid nitrogen and is resuspended in 600µl of fresh Pineapple extraction buffer (Tris 1M pH 7.5 adjusted with boric acid, SDS 10%, EDTA 0.5M pH 8.0, β-Mercaptoethanol 1%). Next, 150 µl of EtOH 100% and 66µl of potassium acetate 5M were added and mixed for 1 minute. Then, 700µl of phenol:chloroform:isoamyl alcohol (25:24:1) were added and the sample was centrifuged at top speed for 3 minutes. After that, 500µl of the supernatant were added to 1mL of 100% EtOH, vortexed, and incubated at -80°C for 30 minutes. The samples were then centrifuged at 14000 rpm at 4°C for 30 more minutes, and the supernatant was discarded. 170µl of 80% EtOH were added to the pellet and the samples were centrifuged at max speed for 3 minutes. After that, the supernatant was discarded, and the pellet was resuspended in 150µl of MilliQ water with 50µl of LiCl 8M, and left at 4°C overnight for RNA precipitation. The samples were centrifuged at 14000 rpm at 4°C for 30 minutes and the pellet was washed with 80% EtOH. Finally, the pellet was resuspended with 50µl of sterile MilliQ water.



cDNA synthesis was performed with 1 µg of RNA using NZY First-Strand cDNA Synthesis Kit (NZYTech) according to the manufacturer's instructions. The resulting cDNA was used for semi-quantitative PCR reaction. The primers used for the semi-quantitative PCR are listed in **Table 3**.

	Forward	Reverse	cDNA product (bp)	gDNA product (bp)
<i>AthACL5</i>	AACATTCTCAAACCCAAGCTTAGC	ATGGTGTTGTAGATTGATGTGAAGACT	107	213
<i>PabACL5.1</i>	CCGCCTTGAGCTCGTTATCAAC	CTGGGTCTGCAAGGTCTCTAC	92	160
<i>PpaACL5.1</i>	CAGTGGCAGGAGGTCTCTGTTA	GGAGTAGACCTCTGTGTGCGTT	140	277
<i>MpaACL5</i>	GTGAGAAAATCGTTGCCCAAGG	TTCGATTGGTTCCATGTCC	83	–
<i>CreACL5</i>	TCACGCTCATCAACGACGAC	ACCACGTTGCGGTAAAACCT	145	291

Table 3. Primers used for PCR analyses

Gene cloning and expression in yeast

Coding sequence (CDS) regions of TSPMS genes from the selected species were obtained either from cDNA (*M. polymorpha* - Mp8g03070, *S. lepidophylla* - onekp:ABIJ-_scaffold_2009837, and *A. thaliana* - AT5G19530) or synthesized (Integrated DNA Technologies, IDT), for *P. abies* – PAV0026429, *P. patens* - Pp3c5_6270V3, and *C. reinhardtii* - Cre06.g251500. The primers used for amplification are summarized in **Table 4**. For plasmid construction, the CDS of the genes were cloned into pDONR207 through Gateway recombination (Invitrogen) or a modified pCR8 with Gateway and Golden Braid overhangs (Sarrion-Perdigones et al., 2011) and eventually into the destination vector pAG426GPD-ccdb-HA (a gift from Susan Lindquist; Addgene plasmid number 14252) for expression in yeast.

Yeast strain BY4741 (MATa his3 leu2 met15 ura3), kindly provided by Ramón Serrano's lab (IBMCP-Valencia, Spain), was grown on Synthetic Defined (SD) medium and transformed with the pAG426GPD containing the CDS of interest by LiAc/ssDNA/PEG (Schiestl & Gietz, 1989). Selected transformants were grown on 50 mL liquid SD medium lacking Trp and Ura for 2 days, then harvested by centrifugation (about 200 mg of pellet) and frozen for further polyamine quantification.



Species	Gene	Direction	Sequence	Overhangs
<i>A. thaliana</i>	<i>AtACL5</i>	Foward	CGGTCTCGCCTTATGGGTGAAGCCGTAGAG	Golden Braid
		Reverse	CGGTCTCGCCTTTTAAATATGCCGGTACGCCA	Golden Braid
<i>P. abies</i>	<i>PabACL5.1</i>	Foward	From GBLOCKS	Gateway
		Reverse	From GBLOCKS	Gateway
<i>S. lepidophylla</i>	<i>SleACL5.1</i>	Foward	GGGGACAAGTTTGTACAAAAAAGCAGGCTCGATGGGGAAAGTTCACGTCAATGGC	Gateway
		Reverse	GGGGACCACCTTTGTACAAGAAAGCTGGGTATTAAAGCTGCTGTGTGGCTGC	Gateway
<i>P. patens</i>	<i>PpaACL5.1</i>	Foward	From GBLOCKS	Gateway
		Reverse	From GBLOCKS	Gateway
<i>M. polymorpha</i>	<i>MpoACL5</i>	Foward	GGGGACAAGTTTGTACAAAAAAGCAGGCTTAATGGCTGAAGCCATTACGACTAC	Gateway
		Reverse	GGGGACCACCTTTGTACAAGAAAGCTGGGTAAATGGGATTTCCGATTTGGTTCC	Gateway
<i>C. reinhardtii</i>	<i>CreACL5</i>	Foward	From GBLOCKS	Gateway
		Reverse	From GBLOCKS	Gateway

Table 4. Primers used for cloning and expression in yeast.

Polyamine Quantification

The tissues used for polyamine quantification were *A. thaliana* 15-day-old seedlings; *P. abies* shoots from adult trees; *S. lepidophylla* a mixture of rehydrated shoot and root tissues; *P. patens* 10-day-old gametophytes; and *C. reinhardtii* 200 mg of centrifuged liquid culture. For quantification in yeast, 200 mg worth of pellets were used for every TSPMS gene. Polyamine measurements were performed on at least 3 biological replicates for plant tissues and yeast extracts. Polyamine extraction was performed using 1 g of plant samples (except for *C. reinhardtii*). The tissue was ground with mortar and pestle in liquid nitrogen (in the case of yeast pellets, the cells were broken with glass balls) and resuspended in 2.5 mL of 5% perchloric acid (PCA) in a 15-mL tube. At this point 500 μ L of the internal standard (diethylamine 1mM, DEA) was added to the 5% PCA. The samples were kept on ice for 1h and centrifuged at 4°C for 20 min at 15000 x g. The whole supernatant was collected (between 2 mL and 3.5 mL) and transferred to a fresh 15 mL falcon tube. For each mL of supernatant, 0.66 mL of 2M NaOH was added. Then, benzylation started with the addition of 10 μ L of benzoyl chloride. After 1 min vortex, plant extracts were left at room temperature for 20 min. Next, for each mL of initial supernatant used, 1.33 mL of saturated NaCl solution was added. Two mL of diethyl ether was added, vortexed, and centrifuged at 3000g for 1 min for the separation of the phases. The supernatant was transferred to a new pyrex vial and dried completely using N₂. The remaining polyamines were resuspended in 130 μ L methanol and filtered with a filter syringe (pore size 0.2 μ m). Then, the filtrate was transferred to a plastic vial for HPLC analysis.



Briefly, 30- μ L aliquots were injected through a Waters 717plus autosampler into a 1525 Waters Binary HPLC pump equipped with a 996 Waters PDA detector and using a Luna C18(2) (Phenomenex) column (250 \times 4.6 mm, i.d. 5 μ m). The column was equilibrated with 58% solvent A (acidic H₂O containing 10 mL acetic acid for each liter of distilled water) and 42% solvent B (acetonitrile). Elution was carried out at room temperature; for polyamine separation, a 1 mL min⁻¹ flow rate was used in an isocratic gradient of 42% acetonitrile for 25 min. Then, the column was washed with 42-100% acetonitrile within 3 min and kept at 100% acetonitrile for 10 min. Eventually, the column was equilibrated with 42% acetonitrile for 17 min before the next injection. Detection of polyamines was performed at 254 nm.

Tspm-dependent translation assays in *N. benthamiana* leaves

Prior to the translation assays, the 5' leader sequence of different *SACL* transcripts was cloned into a modified pGreenII0800-LUC (Hellens et al., 2005) carrying a 2x35S promoter derived from pGJ1425 (Jach et al., 2001) at the 5' of the *Firefly* gene. The full 5' leader sequences of *M. polymorpha*, *I. tegetiformans*, *D. digitatum*, *L. deuterodensum*, *S. kraussiana*, *L. japonicum*, *C. glaucum*, *P. hesperium*, *C. richardii* and *A. thaliana* *SACLs* were synthesized (Integrated DNA Technologies) and cloned by restriction-ligation between the 2x35S and the *Firefly* gene. In addition, modified versions of the 5' leader of *M. polymorpha*, *S. kraussiana*, *C. richardii* and *A. thaliana* were designed *in silico* for ATG-to-CTG substitution in the uORF sequence, synthesized (Integrated DNA Technologies) and cloned into the modified pGreenII0800-LUC. The primers used for this experiment are listed in **Table 5**. The final vectors were transformed into *A. tumefaciens* previously carrying the pSOUP plasmid by electroporation and infiltrated into fully grown *N. benthamiana* leaves together with an *A. tumefaciens* carrying the p19 helper plasmid. The infiltration was carried out creating various 2cm diameter "infiltration spots" that were collected after 2 days incubation under continuous light at room temperature. Tspm Treatments were performed in 12-well sterile plates containing one leaf disc per well with liquid 1/2 strength Gamborg's medium (Gamborg's B5 medium 1.58g/L, MES monohydrate 0.5g/L) at pH 5.7 with either mock treatment (water) or 0.01, 0.1, 1 or 10 μ M Thermospermine (Thermospermine hydrochloride, EPICA S.L.). The treated leaf discs



ACL5.2 (Thupl.29381919s0016) were retrieved from the Phytozome (<https://phytozome-next.jgi.doe.gov/pz/portal.html>) and the Gymnosperm Plaza (<https://bioinformatics.psb.ugent.be/plaza/versions/gymno-plaza/>) databases. The retrieved promoters were 4 Kb long, except for *T. plicata* and *P. abies*, which were 2 Kb. Promoters were scanned for C3HDZ bs with the Morpheus (Minguet et al., 2015) “score” tool (<http://biodev.cea.fr/morpheus/>) using a DAP-seq based position frequency matrix (PFM) for AtCNA (At1G52150) (O’Malley et al., 2016), which was obtained from the JASPAR database (Castro-Mondragon et al., 2022).

REFERENCES

- Baima, S., Forte, V., Possenti, M., Peñalosa, A., Leoni, G., Salvi, S., Felici, B., Ruberti, I., & Morelli, G.** (2014). Negative feedback regulation of auxin signaling by ATHB8/ACL5-BUD2 transcription module. *Molecular Plant*, 7(6). <https://doi.org/10.1093/mp/ssu051>
- Cai, Q., Fukushima, H., Yamamoto, M., Ishii, N., Sakamoto, T., Kurata, T., Motose, H., & Takahashi, T.** (2016). The SAC51 family plays a central role in thermospermine respons 83 elevant 83 isdopsis. *Plant and Cell Physiology*, 57(8). <https://doi.org/10.1093/pcp/pcw113>
- Carretero-Paulet, L., Galstyan, A., Roig-Villanova, I., Martínez-García, J. F., Bilbao-Castro, J. R., & Robertson, D. L.** (2010). Genome-wide classification and evolutionary analysis of the bHLH family of transcription factors in Arabidopsis, poplar, rice, moss, and algae. *Plant Physiology*, 153(3), 1398–1412. <https://doi.org/10.1104/PP.110.153593>
- Castro-Mondragon, J. A., Riudavets-Puig, R., Rauluseviciute, I., Berhanu Lemma, R., Turchi, L., Blanc-Mathieu, R., Lucas, J., Boddie, P., Khan, A., Perez, N. M., Fornes, O., Leung, T. Y., Aguirre, A., Hammal, F., Schmelter, D., Baranasic, D., Ballester, B., Sandelin, A., Lenhard, B., ... Mathelier, A.** (2022). JASPAR 2022: The 9th release of the open-access database of transcription factor binding profiles. *Nucleic Acids Research*, 50(D1). <https://doi.org/10.1093/nar/gkab1113>
- Catarino, B., Hetherington, A. J., Emms, D. M., Kelly, S., & Dolan, L.** (2016). The Stepwise Increase in the Number of Transcription Factor Families in the Precambrian Predated the Diversification of Plants on Land. *Molecular Biology and Evolution*, 33(11). <https://doi.org/10.1093/molbev/msw155>



- Cove, D. J., Perroud, P. F., Charron, A. J., McDaniel, S. F., Khandelwal, A., & Quatrano, R. S.** (2009). Culturing the moss *Physcomitrella patens*. *Cold Spring Harbor Protocols*, 4(2). <https://doi.org/10.1101/pdb.prot5136>
- Exposito-Alonso, M., Drost, H. G., Burbano, H. A., & Weigel, D.** (2020). The Earth BioGenome project: opportunities and challenges for plant genomics and conservation. *Plant Journal*, 102(2). <https://doi.org/10.1111/tpj.14631>
- Ferré-D'Amaré, A. R., Prendergast, G. C., Ziff, E. B., & Burley, S. K.** (1993). Recognition by Max of its cognate DNA through a dimeric b/HLH/Z domain. *Nature*, 363(6424). <https://doi.org/10.1038/363038a0>
- Floyd, S. K., & Bowman, J. L.** (2006). Distinct Developmental Mechanisms Reflect the Independent Origins of Leaves in Vascular Plants. *Current Biology*, 16(19). <https://doi.org/10.1016/j.cub.2006.07.067>
- Floyd, S. K., Ryan, J. G., Conway, S. J., Brenner, E., Burris, K. P., Burris, J. N., Chen, T., Edger, P. P., Graham, S. W., Leebens-Mack, J. H., Pires, J. C., Rothfels, C. J., Sigel, E. M., Stevenson, D. W., Neal Stewart, C., Wong, G. K. S., & Bowman, J. L.** (2014). Origin of a novel regulatory module by duplication and degeneration of an ancient plant transcription factor. *Molecular Phylogenetics and Evolution*, 81. <https://doi.org/10.1016/j.ympev.2014.06.017>
- Floyd, S. K., Zalewski, C. S., & Bowman, J. L.** (2006). Evolution of class III homeodomain-leucine zipper genes in streptophytes. *Genetics*, 173(1). <https://doi.org/10.1534/genetics.105.054239>
- Fuütterer, J., & Hohn, T.** (1992). Role of an upstream open reading frame in the translation of polycistronic mRNAs in plant cells. *Nucleic Acids Research*, 20(15). <https://doi.org/10.1093/nar/20.15.3851>
- Gonzalez, M. E., Marco, F., Minguet, E. G., Carrasco-Sorli, P., Blázquez, M. A., Carbonell, J., Ruiz, O. A., & Pieckenstain, F. L.** (2011). Perturbation of spermine synthase gene expression and transcript profiling provide new insights on the role of the tetraamine spermine in *Arabidopsis* defense against *Pseudomonas viridiflava*. *Plant Physiology*, 156(4). <https://doi.org/10.1104/pp.110.171413>
- Goodstein, D. M., Shu, S., Howson, R., Neupane, R., Hayes, R. D., Fazo, J., Mitros, T., Dirks, W., Hellsten, U., Putnam, N., & Rokhsar, D. S.** (2012). Phytosome: A comparative platform for green plant genomics. *Nucleic Acids Research*, 40(D1). <https://doi.org/10.1093/nar/gkr944>



- Harris, B. J., Clark, J. W., Schrepf, D., Szöllösi, G. J., Donoghue, P. C. J., Hetherington, A. M., & Williams, T. A.** (2022). Divergent evolutionary trajectories of bryophytes and tracheophytes from a complex common ancestor of land plants. *Nature Ecology and Evolution*, 6(11). <https://doi.org/10.1038/s41559-022-01885-x>
- Harris, B. J., Harrison, C. J., Hetherington, A. M., & Williams, T. A.** (2020). Phylogenomic Evidence for the Monophyly of Bryophytes and the Reductive Evolution of Stomata. *Current Biology*, 30(11). <https://doi.org/10.1016/j.cub.2020.03.048>
- Hashimoto, T., Tamaki, K., Suzuki, K. I., & Yamada, Y.** (1998). Molecular cloning of plant spermidine synthases. *Plant and Cell Physiology*, 39(1). <https://doi.org/10.1093/oxfordjournals.pcp.a029291>
- Hayden, C. A., & Jorgensen, R. A.** (2007). Identification of novel conserved peptide uORF homology groups in Arabidopsis and rice reveals ancient eukaryotic origin of select groups and preferential association with transcription factor-encoding genes. *BMC Biology*, 5(1), 32. <https://doi.org/10.1186/1741-7007-5-32>
- Hellens, R. P., Allan, A. C., Friel, E. N., Bolitho, K., Grafton, K., Templeton, M. D., Karunairetnam, S., Gleave, A. P., & Laing, W. A.** (2005). Transient expression vectors for functional genomics, quantification of promoter activity and RNA silencing in plants. *Plant Methods*, 1(1). <https://doi.org/10.1186/1746-4811-1-13>
- Imai, A., Hanzawa, Y., Komura, M., Yamamoto, K. T., Komeda, Y., & Takahashi, T.** (2006). The dwarf phenotype of the Arabidopsis ac15 mutant is suppressed by a mutation in an upstream ORF of a bHLH gene. *Development*, 133(18). <https://doi.org/10.1242/dev.02535>
- Ishitsuka, S., Yamamoto, M., Miyamoto, M., Kuwashiro, Y., Imai, A., Motose, H., & Takahashi, T.** (2019). Complexity and Conservation of Thermospermine-Responsive uORFs of SAC51 Family Genes in Angiosperms. *Frontiers in Plant Science*, 10. <https://doi.org/10.3389/fpls.2019.00564>
- Jach, G., Binot, E., Frings, S., Luxa, K., & Schell, J.** (2001). Use of red fluorescent protein from *Discosoma* sp. (dsRED) as a reporter for plant gene expression. *Plant Journal*, 28(4). <https://doi.org/10.1046/j.1365-313X.2001.01153.x>
- Jiao, Y., Wickett, N. J., Ayyampalayam, S., Chanderbali, A. S., Landherr, L., Ralph, P. E., Tomsho, L. P., Hu, Y., Liang, H., Soltis, P. S., Soltis, D. E., Clifton, S. W., Schlarbaum, S. E., Schuster, S. C., Ma, H., Leebens-Mack, J., & Depamphilis, C. W.** (2011). Ancestral polyploidy in seed plants and angiosperms. *Nature*, 473(7345). <https://doi.org/10.1038/nature09916>



- Katayama, H., Iwamoto, K., Kariya, Y., Asakawa, T., Kan, T., Fukuda, H., & Ohashi-Ito, K.** (2015). A negative feedback loop controlling bHLH complexes is involved in vascular cell division and differentiation in the root apical meristem. *Current Biology*, 25(23). <https://doi.org/10.1016/j.cub.2015.10.051>
- Katoh, K., & Standley, D. M.** (2013). MAFFT multiple sequence alignment software version 7: Improvements in performance and usability. *Molecular Biology and Evolution*, 30(4). <https://doi.org/10.1093/molbev/mst010>
- Kozak, M.** (1987). Effects of intercistronic length on the efficiency of reinitiation by eucaryotic ribosomes. *Molecular and Cellular Biology*, 7(10). <https://doi.org/10.1128/mcb.7.10.3438-3445.1987>
- Kozak, M.** (2002). Pushing the limits of the scanning mechanism for initiation of translation. In *Gene* (Vol. 299, Issues 1–2). [https://doi.org/10.1016/S0378-1119\(02\)01056-9](https://doi.org/10.1016/S0378-1119(02)01056-9)
- Kumar, S., Stecher, G., Li, M., Knyaz, C., & Tamura, K.** (2018). MEGA X: Molecular evolutionary genetics analysis across computing platforms. *Molecular Biology and Evolution*, 35(6). <https://doi.org/10.1093/molbev/msy096>
- Leebens-Mack, J. H., Barker, M. S., Carpenter, E. J., Deyholos, M. K., Gitzendanner, M. A., Graham, S. W., Grosse, I., Li, Z., Melkonian, M., Mirarab, S., Porsch, M., Quint, M., Rensing, S. A., Soltis, D. E., Soltis, P. S., Stevenson, D. W., Ullrich, K. K., Wickett, N. J., DeGironimo, L., ... Wong, G. K. S.** (2019). One thousand plant transcriptomes and the phylogenomics of green plants. *Nature*, 574(7780). <https://doi.org/10.1038/s41586-019-1693-2>
- Lemoine, F., Correia, D., Lefort, V., Doppelt-Azeroual, O., Mareuil, F., Cohen-Boulakia, S., & Gascuel, O.** (2019). NGPhylogeny.fr: New generation phylogenetic services for non-specialists. *Nucleic Acids Research*, 47(W1). <https://doi.org/10.1093/nar/gkz303>
- Li, Z., Baniaga, A. E., Sessa, E. B., Scascitelli, M., Graham, S. W., Rieseberg, L. H., & Barker, M. S.** (2015). Early genome duplications in conifers and other seed plants. *Science Advances*, 1(10). <https://doi.org/10.1126/sciadv.1501084>
- Minguet, E. G., Segard, S., Charavay, C., & Parcy, F.** (2015). MORPHEUS, a Webtool for Transcription Factor Binding Analysis Using Position Weight Matrices with Dependency. *PLOS ONE*, 10(8), e0135586. <https://doi.org/10.1371/JOURNAL.PONE.0135586>
- Minguet, E. G., Vera-Sirera, F., Marina, A., Carbonell, J., & Blázquez, M. A.** (2008). Evolutionary diversification in polyamine biosynthesis. *Molecular Biology and Evolution*, 25(10). <https://doi.org/10.1093/molbev/msn161>



- O'Malley, R. C., Huang, S. S. C., Song, L., Lewsey, M. G., Bartlett, A., Nery, J. R., Galli, M., Gallavotti, A., & Ecker, J. R.** (2016). Cistrome and Epicistrome Features Shape the Regulatory DNA Landscape. *Cell*, 165(5). <https://doi.org/10.1016/j.cell.2016.04.038>
- Panicot, M., Minguet, E. G., Ferrando, A., Alcázar, R., Blázquez, M. A., Carbonell, J., Altabella, T., Koncz, C., & Tiburcio, A. F.** (2002). A polyamine metabolon involving aminopropyl transferase complexes in *Arabidopsis*. *Plant Cell*, 14(10). <https://doi.org/10.1105/tpc.004077>
- Pires, N., & Dolan, L.** (2010). Origin and diversification of basic-helix-loop-helix proteins in plants. *Molecular Biology and Evolution*, 27(4), 862–874. <https://doi.org/10.1093/MOLBEV/MSP288>
- Prigge, M. J., & Clark, S. E.** (2006). Evolution of the class III HD-Zip gene family in land plants. *Evolution and Development*, 8(4), 350–361. <https://doi.org/10.1111/j.1525-142X.2006.00107.x>
- Proost, S., Bel, M. van, Vanechoutte, D., van de Peer, Y., Inzé, D., Mueller-Roeber, B., & Vandepoele, K.** (2015). PLAZA 3.0: An access point for plant comparative genomics. *Nucleic Acids Research*, 43(D1). <https://doi.org/10.1093/nar/gku986>
- Rambla, J. L., Vera-Sirera, F., Blázquez, M. A., Carbonell, J., & Granell, A.** (2010). Quantitation of biogenic tetraamines in *Arabidopsis thaliana*. *Analytical Biochemistry*, 397(2). <https://doi.org/10.1016/j.ab.2009.10.013>
- Romani, F., Reinheimer, R., Florent, S. N., Bowman, J. L., & Moreno, J. E.** (2018). Evolutionary history of HOMEODOMAIN LEUCINE ZIPPER transcription factors during plant transition to land. *New Phytologist*, 219(1), 408–421. <https://doi.org/10.1111/nph.15133>
- Sarrion-Perdigones, A., Falconi, E. E., Zandalinas, S. I., Juárez, P., Fernández-del-Carmen, A., Granell, A., & Orzaez, D.** (2011). GoldenBraid: An iterative cloning system for standardized assembly of reusable genetic modules. *PLoS ONE*, 6(7). <https://doi.org/10.1371/journal.pone.0021622>
- Schiestl, R. H., & Gietz, R. D.** (1989). High efficiency transformation of intact yeast cells using single stranded nucleic acids as a carrier. *Current Genetics*, 16(5–6). <https://doi.org/10.1007/BF00340712>
- Siebers, T., Catarino, B., & Agusti, J.** (2017). Identification and expression analyses of new potential regulators of xylem development and cambium activity in cassava (*Manihot esculenta*). *Planta*, 245(3). <https://doi.org/10.1007/s00425-016-2623-2>



- Solé-Gil, A., Hernández-García, J., López-Gresa, M. P., Blázquez, M. A., & Agustí, J.** (2019). Conservation of thermospermine synthase activity in vascular and non-vascular plants. *Frontiers in Plant Science*, 10. <https://doi.org/10.3389/fpls.2019.00663>
- Takahashi, T., & Kakehi, J. I.** (2010). Polyamines: Ubiquitous polycations with unique roles in growth and stress responses. In *Annals of Botany* (Vol. 105, Issue 1). <https://doi.org/10.1093/aob/mcp259>
- Takano, A., Kakehi, J. I., & Takahashi, T.** (2012). Thermospermine is not a minor polyamine in the plant kingdom. In *Plant and Cell Physiology* (Vol. 53, Issue 4). <https://doi.org/10.1093/pccp/pcs019>
- Teuber, M., Azemi, M. E., Namjohan, F., Meier, A. C., Wodak, A., Brandt, W., & Dräger, B.** (2007). Putrescine N-methyltransferases - A structure-function analysis. *Plant Molecular Biology*, 63(6). <https://doi.org/10.1007/s11103-006-9126-7>
- Vasco, A., Smalls, T. L., Graham, S. W., Cooper, E. D., Wong, G. K. S., Stevenson, D. W., Moran, R. C., & Ambrose, B. A.** (2016). Challenging the paradigms of leaf evolution: Class III HD-Zips in ferns and lycophytes. *New Phytologist*, 212(3). <https://doi.org/10.1111/nph.14075>
- Vera-Sirera, F., De Rybel, B., Úrbez, C., Kouklas, E., Pesquera, M., Álvarez-Mahecha, J. C., Minguet, E. G., Tuominen, H., Carbonell, J., Borst, J. W., Weijers, D., & Blázquez, M. A.** (2015). A bHLH-Based Feedback Loop Restricts Vascular Cell Proliferation in Plants. *Developmental Cell*, 35(4), 432–443. <https://doi.org/10.1016/j.devcel.2015.10.022>
- Vuosku, J., Karppinen, K., Muilu-Mäkelä, R., Kusano, T., Sagor, G. H. M., Avia, K., Alakärppä, E., Kestilä, J., Suokas, M., Nickolov, K., Hamberg, L., Savolainen, O., Häggman, H., & Sarjala, T.** (2018). Scots pine aminopropyltransferases shed new light on evolution of the polyamine biosynthesis pathway in seed plants. *Annals of Botany*, 121(6). <https://doi.org/10.1093/aob/mcy012>
- Wood, T. E., Takebayashi, N., Barker, M. S., Mayrose, I., Greenspoon, P. B., & Rieseberg, L. H.** (2009). The frequency of polyploid speciation in vascular plants. *Proceedings of the National Academy of Sciences of the United States of America*, 106(33). <https://doi.org/10.1073/pnas.0811575106>
- Yamamoto, M., & Takahashi, T.** (2017). Thermospermine enhances translation of SAC51 and SACL1 in Arabidopsis. *Plant Signaling & Behavior*, 12(1), e1276685. <https://doi.org/10.1080/15592324.2016.1276685>



CHAPTER 2

The role of *C3HDZ*,
ACL5 and *SACL* genes
in *M. polymorpha*

The work described in **Chapter 1** confirms that the main elements of the genetic circuit that regulates vascular cell proliferation are conserved at least in all land plants. Our *in silico* analysis suggests that transcriptional regulation of *ACL5* by C3HDZ might be ancestral to all land plants, but the study of Tspm-sensitive uORFs in the 5'-leader sequence of *SACL* transcripts suggests that *ACL5* (or Tspm) would regulate *SACL* function only in tracheophytes. However, these ideas require further experimental evidence, which we planned to achieve using the liverwort *M. polymorpha*.

Previously published studies have shown that certain parts of the module that regulates vascular cell proliferation in *A. thaliana* are functionally conserved in *M. polymorpha*. First, it has canonical auxin signaling (Flores-Sandoval et al., 2015; Kato et al., 2015), which, in angiosperms, is required for the activation of C3HDZ and *ACL5* responses in vascular development (Baima et al., 2014; Milhinhos et al., 2013). However, MpLHW and MpTMO5 do not share downstream regulation –which might be explained by the missing ACT-like domain in MpLHW (Lu et al., 2020).

In this chapter we will perform a functional analysis of MpC3HDZ, MpACL5 and MpSACL genes in the liverwort *M. polymorpha*, through a combination of two approaches: (i) analysis of the expression pattern and the regulation of promoter- β -GLUCURONIDASE (GUS) fusions or protein-citrine (Cit) fusions for the three genes; and (ii) genetic analysis of gain and loss of function mutants in each of the three genes. These experiments will allow to describe how MpC3HDZ and auxin can upregulate MpACL5, and together influence growth in the gametophyte; while MpSACL regulates the development of epidermal structures through another bHLH TF, MpRSL1. Together, our results suggest that the C3HDZ-ACL5-SACL module has undergone divergent evolutionary trajectories in bryophytes and tracheophytes.



RESULTS AND DISCUSSION

MpC3HDZ and MpACL5 expression overlap in apical notches, where MpSACL is excluded

GUS lines were generated as described in Materials of this chapter. We analyzed two independent promoter-fusion lines for *proMpC3HDZ::GUS* (2 and 6). MpC3HDZ promoter activity was consistent in both lines and the GUS signal was found at the apical notches and midribs (see Glossary) in adult 21-day-old plants (**Figure 1 A and B**). We did not observe any GUS signal in mature dormant gemmae or in gemma cups (**Figure 1 C and D**, respectively).

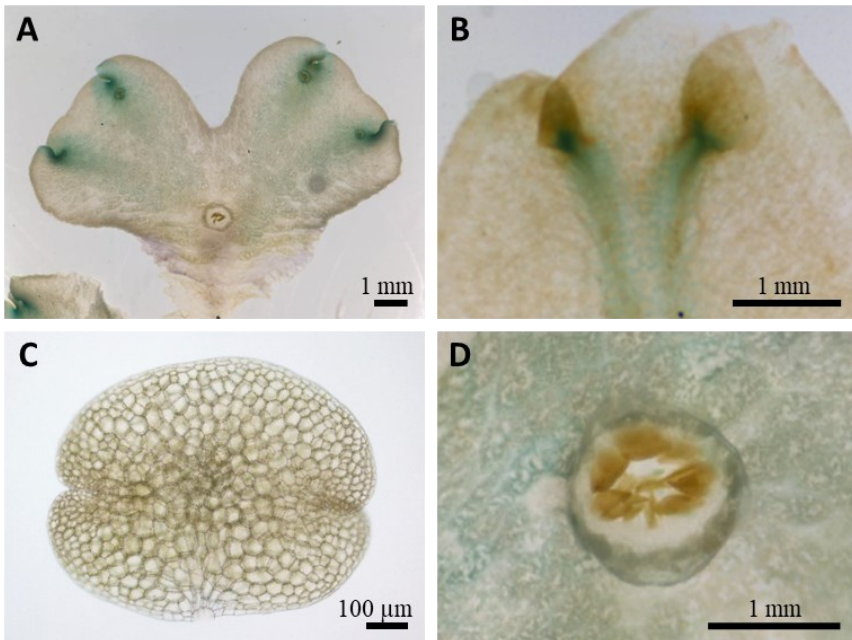


Figure 1. MpC3HDZ promoter is active in apical notches in adult plants. Expression analysis of *proMpC3HDZ::GUS-2* during *M. polymorpha* vegetative development after GUS staining. **A**, thallus; **B**, close view of apical notch regions; **C**, mature dormant gemma; **D**, gemma cup.



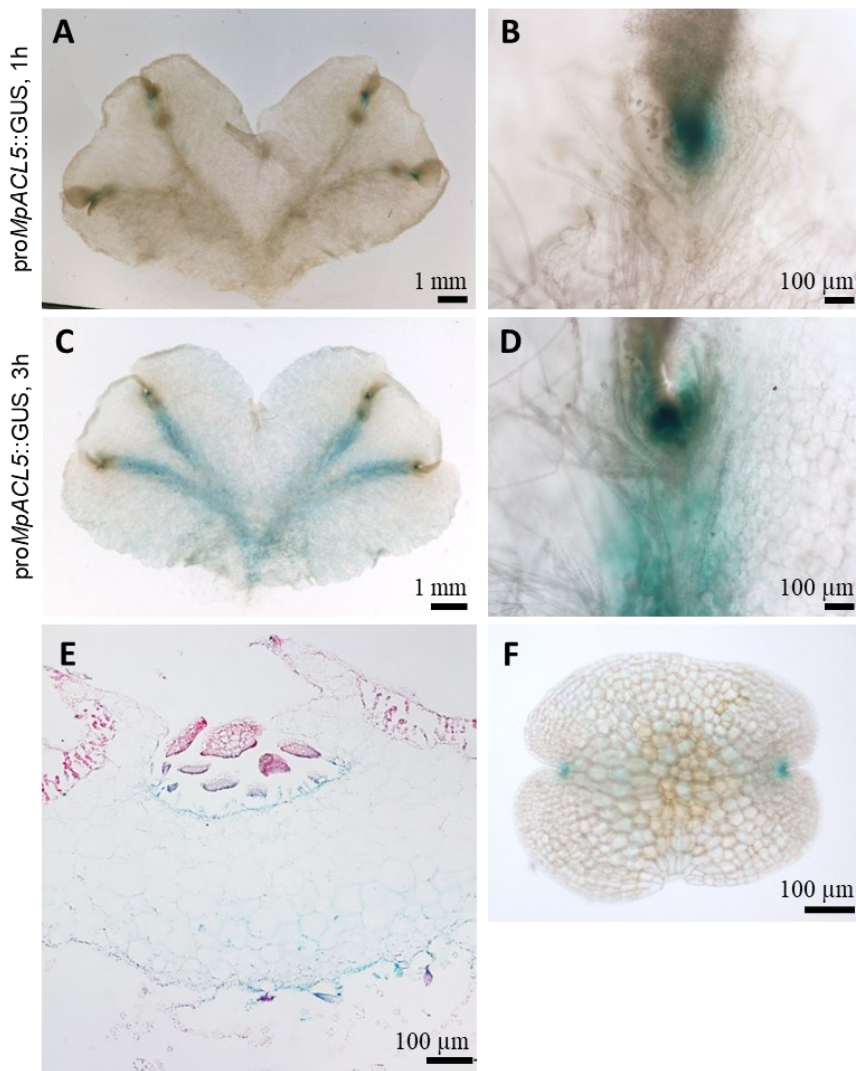


Figure 2. *MpACL5* promoter is active in apical notches, midribs and base of gemma cups. Expression analysis of *proMpACL5::GUS-8* during *M. polymorpha* gametophyte development with GUS staining. **A, B:** thallus (**A**) and close view of apical notches (**B**) of 21-day-old *M. polymorpha* gemmalings after 1 hour of GUS staining; **C, D:** thallus (**C**) and close view of apical notches (**D**) of 21-day-old *M. polymorpha* gemmalings after 3 hours of GUS staining; **E,** cross section of gemma cup after 3 hours of GUS staining; **F,** mature dormant gemmae after 1 hour of GUS staining.



To examine MpACL5 promoter activity, we analyzed three independent lines (*proMpACL5::GUS*-6, -8, and -11). The most intense GUS signal for MpACL5 promoter was observed at apical notches in adult plants and gemmae (**Figure 2 A, B, D, and F**). After the plants were left in the staining solution for a longer time, we could observe a strong GUS signal at the midrib and base of gemma cups, as well as in the apical notch (**Figure 2 C-E**). The expression at the base of gemma cups suggested that MpACL5 might be required for gemmae development, so we characterized MpACL5 localization with several protein fusion lines that allowed a better cellular resolution: *proMpACL5::MpACL5:citrine-1*, -2 and -3. The signal appeared very early during gemmae development and was visible in whole gemmae through all developmental stages (**Figure 3 A-C**) until the completion of gemma formation, when the signal was restricted to the apical notches (**Figure 3D**).

The expression of MpSACL was, on the other hand, mostly absent from apical notches. By analyzing two *proMpSACL::GUS* lines (2 and 6), we observed that the GUS signal accumulated in an irregular pattern all through the 21-day-old thallus (**Figure 4 A and B**), and was especially strong in developing gemma cups (**Figure 4C**), but not at the base of gemma cups (unlike the observed signal in MpACL5 marker lines). We found no GUS signal at the apical notch or mature dormant gemmae (**Figure 4 B and D** respectively).

To complement the information obtained from the marker lines, we performed a Retro-Transcribed Quantitative Real Time Polymerase Chain Reaction (RT-qPCR) analysis for the three genes in dissected regions of 21-day-old gemmalings (**Figure 5**). MpC3HDZ and MpACL5 expressions were the highest at the apical notches, although MpACL5 transcript was also found in intermediate zones (which include the midrib and young gemma cups). MpSACL expression, in turn, was higher at intermediate zones, followed by mature thallus tissues, and its expression was diminished in apical notches. Taken together, the RT-qPCR results are in line with the promoter activity patterns inferred from the analysis of the reporter lines.



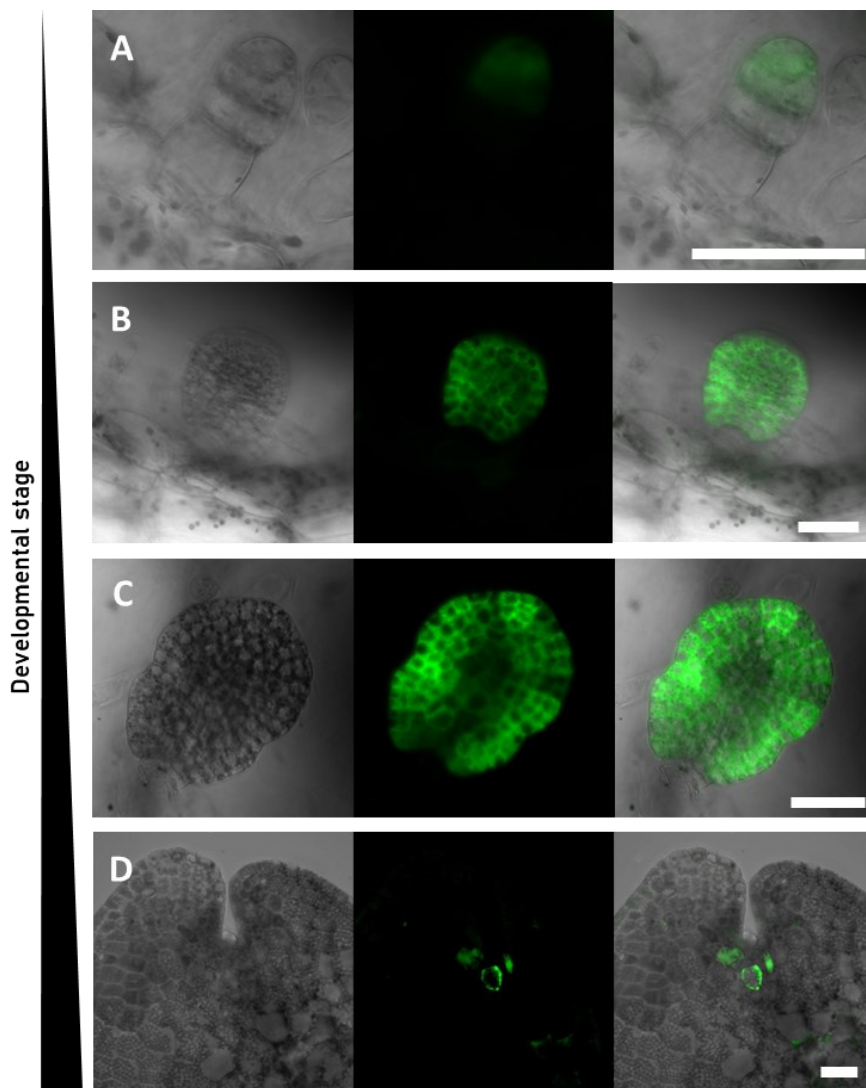


Figure 3. MpACL5 localizes in developing gemmae and shifts towards apical notches in mature dormant gemmae. Expression of *proMpACL5::MpACL5:citrine (Tak-1)-1* during gemmae development. **A**, 2-cell stage, showing citrine accumulation at the most apical cell in the gemma primordia; **B** and **C**, advanced pluricellular gemmae under development showing MpACL5:citrine accumulation in the whole gemma body; **D**, mature dormant gemmae showing MpACL5:citrine accumulation in the apical merophytes. White scale bars represent 50 μm .



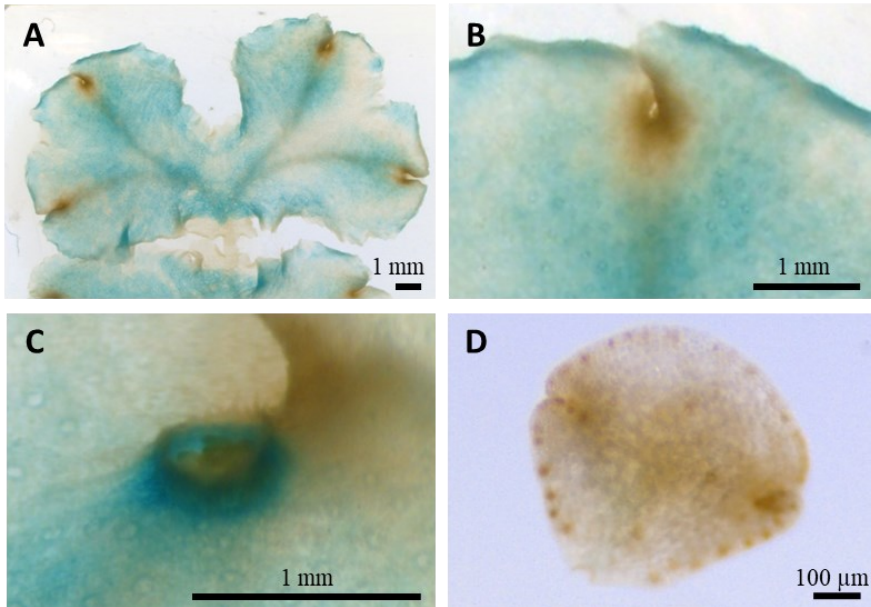


Figure 4. MpSACL promoter is active in epidermal tissues and developing gemma cups, but it is excluded from the apical region. Expression analysis of *proMpSACL::GUS-2* during *M. polymorpha* gametophyte development. **A**, thallus; **B**, close view of apical notch regions; **C**, early gemma cup; **D**, mature dormant gemma

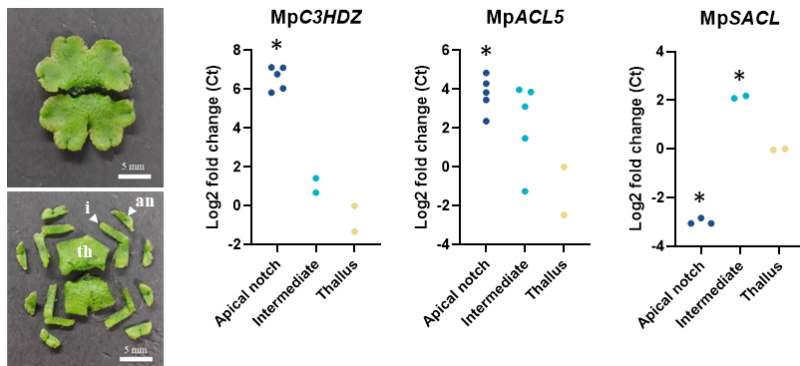


Figure 5. Analysis of MpC3HDZ, MpACL5 and MpSACL transcript abundances in *M. polymorpha* gametophyte tissues: apical notch, thallus, and intermediate zones. Tissue collection for RNA extraction is represented in the pictures and white arrowheads indicate



Continuation Figure 5.

the apical notch (an), intermediate zones (i), and thallus (th). RNA extraction was performed using several pools of these tissues as biological replicates; RT-qPCR were performed in these replicates with a minimum of n=2 and a maximum of n=5. The relative fold-expressions of MpC3HDZ, MpACL5 and MpSACL are shown as Log₂ fold-change of Ct using the "Thallus" values as reference. Asterisks mark statistical significance (p<0.05).

In summary, the expression patterns of MpC3HDZ and MpACL5 clearly overlap in the apical notches, which is consistent with a molecular interaction between these two genes in *M. polymorpha*. MpSACL, in turn, would remain excluded from this region; nevertheless, its ubiquitous expression at the rest of the mature thallus does not exclude the midrib zone, where MpACL5 promoter is active, and is therefore a tissue that could host a putative molecular interaction between MpACL5 and MpSACL. However, this interaction is unlikely, since MpSACL 5' leader does not harbor the Tspm-sensitive uORF.

MpC3HDZ is a fundamental regulator of meristematic activity

The role of C3HDZ TFs with respect to apical growth and dorsoventral patterning has been profusely studied in tracheophytes, especially in seed plants (Carlsbecker et al., 2010; Emery et al., 2003; Floyd et al., 2006; Ilegems et al., 2010; McConnell et al., 2001; Prigge & Clark, 2006b; Ramachandran et al., 2017). However, C3HDZ orthologs in the moss *P. patens* regulate phyllid development instead (Yip et al., 2016), which indicates that not all roles of C3HDZ are necessarily conserved between bryophytes and tracheophytes. To determine C3HDZ function in the liverwort *M. polymorpha*, we analyzed a T-DNA insertion mutant at the exon 6 of MpC3HDZ, *Mpc3hdz* (**Figure 6**) and generated two gain of function lines that constitutively express MpC3HDZ fused to citrine (*EF1::MpC3HDZ:citrine-2* and *-4*). We used a 526-bp region containing exons 4 to 7 and part of the third and eighth exons to quantify the MpC3HDZ transcripts in a semi-quantitative PCR from cDNA. As expected, the gain of function lines displayed a higher abundance of the MpC3HDZ transcript, while *Mpc3hdz* showed lower transcript abundance compared to Tak-1 (**Figure 6A**). However, the semi-quantitative PCR results revealed the presence of two bands in *Mpc3hdz* extracts that did not match the size of the Tak-1

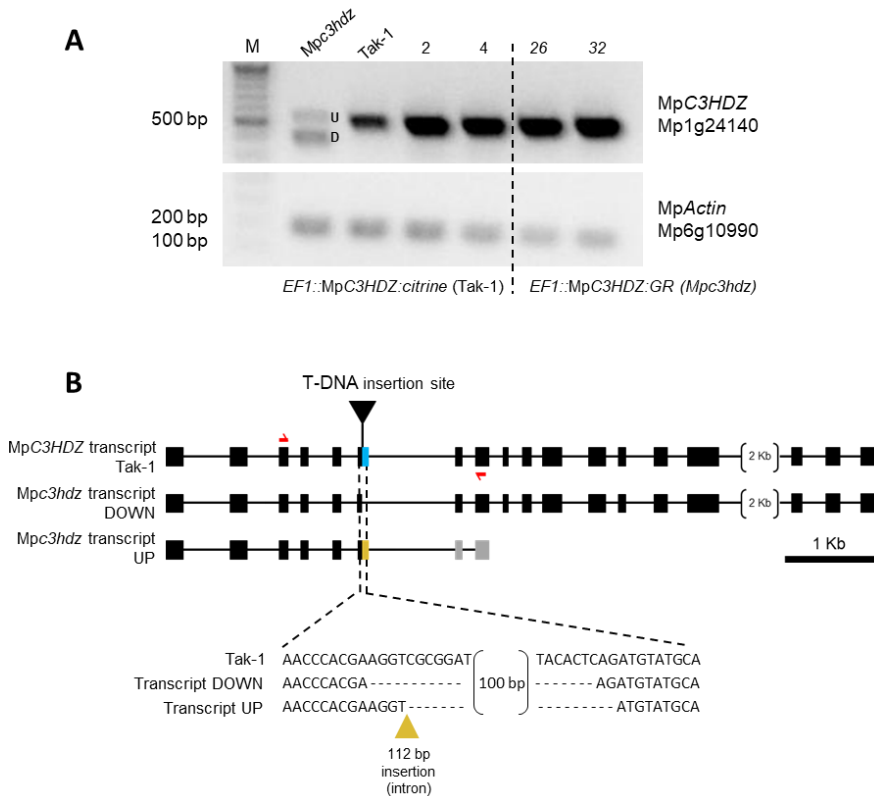


Figure 6. Genetic characterization of MpC3HDZ loss and gain of function mutations. A, Semi-quantitative PCR of MpC3HDZ transcript in *Mpc3hdz*, *Tak-1*, *EF1::MpC3HDZ:citrine-2* and *-4*, and *EF1::MpC3HDZ:GR (Mpc3hdz)-26* and *-32* at 28 cycles. MpActin (Mp6g10990) was used as a reference gene. **B,** Graphic representation of MpC3HDZ transcripts for *Tak-1* and the two versions in *Mpc3hdz* mutant, showing the site of T-DNA insertion. Thick black boxes indicate wild type exons, while thin lines indicate introns. Blue thick box marks the sequence lost in both *Mpc3hdz* transcripts; yellow thick box represents the 112 bp insertion in the “UP” version of *Mpc3hdz* transcript; grey thick boxes represent a change in frame prior to the premature STOP in *Mpc3hdz* “DOWN” transcript version. Red lines indicate the binding site of the primers used for semi-quantitative PCR. The region englobing the blue box is represented to illustrate the sequence changes in both *Mpc3hdz* transcript versions. , M, 100 bp plus ladder; U, UP; D, DOWN; Kb, Kilobase; bp, base pairs.



or gain of function lines. After sequencing and subsequently performing a Nucleotide Basic Local Alignment Search (BLAST) to *M. polymorpha* genome, we confirmed that both bands were from different versions of MpC3HDZ transcripts, likely caused by the T-DNA insertion (**Figure 6B**).

Both loss and gain of function mutants displayed stunted growth and other major defects in the thallus structure (**Figure 7**). *EF1::MpC3HDZ:citrine* lines developed a pale, narrow and irregular thallus that bent upwards, probably due to excessive ventral tissue formation (**Figure 7 C and F**). However, the thallus conserved the bilateral symmetry, and structures like apical notches, ventral scales, gemma cups or rhizoids were recognizable (**Figure 7 C and F**). The severity of the defective phenotype correlated with the level of overexpression of MpC3HDZ in each of the lines (3.5x and 10.2x, respectively in lines 2 and 4).

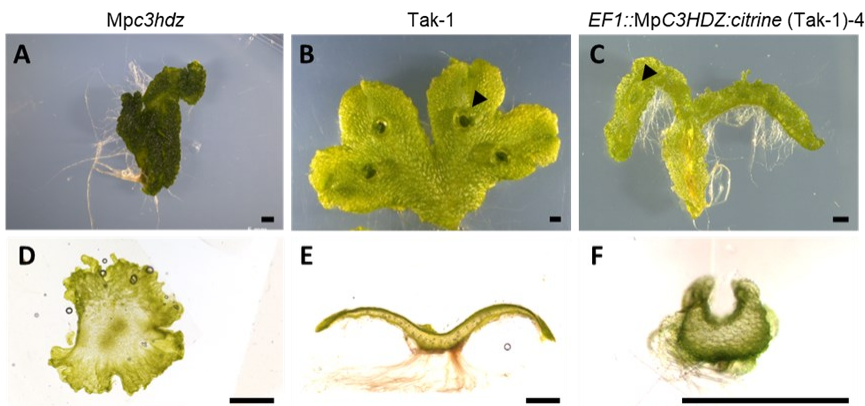


Figure 7. MpC3HDZ regulates meristem identity and dorsoventral patterning. Overview of MpC3HDZ loss- and gain of function phenotypes during vegetative development. **A-C**, Thallus of 21-day-old plants of *Mpc3hdz* (**A**), *Tak-1* (**B**) and *EF1::MpC3HDZ:citrine-4* (**C**). Due to lack of gemma production in the *Mpc3hdz* line, the picture shows thallus recovery after 21 days from the excision of an apical region. Black arrowheads indicate gemma cups. **D-F**, cross sections of the thallus of *Mpc3hdz* (**D**), *Tak-1* (**E**) and *EF1::MpC3HDZ:citrine-4* (**F**). Scale bars: 1 mm.

Mpc3hdz thallus, on the contrary, displayed a significant dorsal dominance. It was dark green, perhaps due to an enhanced production of photosynthetic cells, which are produced mostly in the adaxial part of the thallus in the wild type and can be observed in cross-sections (**Figure 7 A and B, D and E**). This mutant also showed excessive cell proliferation and multidirectional growth; it resulted in an irregular circular-shaped thallus with unrecognizable apical notches instead of the flat bilateral thallus in the wild type with distinguishable notches (**Figure 7 B and E**). The *Mpc3hdz*

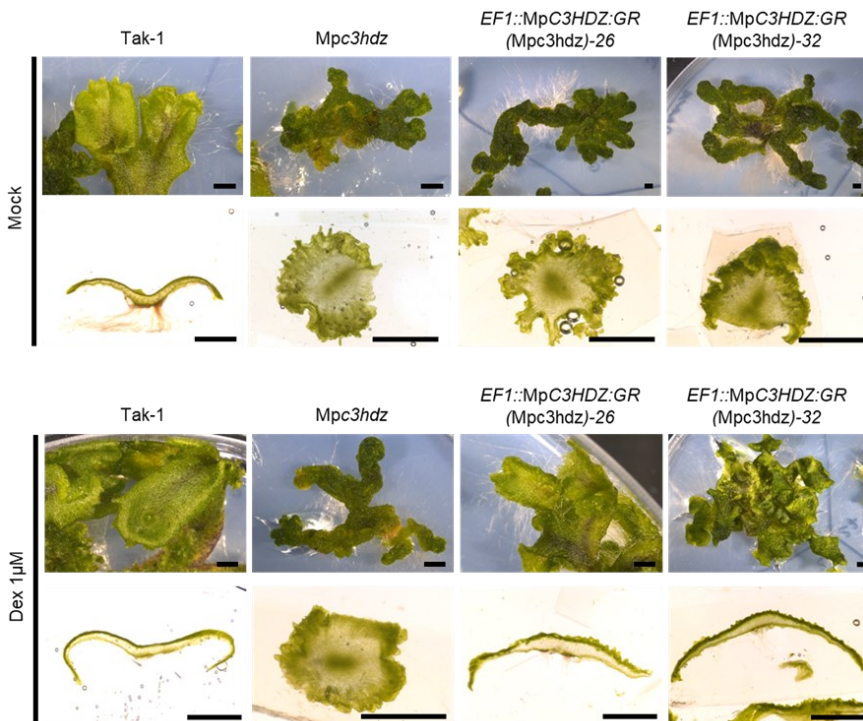


Figure 8. *Mpc3hdz* phenotype is alleviated by conditional constitutive expression of *MpC3HDZ*. Recovery of *EF1::MpC3HDZ:GR (Mpc3hdz)-26* and *-32* lines after 45 days in mock or 1 µM dexamethasone treatments with Tak-1 and *Mpc3hdz* mutant for reference. Pictures display the top view of *M. polymorpha* plants (top) and fresh cross-sections from plants from the same plate (bottom). Scale bars: 2 mm. Dex, dexamethasone; µM, micromolar; mm, millimeters



mutant did not develop any gemmae or gemma cups and had reduced rhizoid production. This defective phenotype was alleviated when *Mpc3hdz* was complemented with inducible ectopic expression of *MpC3HDZ* (**Figure 8**). We analyzed two independent *EF1::MpC3HDZ:GR* (*Mpc3hdz*) lines (-26 and -32). In both lines, *MpC3HDZ* transcript abundance was higher than in Tak-1 and *Mpc3hdz* (**Figure 6A**). After forty-five days in the presence of Dexamethasone (Dex), the newly developed thalli recovered the bilateral symmetry; rhizoids were produced, and apical notch-like structures were distinguishable (**Figure 8**). We could also observe *de novo* gemma cup formation with active gemmae development; however, gemma cups were produced less frequently and only in the *EF1::MpC3HDZ:GR* (*Mpc3hdz*)-26 line. These observations confirmed that the loss of function mutant phenotype was due to *MpC3HDZ* disrupted function in the *Mpc3hdz* mutant.

As a summary, we have provided evidence of *MpC3HDZ* involvement in apical growth, meristem identity, and dorsoventral patterning in the gametophyte of *M. polymorpha*. However, while C3HDZ TFs in tracheophytes are reported as a dorsalizing factor (Emery et al., 2003; Izhaki & Bowman, 2007; McConnell et al., 2001; Ramachandran et al., 2017; Vasco et al., 2016), our phenotypic analysis reveals that *MpC3HDZ* promotes ventralization in *M. polymorpha*. Given that the *MpC3HDZ* promoter is almost exclusively active in the apical notches, the observation that the loss of function mutations repercute in the whole thallus structure can have at least one of these three explanations: either (i) *MpC3HDZ* can move from the apical notches towards non-meristematic tissues; (ii) *MpC3HDZ* functions non-cell-autonomously from the apical notches, or (iii) the cell fate is established after a few divisions of the apical cell and merophytes in the gametophyte of *M. polymorpha*, inside *MpC3HDZ* domain.

Another implication of our results is that C3HDZ regulate apical growth in bryophytes, which is in contrast with previous analyses in a moss, *P. patens*, that suggest that C3HDZ do not regulate apical growth or patterning in bryophytes (Yip et al., 2016). Thus, we envision two possible scenarios: (i) apical meristem regulation by C3HDZ is an ancestral trait that was lost in mosses; or (ii) some or all liverworts, as well as tracheophytes, co-opted (see Glossary) C3HDZ for apical regulation in two

independent events. Given that the function of C3HDZ in *P. patens* is still required for a lateral determinate meristem in the gametophyte, the most parsimonious option would be the former. Future studies regarding C3HDZ function in other model bryophytes, such as *A. agrestis*, would be key to infer the role of C3HDZ in the land plant common ancestor.

Tspm is a positive regulator of meristem growth in the gametophyte of *M. polymorpha*

M. polymorpha contains a functional Tspm synthase, MpACL5, and polyamine quantifications confirm the presence of Tspm in the gametophyte (**Chapter 1**). To investigate the function of Tspm in this species, we generated two loss of function mutants with CRISPR-Cas9 technology: *Mpac15-4*, with a 2 bp deletion at the exon 1 that led to a premature STOP codon at the beginning of exon 2; and *Mpac15-13*, with a partial deletion in exon 1 that led to a premature STOP codon at exon 3 (**Figure 9**). We also generated two gain of function mutants in the Tak-1 background, namely *EF1::MpACL5:citrine-1* and *-20*.



Figure 9. Characterization of *MpACL5* loss of function mutants. Graphic representation of *MpACL5* transcripts for Tak-1, *Mpac15-4*, and *Mpac15-13* mutants. Thick black boxes indicate exons, while thin lines indicate introns. Blue arrowheads mark the sites for the 2 bp deletion and premature STOP of the *Mpac15-4* mutant, and yellow arrowheads mark the sites for the 82 bp deletion and premature STOP of the *Mpac15-13* mutant. The gRNA region is represented below, illustrating the different modifications. Pink box marks the PAM region. Bp, base pairs.



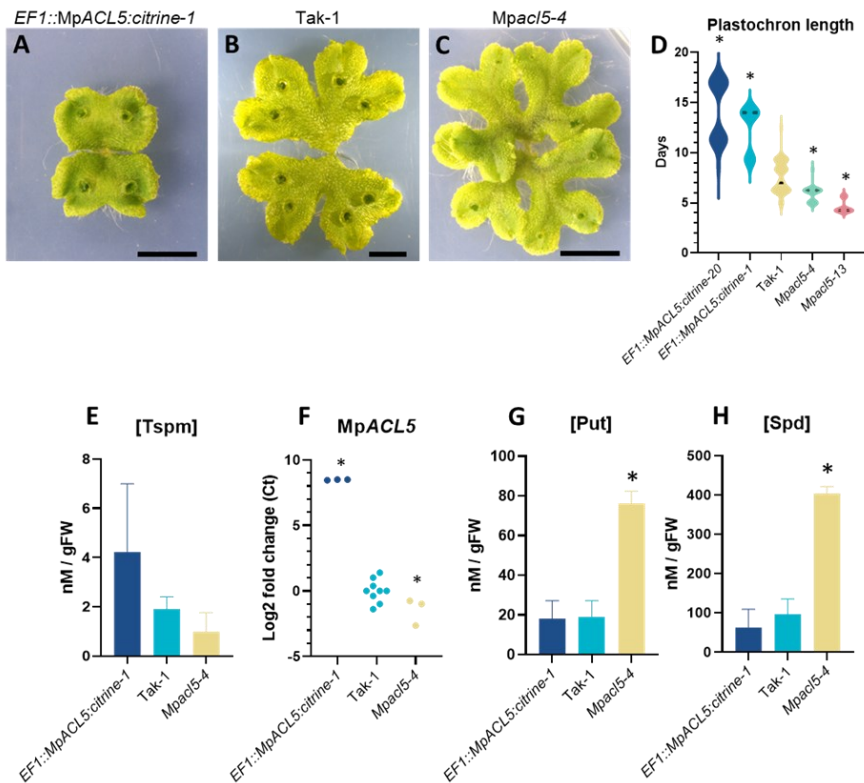


Figure 10. MpACL5 regulates plastochron length and correlates with Tspm levels in *M. polymorpha*. Overview of MpACL5 loss- and gain of function phenotypes during *M. polymorpha* gametophyte development. **A-C**, Thalli in 28-day-old plants of *EF1::MpACL5:citrine-1* (**A**) *Tak-1* (**B**) and *MpacI5-4* (**C**). Scale bars represent 5mm. **D**, Plastochron measurements after 21 days in gain and loss of function *MpACL5* mutants ($12 \leq n \leq 79$). **E**, Tspm quantification by HPLC ($n = 2$). **F**, Relative fold-expression of *MpACL5* transcript abundance ($3 \leq n \leq 9$). **G-H**, Put and Spd quantifications by HPLC, respectively ($n = 2$). Asterisks mark statistical significance ($p < 0.05$). nM, nanomoles; gFW, grams of fresh weight.

Loss- and gain of function lines clearly differed in growth rate compared to *Tak-1* (**Figure 10 A-C**). In *M. polymorpha* and other species with dichotomous branching, growth dynamics can be expressed through the plastochron (see Glossary), which indicates the time that the apical meristem takes to fulfill each

dichotomous bifurcation. The plastochron averaged 7.58 days in Tak-1 in our conditions (**Figure 10D**), which agrees with previously reported values (Solly et al., 2017). Our gain of function lines had a significantly longer plastochron with an average of 12.36 days for line 1 and 14.03 days for line 20, while loss of function lines were characterized by a shorter plastochron of 5.93 days for line 4 and 4.60 days for line 13 (**Figure 10D**).

Since the plastochron was consistently longer in both gain of function lines and shorter in loss of function lines, we used *EF1::MpACL5:citrine-1* and *Mpac5-4* for all subsequent experiments. We performed polyamine quantifications by HPLC in those lines. Tspm abundance correlated directly with MpACL5 transcript levels quantified by RT-qPCR, as well with plastochron length (**Figure 10 D-F**). We were not able to detect Spm in any of the measurements; however, Put and Spd levels increased significantly in *Mpac5-4*, although no significant changes were observed in the *EF1::MpACL5:citrine-1* line in regard to Put and Spd content (**Figure 10 G and H**). Considering that Put and Spd precede Tspm in the polyamine biosynthesis pathway, their increased levels in *Mpac5-4* are perhaps a consequence of a reduction in Tspm production. Nevertheless, to establish which polyamine may be relevant for plastochron regulation, we treated Tak-1 plants with 100 μ M Put, 100 μ M Spd, the combination of 100 μ M Put+Spd, or 100 μ M Tspm and measured the plastochron after 7 days. Tak-1 maintained the same plastochron length as in mock conditions in Put and Spd treatments; however, in high Tspm the plastochron was significantly increased (**Figure 11**), which agrees with the idea that the plastochron defects in the mutants are a consequence of differential Tspm concentration.

Based on the apical notch expression and the defects on plastochron, we hypothesized that MpACL5, and therefore Tspm, delay growth by repressing cell divisions in the apical notch. To investigate the relevance of MpACL5 for cell division in *M. polymorpha*, we performed a 5-ethynyl-2'-deoxyuridine (EdU) assay in Tak-1, *EF1::MpACL5:citrine-1* and *Mpac5-4*. For this experiment, we collected mature dormant gemmae that were subsequently EdU-labelled after one day of growth, which was sufficient to document growth in our conditions (see Materials for details). In Tak-1 gemmae, most of the S-phase cells (see Glossary) were found in the apical



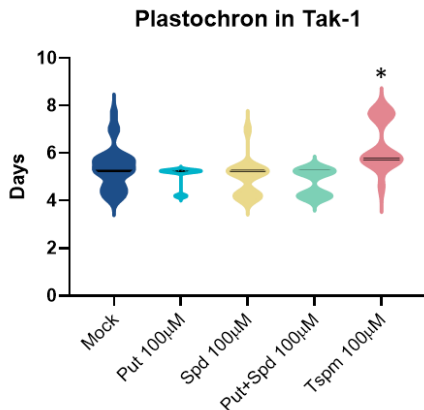
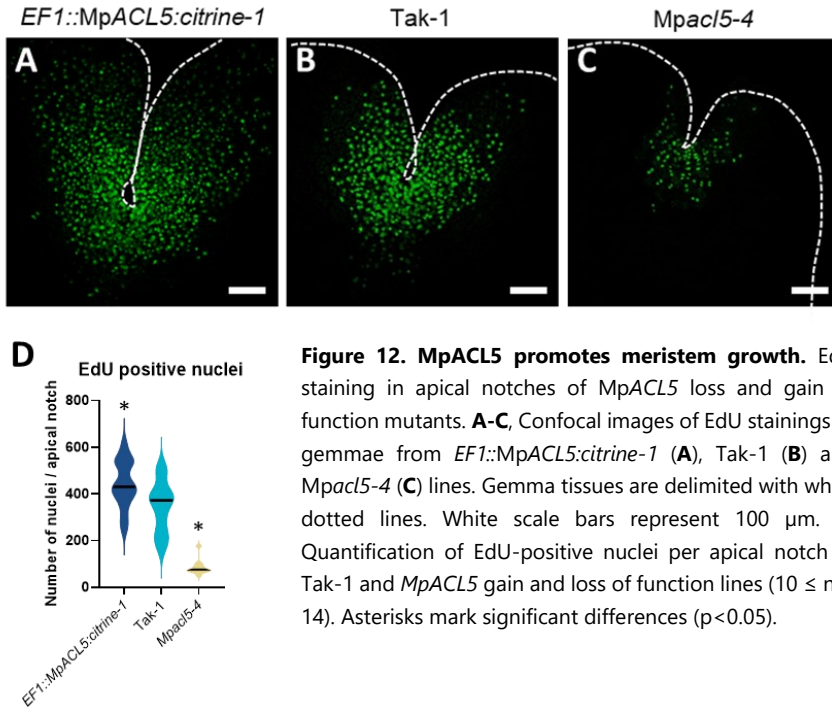


Figure 11. Tspm is the only polyamine that influences plastochron length. Plastochron measurements in Tak-1 after 7 days of mock, 100 µM Put, 100 µM Spd, 100 µM Put + Spd, or 100 µM Tspm ($11 \leq n \leq 27$). Asterisks mark significant differences ($p < 0.05$). Spd, Spermidine; Put, Putrescine; Tspm, Thermospermine; µM, micromolar.

notch (**Figure 12B**). The area of EdU-positive nuclei was circular and extended into the center of the gemmae and the lobes next to the apical notch. In comparison, *EF1::MpACL5:citrine-1* had a significant increase of EdU-labelled nuclei comprised in a much wider area (**Figure 12 A and D**). *Mpac15-4* line, in turn, had fewer S-phase cells that were included in a much smaller area than Tak-1 (**Figure 12 C and D**). These results can be interpreted in at least two ways: (i) MpACL5 promotes cell divisions and there is an inverse correlation between cell divisions and meristem bifurcation, so that a slower cell division rate (in *Mpac15* mutants) is interpreted as a signal to induce bifurcation; or (ii) MpACL5 is an inhibitor of bifurcation but does not target cell divisions, in which case the reduction in EdU-labelled cells in the *Mpac15* mutant is a secondary consequence of precocious splitting of one meristem into two new meristems.

In support of the second interpretation is the observation that thallus thickness and the number of cell layers below the gemma cups (a structure directly derived from apical notches) is directly correlated with the number of S-phase labelled cells in the meristems (**Figure 13**). In other words, gemma cups in *Mpac15-4*

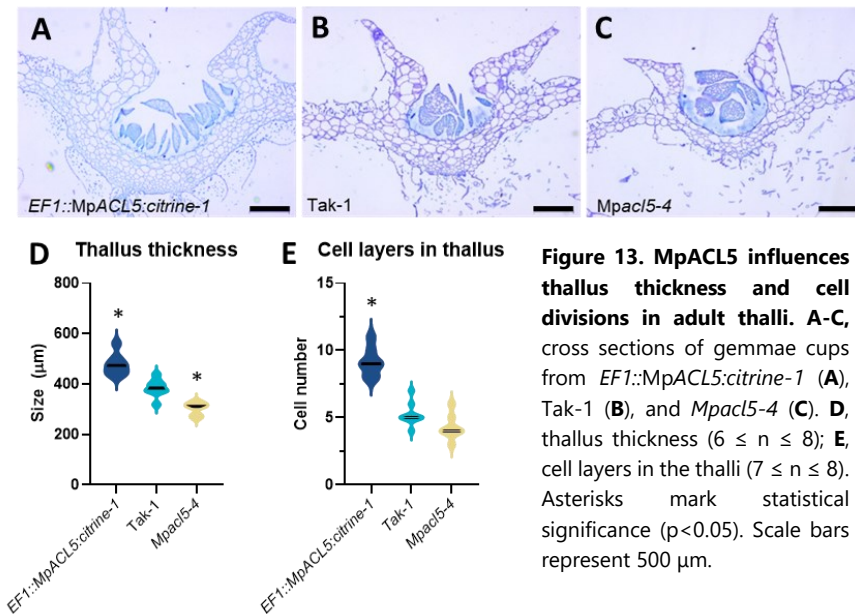




had fewer (and bigger) floor cells than *Tak-1*, whereas *EF1::MpACL5:citrine-1* cups had a higher number of smaller floor cells (**Figure 13 A-C**). And the same happened with the thickness of the thallus and the number of cell layers below the gemma cups (**Figure 13 D-E**).

Given that MpACL5 protein is not only found in apical notches of mature gemmalings, but also throughout the entire gemma during gemmae development, we investigated its possible function on the regulation of cell divisions at that early developmental stage. We performed a cellular profiling analysis of mature dormant gemmae from *Tak-1*, *EF1::MpACL5:citrine-1* and *Mpac15-4* lines and found an inverse correlation between the amount of Tspm and the size of the gemmae (**Figure 14A**). The average cell number was similar in both lines and *Tak-1* (**Figure 14B**), which implies that the differences in gemmae size should be due to differences in cell size.





In *Tak-1*, the smallest cells ($\leq 100 \mu\text{m}^2$) accumulate at the periphery of the gemma, oil bodies (see Glossary), and apical notches, and represent nearly 40% of the epidermal cells. The rest of the cell sizes increase in a continuous distribution that rarely exceeds the $2100 \mu\text{m}^2$, with the largest cells – rhizoid precursor cells – that accumulate at the center of the gemmae (**Figure 14 A** and **C**). Compared to *Tak-1*, cells with sizes up to $100 \mu\text{m}^2$ represented only 25% of the normalized cell number in *Mpacl5-4*, while in *EF1::MpACL5:citrine-1* it was close to 50% (**Figure 14B**). Maximum cell areas were $1500 \mu\text{m}^2$ in *EF1::MpACL5:citrine-1*, and $2500 \mu\text{m}^2$ in *Mpacl5-4*. Notwithstanding, the spatial distribution was as in *Tak-1*, with the smallest cells at the apical notch and peripheral tissues, and the largest cells at the center. These results suggest that *Tspm* plays a role in cell expansion in *M. polymorpha* but is not required for cell divisions during gemmae development.

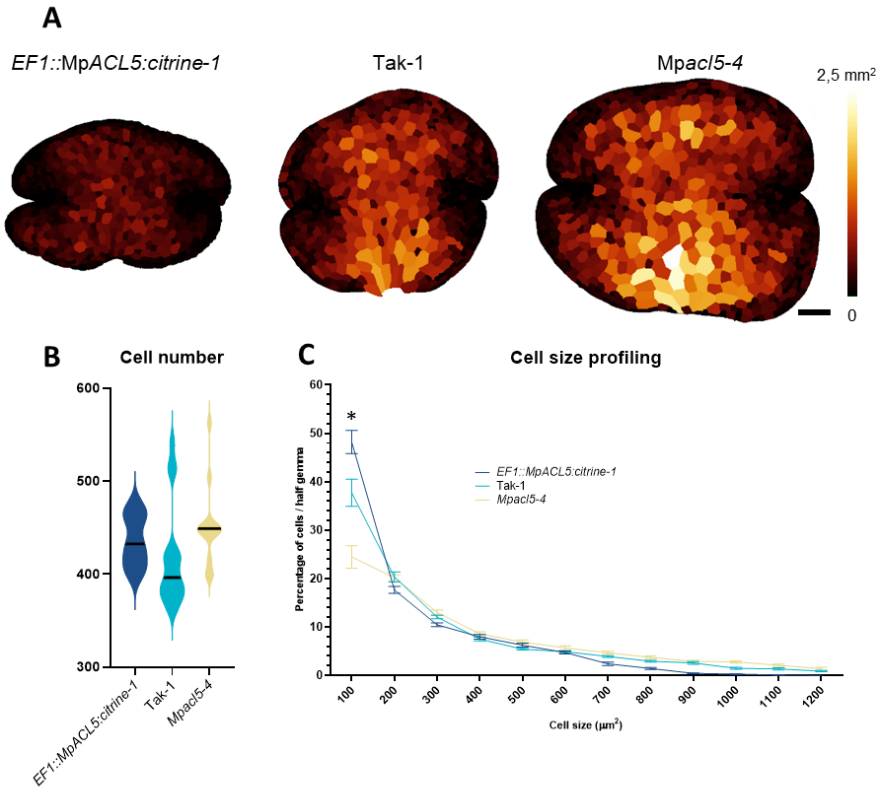


Figure 14. Tspm is a positive regulator of cell size during gemma development. **A**, Cell size distribution in representative mature dormant gemmae of Tak-1 and MpACL5 gain and loss of function lines, based on the cell profiling analysis ($n = 6$). Black scale bar represents 200 μm . **B**, Cell number measurements in Tak-1 and MpACL5 gain and loss of function lines ($6 \leq n \leq 16$). **C**, Proportional cell sizes per gemma in Tak-1 and MpACL5 gain and loss of function lines ($n = 6$). Asterisks mark significant differences ($p < 0.05$).

MpSACL is a negative regulator of rhizoid, mucilage cell and gemma development

In Arabidopsis, SACL TFs inhibit periclinal cell divisions in vascular tissues by disrupting the formation of the AtLHW-AtTMO5 heterodimer (Katayama et al., 2015b;



Vera-Sirera et al., 2015). To investigate the function of MpSACL in *M. polymorpha*, we analyzed two independent loss of function alleles: *Mpsacl-13* and *Mpsacl-16*, with 1 bp insertion and 2 bp deletion at the N-terminus, respectively (**Figure 15**). Both insertions and deletions (INDELs) led to a frameshift with premature STOP codons before the HLH domain, although a RT-qPCR analysis showed a slight, significant increase in MpSACL expression in these lines (**Figure 16A**). We also analyzed two independent gain of function mutants in the Tak-1 background, *EF1::MpSACL:citrine-1* and -2. These lines showed between 23- and 25-fold higher abundance of MpSACL transcript compared to Tak-1 (**Figure 16A**).

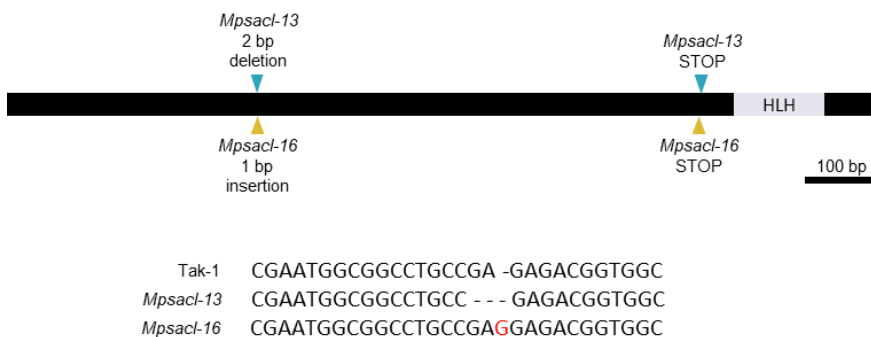


Figure 15. Molecular characterization of *Mpsacl* loss of function mutants. Graphic representation of MpSACL transcripts for Tak-1, *Mpsacl-13* and *Mpsacl-16* mutants. Thick black box indicates the sole exon of MpSACL transcript. Grey box indicates the HLH domain. Blue arrowheads mark the sites for the 2 bp deletion and premature STOP of the *Mpsacl-13* mutant, and yellow arrowheads mark the sites for the 1 bp insertion and premature STOP of the *Mpsacl-16* mutant. The gRNA genetic region is represented below, illustrating the different modifications. bp, base pairs.

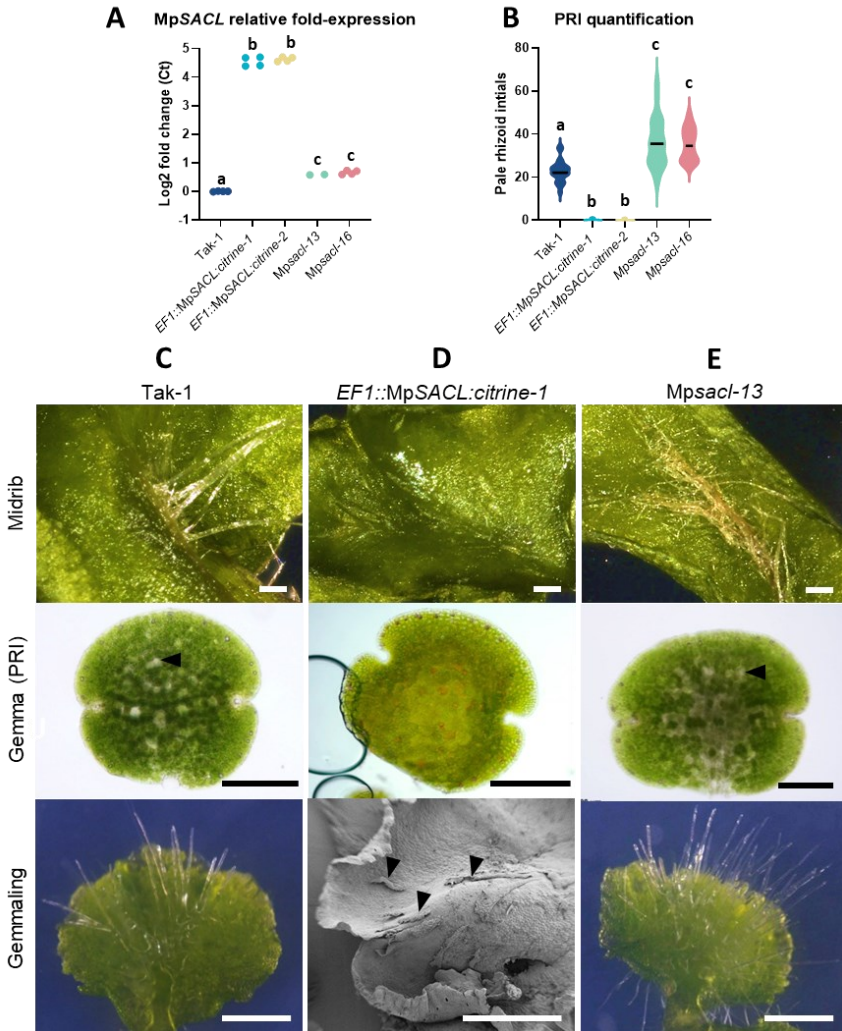


Figure 16. MpSACL is a negative regulator of rhizoid development. **A**, MpSACL fold-expression in Tak-1, MpSACL gain and loss of function mutants measured by RT-qPCR ($2 \leq n \leq 4$). **B**, PRI quantification in Tak-1, MpSACL gain and loss of function mutants ($5 \leq n \leq 22$). Lowercase letters represent statistical significance groups ($p < 0.05$). **C-E**, Tak-1, EF1::MpSACL:citrine-1 and Mpsacl-13 phenotypes in the midrib, gemma and gemmaling with special emphasis on rhizoid development. Gemmalings of EF1::MpSACL:citrine-1 were observed in a Cryo-scanning electron microscope. Black arrowheads indicate pale rhizoid initials. White scale bars represent 1 mm, black scale bars represent 200 μ m.



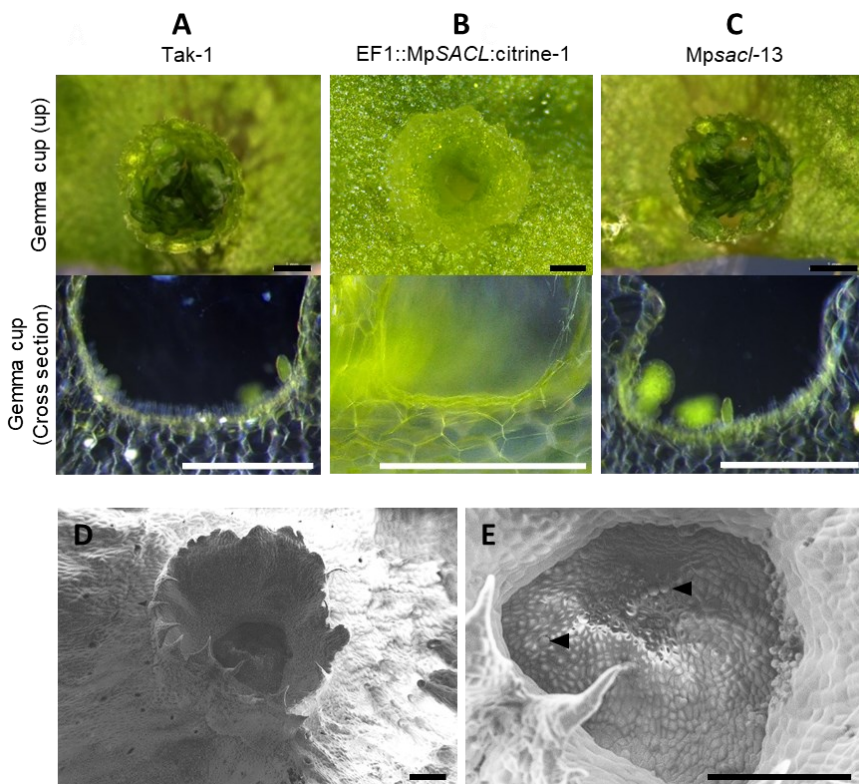


Figure 17. MpsACL is a negative regulator of gemma and mucilage cell development. **A-C**, Top vision of gemma cups and fresh cross sections of gemma cups in 28 day-old plants of *Tak-1* (**A**), *EF1::MpSACL:citrine-1* (**B**) and *Mpsacl-13* (**C**). Mature gemmae were removed to ease visualization of gemma initials and mucilage cells in fresh cross sections. Black scale bars represent 1 mm, white scale bars represent 500 μm. **D, E**, Cryo-FESEM pictures of *EF1::MpSACL:citrine-1* showing empty gemma cups and gemma or mucilage cell initials (black arrowheads). Black scale bars represent 200 μm.

Gain of function mutants had very little to no rhizoid development (**Figure 16 B-D**); in contrast, loss of function mutants displayed increased –although not ectopic– rhizoid production (**Figure 16E**). The primary defect in rhizoid production might be related to the initial acquisition of rhizoid cell identity, since we did not find PRI in mature gemmae of *MpSACL* overexpressors and observed a higher number of PRI in loss of function mutants (**Figure 16B**). Although gain of function mutants had



impaired rhizoid development, ventral scales could be observed in adult plants (**Figure 16D**), which indicates that MpSACL does not regulate the development of these structures.

Although gemmae production was normal in the *Mpsacl* mutant, it was severely impaired in gain of function lines (**Figure 17**). Cross sections of gemma cups showed a severe reduction of mucilage cells in addition to gemma initials (**Figure 17B**), and only in older gemma cups were sometimes gemma or mucilage initials visible (**Figure 17 D and E**).

Our results suggest that MpSACL acts as a negative regulator of rhizoid production, and perhaps of gemmae and mucilage cell development. The fact that this process in particular is affected only in ectopic overexpression lines does not allow to rule out that the impairment of gemmae formation is an artifact due to ectopic MpSACL activity. However, we investigated the possibility of this relevant function. Development of both rhizoid, mucilage cells and gemmae is specifically triggered by activity of the same bHLH TF, MpRSL1 (Honkanen et al., 2018; Proust et al., 2016; Thamm et al., 2020). *Mprsl1* loss of function mutant lines do not produce any rhizoid, mucilage cell or gemma initials, very similarly to our *EF1::MpSACL:citrine* transgenic lines. We hence hypothesized that MpSACL could regulate rhizoid and gemma development through MpRSL1. To test this hypothesis, we analyzed *Mprsl1* loss of function mutants in Tak-1 and *Mpsacl-13* backgrounds to determine whether there is genetic interaction between MpSACL and MpRSL1. We obtained two independent lines for *Mprsl1* in Tak-1 background (*Mprsl1-1* and *Mprsl1-2*), which had a 11 bp deletion and a 1 bp insertion at the first exon, respectively (**Figure 18**). We also obtained two independent double mutant lines *Mpsacl Mprsl1-1*, with a 1 bp insertion and *Mpsacl Mprsl1-2* with a 10 bp deletion at the first exon of MpRSL1 (**Figure 18**). All INDELS led to premature STOP codons before the bHLH domain of MpRSL1. As expected, *Mprsl1* loss of function mutants had reduced rhizoid and mucilage cell production; gemmae development was also severely impaired in Tak-1 background (**Figure 19 A and C**). However, mutating MpSACL was not sufficient to rescue the *Mprsl1* phenotype (**Figure 19 B and D**), which implies that MpRSL1 is epistatic to MpSACL with respect to rhizoid and gemmae development.



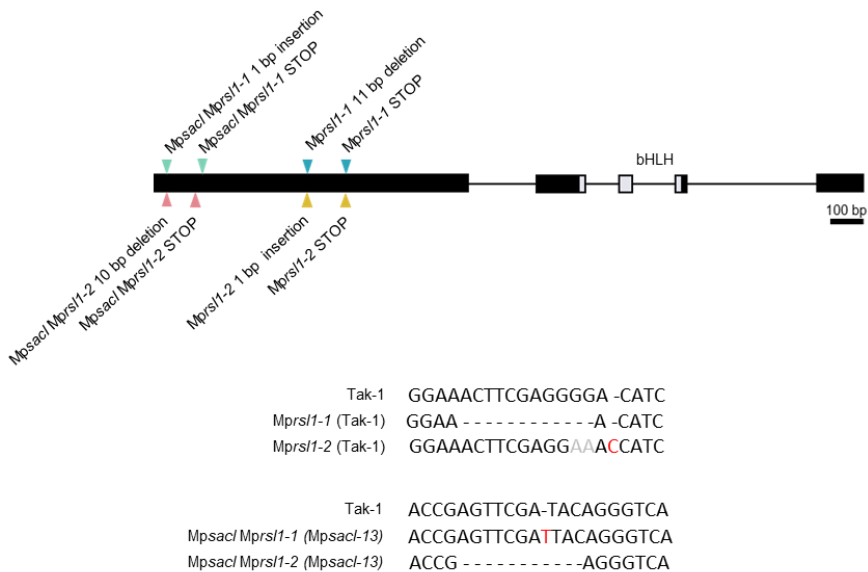


Figure 18. Characterization of *Mprsl1* loss-of-function mutants. Graphic representation of *MpRSL1* transcripts for Tak-1, *Mpsacl Mprsl1-1*, *Mpsacl Mprsl1-2*, *Mprsl1-1* and *Mprsl1-2* mutants. Thick black boxes indicate exons, and thin line represents introns. Grey boxes indicate the bHLH domain. Blue arrowheads mark the sites for the 11 bp deletion and premature STOP of the *Mprsl1-1* mutant; turquoise arrowheads mark the 1 bp insertion and premature STOP of the *Mpsacl Mprsl1-1* mutant; yellow arrowheads mark the 1 bp insertion and premature STOP of the *Mprsl1-2* mutant; pink arrowheads mark the 10 bp deletion and premature STOP of the *Mpsacl Mprsl1-2* mutant. The gRNA genetic region for *Mpsacl Mprsl1* and *Mprsl1* transformation events is represented, illustrating the different modifications. Red letters indicate insertion, and grey letters indicate change of base.

Based on the epistasis analysis, two non-mutually exclusive molecular mechanisms would be possible: (i) MpSACL modulates *MpRSL1* expression; or (ii) MpSACL modulates *MpRSL1* activity. To check if *MpRSL1* expression is affected by MpSACL, we introduced a red fluorescent protein (TdTomato) fused to a Nuclear Localization Sequence (NLS) under the *MpRSL1* promoter (*proMpRSL1::TdTomato-NLS*) reporter construct into the *Mpsacl-13* mutant and analyzed its expression pattern all along gemma development until the differentiation of PRI. In the wild

type, *MpRSL1* promoter activity is found as early as in the gemma initials at the 2-3 cells tage, eventually concentrating around the apical notches at later stages, and

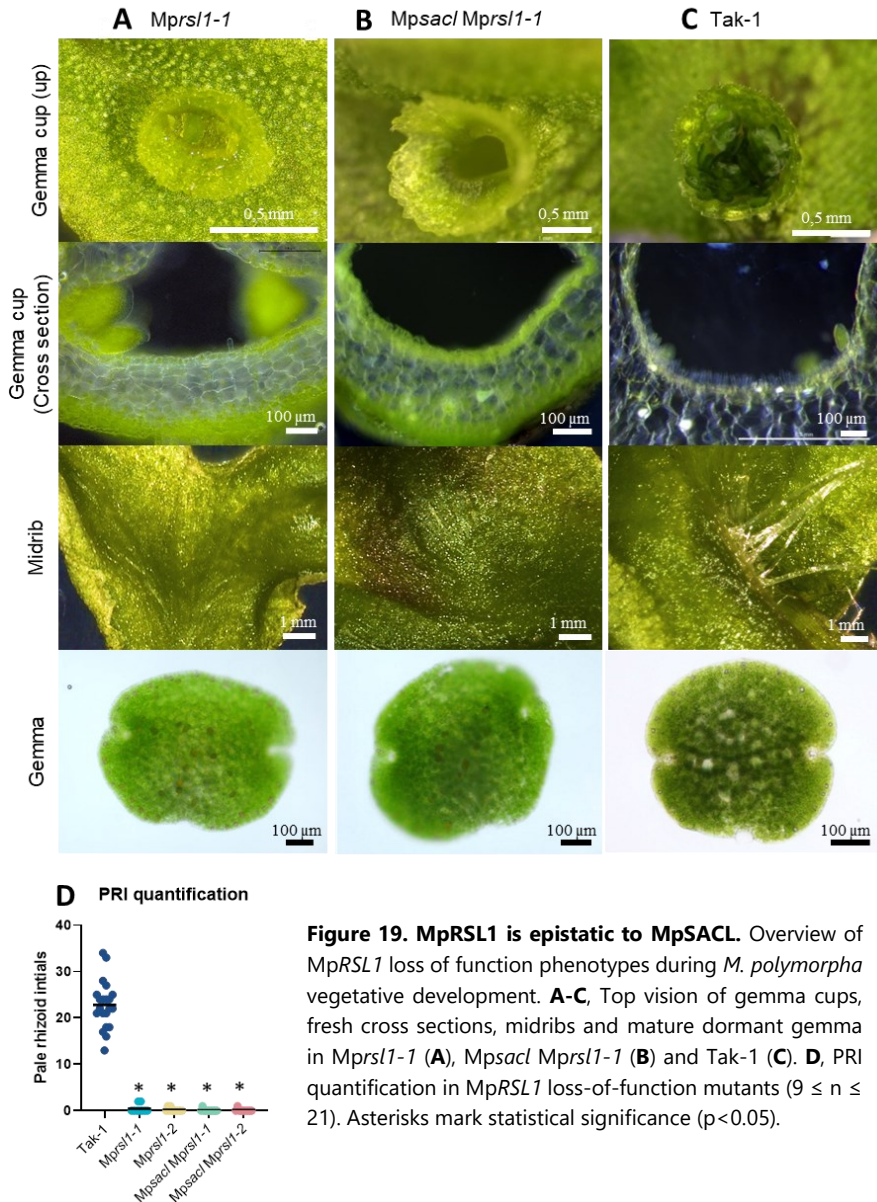
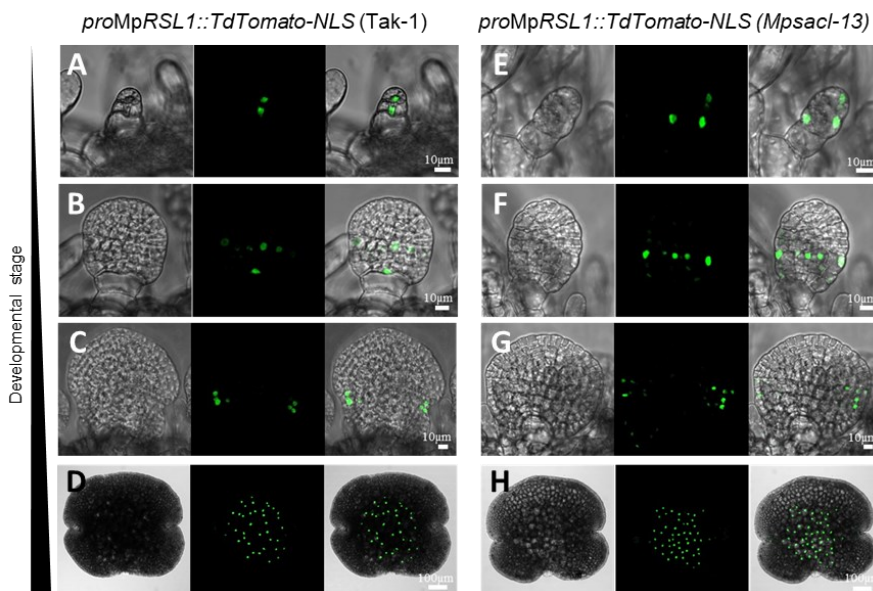


Figure 19. *MpRSL1* is epistatic to *MpSACL*. Overview of *MpRSL1* loss of function phenotypes during *M. polymorpha* vegetative development. **A-C**, Top vision of gemma cups, fresh cross sections, midribs and mature dormant gemma in *Mprsl1-1* (**A**), *Mpsacl Mprsl1-1* (**B**) and *Tak-1* (**C**). **D**, PRI quantification in *MpRSL1* loss-of-function mutants ($9 \leq n \leq 21$). Asterisks mark statistical significance ($p < 0.05$).



marking the PRI in fully developed gemmae (**Figure 20 A-D**). In the *Mpsacl* mutant, *MpRSL1* promoter activity was not affected during gemma development with respect to the timing and spatial localization (**Figure 20 E-H**). The only difference was the number of cells that expressed *MpRSL1* in the fully developed gemmae, which was



I *MpRSL1* positive nuclei

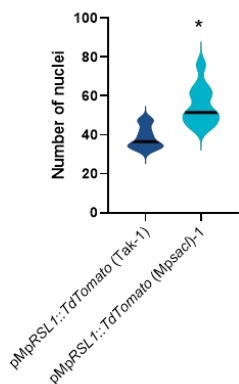


Figure 20. MpSACL does not regulate *MpRSL1* expression during early stages of gemma development. Analysis of *proMpRSL1::TdTomato-NLS* expression during gemma development in *Tak-1* and *Mpsacl-13* backgrounds. **A-D**, confocal images of *proMpRSL1::TdTomato-NLS* (*Tak-1*) background. **E-H**, confocal images of *proMpRSL1::TdTomato-NLS* (*Mpsacl-13*) background. **A, E**, 2-3 cell stage; **B, F**, globular stage; **C, G**, advanced stage; **D, H**, mature gemma. **I**, quantification of *MpRSL1*-positive nuclei in mature gemmae ($n = 10$). Asterisks mark statistical significance ($p < 0.05$)



higher in the *Mpsacl* mutant (**Figure 20 H and I**), in agreement with our previous observations that the mutant had more rhizoid initial cells (**Figure 17E**). This result suggests that MpSACL affects the establishment of PRI identity at a very early stage, which would still be compatible with MpSACL regulating MpRSL1 activity.

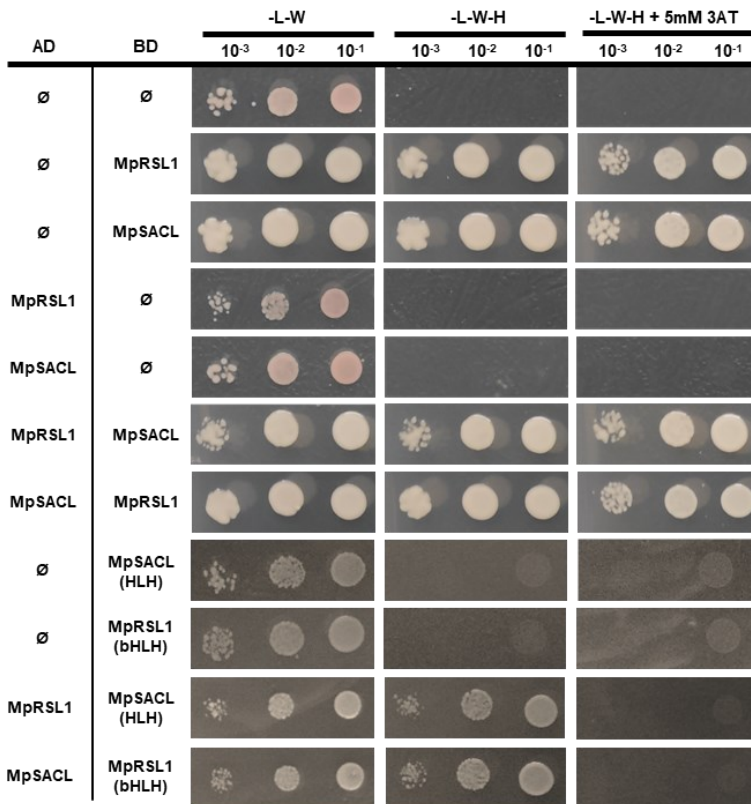


Figure 21. MpSACL interacts with MpRSL1 in Yeast-two hybrid (Y2H) assays.

Reciprocal Y2H assays between MpSACL and MpRSL1 in growth control (-L-W), in histidine-free SD media (-L-W-H) and histidine-free media complemented with 5μM 3-aminotriazole (3AT) (-L-W-H+5μM 3AT). Both MpSACL and MpRSL1 auto-activate when fused with Gal4 binding domain (BD). Y2H Empty vectors (pGADT7 and pGBKT7) containing Gal4 Activation Domain (AD) or Binding Domain (BD) respectively were used as negative control.



To test this possibility, we examined the interaction between MpSACL and MpRSL1 in a Y2H assay. Given that both full-length proteins exhibited autoactivation when fused to the GAL4 DNA binding domain (**Figure 21**), we examined the possible interaction of each full-length protein fused to the GAL4 activation domain, with the (b)HLH domains of the other proteins fused to the GAL4 DNA-binding domain. Indeed, the results show that MpRSL1 and MpSACL interact with each other's (b)HLH domains (**Figure 21**). Further confirmation of the interaction between MpSACL and MpRSL1 was provided by a Bi-Fluorescence Complementation (BiFC) assay, in which we observed reconstitution of yellow fluorescent protein (YFP) only when MpRSL1-YFC and MpSACL-YFN full proteins were co-infiltrated (**Figure 22**).

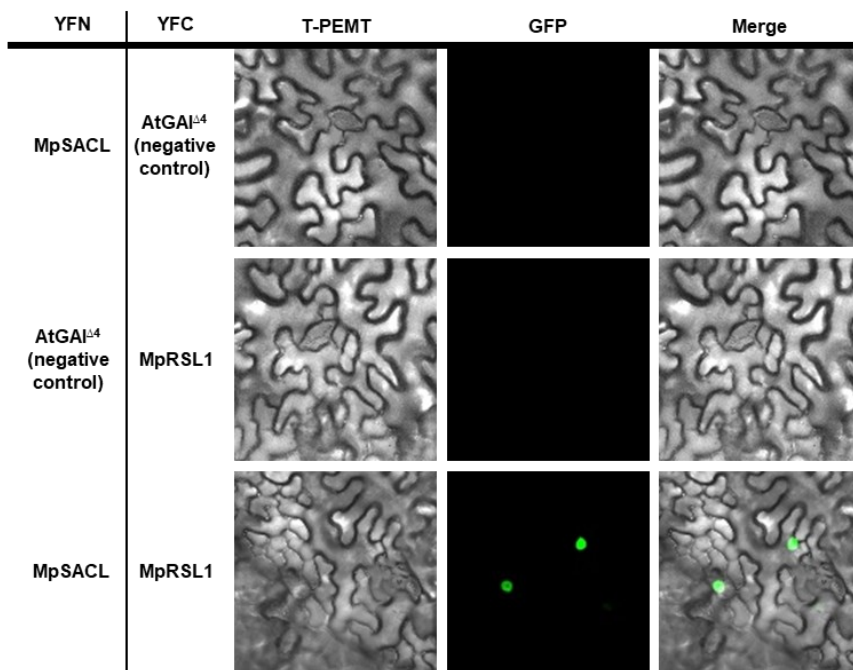


Figure 22. MpRSL1 can interact with MpSACL in a BiFC. Assay on *N. benthamiana* leaves between *MpSACL* and *MpRSL1*, GIBBERELLIN A INSENSITIVE DEL. 4 (AtGAI^{Δ4}) was used as a negative control.



SACL proteins have been shown to act in *A. thaliana* as inhibitors of the activity of LHW, another bHLH TF (Katayama et al., 2015b; Vera-Sirera et al., 2015). Based on this information, the ability of MpSACL to interact with MpRSL1, and the epistasis relationship between MpRSL1 and MpSACL, we propose that MpSACL is a negative regulator of MpRSL1 activity during the specification of rhizoid identity, and perhaps also during gemma and mucilage cell identity -although this might still be an artifact due to ectopic expression of MpSACL in the overexpression lines, and not reflecting a role for the endogenous protein in that process. Given the lack of information about downstream genetic targets of MpRSL1, it is difficult to further test this model at present.

The C3HDZ-ACL5-SACL module is only partially assembled in *M. polymorpha*

In *A. thaliana*, the mechanism mediated by AtACL5, AtHB8 and AtSACLs depends on (i) the precise upregulation of AtACL5 by AtHB8 and auxin; and (ii) the Tspm-dependent translation of AtSACL transcripts (Baima et al., 2014; Imai et al., 2006; Milhinhos et al., 2013; Vera-Sirera et al., 2015). In *M. polymorpha*, MpSACL translation is insensitive to Tspm (**Chapter 1**), and we have demonstrated that MpACL5 and MpSACL functions are unrelated, which indicates that at least these two pieces of the module are not connected in this species. However, we found evidence of a possible conserved interaction between MpC3HDZ and MpACL5 at the genetic level, since they colocalize in apical notches and have a similar role in the apical notch coordinating meristematic activity. In addition, *M. polymorpha* has canonical auxin signaling (Flores-Sandoval et al., 2015; Kato et al., 2015, 2017, 2020), which transcriptional activator, MpARF1, also shares expression domain with MpACL5 in apical notches and gemma cups (Kato et al., 2017). Remarkably, MpACL5 expression pattern resembles the auxin reporter GH3 and MpYUCCA2 expression (MpYUC2), an auxin biosynthesis gene, at apical notches, base of gemma cups and midribs (Eklund et al., 2015; Ishizaki et al., 2012), which suggests that MpACL5 expression might as well be tightly linked with auxin in *M. polymorpha*.

To test the importance of MpC3HDZ and auxin for MpACL5 expression in *M. polymorpha*, we searched 2.8 Kb worth of MpACL5 promoter for putative C3HDZ and



ARF bs using an *in silico* analysis. We used available published binding matrices for AtCNA and AtPHV, both C3HDZ paralogs from *A. thaliana* belonging to the HB8/CNA clade and PHV/PHB/REV clade respectively (**Chapter 1**), as well as for the auxin response factors (ARF) AtMP and AtARF8. Those two *A. thaliana* ARFs, together with AtARF6, 7, and 19, belong to the same clade as MpARF1 and are the most closely related transcriptional activator ARFs (Kato et al., 2015). We found at least three coincident putative C3HDZ bs for AtCNA and AtPHV in the MpACL5 promoter (**Figure 23 A and C**, respectively), ranging from 1.5 to 2.4 Kb upstream of the start codon. Regarding auxin response factors, we found more than ten putative ARF bs in MpACL5 promoter (**Figure 23 B and D**). Taken together, these data suggest that both MpC3HDZ and MpARF1 might be able to bind the MpACL5 promoter.

To test the relevance of these putative binding sites, we designed a dual luciferase transactivation assay in *N. benthamiana*. For this experiment, we used a region of the MpACL5 promoter containing a C3HDZ bs (**Figure 23 A and C**) and another region containing ARF1bs (**Figure 23 B and D**), that drove the expression of the *LUC* gene. As effectors we used 35S::3xHA:MpC3HDZ or 35S::3xHA:MpARF1 in *N. benthamiana* (see Materials for details). In both cases we observed an increased luminescence in the presence of MpC3HDZ or MpARF1 compared to control conditions (**Figure 23 E and F**, respectively), which confirms that MpC3HDZ and MpARF1 can activate the MpACL5 promoter through the identified CRE *in vivo*.

To test whether MpC3HDZ is necessary for the regulation of MpACL5 in *M. polymorpha*, we analyzed MpACL5 expression in *Mpc3hdz*, *EF1::MpC3HDZ:GR* (*Mpc3hdz*), and *EF1::MpC3HDZ:citrine* (Tak-1) lines by a RT-qPCR (**Figure 24A**). On one hand, the MpACL5 expression was 2- to 4-fold higher in *EF1::MpC3HDZ:citrine* (Tak-1)-4 than in Tak-1. On the other hand, MpACL5 expression in *Mpc3hdz* was approximately 3-fold lower than in Tak-1; likewise, there was a decreased –but not significant– MpACL5 expression in *EF1::MpC3HDZ:GR* (*Mpc3hdz*)-26 line, which may indicate a leaky conditional overexpression. These results suggest that MpACL5 expression is upregulated by MpC3HDZ in *M. polymorpha*.

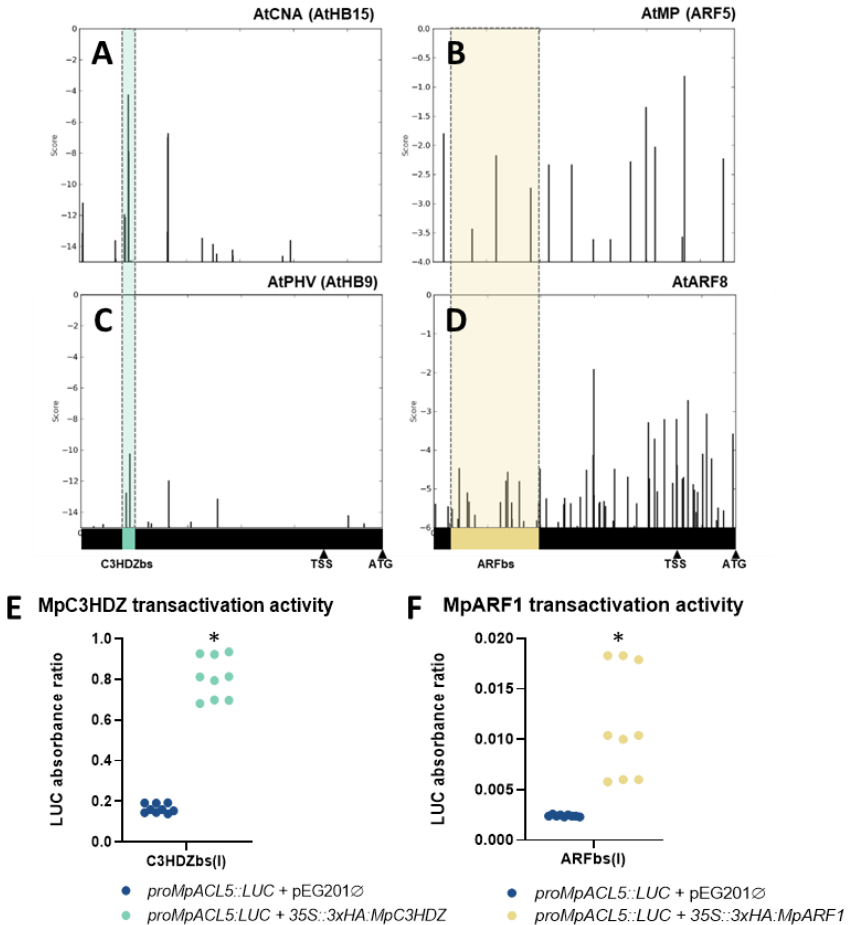


Figure 23. MpC3HDZ and MpARF1 are transcriptional activators of MpACL5. A-D; *in silico* binding site analysis of 2.8 Kb of *MpACL5* promoter with the binding matrix of AtCNA (**A**), AtMP (**B**), AtPHV (**C**), and AtARF8 (**D**). Peaks correspond to a high binding score after MORPHEUS scan. Colored regions represent the regions of *MpACL5* promoter that were used for the dual luciferase assay; C3HDZ bs, in turquoise (**A** and **C**) and ARF bs, in mustard yellow (**B** and **D**). Arrowheads mark the transcription start site and ATG codon in *MpACL5* promoter. **E, F;** Dual luciferase assays showing the LUC absorbance normalized ratios for MpC3HDZ (**E**) and MpARF1 (**F**) of 3 biological replicates with 3 technical replicates each. Asterisks represent statistical significance ($p < 0.05$). TSS, transcription start site; ATG: Start codon; AtCNA, CORONA; AtHB, ARABIDOPSIS HOMEBOX; AtMP, MONOPTEROS; ARF, AUXIN RESPONSE FACTOR; AtPHV, PHAVOLUTA; LUC, Luciferase.



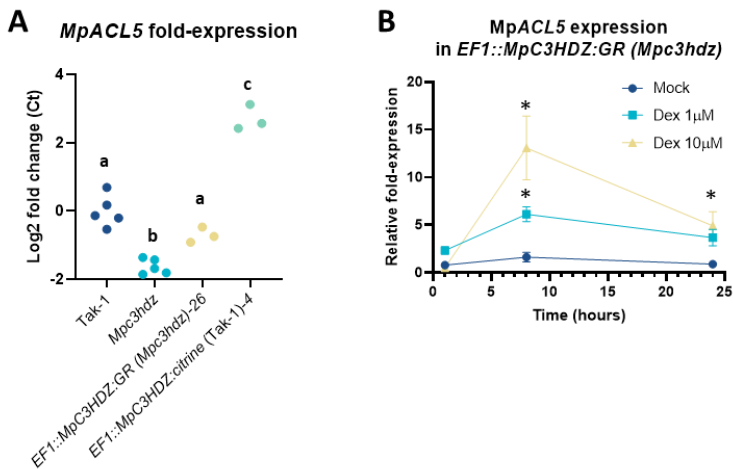


Figure 24. MpC3HDZ regulates MpACL5 transcription *in vivo*. **A**, Relative MpACL5 fold-expression in MpC3HDZ mutant lines, represented as a log₂ scale ($3 \leq n \leq 5$). Letters represent statistical significance groups ($p < 0.05$). **B**, Timecourse of relative MpACL5 fold-expression in *EF1::MpC3HDZ:GR (Mpc3hdz)-26* after mock, 1 μ M Dex, and 10 μ M Dex treatments for 1, 8 and 24 hours ($3 \leq n \leq 5$). Asterisks mark statistical significance ($p < 0.05$). Dex, dexamethasone; μ M, micromolar.

To determine whether MpACL5 is induced in *EF1::MpC3HDZ:GR (Mpc3hdz)* and –if it is– how rapidly does it occur, we treated *EF1::MpC3HDZ:GR (Mpc3hdz)-26* with 1 μ M or 10 μ M Dex and analyzed MpACL5 expression after 1, 8, and 24 hours of treatment (**Figure 24B**). MpACL5 expression peaked at 8 hours; in addition, its expression levels varied concomitantly with the applied Dex concentration.

To test whether auxin has also a positive effect on MpACL5 expression, a similar experiment was performed in which Tak-1 gemmalings were treated with 10 μ M indole-3-acetic-acid (IAA) for 2, 4, and 8 hours. At 4 hours, MpACL5 expression was approximately 4-fold higher than in mock conditions (**Figure 25**). Consistently with our observations, *Mparf1* mutants display decreased MpACL5 expression compared to Tak-1 (Dolf Weijers, personal communication). Taken together, our



results indicate that MpC3HDZ and auxin are positive regulators of MpACL5 expression *in vivo* in *M. polymorpha*.

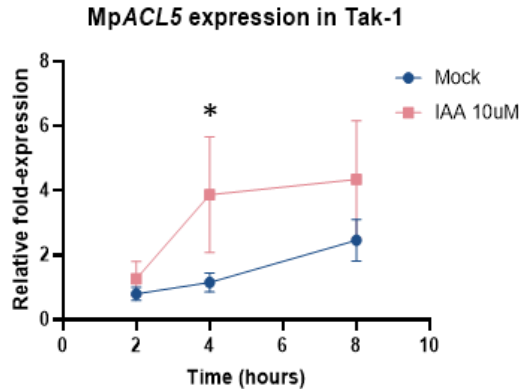


Figure 25. MpACL5 is induced in auxin treatments. MpACL5 fold-expression in Tak-1 after 2, 4, and 8 hours of mock and 10 µM IAA treatments ($3 \leq n \leq 4$). Asterisks mark statistical significance ($p < 0.05$). IAA, Indole-Acetic Acid; µM, micromolar.

Finally, to determine whether MpC3HDZ and auxin are sufficient to establish the MpACL5 spatial pattern in apical notches in *M. polymorpha*, we generated three double transgenic lines carrying the *proMpACL5::GUS* and *EF1::MpC3HDZ:GR* transgenes in Tak-1 background. These lines were created in a two-step transformation of *EF1::MpC3HDZ:GR* in Tak-1 background, from where we identified a conditional ectopic constitutive expressor (*EF1::MpC3HDZ:GR-7*) with 1.96-fold expression of MpC3HDZ (**Figure 26A**). This line was subsequently transformed with the *proMpACL5::GUS* transgene to be able to track changes in MpACL5 expression and to ensure the same constitutive expression levels of MpC3HDZ in all GUS lines. We then performed mock, 1 µM Dex, 10 µM IAA, or the combination of both treatments and performed a GUS staining at 4 hours. Neither the ectopic expression of MpC3HDZ or the auxin treatments were sufficient to drive the GUS signal outside of the apical notch, and only the combined 1 µM Dex + 10 µM IAA showed a slight



expansion towards the midribs (**Figure 26B**), which appeared in two out of three *proMpACL5::GUS (EF1::MpC3HDZ:GR)* lines. Altogether, our results indicate that *MpC3HDZ* and auxin are regulators of *MpACL5* expression levels in *M. polymorpha*. It is interesting, however, how the ectopic expression of *MpC3HDZ*, auxin treatments, or the combination of both are not able to drive *MpACL5* expression ectopically; a possible explanation would require the presence of other main upstream *MpACL5* regulators, which would be also responsible for *MpACL5* expression.

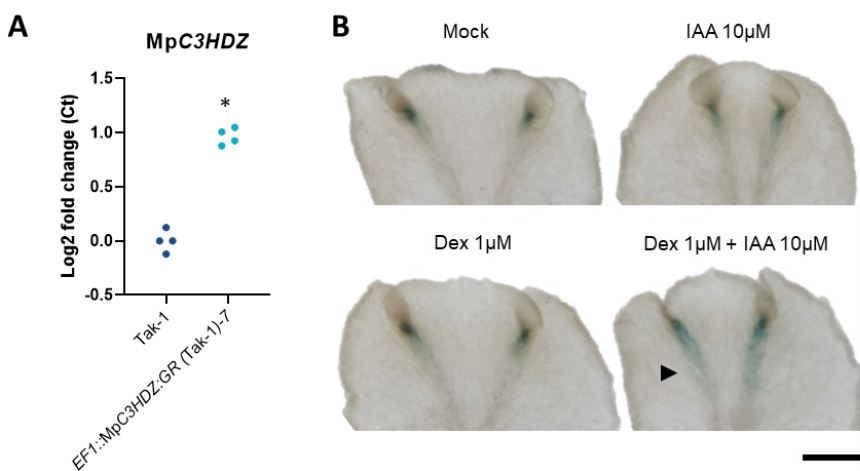


Figure 26. Ectopic *MpC3HDZ* or IAA treatments are not sufficient to drive ectopic *MpACL5* expression. **A**, quantification of *MpC3HDZ* transcript levels by RT-qPCR ($n = 4$). **B**, GUS staining of *proMpACL5::GUS (EF1::MpC3HDZ:GR)-3* after 4 hours of mock, 1 µM Dex, 10 µM IAA and 1 µM Dex + 10 µM IAA treatments. *proMpACL5::GUS (EF1::MpC3HDZ:GR)-3* expression is maintained at the apical notch and is expanded slightly towards the midribs (marked with a black arrowhead) after 10 µM IAA and 1 µM Dex treatment. Scale bar represents 2 mm. Dex, dexamethasone; IAA, Indole-Acetic Acid; µM, micromolar.

Altogether, we have demonstrated that a genetic link between *MpC3HDZ*, auxin and *MpACL5* occurs in *M. polymorpha*. Considering the lack of connection between *MpACL5* and *MpSACL*, our results indicate that the C3HDZ-ACL5-SACL module is only partially assembled in *M. polymorpha*: on the one hand, *MpC3HDZ*



and MpACL5 genetic regulation is relevant for the meristematic activity in the apical notch and is reflected in patterning and growth defects. On the other hand, MpSACL regulates epidermal structures such as rhizoid, mucilage cell and gemma development possibly through interaction with MpRSL1 (**Figure 27**). Hence, these results suggest that the evolutionary trajectory C3HDZ-ACL5-SACL module in bryophytes is divergent from the angiosperm lineage.

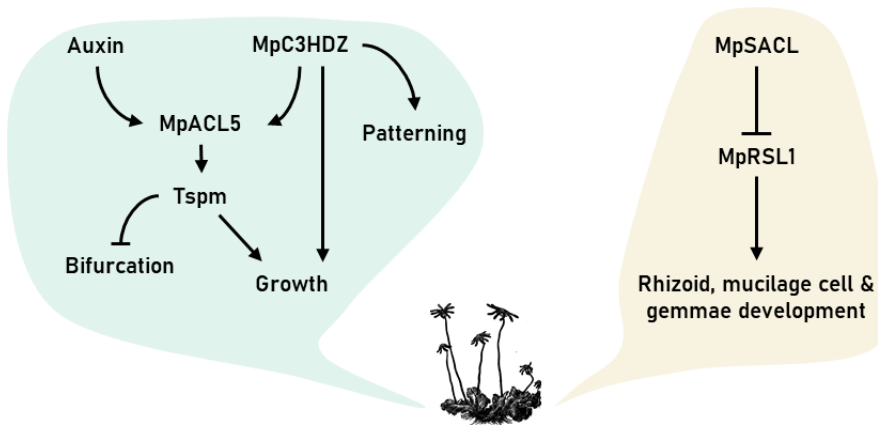


Figure 27. Overview of MpC3HDZ, MpACL5 and MpSACL roles in *M. polymorpha* and their functional connections.

MATERIALS

RNA and gDNA extraction, cDNA synthesis and PCR analysis

Total RNA was isolated using the NucleoSpin™ RNA Plant Kit from Macherey-Nagel, and cDNA synthesis was performed with 1 µg of RNA using NZY First-Strand cDNA Synthesis Kit (NZYTech) according to the manufacturer's instructions. The resulting cDNA was used for semi-quantitative PCR reaction (at 28 cycles) and a real time PCR. The primers used for the semi-quantitative and real time PCR are listed in **Table 1**. The bands containing Mpc3hdz UP and DOWN transcripts were extracted from the gel using the Nucleospin Gel and PCR clean-up kit (Macherey



Nagel) according to the manufacturer's instructions. The sequencing was carried out by the Genomics Service of the University of Valencia.

Name	Locus [MpTak v6.1]	Sequence	Use
MpC3HDZ_F	Mp1g24140	TCTTGTGATTTGCGAGCGTTCC	qPCR
MpC3HDZ_R		TGCTCGAACGAAGAATTGCACC	qPCR, semi-quantitative PCR
MpACL5_F	Mp8g03070	GCTCCACCAAAGGTTCCATTG	qPCR
MpACL5_R		AAGTACCATTTCGCGGCTTTTGG	qPCR
MpSACL_F	Mp5g09710	TAGTAGAGCGGTGGCAGTCC	qPCR
MpSACL_R		CGAGAAGGGTGTGGAAGAT	qPCR
MpACT_F	Mp6g10990	TGTGTTGTCTGGAGGAACCA	qPCR, semi-quantitative PCR
MpACT_R		AGGTGCTGAGAGAAGCCAAG	qPCR, semi-quantitative PCR
MpRSL1_F	Mp3g17930	AGATGAGTCTGGGGCAACC	qPCR
MpRSL1_R		GGATGAGCGCTTTAGAGTG	qPCR
MpC3HDZ_sqF	Mp1g24140	GTTGTACCGGGTGGACTTCAAC	Semi-quantitative PCR

Table 1. Primers used for PCR analyses

Genomic DNA was extracted using a modified version of the CTAB method. For this protocol, the plant material was also grinded with liquid nitrogen and resuspended into 10mL of freshly made CTAB extraction buffer (Tris-HCl pH 8.0 100mM, NaCl 1.42M, CTAB 2%, EDTA 20mM, PCP-40 2%, β -Mercaptoethanol (7 μ l/10mL), and Ascorbic acid (1mg/mL)). Then, 10mL of chloroform:Isoamyl alcohol (24:1) was added and the samples were spun at 4500 x g for 10 minutes at room temperature. The aqueous upper layer was transferred to a conical tube and added 0.7 volumes of isopropanol. Next, the samples were spun at 4500 x g for 10 minutes at room temperature and the supernatant was discarded. To clean the DNA, 1mL of 70% was added and centrifuged at max speed for 2 minutes. The supernatant was discarded, and the tube was left to dry completely before resuspending the pellet in TE buffer.

Generation of *M. polymorpha* transgenic lines

MpTak1v6.1 genome and transcriptome from the MarpolBase (<https://marchantia.info/>) was used as the reference for transgenic line and primer



design using Benchling (<https://benchling.com/>). For PCR amplification, either Phusion High-Fidelity Polymerase (Thermo Fisher Scientific) or KOD Hot Start DNA polymerase (Sigma-Aldrich) were used with similar results. Regarding destination vectors, all Gateway-based pMpGWB series used for this chapter were created by Ishizaki et al. (2015) and thalli transformation was performed according to Ishizaki et al. (2008). All primers used for transgenic line generation and genotyping are listed in **Table 2**.

Name	Type	Locus	Direction	Sequence	Use
MpACL5	Promoter Promoter	Mp8g03070	Forward	GGGGACAAGTTTGTACAAAAAAGCAGGCTATGTACTCGTAGATGACATGCTCTCA	Cloning Cloning
			Reverse	GGGGACCACCTTTGTACAAGAAAGCTGGTTCCTCTCTCTCTCTTC	
MpC3HDZ	Promoter Promoter	Mp1g24140	Forward	GGGGACAAGTTTGTACAAAAAAGCAGGCTTGCCTGACTGGCTCCTATCAAGT	Cloning Cloning
			Reverse	GGGGACCACCTTTGTACAAGAAAGCTGGTTCACGCTCCTACTTTCTCTTTTC	
MpSACL	Promoter Promoter	Mp5g09710	Forward	GGGGACAAGTTTGTACAAAAAAGCAGGCTCTCAATTGTCAATGAAAGAGGAGA	Cloning Cloning
			Reverse	GGGGACCACCTTTGTACAAGAAAGCTGGTATTCCAGTCTTCA CGTA CG	
<i>uidA</i>	CDS	-	Reverse	CGTCGGGTGAGTTTACC CGT	Genotyping
<i>Citrine</i>	CDS	-	Forward	CTTCTTCAAGGACGACGGCAA C	Genotyping
			Reverse	CTTGAAGTGAATGCCCTTCAGC	Genotyping
MpACL5	CDS CDS	Mp8g03070	Forward	GGGGACAAGTTTGTACAAAAAAGCAGGCTTAATGCTGGAAGCATTACCGACTAC	Cloning Cloning
			Reverse	GGGGACCACCTTTGTACAAGAAAGCTGGTAAATGGATTTCGCTGTTCC	
MpC3HDZ	CDS CDS	Mp1g24140	Forward	GGGGACAAGTTTGTACAAAAAAGCAGGCTATGCTTCGCGCAA GTATG	Cloning Cloning
			Reverse	GGGGACCACCTTTGTACAAGAAAGCTGGTTCACAAAATGACA CCA GTTCTGTAACA	
MpSACL	CDS CDS	Mp5g09710	Forward	GGGGACAAGTTTGTACAAAAAAGCAGGCTGGATGTCGAGGATTTGGATTTG	Cloning Cloning
			Reverse	GGGGACCACCTTTGTACAAGAAAGCTGGTGGTGTCCAGCGAACTCTCTCA	
MpRSL1	CDS CDS	Mp3g17930	Forward	GGGGACAAGTTTGTACAAAAAAGCAGGCTGTGATGACTCGAGAAACGCTGACAT	Cloning Cloning
			Reverse	GGGGACCACCTTTGTACAAGAAAGCTGGTGGCGAGGATTTGTTGCTCTGCTGATTGG	
MpACL5	Promoter+CDS Promoter+CDS	Mp8g03070	Forward	ACATATTTTGGGATGAAATTTGAAAGAAATTTTATGTACTCGTAGATGA CATGCTCTCA	Overlapping PCR Overlapping PCR
			Reverse	TGAGAGCATGTCACTACGAGTACATAAAAATTTCTTCAAAATTTCACTCCAAAATATGT	
MpACL5	gRNA 1 gRNA 1	Mp8g03070	Forward	CTCGACAACCTCCAAAAGCCGCGAA	CRISPR CRISPR
			Reverse	AAACTTCGGGGCTTTTGGAGTTGT	
MpSACL	gRNA 1 gRNA 1	Mp5g09710	Forward	CTCGAATGGCGGCTCGCCGAGA GA	CRISPR CRISPR
			Reverse	AAACTCTCTCGCAGGCCGCCATT	
MpRSL1	gRNA 1 gRNA 1	Mp3g17930	Forward	AAACTATCAATATGCAAGGGGTAC	CRISPR CRISPR
			Reverse	CTCGGTACGCCCTGCAATATTGATAG	
MpRSL1	gRNA 2 gRNA 2	Mp3g17930	Forward	CTCGGGGAAACTCGAGGGGGA CAT	CRISPR CRISPR
			Reverse	AAAACATGTCCCTCGAAGTTTCCC	
MpACL5	CDS (gRNA1) CDS (gRNA1)	Mp8g03070	Forward	GCTCCCAACAAAGGTTCCATTG	Genotyping Genotyping
			Reverse	CCGGTGTGCAAGATTTTTGAG	
MpSACL	CDS (gRNA1) CDS (gRNA1)	Mp5g09710	Forward	TAGTAGAGGGGTGGCAGTCC	Genotyping Genotyping
			Reverse	GATTCCTCTCGCTCGCTTGA	
MpRSL1	CDS (gRNA1+2) CDS (gRNA1+2)	Mp3g17930	Forward	CTCGAGTCTACGAGGTTGATACA	Genotyping Genotyping
			Reverse	CGGCTCGCTGCTGCGGTAACCGGATCC	

Table 2. Primers used for transgenic line construction, Y2H and BiFC assays

Promoters from *MpC3HDZ* (Mp1g24140), *MpACL5* (Mp8g03070) and *MpSACL* (Mp5g09710) of 1.5Kb, 2.6Kb, and 1.5Kb respectively were retrieved from genomic DNA of Tak-1 *M. polymorpha* plants. The promoters were introduced into a pDONR207 and subsequently into pMpGWB104 (HygR) or pMpGWB304 (ChlSR)



pDEST plasmids, which were used for Tak-1 thalli transformation. In order to examine the upstream regulation of MpC3HDZ to MpACL5 expression, the thalli of *EF1::MpC3HDZ:GR* (Tak-1) were used for agrobacterium transformation with *proMpACL5::GUS* (cloned with pMpGWB304 – ChIsR). T1 transformants were selected on antibiotic media and genotyped for the *uidA* gene. *proMpRSL1::TdTomato:NLS* in Tak-1 background were obtained from Prof. Kimitsune Ishizaki laboratory in Kobe (Japan), as well as the pDEST vector *proMpRSL1::TdTomato:NLS*, which was used for *Mpsacl-13* thalli transformation.

Translational fusion marker lines were created to observe MpACL5 expression during gemmae development. For this purpose, MpACL5 CDS was isolated from cDNA and fused with its own promoter with an overlapping-PCR (Hilgarth & Lanigan, 2020). The final PCR reaction was used for gel electrophoresis and purified with the Nucleospin Gel and PCR clean-up kit (Cultek). The promoter-CDS fusion PCR products with AttB overhangs were cloned into a pDONR207 and subsequently into a pMpGWB307 (ChIsR). Tak-1 thalli were used for agrobacterium transformation for *proMpACL5::MpACL5:citrine*, and genotyped for citrine.

For the gain of function lines, CDS were generated by synthesis of MpC3HDZ and MpSACL CDS (Integrated DNA Technologies) or obtained from cDNA (MpACL5), and subsequently cloned into a pDONR207. *EF1::MpC3HDZ:citrine*, *EF1::MpACL5:citrine* and *EF1::MpSACL:citrine* were generated by cloning of the CDS into a pMpGWB108 (HygR) and Tak-1 thalli transformation. Conditional MpC3HDZ overexpressors (*EF1::MpC3HDZ:GR*) were created by cloning the MpC3HDZ CDS into a pMpGWB113 (HygR) and subsequent Tak-1 or *Mpc3hdz* thalli transformation. These lines were genotyped by RT-qPCR.

Mpac15, *Mpsacl*, *Mprsl1* and *Mprsl1Mpsacl* mutants were created with CRISPR-Cas9 technology using the plasmids published in Sugano et al. (2018). Single gRNAs were designed to be 20 bp long with a PAM at 3' "NGG". For MpACL5 (Mp8g03070) and MpSACL (Mp5g09710), only one guide RNA was used and cloned into the final vector pMpGE010 (HygR) for MpACL5 or pMpGE011 (ChIsR) for MpSACL. Both final vectors were used for Tak-1 thalli transformation. For *Mprsl1*



(Mp3g17930), two gRNA were designed to target the first exon, separated by 100 bp. Both gRNAs were cloned into pMpGE010 (HygR) and were used for Tak-1 or *Mpsacl-13* thalli transformation. *Mpc3hdz* T-DNA insertion mutant was kindly provided by Dr. Victor Jones (Prof. Liam Dolan laboratory, Austria). For genotyping, genomic regions containing the target sequence for gDNA were amplified and sequenced.

GUS staining

For the GUS assay, plants were fixed in ice cold acetone for 20 minutes, washed with phosphate buffer, and vacuum-infiltrated with GUS staining solution (50 mM sodium phosphate buffer pH 7.2, 0.5 mM potassium-ferrocyanide, 0.5 mM potassium-ferricyanide, 10 mM EDTA, 0.01% Triton X-100 and 1 mM 5-bromo-4-chloro-3-indolyl- β -D-glucuronic acid) for 15 min, and then incubated at 37 °C for 1h, 3h, or overnight. Tissue was clarified with EtOH dehydration series and imaged under a Nikon Eclipse E600 microscope and a Leica DMS 1000 macroscope in the bright field.

Polyamine extraction and quantification

Total polyamine extraction was performed on 1g of tissue from 3 biological replicates from Tak-1, *EF1::MpACL5:citrine-1* and *Mpac15-4* lines according to polyamine extraction methods described in **Chapter 1**.

Dex and IAA treatments

For the timecourse for *MpACL5* expression in *EF1::MpC3HDZ:GR* (*Mpc3hdz*) backgrounds, the lines *EF1::MpC3HDZ:GR* (*Mpc3hdz*)-26 and -32 were treated with mock, 1 μ M Dex (11 β ,16 α)-9-Fluoro-11,17,21-trihydroxy-16-methylpregna-1,4-diene-3,20-dione, Sigma), and 10 μ M Dex treatments for 1, 8 and 24 hours on liquid 1/2 strength Gamborg's medium. For the timecourse for *MpACL5* expression after IAA treatments, Tak-1 plants were treated with mock or 10 μ M IAA for 2, 4, and 8 hours. Three biological replicates were obtained from each treatment for the RNA extraction and RT-qPCR analysis.



For the analysis of the proMpACL5 expression in the presence of a gain of function MpC3HDZ and IAA, proMpACL5::GUS (*EF1::MpC3HDZ:GR*) 14-day-old plants grown on ½ strength Gamborg's B5 medium were moved into liquid ½ strength Gamborg's B5 medium containing mock (EtOH and DMSO), 10 µM IAA, 1 µM Dex, or the combination of 10 µM IAA and 1 µM Dex for 4 hours. After this time, a GUS staining was performed.

Confocal microscopy

Fresh gemma cup slices embedded in 6% agar from *proMpRSL1::TdTomato-NLS* (Tak-1), *proMpRSL1::TdTomato-NLS* (*Mpsacl-13*) and *proMpACL5::MpACL5:citrine* (Tak-1) were analyzed with a Zeiss LSM 780 confocal microscope targeting developing gemmae. TdTomato signal was detected at 581 nm, and citrine was detected at 530 nm.

***In silico* promoter analysis**

To investigate the upstream regulation of *ACL5*, C3HDZ and ARF bs were examined in 2.6 Kb worth of MpACL5 promoter, which was retrieved from MarpolBase (<https://marchantia.info/>). C3HDZ and ARF binding profiles from *A. thaliana* were obtained from the JASPAR database (Castro-Mondragon et al., 2022): a DAP-seq based position frequency matrix (PFM) for AtCNA-At1G52150 (O'Malley et al., 2016), a SELEX-based PFM for AtPHV-At1G30490 (Sessa et al., 1998), a protein binding microarray (PBM)-based PFM for AtMP (AtARF5)- At1G19850 (Boer et al., 2014) and a PBM-based PFM for AtARF8-At5G37020 (Weirauch et al., 2014). Using MORPHEUS score tool (Minguet et al., 2015), these binding profiles were used to search for binding sites in the MpACL5 promoter. The obtained scores were limited for optimal visualization at -15 (-6 for AtARF8), and final figures were produced manually.

Dual luciferase transactivation assay

A region of 131 bp containing the highest score of AtCNA and AtPHV bs (2298 bp from the ATG), named C3HDZ bs, was amplified from Tak-1 genomic DNA and cloned into a pUPD2 with GoldenBraid technology (Sarrion-Perdigones et al.,



2011, 2013). Next, the C3HDZ bs was fused to a 35S minimal promoter derived from GB0050 from the GoldenBraid collection (Diego Orzáez laboratory, IBMCP, Valencia, Spain) into a $\alpha 2$ level vector. This was used as a template to amplify the C3HDZ bs-35Smin sequence with HindIII and NcoI overhangs, that was subsequently cloned into a HindIII-NcoI digested pGreenII0800-LUC (Hellens et al., 2005). Another region of 826 bp containing AtARF5 and AtARF8 bs (1825 bp from the ATG), named ARF bs, was amplified from Tak-1 genomic DNA with HindIII and NcoI overhangs, and was subsequently cloned into a HindIII-NcoI digested pGreenII0800-LUC. Regarding the effector vectors, a pDONR207 entry vector with MpARF1 was kindly provided by Dr. Jorge Hernández García (Wageningen University). Both MpARF1 and MpC3HDZ CDS were cloned into pEarleyGate104 and pEarleyGate201, respectively (Earley et al., 2006). Expression vectors containing the binding sequences were transformed into *A. tumefaciens* C58 strain with pSOUP, and effector vectors were transformed into *A. tumefaciens* C58 strain. The infiltration of fully grown *N. benthamiana* leaves was performed with the combination of 3 *A. tumefaciens* carrying: (i) Effector vector; (ii) Expression vector; and (iii) p19 helper plasmid. After 3 days at room temperature in continuous light, leaf discs were collected, grinded with liquid nitrogen, and resuspended in 150 μ L 1x Passive Lysis Buffer (Promega). The *Firefly* and *Renilla* luciferase translation was assessed with a Dual-Glo[®] Luciferase assay (Promega) according to the manufacturer's instructions, with the following modifications: 5 μ L of the plant extract was added to 40 μ L Dual-Glo Luciferase. *Firefly* and *Renilla* luminescence were measured with a GloMax 96 Microplate Luminometer (Promega). Statistical differences were analyzed by T-student test with $\alpha=0.05$.

EdU assay

Gemmae from Tak-1, EF1::MpACL5:citrine-1 and MpACL5-4 were grown on liquid media for 1 day previous to the EdU labelling. EdU staining assay was performed with a modified protocol from Click-iT EdU imaging kit with Alexa Fluor 488 Azide (Thermo Fisher Scientific). As a summary, 1-day-old gemmae were EdU-labelled in a 1.5 mL Eppendorf tube with $\frac{1}{2}$ strength Gamborg's B5 medium supplemented with 10 μ M EdU for one hour. Then, they were fixed in 1 mL 3.7% paraformaldehyde in PBS for 15 minutes and washed with 1 mL 3% BSA in PBS twice.



The tissue was permeabilized with 1 mL 0.5% Triton X-100 in PBS for 20 min before EdU detection. For the detection of EdU-labelled cells, the permeabilization buffer was removed and the tissues were washed with 1 mL 3% BSA in PBS twice. Then, the wash solution was substituted with the Click-iT® reaction cocktail (Alexa Fluor 488 Azide, 10% v/v Click-iT® reaction buffer, 80% v/v CuSO₄ and 10% v/v 1X Click-iT® reaction buffer) for 30 minutes in the dark. Finally, the samples were washed with 1 mL 3% BSA in PBS twice before optical observation. The EdU-labelled gemmae were mounted to slides with 50% glycerol and observed in a AxioObserver 780 confocal laser scanning microscope (Zeiss) at 488 nm. To quantify EdU positive nuclei, confocal images were converted to binary (8 bit) and threshold was adjusted to maximize nuclei visualization in Fiji. Lastly, the EdU nuclei were quantified with the “Analyze particles” tool in Fiji.

Cryo-field emission scanning electron microscopy (cryo-FESEM) and cellular profiling

M. polymorpha tissues (thalli and mature gemmae) were deposited on a mix of Tissue+ OCT compound and colloidal graphite and frozen on sleet nitrogen by immersion in a PP3010T Cryo Preparation System (Quorum). Samples were kept in vacuum inside the Cryo-FESEM. Samples were cleaned by sublimation at -90°C for 7 minutes and subsequently recovered with platinum by sputtering for 5 seconds with a current of 5mA. After that, the samples were observed at 1-2 KV, 4-6mm distance, and pictures were obtained with an SE2 detector in a Ultra55 Scanning Electron Microscope (Zeiss). For the cellular profiling, gemmae pictures were converted to binary (8 bit) and threshold was adjusted to maximize cell size visualization in Fiji. Cells were then identified, and area measurements were performed using “Analyze particles” tool in Fiji. Color coding according to the measured cell size was performed using the plugin ROI_color_coder from Fiji, and final pictures were manually edited.

Y2H assay

MpRSL1 CDS was amplified from Tak-1 cDNA and cloned into a pDONR207 with Gateway technology. The primers used for MpRSL1 amplification are listed in Table 2. MpSACL and MpRSL1 CDS were fused to Gal4-binding domain and to Gal4-



activation domain by cloning into pGBKT7 and pGADT7 respectively via LR clonase II (Invitrogen).

Direct interaction assays in yeast were performed following Clontech's small-scale yeast transformation procedure. Transformed yeast strains were selected in Synthetic Defined medium (SD) without Leu (for pGADT7) or Trp (for pGBKT7). Diploid cells were obtained after mating and subsequent selection in SD -Leu -Trp. Interaction assays were performed by 1:1, 1:10, 1:100 and 1:1000 diploid culture dripping in SD -Leu -Trp and -His, in 5 mM 3AT (Sigma Aldrich).

BiFC assays

MpSACL and MpRSL1 were cloned into pMDC43-YFN and pMDC43-YFC (Belda-Palazón et al., 2012), respectively. *A. tumefaciens* C58 strain containing binary plasmids was used to infiltrate 3-week-old *Nicotiana benthamiana* leaves. Three days after infiltration, leaves were analyzed with a Zeiss LSM 780 confocal microscope. Reconstituted YFP signal was detected in abaxial epidermal cells at 503-517 nm and transmitted light.

Histological analyses

Plastochron measurements

For the plastochron measurements, Tak-1, *EF1::MpACL5:citrine-1* and -20, and *Mpacl5-4* and -13 were grown on ½ strength Gamborg's B5 medium (Gamborg's B5 medium 1.58g/L, MES monohydrate 0.5g/L, Plant Propagation Agar PPA 10g/L) at pH 5.7 under continuous light in a growth chamber. After 5 weeks, the number of apical notch bifurcations was measured for half of the adult plant. Similarly, plastochron measurements were performed on Tak-1 grown on ½ strength Gamborg's B5 medium supplemented with 100 µM Put (Putrescine dihydrochloride, Sigma), 100 µM Spd (Spermidine trihydrochloride, Sigma), 100 µM Put + Spd or 100 µM Tspm (Thermospermine hydrochloride, EPICA S.L.) for 7 days.

PRI quantification



Mature dormant gemmae from Tak-1, *EF1::MpSACL:citrine*, *Mpsacl*, *Mprsl1*, and *Mpsacl Mprsl1* backgrounds were extracted from gemma cups and introduced into a 0.5% Tween 20 solution (Sigma). PRI were quantified using a Nikon Eclipse E600 microscope in bright field.

Fixation and paraffin embedding

For histological analyses, derived from the described protocol in Feder & O'Brien (1968) plants were fixed in FAA solution (50% absolute EtOH, 5% glacial acetic acid, 5% formaldehyde) for 1 hour, and then dehydrated with an Ethanol series up to 70%. They were then automatically incubated with sequential 70%, 95% with 0.2% Eosin-Y, 100% EtOH, and gradual Histoclear (National Diagnostics):EtOH concentrations (% v/v): 25:75; 50:50; 75:25 and 100:0 in a tissue processor. Lastly, samples were included in 100% paraffin (Paraplast Plus, McCormick Scientific) at 58°C in vacuum conditions. After the inclusion, samples were placed in aluminium moulds with liquid paraffin, and solidified at 4°C. The plant tissues were sliced at 10 µm thickness with a HM325 microtome (Microm), deposited into wet slides, and dried on a heat block at 42°C. For the Toluidine blue staining, the slides were de-parafined twice with Histoclear II (National Diagnostics) for 10 minutes each. Samples were then rehydrated with EtOH series: 100%, 90%, 70%, 50%, 30% for 5 minutes each. Then, samples were washed with distilled water for 10 minutes and dipped into 0.02% Toluidine blue solution for 30 seconds, washed with EtOH 70%, and air-dried. Samples were then fixed with Merckoglass (Sigma) and a coverslip, and let air dry until solidified. Pictures of histological cuts were taken with the Nikon Eclipse E600 microscope in bright field. Thallus thickness and cell layers were measured from tissues surrounding the midrib or at the center of the gemmae.

Fresh sectioning in 6% agar

Fresh tissue was embedded in 6% agar (Granulated agar DIFCO, ThermoFisher). After solidification, the samples were sliced with a vibrating microtome Leica VT1200S at 85 Hz with a 50 µm thickness and visualized in a Nikon Eclipse E600 microscope in bright field or a Leica DMS 1000 macroscope.



REFERENCES

- Baima, S., Forte, V., Possenti, M., Peñalosa, A., Leoni, G., Salvi, S., Felici, B., Ruberti, I., & Morelli, G.** (2014). Negative feedback regulation of auxin signaling by ATHB8/ACL5-BUD2 transcription module. *Molecular Plant*, 7(6). <https://doi.org/10.1093/mp/ssu051>
- Belda-Palazón, B., Ruiz, L., Martí, E., Tárraga, S., Tiburcio, A. F., Culiáñez, F., Farràs, R., Carrasco, P., & Ferrando, A.** (2012). Aminopropyltransferases Involved in Polyamine Biosynthesis Localize Preferentially in the Nucleus of Plant Cells. *PLoS ONE*, 7(10). <https://doi.org/10.1371/journal.pone.0046907>
- Boer, D. R., Freire-Rios, A., van den Berg, W. A. M., Saaki, T., Manfield, I. W., Kepinski, S., López-Vidriero, I., Franco-Zorrilla, J. M., de Vries, S. C., Solano, R., Weijers, D., & Coll, M.** (2014). Structural basis for DNA binding specificity by the auxin-dependent ARF transcription factors. *Cell*, 156(3). <https://doi.org/10.1016/j.cell.2013.12.027>
- Carlsbecker, A., Lee, J. Y., Roberts, C. J., Dettmer, J., Lehesranta, S., Zhou, J., Lindgren, O., Moreno-Risueno, M. A., Vatén, A., Thitamadee, S., Campilho, A., Sebastian, J., Bowman, J. L., Helariutta, Y., & Benfey, P. N.** (2010). Cell signalling by microRNA165/6 directs gene dose-dependent root cell fate. *Nature*, 465(7296). <https://doi.org/10.1038/nature08977>
- Castro-Mondragon, J. A., Riudavets-Puig, R., Rauluseviciute, I., Berhanu Lemma, R., Turchi, L., Blanc-Mathieu, R., Lucas, J., Boddie, P., Khan, A., Perez, N. M., Fornes, O., Leung, T. Y., Aguirre, A., Hammal, F., Schmelter, D., Baranasic, D., Ballester, B., Sandelin, A., Lenhard, B., ... Mathelier, A.** (2022). JASPAR 2022: The 9th release of the open-access database of transcription factor binding profiles. *Nucleic Acids Research*, 50(D1). <https://doi.org/10.1093/nar/gkab1113>
- Earley, K. W., Haag, J. R., Pontes, O., Opper, K., Juehne, T., Song, K., & Pikaard, C. S.** (2006). Gateway-compatible vectors for plant functional genomics and proteomics. In *Plant Journal* (Vol. 45, Issue 4). <https://doi.org/10.1111/j.1365-313X.2005.02617.x>
- Eklund, D. M., Ishizaki, K., Flores-Sandoval, E., Kikuchi, S., Takebayashi, Y., Tsukamoto, S., Hirakawa, Y., Nonomura, M., Kato, H., Kouno, M., Bhalariao, R. P., Lagercrantz, U., Kasahara, H., Kohchi, T., & Bowman, J. L.** (2015). Auxin Produced by the Indole-3-Pyruvic Acid Pathway Regulates Development and Gemmae Dormancy in the Liverwort *Marchantia polymorpha*. *The Plant Cell*, 27(6), 1650–1669. <https://doi.org/10.1105/TPC.15.00065>
- Emery, J. F., Floyd, S. K., Alvarez, J., Eshed, Y., Hawker, N. P., Izhaki, A., Baum, S. F., & Bowman, J. L.** (2003). Radial Patterning of Arabidopsis Shoots by Class III HD-ZIP and KANADI Genes. *Current Biology*, 13(20). <https://doi.org/10.1016/j.cub.2003.09.035>



- Feder, N., & O'Brien, T. P.** (1968). Plant Microtechnique: Some Principles and New Methods. *American Journal of Botany*, 55(1). <https://doi.org/10.2307/2440500>
- Flores-Sandoval, E., Eklund, D. M., & Bowman, J. L.** (2015). A Simple Auxin Transcriptional Response System Regulates Multiple Morphogenetic Processes in the Liverwort *Marchantia polymorpha*. *PLoS Genetics*, 11(5). <https://doi.org/10.1371/journal.pgen.1005207>
- Floyd, S. K., Zalewski, C. S., & Bowman, J. L.** (2006). Evolution of class III homeodomain-leucine zipper genes in streptophytes. *Genetics*, 173(1). <https://doi.org/10.1534/genetics.105.054239>
- Hellens, R. P., Allan, A. C., Friel, E. N., Bolitho, K., Grafton, K., Templeton, M. D., Karunairetnam, S., Gleave, A. P., & Laing, W. A.** (2005). Transient expression vectors for functional genomics, quantification of promoter activity and RNA silencing in plants. *Plant Methods*, 1(1). <https://doi.org/10.1186/1746-4811-1-13>
- Hilgarth, R. S., & Lanigan, T. M.** (2020). Optimization of overlap extension PCR for efficient transgene construction. *MethodsX*, 7. <https://doi.org/10.1016/j.mex.2019.12.001>
- Honkanen, S., Thamm, A., Arteaga-Vazquez, M. A., & Dolan, L.** (2018). Negative regulation of conserved RSL class I bHLH transcription factors evolved independently among land plants. *ELife*, 7. <https://doi.org/10.7554/eLife.38529>
- Ilegems, M., Douet, V., Meylan-Bettex, M., Uyttewaal, M., Brand, L., Bowman, J. L., & Stieger, P. A.** (2010). Interplay of auxin, KANADI and Class III HD-ZIP transcription factors in vascular tissue formation. *Development*, 137(6), 975–984. <https://doi.org/10.1242/dev.047662>
- Imai, A., Hanzawa, Y., Komura, M., Yamamoto, K. T., Komeda, Y., & Takahashi, T.** (2006). The dwarf phenotype of the *Arabidopsis* ac15 mutant is suppressed by a mutation in an upstream ORF of a bHLH gene. *Development*, 133(18). <https://doi.org/10.1242/dev.02535>
- Ishizaki, K., Nonomura, M., Kato, H., Yamato, K. T., & Kohchi, T.** (2012). Visualization of auxin-mediated transcriptional activation using a common auxin-responsive reporter system in the liverwort *Marchantia polymorpha*. *Journal of Plant Research*, 125(5). <https://doi.org/10.1007/s10265-012-0477-7>
- Izhaki, A., & Bowman, J. L.** (2007). KANADI and class III HD-Zip gene families regulate embryo patterning and modulate auxin flow during embryogenesis in *Arabidopsis*. *Plant Cell*, 19(2). <https://doi.org/10.1105/tpc.106.047472>



- Katayama, H., Iwamoto, K., Kariya, Y., Asakawa, T., Kan, T., Fukuda, H., & Ohashi-Ito, K.** (2015). A Negative Feedback Loop Controlling bHLH Complexes Is Involved in Vascular Cell Division and Differentiation in the Root Apical Meristem. *Current Biology*, 25(23), 3144–3150. <https://doi.org/10.1016/j.cub.2015.10.051>
- Kato, H., Ishizaki, K., Kouno, M., Shirakawa, M., Bowman, J. L., Nishihama, R., & Kohchi, T.** (2015). Auxin-Mediated Transcriptional System with a Minimal Set of Components Is Critical for Morphogenesis through the Life Cycle in *Marchantia polymorpha*. *PLoS Genetics*, 11(5). <https://doi.org/10.1371/journal.pgen.1005084>
- Kato, H., Kouno, M., Takeda, M., Suzuki, H., Ishizaki, K., Nishihama, R., & Kohchi, T.** (2017). The roles of the sole activator-type auxin response factor in pattern formation of *Marchantia polymorpha*. *Plant and Cell Physiology*, 58(10). <https://doi.org/10.1093/pcp/pcx095>
- Kato, H., Yasui, Y., & Ishizaki, K.** (2020). Gemma cup and gemma development in *Marchantia polymorpha*. *New Phytologist*, 228(2), 459–465. <https://doi.org/10.1111/nph.16655>
- Kohchi, T., Yamato, K. T., Ishizaki, K., Yamaoka, S., & Nishihama, R.** (2021). Development and Molecular Genetics of *Marchantia polymorpha*. <https://doi.org/10.1146/annurev-arplant-082520-094256>, 72, 677–702. <https://doi.org/10.1146/annurev-arplant-082520-094256>
- Lu, K. J., van't Wout Hofland, N., Mor, E., Mutte, S., Abrahams, P., Kato, H., Vandepoele, K., Weijers, D., & de Rybel, B.** (2020). Evolution of vascular plants through redeployment of ancient developmental regulators. *Proceedings of the National Academy of Sciences of the United States of America*, 117(1). <https://doi.org/10.1073/pnas.1912470117>
- McConnell, J. R., Emery, J., Eshed, Y., Bao, N., Bowman, J., & Barton, M. K.** (2001). Role of PHABULOSA and PHAVOLUTA in determining radial patterning in shoots. *Nature*, 411(6838). <https://doi.org/10.1038/35079635>
- Milhinhos, A., Prestele, J., Bollhöner, B., Matos, A., Vera-Sirera, F., Rambla, J. L., Ljung, K., Carbonell, J., Blázquez, M. A., Tuominen, H., & Miguel, C. M.** (2013). Thermospermine levels are controlled by an auxin-dependent feedback loop mechanism in *Populus* xylem. *The Plant Journal*, 75(4), 685–698. <https://doi.org/10.1111/tpj.12231>
- Minguet, E. G., Segard, S., Charavay, C., & Parcy, F.** (2015). MORPHEUS, a Webtool for Transcription Factor Binding Analysis Using Position Weight Matrices with Dependency. *PLOS ONE*, 10(8), e0135586. <https://doi.org/10.1371/JOURNAL.PONE.0135586>



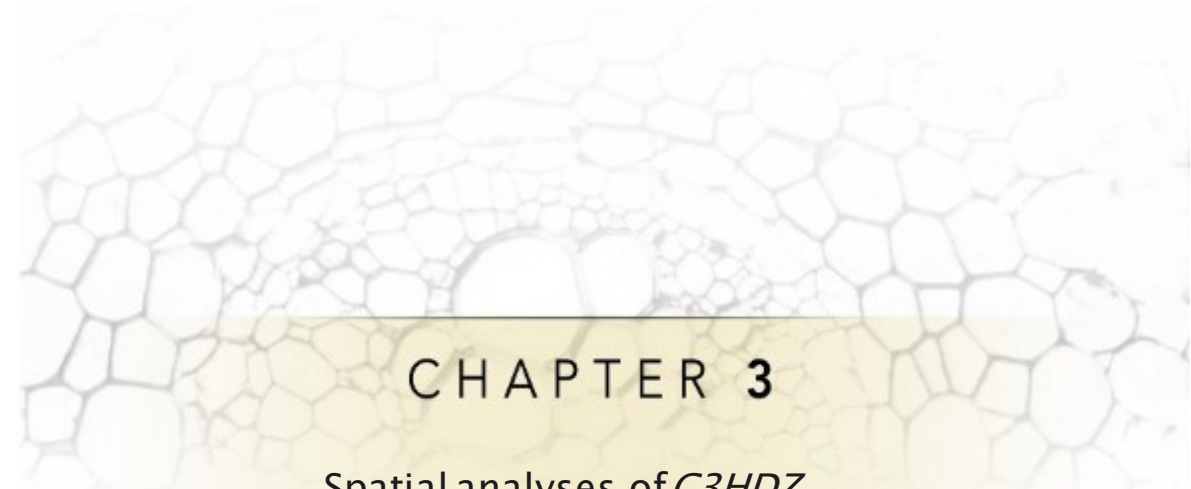
- O'Malley, R. C., Huang, S. S. C., Song, L., Lewsey, M. G., Bartlett, A., Nery, J. R., Galli, M., Gallavotti, A., & Ecker, J. R.** (2016). Cistrome and Epicistrome Features Shape the Regulatory DNA Landscape. *Cell*, 165(5). <https://doi.org/10.1016/j.cell.2016.04.038>
- Prigge, M. J., & Clark, S. E.** (2006). Evolution of the class III HD-Zip gene family in land plants. *Evolution and Development*, 8(4), 350–361. <https://doi.org/10.1111/j.1525-142X.2006.00107.x>
- Proust, H., Honkanen, S., Jones, V. A. S., Morieri, G., Prescott, H., Kelly, S., Ishizaki, K., Kohchi, T., & Dolan, L.** (2016). RSL Class I Genes Controlled the Development of Epidermal Structures in the Common Ancestor of Land Plants. *Current Biology*, 26(1). <https://doi.org/10.1016/j.cub.2015.11.042>
- Ramachandran, P., Carlsbecker, A., Etchells, J. P., & Turner, S.** (2017). Class III HD-ZIPs govern vascular cell fate: An HD view on patterning and differentiation. In *Journal of Experimental Botany* (Vol. 68, Issue 1). <https://doi.org/10.1093/jxb/erw370>
- Sarrion-Perdigones, A., Falconi, E. E., Zandalinas, S. I., Juárez, P., Fernández-del-Carmen, A., Granell, A., & Orzaez, D.** (2011). GoldenBraid: An iterative cloning system for standardized assembly of reusable genetic modules. *PLoS ONE*, 6(7). <https://doi.org/10.1371/journal.pone.0021622>
- Sarrion-Perdigones, A., Vazquez-Vilar, M., Palací, J., Castelijns, B., Forment, J., Ziarsolo, P., Blanca, J., Granell, A., & Orzaez, D.** (2013). Goldenbraid 2.0: A comprehensive DNA assembly framework for plant synthetic biology. *Plant Physiology*, 162(3). <https://doi.org/10.1104/pp.113.217661>
- Sessa, G., Steindler, C., Morelli, G., & Ruberti, I.** (1998). The Arabidopsis Athb-8, -9 and -14 genes are members of a small gene family coding for highly related HD-ZIP proteins. *Plant Molecular Biology*, 38(4). <https://doi.org/10.1023/A:1006016319613>
- Solly, J. E., Cunniffe, N. J., & Harrison, C. J.** (2017). Regional Growth Rate Differences Specified by Apical Notch Activities Regulate Liverwort Thallus Shape. *Current Biology*, 27(1). <https://doi.org/10.1016/j.cub.2016.10.056>
- Sugano, S. S., Nishihama, R., Shirakawa, M., Takagi, J., Matsuda, Y., Ishida, S., Shimada, T., Hara-Nishimura, I., Osakabe, K., & Kohchi, T.** (2018). Efficient CRISPR/Cas9-based genome editing and its application to conditional genetic analysis in *Marchantia polymorpha*. *PLoS ONE*, 13(10). <https://doi.org/10.1371/journal.pone.0205117>
- Thamm, A., Saunders, T. E., & Dolan, L.** (2020). MpFEW RHIZOIDS1 miRNA-Mediated Lateral Inhibition Controls Rhizoid Cell Patterning in *Marchantia polymorpha*. *Current Biology*, 30(10). <https://doi.org/10.1016/j.cub.2020.03.032>



- Vasco, A., Smalls, T. L., Graham, S. W., Cooper, E. D., Wong, G. K. S., Stevenson, D. W., Moran, R. C., & Ambrose, B. A.** (2016). Challenging the paradigms of leaf evolution: Class III HD-Zips in ferns and lycophytes. *New Phytologist*, 212(3). <https://doi.org/10.1111/nph.14075>
- Vera-Sirera, F., De Rybel, B., Úrbez, C., Kouklas, E., Pesquera, M., Álvarez-Mahecha, J. C., Minguet, E. G., Tuominen, H., Carbonell, J., Borst, J. W., Weijers, D., & Blázquez, M. A.** (2015). A bHLH-Based Feedback Loop Restricts Vascular Cell Proliferation in Plants. *Developmental Cell*, 35(4), 432–443. <https://doi.org/10.1016/j.devcel.2015.10.022>
- Weirauch, M. T., Yang, A., Albu, M., Cote, A. G., Montenegro-Montero, A., Drewe, P., Najafabadi, H. S., Lambert, S. A., Mann, I., Cook, K., Zheng, H., Goity, A., van Bakel, H., Lozano, J. C., Galli, M., Lewsey, M. G., Huang, E., Mukherjee, T., Chen, X., ... Hughes, T. R.** (2014). Determination and inference of eukaryotic transcription factor sequence specificity. *Cell*, 158(6). <https://doi.org/10.1016/j.cell.2014.08.009>
- Yip, H. K., Floyd, S. K., Sakakibara, K., & Bowman, J. L.** (2016). Class III HD-Zip activity coordinates leaf development in *Physcomitrella patens*. *Developmental Biology*, 419(1). <https://doi.org/10.1016/j.ydbio.2016.01.012>






A microscopic view of plant tissue cells, showing a network of cell walls forming a honeycomb-like pattern. The cells are mostly polygonal in shape. A central circular structure, possibly a vascular bundle, is visible in the middle of the field of view.

CHAPTER 3

Spatial analyses of *C3HDZ*,
ACL5 and *SACL* expression in
extant tracheophyte lineages

A collection of bright green, fan-shaped Ginkgo leaves (Ginkgo biloba) against a white background. The leaves are arranged in a dense, overlapping pattern at the bottom of the page. Each leaf shows a distinct venation pattern with multiple primary veins radiating from the base.

As we propose in the previous chapter, C3HDZ, ACL5 and SACL do not operate together as a module in bryophytes (**Chapter 2**), which suggests that these genes have followed divergent evolutionary trajectories in bryophytes and tracheophytes. Thus, one pressing question would be when, during the evolution of tracheophytes, was the regulatory module assembled and co-opted for vascular cell proliferation. In other words: is this module a shared mechanism for the control of xylem production in all tracheophytes, or is it restricted to certain lineages?

Considering the paucity of standard molecular genetic tools for functional studies in most vascular lineages (gymnosperms, ferns, lycophytes), we performed RNA *in situ* hybridizations of *C3HDZ*, *ACL5* and *SACL* orthologs in these lineages, as well as protein-protein interaction studies with SACL proteins from divergent land plant lineages. These techniques allowed to establish that the co-option of C3HDZ, ACL5 and SACL genes towards vascular tissues predated the divergence of the tracheophytes, but also revealed other co-options of these genes (as a module or independently) in apical meristems. In addition, we have demonstrated that the ability of SACL to interact with other partners has diverged in the tracheophyte and bryophyte lineages.



RESULTS AND DISCUSSION

Anatomy and vascular development of *G. biloba*, *C. richardii* and *S. kraussiana*

To investigate the possible association between vascular structures and the expression of *C3HDZ*, *ACL5* and *SACL* orthologs across the tracheophyte lineage –in addition to angiosperms–, we have selected the following species: *Ginkgo biloba* (gymnosperm), *Ceratopteris richardii* (fern) and *Selaginella kraussiana* (lycophyte). As vasculature-bearing tissues, we analyzed the SAM of *G. biloba* and *S. kraussiana*, and the primary rooting structures of *G. biloba*, *C. richardii* and *S. kraussiana*.

G. biloba (**Figure 1**) is the only extant species of the order of Ginkgoales. It has two types of vegetative shoots: dwarf shoots with short internodes and relatively large pith and cortex, and long shoots, with long internodes and small pith and cortex. Despite these differences in shoots, the cellular organization of both SAM remains the same (reviewed in Foster, 1938; Hara, 1997). For our analyses we used long shoot-SAMs (**Figure 1**; **Figure 2 A** and **B**) since they are the principal shoot type in *G. biloba* seedlings. *G. biloba* SAMs are composed of a group of apical cells (or cell initials) that are surrounded by many layers of merophytes. These merophytes will give rise to the

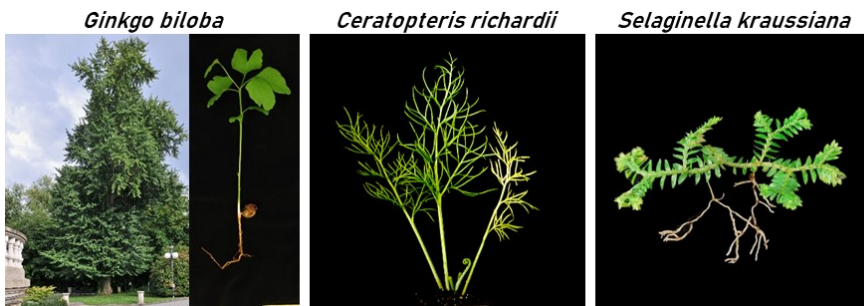


Figure 1. Anatomy overview of *G. biloba*, *C. richardii*, and *S. kraussiana*. *G. biloba* (adult tree, left; seedling with long shoots, right), *C. richardii* and *S. kraussiana* used for the *in situ* hybridization. Picture of an adult *G. biloba* tree was obtained from Wikipedia (<https://commons.wikimedia.org/wiki/>); *C. richardii* adult from C-Fern (<https://c-fern.org/>); and *S. kraussiana* courtesy of Dr. Eugenio Gómez Minguet (University of Valencia).



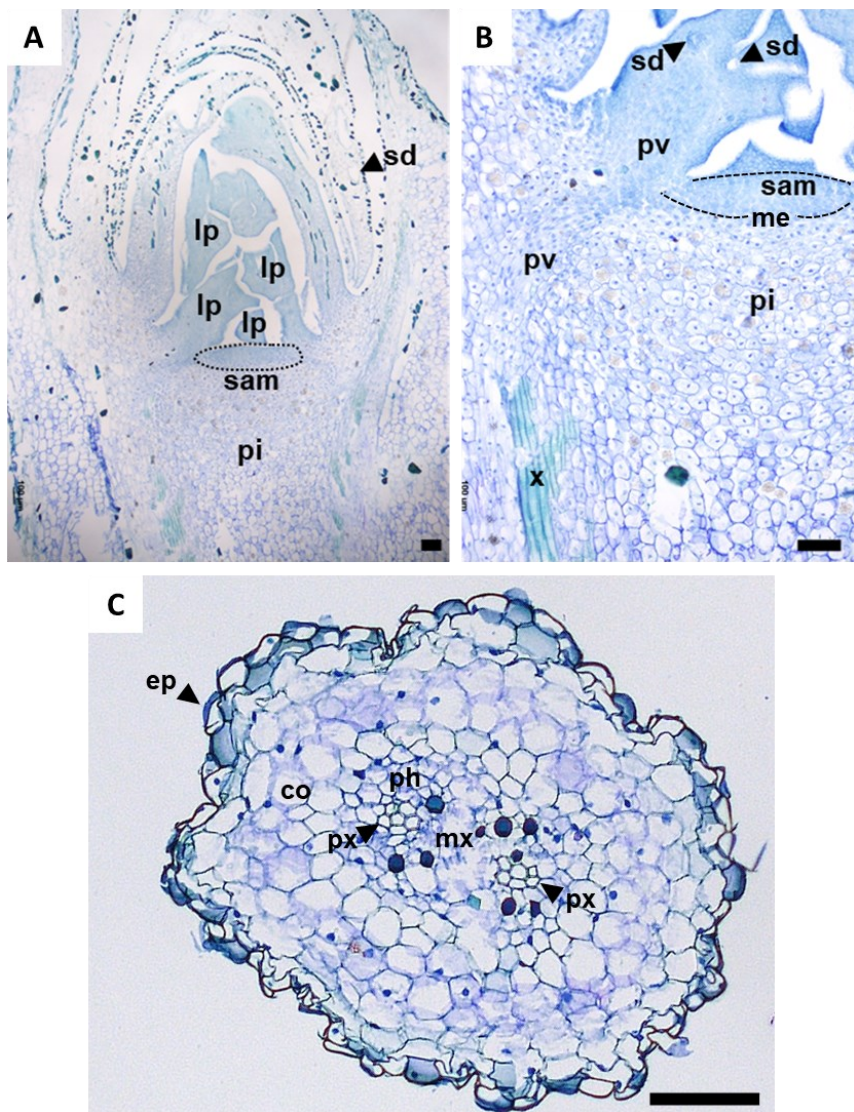


Figure 2. Anatomy of the SAM and primary root of *G. biloba* in cross sections after toluidine blue staining. A, B: Long-SAMs (longitudinal cross sections). **C:** Root during primary development. Scale bars represent 100 μm. Dotted black lines are used to delimitate SAM or merophyte domain. co, cortex; ep, epidermis; lp, leaf primordia; me, merophytes; mx, metaxylem; ph, phloem; pi, pith; pv, provascular tissues; px, protoxylem; sam, shoot apical meristem; sd, secretory duct; x, xylem.



leaf primordia, the pith, and the provascular tissues (see Glossary) in the leaf primordia and the rest of the shoot (Reviewed in Foster, 1938; Hara, 1997) (**Figure 2 A and B**). In addition to these cell types, *G. biloba* also produces a special type of conducts, the secretory ducts, hollow structures derived from PCD where secondary metabolites and mucilage are accumulated (**Figure 2 A and B**) (Cartayrade et al., 1990; Dörken, 2014; Pillai, 1963). Another tissue bearing vasculature is the root; the stele of *G. biloba* root displays diarch symmetry during primary development (**Figure 2C**), and eventually becomes tetrarch (or up to hexarch) with the addition of new leaves (Bonacorsi & Seago, 2016; Soh et al., 1988). The procambium produces both phloem and protoxylem during the first stages of root development; in later stages, the procambium transitions to vascular cambium, becomes cylindrical and connects all the xylem poles (Soh et al., 1988). In addition to the stele, the rest of the root tissues are composed of cortex and epidermis.

C. richardii is a semi-aquatic fern from the Pteridaceae family inside the order Polypodiales (**Figure 1**). Its roots are developed laterally with respect to the longitudinal axis of the embryo, also called primary homorhizy (Groff & Kaplan, 1988; G. Hou & Blancaflor, 2018). The root is developed from the hypodermis of the leaf stem, making one root per leaf node (G. C. Hou & Hill, 2002). *C. richardii* roots are heteroblastic (see Glossary) (G. C. Hou & Hill, 2002); however, the development of vascular tissues does not differ within heteroblastic roots. Vascular development starts very early at the meristematic zone of the root (Aragón-Raygoza et al., 2020), and protoxylem is the first to differentiate (**Figure 3A**). At the end of the meristematic zone, the stele of stem-borne roots contains protoxylem, phloem, endodermis and pericycle (**Figure 3**) (Aragón-Raygoza et al., 2020; G. C. Hou & Hill, 2004). In later stages, metaxylem is formed at the center of the root (**Figure 3B**) (Aragón-Raygoza et al., 2020). In addition to these cell types, the root is composed of epidermis and cortex, where aerenchyma (see Glossary) is produced (Aragón-Raygoza et al., 2020; G. C. Hou & Hill, 2004) (**Figure 3A**). We excluded the SAMs of *C. richardii* for the *in situ* hybridization due to its small size at the time of tissue collection (8 cells at stage S2, as described by Conway & di Stilio, 2020) and derived difficulty in identification and handling (G. C. Hou & Hill, 2004).



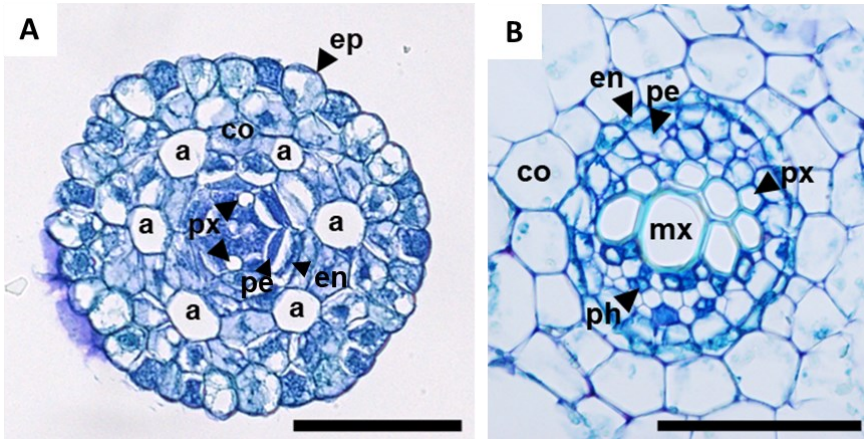


Figure 3. Anatomy of the primary root of *C. richardii*. Cross sections of primary roots after toluidine blue staining, showing the first protoxylem poles (**A**) and metaxylem formation (**B**). Scale bars represent 100 μm . a, aerenchyma; co, cortex; en, endodermis; ep, epidermis; mx, metaxylem; ph, phloem; pe, pericycle; px, protoxylem.

S. kraussiana is a lycophyte from the family of Selaginellaceae, inside the order of Selaginellales (**Figure 1**). Shoots have dorsi-ventral organization; leaf primordia arise in pairs and have a central vascular bundle (Harrison et al., 2005) (**Figure 4A**). During their growth, both SAM and root apical meristems (RAM) have dichotomous branching (Gola, 2014; Gola & Jernstedt, 2016; Harrison et al., 2007; Otreba & Gola, 2011). The SAM consists of one or two apical cells (Gola, 2014; Harrison et al., 2007) that produce the rest of the cells of the shoot, included the provascular cells at either side of the shoot (Gola & Jernstedt, 2016). The *S. kraussiana* shoot vasculature is described as a protostele with two meristeles (see Glossary), or vascular bundles (**Figure 4A**) (Gola & Jernstedt, 2016). As a rooting mechanism, *S. kraussiana* develops the rhizophore, that is a special structure of the genus Selaginella (**Figure 4 B and C**). Rhizophores are developed at every branching point from the shoot (Harrison et al., 2005; Otreba & Gola, 2011). They are cylindrical structures that have both shoot and root features, since they lack a root cap and root hairs (Imaichi, 2008; Imaichi & Kato, 1991; P. Lu & Jernstedt, 1996).



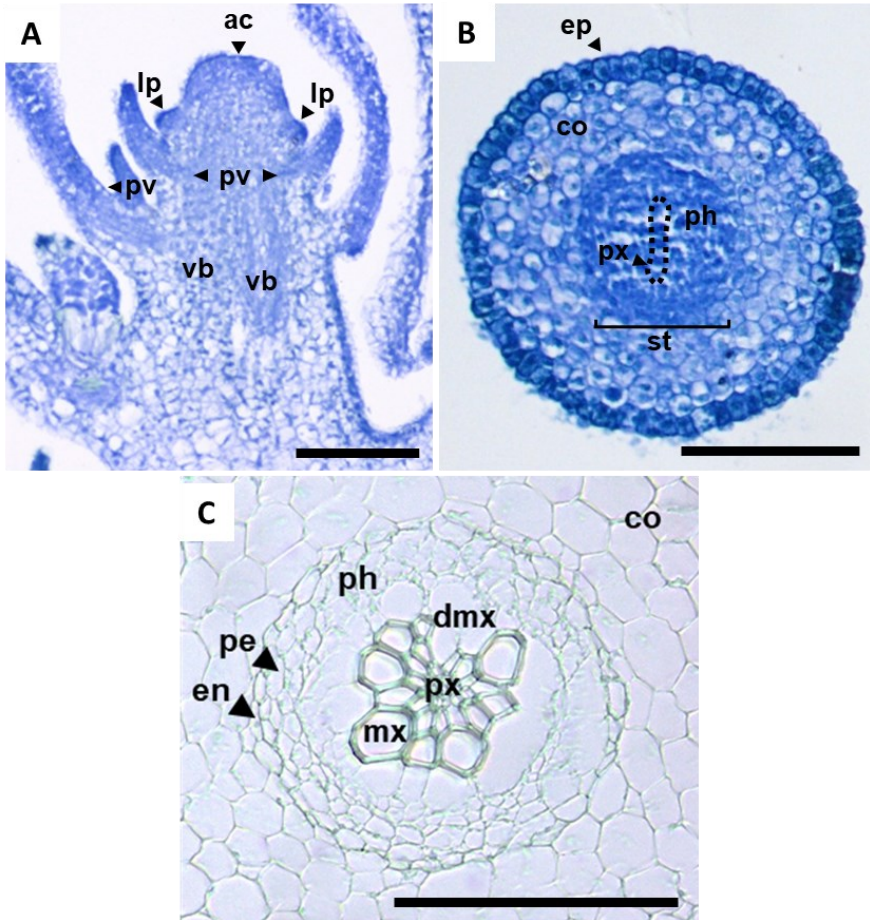


Figure 4. Anatomy of the SAM and rhizophore of *S. kraussiana*. Cross sections after toluidine blue staining. **A**, SAM showing the leaf primordia and shoot vascular bundles. **B** and **C**, rhizophore during first stage (**B**) or later stages of vascular development (**C**). Scale bars represent 100 μm . ac, apical cell; co, cortex; dmx, developing metaxylem; en, endodermis; ep, epidermis; lp, leaf primordia; mx, metaxylem; ph, phloem; pe, pericycle; pv, provascular tissues; px, protoxylem; st, stele; vb: vascular bundle.

The rhizophore has an apical cell that contributes to the initial apical growth of the rhizophore. After a few cell divisions, it loses its identity and two new root apical cells are formed at the tip of the rhizophore, under few layers of parenchymatic



cells. Then, these initials will form a root primordium and emerge from the tip of the rhizophore (Imaichi, 2008; Imaichi & Kato, 1989; P. Lu & Jernstedt, 1996). These root tips can bifurcate dichotomously a few times before reaching the soil and continue their growth as roots (Imaichi & Kato, 1989; P. Lu & Jernstedt, 1996). The vasculature of the rhizophore is formed at a central stele, where xylem and phloem are formed from the procambial cells (**Figure 4 B and C**) (Imaichi & Kato, 1989). The protoxylem is formed at the center, and metaxylem is later formed surrounding the center of protoxylem; the phloem is found surrounding the xylem (**Figure 4C**) (Imaichi & Kato, 1989). The stele is enclosed by a layer of pericycle, a layer of endodermis, cortex, and a layer of epidermis (**Figure 4 B and C**).

***G. biloba*, *C. richardii* and *S. kraussiana* encode C3HDZ, ACL5 and uORF-containing SACL orthologs**

Regarding C3HDZ orthologs (**Table 1**), *G. biloba* contains five *C3HDZ* paralogs that were also identified in previous studies (Zumajo-Cardona et al., 2021; Floyd et al., 2014; Prigge & Clark, 2006). In our phylogenetic analysis, GbiC3HDZ.1 to 3 were grouped into the spermatophyte clade, but GbiC3HDZ.4 and 5 were more similar to the fern *C3HDZ* and were grouped in Ferns 1 and Ferns 2 clades respectively (**Figure 5**). We identified three C3HDZ paralogs in *C. richardii*, of which two (CriC3HDZ.1 and 2) were previously described (Floyd et al., 2014; Prigge & Clark, 2006b). Additionally, a BLAST screening from a non-published transcriptome from this species (personal communication, Chang lab, Iowa State University, USA) revealed a third C3HDZ paralog (CriC3HDZ.3). In the C3HDZ phylogenetic tree, CriC3HDZ.1 and 2 belong to Ferns 2, while CriC3HDZ.3 belong to Ferns 1 (**Figure 5**). Lastly, we identified two *C3HDZ* paralogs in *S. kraussiana* genome, SkrC3HDZ.1 and 2 (**Figure 5**), that were also previously described (Floyd et al., 2014; Floyd & Bowman, 2006; Prigge & Clark, 2006).

Regarding *ACL5* orthologs (**Table 1**), *G. biloba* genome contains two paralogs that belong to the phylogenetic group of Gymnosperms 1 and 2 (GbiACL5.1 and 2, respectively); *C. richardii* has a sole ortholog in the Ferns 1 (CriACL5), and *S.*

kraussiana contains two paralogs inside the lycophyte clade (SkrACL5.1 and 2) (**Figure 5**).

	Name	Origin	Identifier	uORF
<i>G. biloba</i>	GbiC3HDZ.1	Prigge and Clark, 2006	DQ657215 (Genbank)	-
	GbiC3HDZ.2	Prigge and Clark, 2006	DQ657216 (Genbank)	-
	GbiC3HDZ.3	Prigge and Clark, 2006	DQ657217 (Genbank)	-
	GbiC3HDZ.4	Floyd et al., 2014		-
	GbiC3HDZ.5	Floyd et al., 2014		-
	GbiACL5.1	own	Scaffold_2003720 (OneKP)	-
	GbiACL5.2	own	Scaffold_2004590 (OneKP)	-
	GbiSACL.1	own	Scaffold_2002494 (OneKP)	Yes
	GbiSACL.2	own	Scaffold_2037779 (OneKP)	No
<i>C. richardii</i>	CriC3HDZ.1	Prigge and Clark, 2006	DQ657205 (Genbank)	-
	CriC3HDZ.2	Prigge and Clark, 2006	DQ657206 (Genbank)	-
	CriC3HDZ.3	own, Cheng lab	Ceric.18G068400 (Phytozome)	-
	CriACL5	own, Cheng lab	Ceric.07G097200 (Phytozome)	-
	CriSACL.1	own, Cheng lab	Ceric.12G069300 (Phytozome)	Yes
	CriSACL.2	own	Ceric.21G028000 (Phytozome)	Yes
	CriSACL.3	own	Ceric.24G028600 (Phytozome)	Yes
	CriSACL.4	own	Ceric.20G009700 (Phytozome)	No
	CriSACL.5	own	Ceric.16G076700 (Phytozome)	Yes
<i>S. kraussiana</i>	SkrC3HDZ.1	Prigge and Clark, 2006	DQ657196 (Genbank)	-
	SkrC3HDZ.2	Prigge and Clark, 2006	DQ657197 (Genbank)	-
	SkrACL5.1	own	Scaffold_2038638 (OneKP)	-
	SkrACL5.2	own	Scaffold_2040229 (OneKP)	-
	SkrSACL	own	Scaffold_2000249 (OneKP)	Yes

Table 1. List of C3HDZ, ACL5 and SACL orthologs in *G. biloba*, *C. richardii* and *S. kraussiana*.

For SACL orthologs (**Table 1**), *G. biloba* has two SACL paralogs that belong to Gymnosperms 1 and 2, GbiSACL.1 and 2, respectively (**Figure 5**). *C. richardii* possesses five SACL paralogs (CriSACL.1 to 5), of which CriSACL.1-3, and 5 belong to Ferns 1, and CriSACL.4 belong to the Ferns 2 clade (**Figure 5**). *S. kraussiana*, in turn, encodes a sole SACL ortholog (SkrSACL) that belongs to the lycophyte clade (**Figure 5**). We then investigated the presence of the Tspm-sensitive uORF in these orthologs 5' leader sequences. As expected, most SACL transcripts contain the uORF for Tspm regulation in their 5' leaders (**Figure 6A**), and their length and intergenic space meet the requirements for optimal translational regulation (**Figure 6B**) (Fuütterer & Hohn, 1992; Kozak, 1987). Among the described orthologs, we were able to amplify hybridization probes (marked in black circles in **Figure 5**) for the *G. biloba* orthologs:



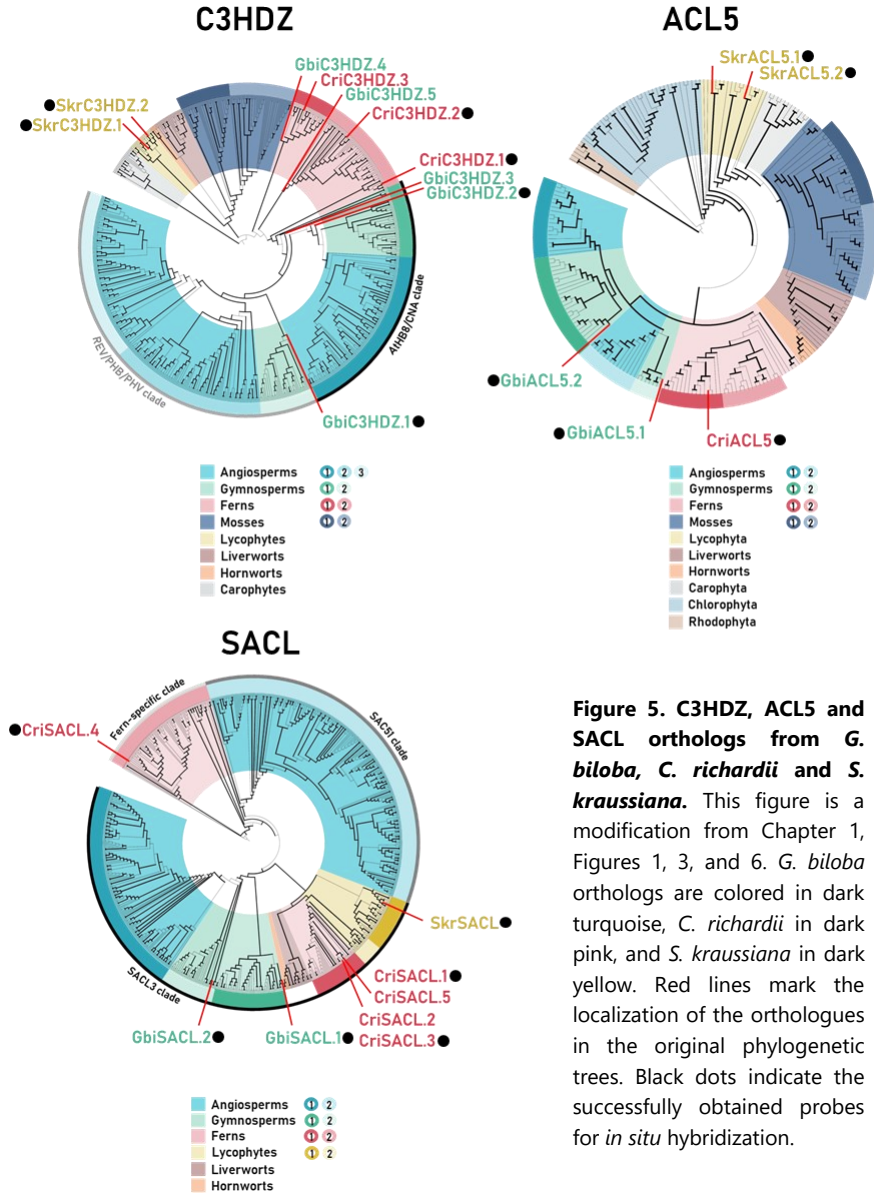


Figure 5. C3HDZ, ACL5 and SACL orthologs from *G. biloba*, *C. richardii* and *S. kraussiana*. This figure is a modification from Chapter 1, Figures 1, 3, and 6. *G. biloba* orthologs are colored in dark turquoise, *C. richardii* in dark pink, and *S. kraussiana* in dark yellow. Red lines mark the localization of the orthologues in the original phylogenetic trees. Black dots indicate the successfully obtained probes for *in situ* hybridization.



GbiC3HDZ.1 and 2; GbiACL5.1 and 2; GbiSACL.1 and 2; for the *C. richardii* orthologs CriC3HDZ.1 and 2; CriACL5; CriSACL.1, 3 and 4; and for the *S. kraussiana* orthologs: SkrC3HDZ.1 and 2; SkrACL5.1 and 2; and SkrSACL.

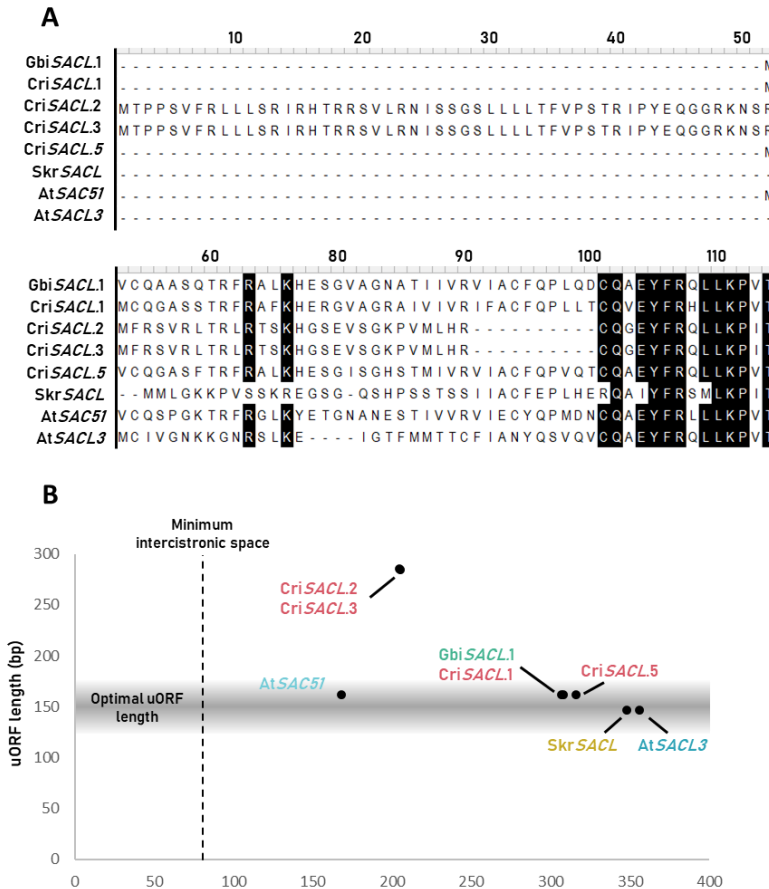


Figure 6. SACL transcripts from *G. biloba*, *C. richardii* and *S. kraussiana* contain the tracheophyte-specific uORF. A, alignment of peptidic uORF sequences, with *A. thaliana* AtSAC51 and AtSACL3 for reference. Black boxes indicate conserved sites in $\geq 80\%$ of the sequences. **B**, graphical representation of uORF length (Y axis) versus intergenic space (X axis), in identified uORF sequences (in bp). Dashed line delimits the minimum intergenic space required for mORF regulation, and grey box marks the optimal uORF length. Both criteria are based on Fütterer & Hohn (1992) and Kozak (1987) research.



C3HDZ, ACL5 and SACL orthologs expression overlaps in the vascular tissues

In *G. biloba*, both GbiC3HDZ orthologs' mRNAs were detected in the provascular tissues in shoots and roots (**Figure 7 A-D**). In the shoot, their expression is particularly strong in the provascular tissues of leaf primordia as well as developing vascular tissues below the SAM (**Figure 7 A and C**). Regarding root vasculature, both GbiC3HDZ mRNAs were detected in the stele, in what appear to be developing protoxylem cells (**Figure 7 B and D**). However, we also observed expression outside of the stele, in some cortex and epidermis cells, especially for GbiC3HDZ.2 (**Figure 7D**). Consistently, a previous study in *G. biloba* has also found GbiC3HDZs expression in the provascular tissues of developing reproductive structures and leaves (Zumajo-Cardona et al., 2021). Regarding GbiACL5 paralogs, their mRNA accumulates in provascular tissues of leaf primordia, shoot and root (**Figure 7 E and F, Figure 8 A and B**). However, while GbiACL5.1 domain is broader and includes all provascular tissues in the stele (**Figure 7 E and F**), GbiACL5.2 appears to be expressed strictly in developing xylem cells in both shoot and root (**Figure 8 A and B**). Similar to the expression pattern of *G. biloba* C3HDZ and ACL5 orthologs, expression of GbiSACLs is detected in all provascular tissues of the shoot and root (**Figure 8 C-F**). In the root, both GbiSACLs are expressed in the stele, although GbiSACL.1 domain is 2-3 cell broader than GbiSACL.2 towards cortical cells (**Figure 8 D and F**). There was no observable unspecific staining in sense probes for any of the *G. biloba* genes (**Supplemental Figure 1**). In summary, we observed that the expression patterns of C3HDZ, ACL5 and SACL largely overlapped in vascular tissues of several organs in *G. biloba*.

In *C. richardii* roots, CriC3HDZ.1 and 2 have a rather ubiquitous expression pattern (**Figure 9 A and B**), and their mRNA was detected in the stele, in addition to all surrounding tissues, namely the epidermis, cortex, and endodermis. CriC3HDZ.1 signal was particularly strong in the protoxylem poles (**Figure 9A**). In line with our observations, other studies have documented C3HDZ expression in the provascular tissues in other fern species as well (Vasco et al., 2016). CriACL5 expression, in turn, is restricted to the developing xylem axis in the root (**Figure 9C**). Interestingly, although all the CriSACL genes examined were expressed in the provascular tissues in the root,

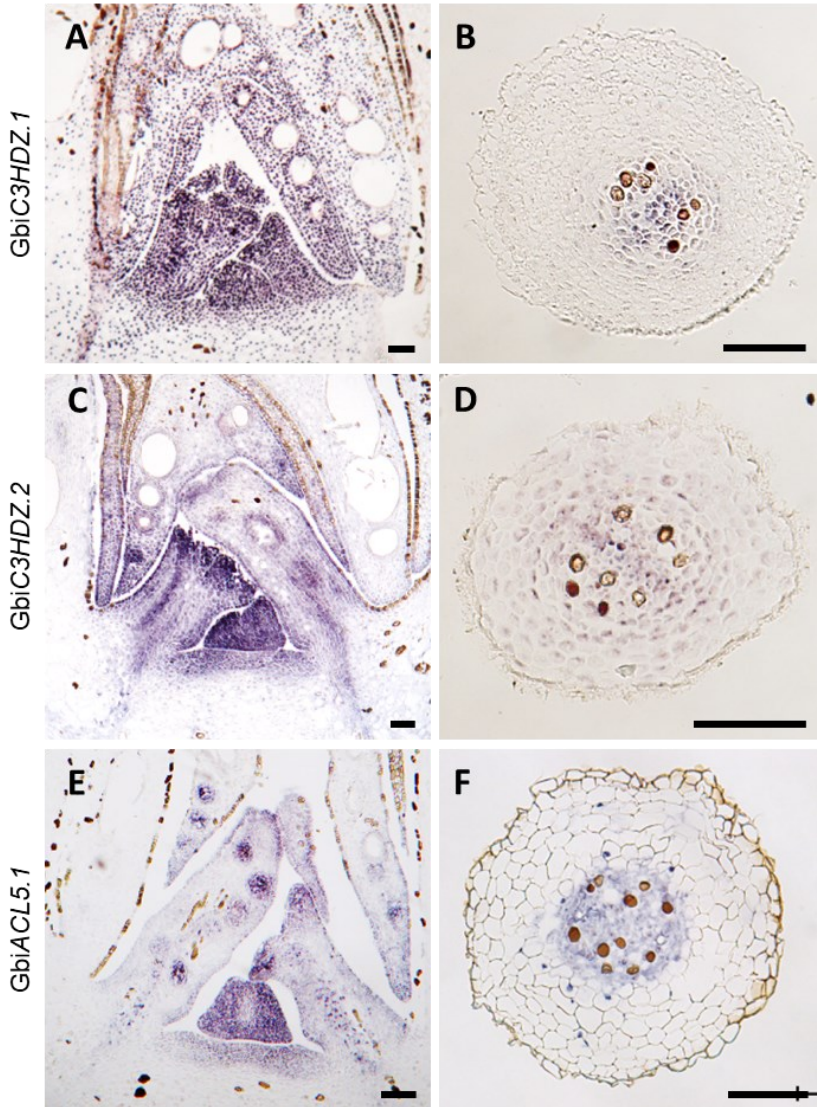


Figure 7. Expression of *GbiC3HDZ.1*, *GbiC3HDZ.2* and *GbiACL5.1* in *G. biloba* shoots and roots. **A, C, E;** *in situ* hybridizations of the antisense probes in longitudinal cross sections of vegetative long-shoot SAM of **(A)** *GbiC3HDZ.1*, **(C)** *GbiC3HDZ.2* and **(E)** *GbiACL5.1*. **B, D, F;** *in situ* hybridizations of the antisense probes in cross sections of *Ginkgo biloba* roots during primary development of **(B)** *GbiC3HDZ.1*, **(D)** *GbiC3HDZ.2* and **(F)** *GbiACL5.1*. Scale bars represent 100 μm .



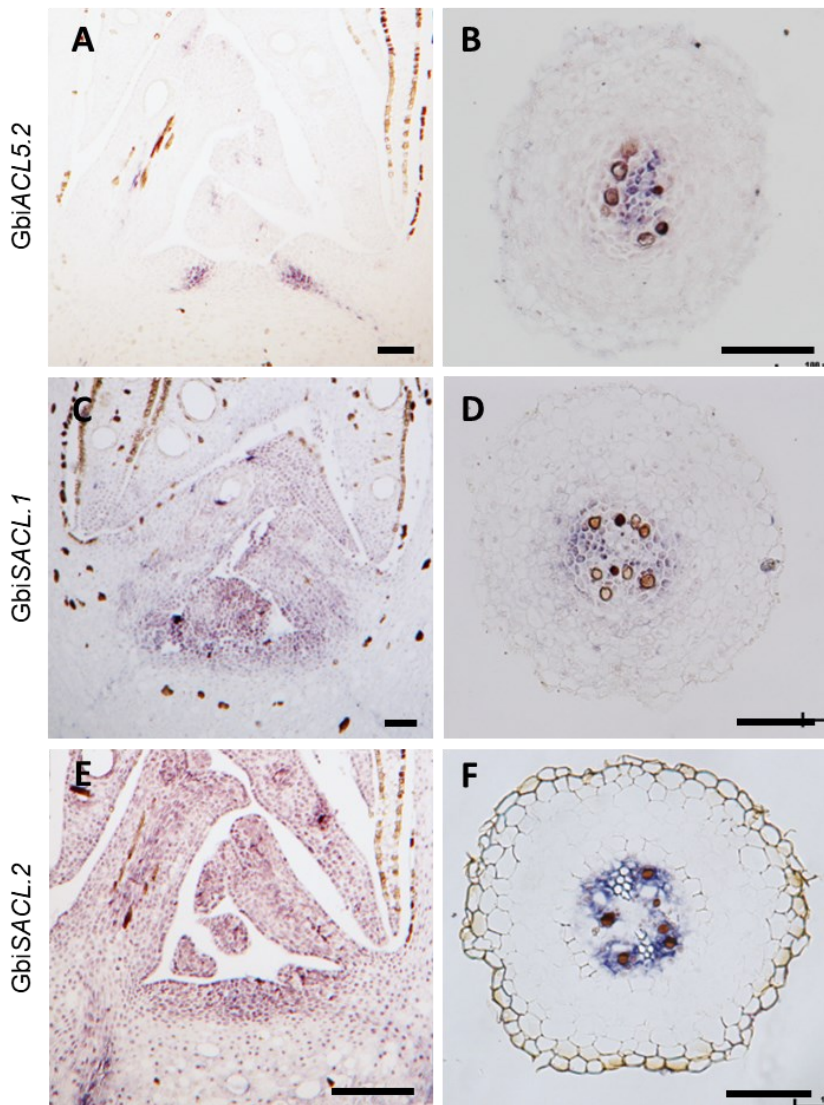


Figure 8. Expression of GbiACL5.2, GbiSACL.1 and GbiSACL.2 from *G. biloba* shoots and roots. A, C, E; *in situ* hybridizations of the antisense probes in longitudinal cross sections of vegetative long-shoot SAM of (A) GbiACL5.2, (C) GbiSACL.1 and (E) GbiSACL.2. B, D, F; *in situ* hybridizations of the antisense probes in cross sections of *Ginkgo biloba* roots during primary development of (B) GbiACL5.2, (D) GbiSACL.1 and (E) GbiSACL.2. Scale bars represent 100 μ m.



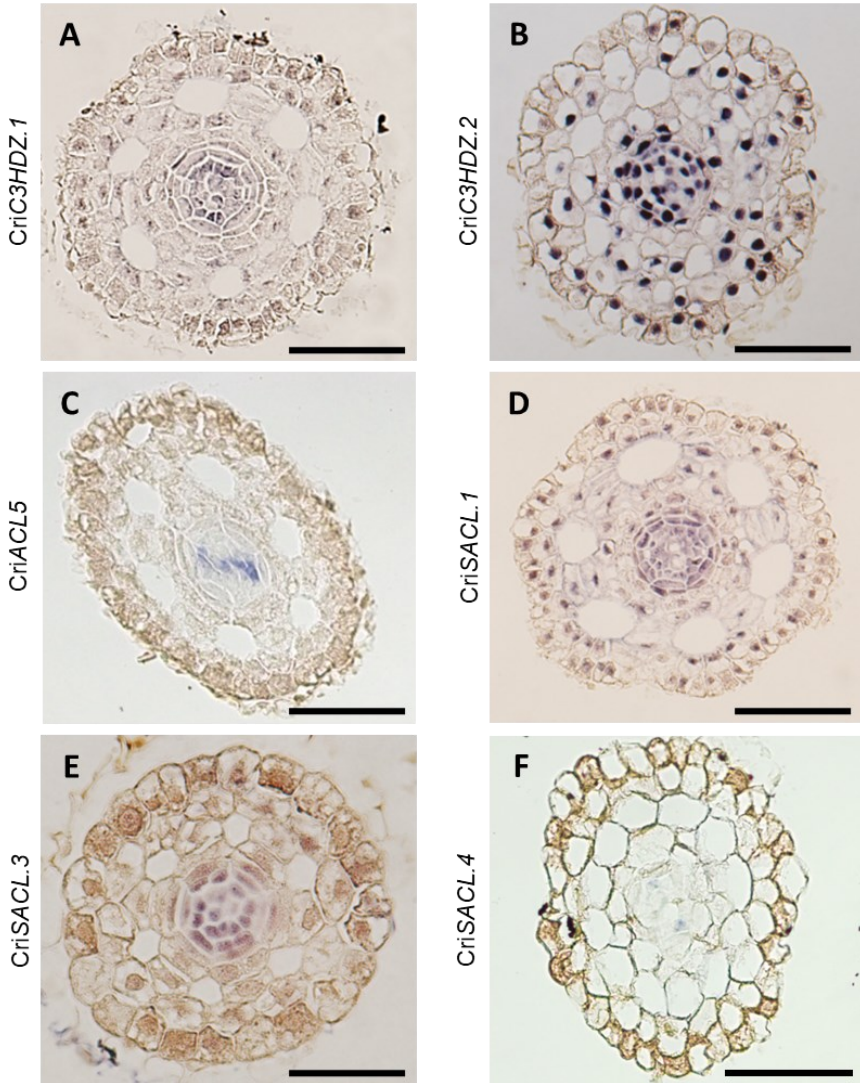


Figure 9. Expression of *C3HDZ*, *ACL5* and *SACL* orthologs in *C. richardii* root. *In situ* hybridizations of the antisense probes for (A) CriC3HDZ.1, (B) CriC3HDZ.2, (C) CriACL5, (D) CriSACL.1, (E) CriSACL.3 and (F) CriSACL.4 in root cross sections. Scale bars represent 100 μ m.



they exhibited different expression patterns, following a pattern fairly similar to that of the AtSACL orthologs in the root of *A. thaliana* (Vera-Sirera et al., 2015): CriSACL.1 expression is ubiquitous (**Figure 9D**), while CriSACL.3 and 4 are specific for the stele. However, CriSACL.3 mRNA was detected in the provascular tissues, endodermis and pericycle (**Figure 9E**), and CriSACL.4 is very specific of xylem precursor cells, at the xylem axis (**Figure 9F**). Regarding the sense probes, we did not observe any unspecific staining for any of the *C. richardii* genes (**Supplemental Figure 2**). In sum, we provide consistent evidence that all analyzed *C3HDZ*, *ACL5* and *SACL* orthologs express within the root provascular domain in *C. richardii*.

In the lycophyte *S. kraussiana*, all *C3HDZ*, *ACL5* and *SACL* orthologs examined were expressed in provascular tissues of the shoot and the rhizophore as well (**Figure 10**), except for SkrACL5.1, which is restricted to the rhizophore (**Figure 10 E, F and M**). In the rhizophore, SkrC3HDZ.1 and 2 accumulate at the stele and some cortex cells (**Figure 10 K and L** respectively); and SkrC3HDZ.2 is especially strong in developing xylem cells (**Figure 10L**). Our observations agree with previous studies that have localized SkrC3HDZ provascular expression in the shoots of *S. kraussiana* (Floyd et al., 2006; Floyd & Bowman, 2006; Prigge & Clark, 2006) and its close relative *S. moellendorffii* (Vasco et al., 2016). Regarding SkrACL5 orthologs, SkrACL5.1 domain is very specific of the xylem axis in the rhizophore (**Figure 10M**). SkrACL5.2, in turn, accumulates at the provascular tissues of the shoots with a similar domain in the rhizophore, in the xylem domain enclosed in the stele (**Figure 10 G, H and N**). SkrSACL mRNA is found in provascular tissues of the shoot (**Figure 10 I and J**) and the stele and 2-3 surrounding cortical cell layers (**Figure 10O**). We did not observe unspecific staining of sense probes for *S. kraussiana* (**Supplemental Figure 3**). In sum, our observations indicate that all *C3HDZ*, *ACL5* and *SACL* orthologs are expressed in provascular tissues in the lycophyte *S. kraussiana*.

The overlapping expression domains of these orthologs in vascular tissues seems to be conserved across tracheophytes. In addition, the fact that all paralogs in these species show different expression breadth or specificity towards vascular tissues argues in favor of an initial recruitment of their expression towards vascular tissues at the common ancestor of tracheophytes, which was followed by internal

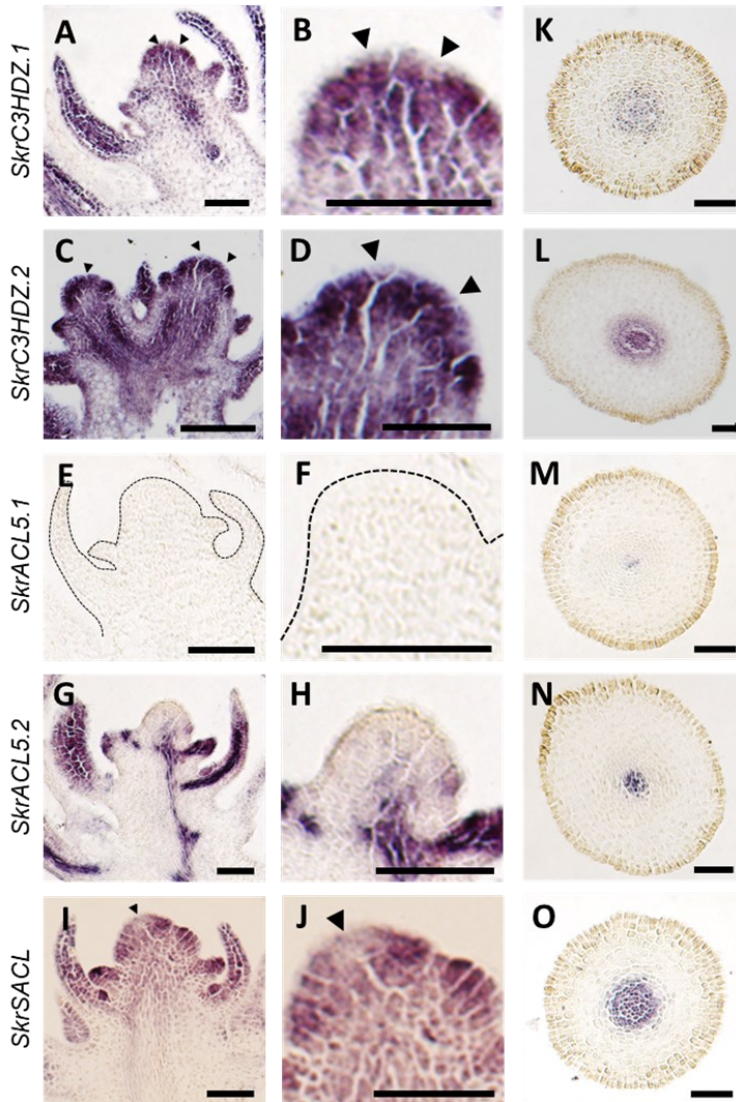


Figure 10. Expression of *C3HDZ*, *ACL5* and *SACL* orthologs in *S. kraussiana*. *In situ* hybridizations of the antisense probes. **A-I**; longitudinal cross sections of vegetative SAM of **(A)** *SkrC3HDZ.1*, **(C)** *SkrC3HDZ.2*, **(E)** *SkrACL5.1*, **(G)** *SkrACL5.2*, and **(I)** *SkrSACL*. **B-J**, close view on SAM on previous longitudinal cross sections; **K-O**, cross sections of rhizophores of **(K)** *SkrC3HDZ.1*, **(L)** *SkrC3HDZ.2*, **(M)** *SkrACL5.1*, **(N)** *SkrACL5.2*, and **(O)** *SkrSACL*. Scale bars represent 50 μm .



lineage duplications and paralog domain diversification. However, their functionality and connections as a module regulating vascular periclinal cell divisions in these species remains to be elucidated.

Expression of C3HDZ, ACL5 and SACL orthologs outside the vasculature in tracheophytes

In addition to the documented expression in the vascular domain, we observed relatively conserved expression patterns of the studied orthologs in other tissues. For instance, all C3HDZ orthologs are found in apical domains; in *G. biloba*, both GbiC3HDZ.1 and GbiC3HDZ.2 paralogs are expressed in the SAM and are especially strong in leaf primordia (**Figure 7 A and C**). However, while GbiC3HDZ.2 expression rapidly decreases in older leaf primordia (**Figure 7C**), GbiC3HDZ.1 expression seems to be maintained for a longer time (**Figure 7A**). The expression of GbiC3HDZ orthologs in apical regions agree with the work of Floyd et al. (2006) and Floyd & Bowman (2006), that documented GbiC3HDZ.1 expression in apical vegetative meristems in *G. biloba* as well as an ortholog from another gymnosperm species, *Pseudotsuga menziesii*. Similar studies have confirmed GbiC3HDZ.1-3 expression in developing leaf primordia, which is consistent with our results as well (Floyd et al., 2006; Zumajo-Cardona et al., 2021). However, they reported preferential expression on the adaxial side of the developing leaves, which would be difficult to observe in our longitudinal sections.

In *S. kraussiana*, all SkrC3HDZ paralogs have apical domains in addition to vascular tissues. Contrary to the observations by Floyd et al. (2006), who reported SkrC3HDZ.1 and 2 expression in apical cells and merophytes in the SAM, we observed specific expression of SkrC3HDZ.1 and 2 in the merophytes but excluding apical cells (**Figure 10 A-D**). This agrees with the findings by Prigge & Clark (2006) and Vasco et al. (2016). Both SkrC3HDZ paralogs in *S. kraussiana* also show an intense signal at leaf primordia, which is the commonly accepted C3HDZ expression domain in lycophytes in all previous studies (Floyd et al., 2006; Prigge & Clark, 2006; Vasco et al., 2016). In addition, C3HDZ orthologs are also found in the meristem of leptosporangiate ferns (see Glossary) (Vasco et al., 2016). Hence, our work with a

lycophyte and a gymnosperm agrees with the putative co-option of C3HDZ orthologs for the regulation of apical growth in the sporophyte in tracheophytes.

Regarding *ACL5* orthologs, we have provided a first evidence of *ACL5* expression in the SAM of lycophytes and gymnosperms; however, while *G. biloba* orthologs are found in the apical meristems and leaf primordia, in the lycophyte *S. kraussiana*, the expression was specifically restricted to leaf primordia. In addition, these expression patterns were not shared by all *ACL5* paralogs in these species. In *G. biloba*, only *GbiACL5.1* is expressed in SAMs and leaf primordia (**Figure 7E**), and the other paralog (*GbiACL5.2*) is restricted to provascular tissues (**Figure 8A**). A similar situation is found in *S. kraussiana* *ACL5* paralogs, one of which (*SkrACL5.2*) is expressed in leaf primordia (**Figure 10 G and H**) but the other paralog (*SkrACL5.1*) is not found in shoots and is specific for rhizophore vasculature (**Figure 10 E and F**). Our results suggest that *ACL5* could have been co-opted in shoot apical tissues in the common ancestor of tracheophytes, where it may participate in the regulation of apical meristems, leaf primordia, or both. Likewise, the *AtACL5* ortholog from the angiosperm *A. thaliana* has been found in the RAM (Baima et al., 2014; Clay & Nelson, 2005) but the expression in the SAM has been overlooked. Hence, future studies should consider revisiting *ACL5* expression in *A. thaliana*, which would allow to infer the possible conservation of *ACL5* function in the regulation of apical meristems. In addition, considering that *ACL5* has been previously identified to participate during embryogenesis in Scots pine, a gymnosperm (Vuosku et al., 2019), the role of *ACL5* outside of vascular development in vascular plants is possibly much broader than what has been hitherto studied.

Interestingly, we documented a strong expression of *GbiACL5.1* in secretory ducts in the shoots of *G. biloba*. These are tissues that later in development undergo cell death to create the final hollow conduct (**Figure 7E**) (Cartayrade et al., 1990), and may indicate that *ACL5* role in plant cell death is conserved in tracheophytes (Muñiz et al., 2008; Vuosku et al., 2019).

As in the case of *ACL5* orthologs, this is the first time that the expression of *SACL* orthologs has been documented in SAMs (Katayama et al., 2015; Vera-Sirera et



al., 2015). We have observed that *SACL* orthologs are expressed in SAMs and leaf primordia in *G. biloba* (**Figure 8 C and E**) as well as in merophytes (but not the apical cell) and leaf primordia of *S. kraussiana* shoots (**Figure 10 I and J**). Hence, our results suggest that *SACL* orthologs may have been co-opted and participate in the regulation of apical meristems and/or leaf primordia development in tracheophytes.

Although the detection of *C3HDZ*, *ACL5* and *SACL* expression in apical meristems in different tracheophytes suggests that they may have a function in those cells, the question still remains if they can operate together as a module (as observed in *A. thaliana* vascular tissues). One interpretation is that they might regulate cell divisions and growth, which is supported by circumstantial evidence from different sources: this is what MpC3HDZ and MpACL5 seem to do in apical notches in *M. polymorpha* (**Chapter 2**), and it is what AtC3HDZ and AtACL5 (together with AtSACLs and AtLHW-AtTMO5) do in differentiating xylem cells (Vera-Sirera et al., 2015). However, the expression of AtLHW and AtTMO5 has only been characterized in roots and AtTMO5 expression has been located in the cotyledon primordia of the embryo (de Rybel et al., 2014), but their expression has been overlooked in the SAM of *A. thaliana* (de Rybel et al., 2013; Katayama et al., 2015; Vera-Sirera et al., 2015). Likewise, it is also possible that the downstream regulation of these genes may be divergent in different tracheophyte apical meristems, given that they might share domain with other putative downstream targets (Hodin, 2000), which would need to be explored.

SACL heterodimerization activity has diverged during land plant evolution

The results shown above suggest that the overlapping expression of *C3HDZ*, *ACL5* and *SACL* genes in the developing vascular tissues in tracheophytes marked the evolutionary origin of their joint action in the control of vascular cell proliferation, together with the appearance of a Tspm-regulated uORF in the 5'-leader sequence of *SACL* transcripts. However, it is still unclear how this module became connected to the LHW/TMO5 heterodimer that ultimately promotes cytokinin synthesis and cell proliferation. Considering that this connection happens in *A. thaliana* through direct physical interaction between AtSACL and AtLHW, we hypothesized that the ability of *SACL* to interact with different partners diverged after the separation of



tracheophytes and bryophytes. We hence tested the intra- and inter-species interactions between SACL and LHW or RSL1 orthologs from the tracheophyte *A. thaliana* and the bryophyte *M. polymorpha*. The results of Y2H and BiFC interaction assays are summarized in **Figure 11**.

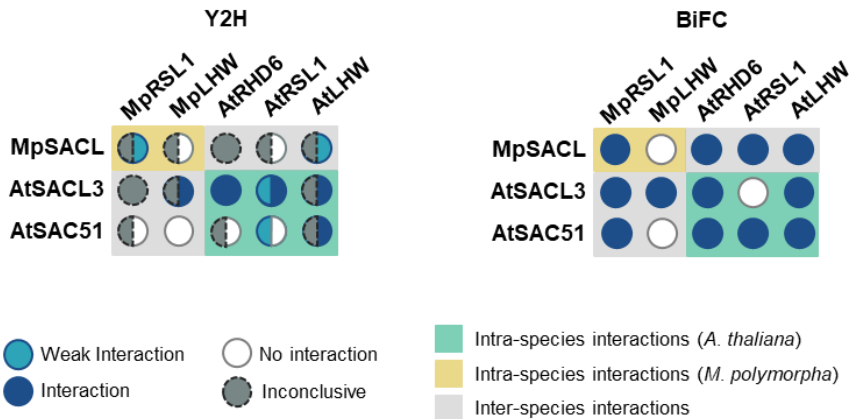


Figure 11. Summary of interactions in Yeast-2-Hybrid and Bimolecular Fluorescence Complementation assays between SACL, LHW and RSL class I orthologs. Dark blue circles indicate positive strong interaction, light blue circles indicate weak interaction; White circles indicate no interaction, and dark grey and dotted circles indicate inconclusive results due to the auto-activation effects on Y2H. Turquoise boxes mark the intra-species interactions in *A. thaliana*, yellow boxes the intra-species interactions in *M. polymorpha*, and grey boxes mark the inter-species interactions. These analyses were based on two replicates performed on different times.

The Y2H assays were limited by the auto-activation of MpSACL, MpRSL1, ROOT HAIR DEFECTIVE 6 (AtRHD6), and AtLHW when fused to the Gal4 DNA Binding Domain (Gal4BD) (**Figure 12A**). Nevertheless, we could confirm interaction between the MpSACL HLH domain and the full-length AtLHW protein fused to the Gal4 Activation Domain (Gal4AD) (**Figure 12B**), as well as with MpRSL1, which was used as a positive control (**Chapter 2**). However, these interactions did not occur when the media was complemented with 5 mM 3AT. Regarding *A. thaliana* SACL orthologs, we only observed positive interaction of AtSAC51-Gal4BD with AtLHW, which was



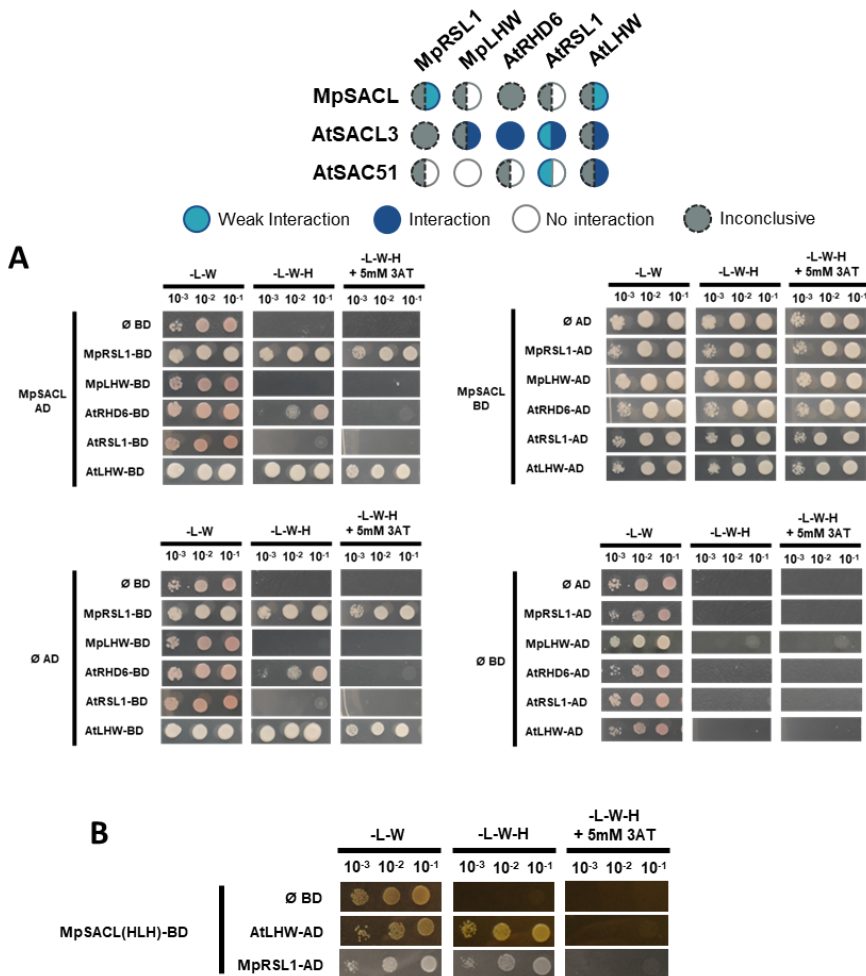


Figure 12. Reciprocal Yeast 2 Hybrid assays between MpSACL, LHW and RSL class I orthologs. Top: summary of Y2H interactions of all SACL orthologs with LHW and RSL class I orthologs to ease comparison (adapted from **Figure 11**). **A**, Reciprocal interactions with full length proteins; **B**, Interactions between the HLH domain of MpSACL and full length MpRSL1 and AtLHW proteins. Different interactions were tested in growth control, lacking leucine and tryptophan (-L-W), in histidine-free SD media (-L-W-H) and histidine-free media complemented with 5 mM 3AT (-L-W-H+5 mM 3AT) to test interaction strength. Y2H Empty vectors (pGADT7 and pGBT7) containing Gal4 Activation Domain (AD) or Binding Domain (BD) respectively were used as negative controls. Analyses were based on two replicates performed on different times.

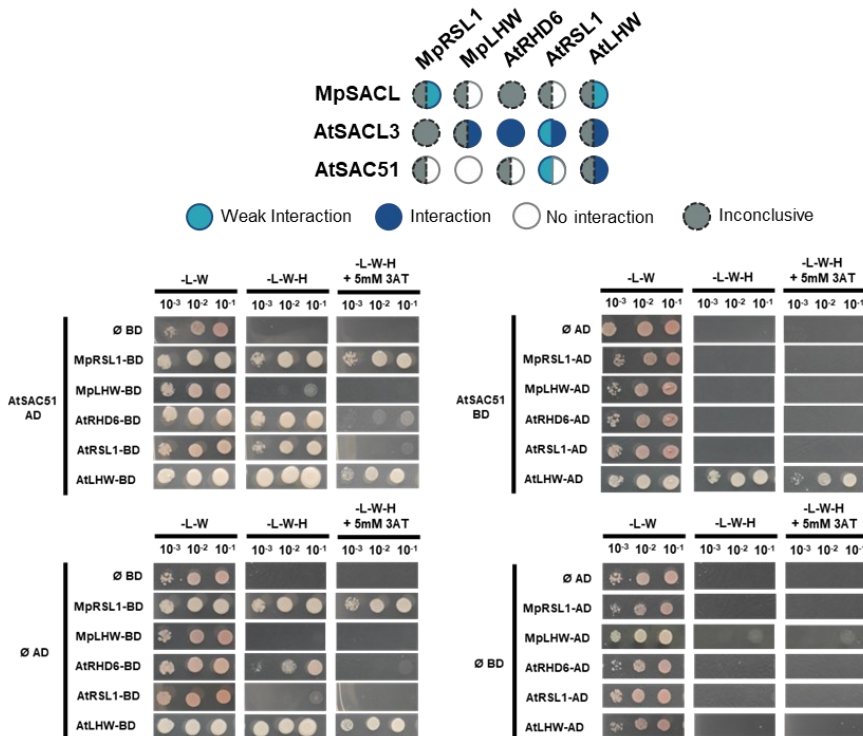


Figure 13. Reciprocal Yeast 2 Hybrid assays between AtSAC51, LHW and RSL class I orthologs. Top: summary of Y2H interactions of all SACL orthologs with LHW and RSL class I orthologs to ease comparison (adapted from **Figure 11**). Different interactions were tested in growth control, lacking leucine and tryptophan (-L-W), in histidine-free SD media (-L-W-H) and histidine-free media complemented with 5 mM 3AT (-L-W-H+5 mM 3AT) to test interaction strength. Y2H Empty vectors (pGADT7 and pGBKT7) containing Gal4 Activation Domain (AD) or Binding Domain (BD) respectively were used as negative controls. Analyses were based on two replicates performed on different times.



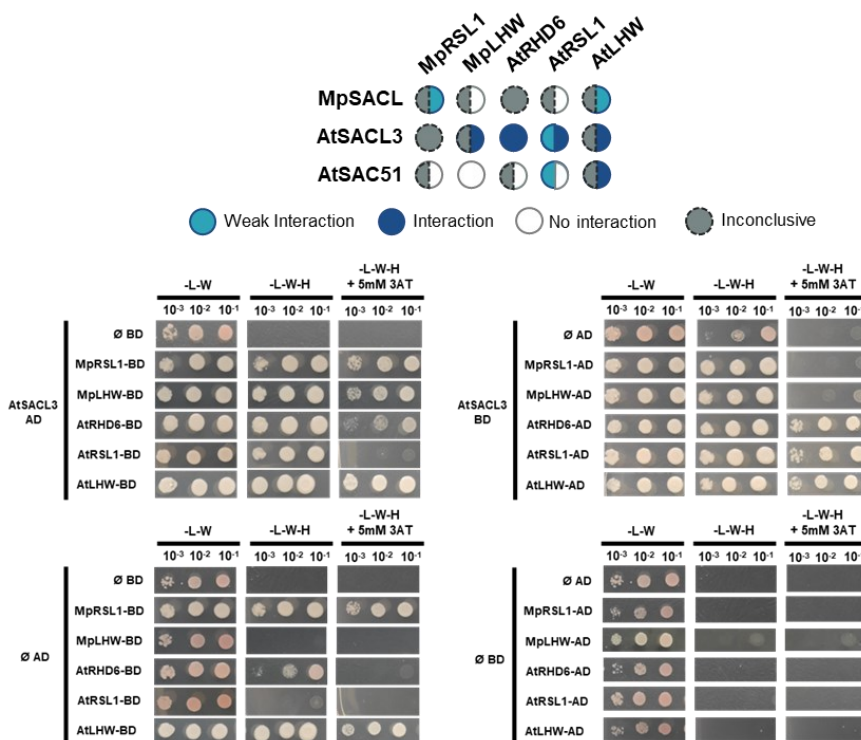


Figure 14. Reciprocal Yeast 2 Hybrid assays between AtSACL3, LHW and RSL class I orthologs. Top: summary of Y2H interactions of all SACL orthologs with LHW and RSL class I orthologs to ease comparison (adapted from **Figure 11**). Different interactions were tested in growth control, lacking leucine and tryptophan (-L-W), in histidine-free SD media (-L-W-H) and histidine-free media complemented with 5 mM 3AT (-L-W-H+5 mM 3AT) to test interaction strength. Y2H Empty vectors (pGADT7 and pGBKT7) containing Gal4 Activation Domain (AD) or Binding Domain (BD) respectively were used as negative controls. Analyses were based on two replicates performed on different times.

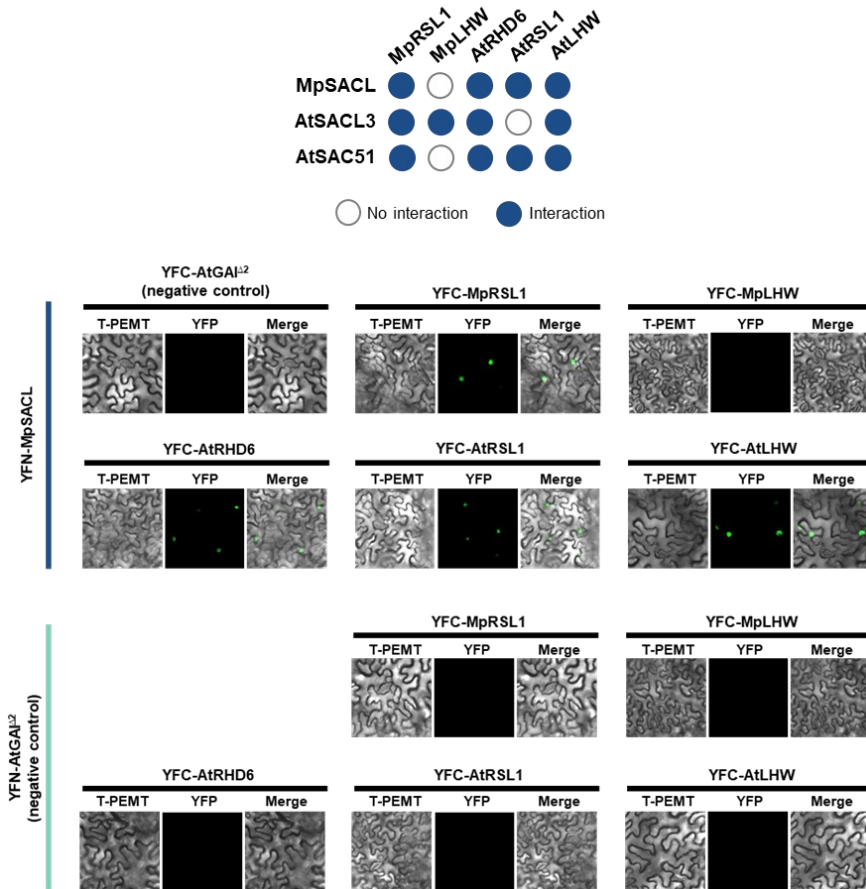


Figure 15. BiFC assay on *N. benthamiana* leaves between MpSACL, LHW and RSL class I orthologs. Top: summary of BiFC interactions of all SACL orthologs with LHW and RSL class I orthologs to ease comparison. Dark blue circles indicate positive interaction and white circles indicate no interaction. For these experiments, MpSACL was always fused to the N-terminal of a YFP - YFN, and interactions were tested with potential partners fused to the C-terminal of YFN (YFC). AtGAI^{Δ2} was used as a negative control in all interactions. Images are shown in transmitted White light (T-PEMT), Emission field for YFP (503-517 nm), or merged channels (T-PEMT + YFP).



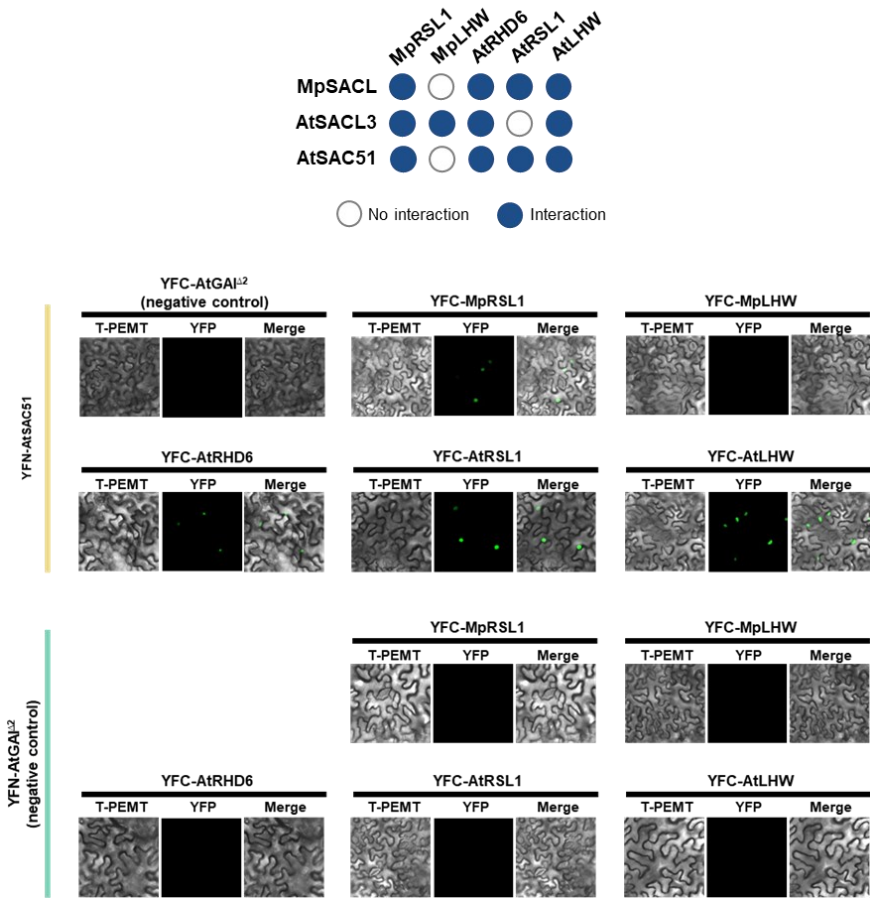


Figure 16. BiFC assay on *N. benthamiana* leaves between AtSAC51, LHW and RSL class I orthologs. Top: summary of BiFC interactions of all SACL orthologs with LHW and RSL class I orthologs to ease comparison. Dark blue circles indicate positive interaction and white circles indicate no interaction. For these experiments, AtSAC51 was always used fused to the N-terminal of a YFP - YFN, and interactions were tested with potential partners fused to the C-terminal of YFN (YFC). AtGAI^{Δ2} was used as a negative control in all interactions. Images are shown in transmitted White light (T-PEMT), Emission field for YFP (503-517 nm), or merged channels (T-PEMT + YFP).



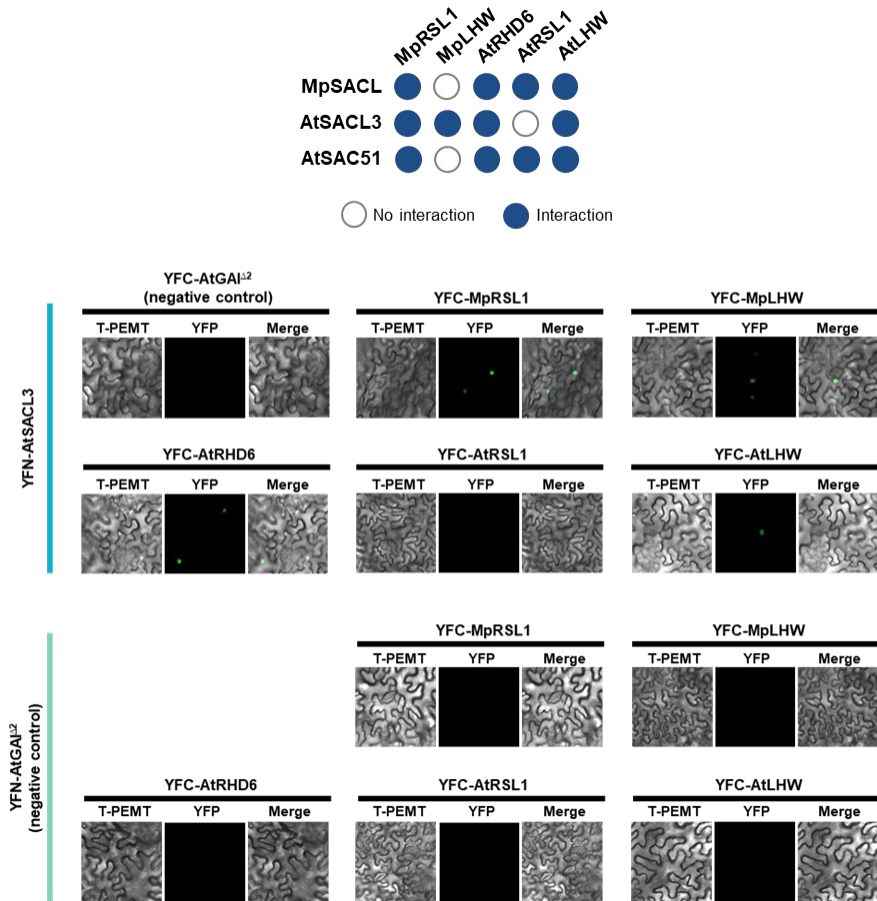


Figure 17. BiFC assay on *N. benthamiana* leaves between AtSACL3, LHW and RSL class I orthologs. Top: summary of BiFC interactions of all SACL orthologs with LHW and RSL class I orthologs to ease comparison. Dark blue circles indicate positive interaction and white circles indicate no interaction. For these experiments, AtSACL3 was always used fused to the N-terminal of a YFP - YFN, and interactions were tested with potential partners fused to the C-terminal of YFN (YFC). AtGAI^{A2} was used as a negative control in all interactions. Images are shown in transmitted White light (T-PEMT), Emission field for YFP (503-517 nm), or merged channels (T-PEMT + YFP).



maintained after 5 mM 3AT; and also, with AtRSL1 when AtSAC51 was fused to Gal4BD, although this interaction was lost in more restrictive conditions (**Figure 13**). AtSACL3-Gal4BD, in turn, showed positive interactions with AtRHD6, AtRSL1 and AtLHW under 5 mM 3AT (**Figure 14**), and AtSACL3-Gal4AD also showed an interaction with MpLHW (**Figure 14**).

In the BiFC assay, MpSACL showed positive interactions with all RSL class I orthologs from *M. polymorpha* and *A. thaliana* (**Figure 15**); however, regarding LHW orthologs, MpSACL was only able to interact with the *A. thaliana* AtLHW, but not MpLHW from *M. polymorpha* (**Figure 15**). AtSAC51, in turn, can interact with all RSL class I orthologs, in addition to AtLHW, but not MpLHW (**Figure 16**). Lastly, AtSACL3 had a positive interaction with all LHW and RSL class I orthologs from both species, except for AtRSL1 (**Figure 17**).

Considering all the positive interactions in either one of the experimental approaches (**Figure 11**), we conclude that the SACL-LHW interaction was acquired at some point during the evolution of the tracheophyte lineage, while the SACL-RSL interaction was probably present in the last common ancestor of land plants. Given that SACL and LHW can establish heterologous interactions, it is difficult to discern whether this interaction in tracheophytes was caused by changes in the SACL or in the LHW proteins. Interestingly, our results in heterodimerization activity between three bHLH members, and by extension, the work of Lu et al. (2020), which confirmed that TMO5 and LHW orthologs are not able to interact in *K. nitens*, a charophyte, suggest that the heterodimerization activity of bHLH proteins is divergent in different land plant lineages. This confirms and at the same time, contrasts the hypotheses by Pires and Dolan (2010a, 2010b) which concluded that bHLH interactions are conserved across land plant lineages. Our results, hence, suggest that although this is true for some bHLH proteins, like SACL and RSL class I orthologs, conserved interactions cannot always be assumed.



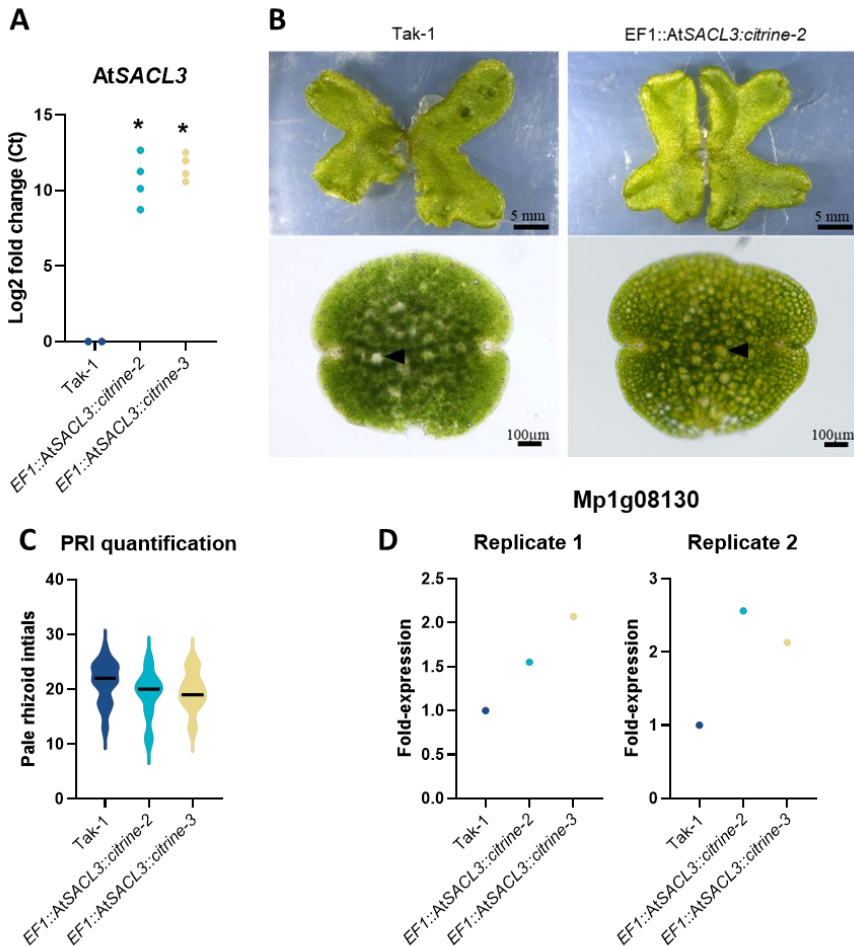


Figure 18. AtSACL3 does not share downstream regulation with MpSACL. **A**, quantification of *AtSACL3* transcripts by RT-qPCR from four biological replicates; **B**, Phenotype in thalli and gemmae from Tak-1 and *EF1::AtSACL3::citrine-2*. Black arrowheads indicate pale rhizoid initials. **C**, PRI quantifications in Tak-1, *EF1::AtSACL3::citrine-2* and *EF1::AtSACL3::citrine-3*, with no significant changes ($18 \geq n \geq 8$). **D**, Relative expression of Mp1g08130 in Tak-1, *EF1::AtSACL3::citrine-2* and *EF1::AtSACL3::citrine-3* quantified by RT-qPCR from 2 biological replicates.



Next, we assessed whether the positive interactions in the Y2H and BiFC had relevant consequences *in vivo*. Hence, we hypothesized that AtSACLs would be functionally equivalent to MpSACL in *M. polymorpha*. To test this hypothesis, we performed a heterologous expression of AtSACL3 in *M. polymorpha* since it is the most closely related ortholog to MpSACL based on our phylogenetic analysis (**Chapter 1**). We generated two independent *EF1::AtSACL3:citrine* lines in Tak-1 background, both with a similar AtSACL3 transcript accumulation (**Figure 18A**).

Since AtSACL3 can interact with MpRSL1 and MplHW, we looked for any defective phenotypes that could derive from a loss of function of MpRSL1 or MplHW in these lines, as a consequence of inhibition through AtSACL3. For MpRSL1, we analyzed gemma development in gemma cups, as well as rhizoid development. However, we did not observe any defective phenotype in *EF1::AtSACL3:citrine* (**Figure 18B**); gemma cups produced gemmae, and PRI developed similarly to Tak-1 (**Figure 18 B and C**), which suggests that AtSACL3 does not compromise MpRSL1 downstream regulation in *M. polymorpha*. As for the interaction with MplHW, we quantified the expression of Mp1g08130, a gene induced in *Mplhw* mutant background, given that *Mplhw* loss of function mutants do not seem to have any observable defective phenotype (Lu et al., 2020). In both constitutive expression lines, the Mp1g08130 transcript abundance was between 1.5 and 2-fold higher in replicate 1, and between 2 and 2.5-fold in replicate 2 compared to Tak-1 (**Figure 18D**), which suggests that MplHW downstream regulation is compromised in constitutive expression of AtSACL3. Taken together, our results suggest that the biochemical properties of SACL orthologs have diverged in the tracheophyte and bryophyte lineages. In other words, changes in SACL biochemical properties may underlie the species-specific functions downstream of SACLs.



MATERIALS

Plant material and growth conditions

Ginkgo biloba SAMs were obtained from adult trees grown in the New York Botanical Garden (NYBG) (1358/97 F Princeton Nurseries) whereas RAM were obtained from seedlings from the same trees grown in a growth chamber (16-hour long day conditions at 23°C). *Ceratopteris richardii* Rn-3 spores were germinated in liquid basal medium (0.5x MS salts at pH 6.0) for 3 days at 28°C at long day conditions (16h light). Then, the germinated spores were grown in the same solution in a shaker (200 rpm) at room temperature for 9 days. The gametophytes were transferred into soil and grown at room temperature and long day conditions. Young roots were collected from 14-day-old sporophytes. SAMs and rhizophores of *Selaginella kraussiana* var. *aurea* were obtained from the NYBG.

Histological analyses and toluidine blue staining

G. biloba, *C. richardii* and *S. kraussiana* tissues were fixed in formaldehyde acetic acid solution (FAA: 50% absolute EtOH, 5% glacial acetic acid, 5% formaldehyde) for 2h at room temperature, starting with a 20' vacuum, and then dehydrated with EtOH series up to 70% EtOH. Paraffin embedding, sectioning and toluidine blue staining was performed as described in **Chapter 2**.

RNA extraction and cDNA synthesis

Previous to the *in situ* hybridizations, probes for C3HDZ, ACL5 and SACL orthologs were designed according to the sequences retrieved from our phylogenetic analyses (**Chapter 1**) and were amplified from RNA extractions from apical tissues (for *G. biloba*) or whole plants (for *C. richardii* and *S. kraussiana*) in individuals identified at the New York Botanical Garden (NYBG). RNA extraction from *Ginkgo biloba* SAMs was performed according to Wang et al. (2005). *Ceratopteris richardii*, *Selaginella kraussiana* var. *aurea* and *M. polymorpha* RNA was extracted with the Nucleospin RNA Plant Macherey Nagel kit (Cultek) following the manufacturer's instructions. cDNA was synthesized from 8μL using the NZY First-Strand cDNA Synthesis kit following the manufacturer's instructions.



Ortholog identification and phylogenetic analysis

Orthologs from *Ginkgo biloba*, *Ceratopteris richardii* and *Selaginella kraussiana* var. *aurea* were previously identified as specified in **Chapter 1**. Additionally, most C3HDZ orthologs were also identified in previous studies, except for CriC3HDZ.3 (Floyd et al., 2014; Prigge & Clark, 2006a). All orthologs were confirmed by phylogenetic analysis (PhyML) with representative members of the C3HDZ family, ACL5, and SACL family from the streptophyte lineage using the NGPhylogeny.fr webtool (Lemoine et al., 2019) and the Interactive Tree of Life webtool (iTOL) version 6.5.8 (<https://itol.embl.de/>) and represented in modified figures from **Chapter 1**. The identification of uORF sequences in *SACL* 5' leaders was performed in the available transcripts from SACL orthologs from *G. biloba*, *C. richardii* and *S. kraussiana*. uORF proteic sequences were aligned in MEGA X (Kumar et al., 2018) using MAFFT ver. 7 in default parameters (Katoh & Standley, 2013).

in situ hybridization

Sense and antisense probes were designed to target a 500bp-long unique sequence for each gene. The PCR fragments were amplified from cDNA with an Econo-Taq PLUS GREEN (Biosearch Technologies). Sense and antisense PCR templates for probes were amplified from the PCR products with primers containing T7 promoter overhangs. The primers used for probe synthesis and gene information are listed in **Table 2**. To ensure that only the PCR product was amplified, PCR products were run in a 1% agarose gel and the 500 bp size bands were cut under UV light and purified with Nucleospin Gel and PCR clean-up kit (Macherey-Nagel) according to manufacturer's instructions. Then, the final PCR products were checked by restriction enzyme digestion to ensure that the sequence was correct. Probe synthesis and DIG labelling were performed according to the manufacturer's instructions (Roche Applied Science). Tissues were fixed in formaldehyde acetic acid for 2h at room temperature, starting with a 20' vacuum, and then dehydrated with EtOH series to 100% EtOH. Tissue embedding, sectioning, hybridization and detection was done as previously described (Ambrose et al., 2000) except for *G. biloba* SAMs sections, whose thickness was 10µm.



Species	Name (gene)	Sequence
<i>Ginkgo biloba</i>	GbiC3HDZ1_F	GTTGTAGCATCTGTGCAGAGGG
	GbiC3HDZ1_R	ATGCAGTGGGTGCTGTCTCG
	GbiC3HDZ1_F_T7	CTAATACGACTCACTATAGGGGTTGTAGCATCTGTGCAGAGGG
	GbiC3HDZ1_R_T7	CTAATACGACTCACTATAGGGGATGCAGTGGGTGCTGTCTCG
	GbiC3HDZ2_F	GGTAATGATGGAACAGATGATGTAACCTATT
	GbiC3HDZ2_R	TAGGAGCAACACAAAGTTCAGCA
	GbiC3HDZ2_F_T7	CTAATACGACTCACTATAGGGGGTAAATGATGGAACAGATGATGTAACCTATT
	GbiC3HDZ2_R_T7	CTAATACGACTCACTATAGGGTAGGAGCAACACAAAGTTCAGCA
	GbiACL5.1_F	ATCATGAATCCCTGGTGATCC
	GbiACL5.1_R	GCCTACGAAGGCACGTGAG
	GbiACL5.1_F_T7	CTAATACGACTCACTATAGGGATCATGAATCCCTGGTGATCC
	GbiACL5.1_R_T7	CTAATACGACTCACTATAGGGCGTACGAAGGCACGTGAG
	GbiACL5.2_F	GTTATAAACGACGCCAGGGCT
	GbiACL5.2_R	CCATGTACAAAACGGGCTGTC
	GbiACL5.2_F_T7	CTAATACGACTCACTATAGGGGTTATAAACGACGCCAGGGCT
	GbiACL5.2_R_T7	CTAATACGACTCACTATAGGGCCATGTACAAAACGGGCTGTC
	GbiSACL1_F	GTGCAAGTAGAGTGAGCTGTAATG
	GbiSACL1_R	AGCTGATCCAAATTGCATTTGC
	GbiSACL1_F_T7	CTAATACGACTCACTATAGGGGTGCAAGTAGAGTGAGCTGTAATG
	GbiSACL1_R_T7	CTAATACGACTCACTATAGGGAGCTGATCCCAAATGCAATTTGC
GbiSACL2_F	GCTGCAGAAAAGACATCTGTTATATCA	
GbiSACL2_R	ACAGAGTAAGCTACAAAGCTATTCCA	
GbiSACL2_F_T7	CTAATACGACTCACTATAGGGGCTGCAGAAAAGACATCTGTTATATCA	
GbiSACL2_R_T7	CTAATACGACTCACTATAGGGACAGAGTAAGCTACAAAGCTATTCCA	
<i>Ceratopteris richardii</i>	CriHDZiPIII.1_F	GATGATTTGCATTAAITCCCTCTGGTTTC
	CriHDZiPIII.1_R	GCCTGCAAATATGCTTCACTACTTC
	CriHDZiPIII.1_F_T7	CTAATACGACTCACTATAGGGGATGATATTGCATTAAITCCCTCTGGTTTC
	CriHDZiPIII.1_R_T7	CTAATACGACTCACTATAGGGGCTGCAAATATGCTTCACTACTTC
	CriHDZiPIII.2_F	AGCTCTGTGAAAATTTCTGAGTCGAG
	CriHDZiPIII.2_R	CTCGAAATAAGTGTGTCAGGATGT
	CriHDZiPIII.2_F_T7	CTAATACGACTCACTATAGGGAGCTCTGTGAAAATTTCTGAGTCGAG
	CriHDZiPIII.2_R_T7	CTAATACGACTCACTATAGGGCTGCAAATAAGTGTGTCAGGATGT
	CriACL5_F	TCGCTCCCTCAGGTGTG
	CriACL5_R	AGTGCCAGGATGAACCAGGCA
	CriACL5_F_T7	CTAATACGACTCACTATAGGGGTGCTCCCTCAGGTGTG
	CriACL5_R_T7	CTAATACGACTCACTATAGGGAGTGCAGGATGAACCAGGCA
	CriSACL1_F	GATGCAATTGCTAGAACAGAGAACCA
	CriSACL1_R	GACAATACTGCATCCACTGGGG
	CriSACL1_F_T7	CTAATACGACTCACTATAGGGGATGCAATTTCTAGAACAGAGAACCA
	CriSACL1_R_T7	CTAATACGACTCACTATAGGGGCAACTGCTCATCCACTGGGG
	CriSACL3_F	CTGGGATGCGAAAGGCATAAATC
	CriSACL3_R	GAATATCCTCATCATGCTCATCATCAGA
	CriSACL3_F_T7	CTAATACGACTCACTATAGGGCTGGGATGCGAAAGGCATAAATC
	CriSACL3_R_T7	CTAATACGACTCACTATAGGGGAATATCCTCATCATGCTCATCATCAGA
CriSACL4_F	CTAGAAAGTGATCACGAATTCACCTTTATCG	
CriSACL4_R	CTTTCAGAATGACTGTAGAGGACTG	
<i>Selaginella kraussiana</i>	SkrHDZiPIII.1_F	TTGCTTCGAGGTGGACAACAG
	SkrHDZiPIII.1_R	GTCCCAGAGACGTTGTCTGTGT
	SkrHDZiPIII.1_F_T7	CTAATACGACTCACTATAGGGTTGCTTCGAGGTGGACAACAG
	SkrHDZiPIII.1_R_T7	CTAATACGACTCACTATAGGGGTCACAGAGACGTTGTCTGTGT
	SkrHDZiPIII.2_F	GAGTCGCTCCCTCCCTCG
	SkrHDZiPIII.2_R	AACTCTTCTCCTCAGAAGAATGAATGAG
	SkrHDZiPIII.2_F_T7	CTAATACGACTCACTATAGGGGAGTGCCTCCGCTCCCG
	SkrHDZiPIII.2_R_T7	CTAATACGACTCACTATAGGGAATCTTCTCCTCAGAAGAATGAATGAG
	SkrACL5.1_F	CCACAGCTCGTGAAGTACTGAGA
	SkrACL5.1_R	TACTCTCACATCAAAGTGGTTGGC
	SkrACL5.1_F_T7	CTAATACGACTCACTATAGGGCCACAGCTGCTGAAGTACTGAGA
	SkrACL5.1_R_T7	CTAATACGACTCACTATAGGGTACTCTCACATCAAAGTGGTTGGC
	SkrACL5.2_F	GAAGTTCACCTCAATGGCACACT
	SkrACL5.2_R	CTTGACATCGTTTTAGCAGAGATCCA
	SkrACL5.2_F_T7	CTAATACGACTCACTATAGGGGAAGTTCACCTCAATGGCACACT
	SkrACL5.2_R_T7	CTAATACGACTCACTATAGGGCTTGCATCGTTTTATGACGAGATCCA
	SkrSACL_F	TGAGTTTCCCAGCAATGGTAATGG
	SkrSACL_R	CGATCAAGGCAGCATTGCTG
SkrSACL_F_T7	CTAATACGACTCACTATAGGGTGAGTTTCCAGCAATGGTAATGG	
SkrSACL_R_T7	CTAATACGACTCACTATAGGGCGATCAAGGCAGCATTGCTG	

Table 2. List of primers used for the synthesis of *In situ* hybridization sense and antisense probes



Y2H assay

The entry clones with CDS of MpSACL and MpRSL1 were previously obtained on **Chapter 2**. The HLH domain of MpSACL was obtained from *M. polymorpha* cDNA and cloned into a pDONR207 through a BP reaction (Gateway technology, Invitrogen); the rest of the entry clones were obtained from Vera-Sirera et al., (2015) (AtSAC51 and AtLHW) or synthesized in GBLOCKS (IDT) and further cloned into a pDONR207 through a BP reaction (MpLHW, AtSACL3, AtRHD6, and AtRSL1). The primers used to amplify CDS for the Y2H, as well as gene information are listed on **Table 3**. The entry clones were used to generate Gal4-binding domain and Gal4-activation domain fused proteins by cloning the CDS into the destination vectors pGBKT7 and pGADT7 respectively via LR clonase II (Invitrogen). MpSACL HLH domain was just used for the fusion with Gal4-binding domain. The rest of the assay was performed as specified in **Chapter 2**.

Name	Gene	Origin	Direction	Sequence
MpSACL	Mp5g09710	cDNA	Forward Reverse	GGGGACAAGTTTGTACAAAAAAGCAGGCTCTCAATTGTCAATGAAGAGGAGAG GGGGACCACCTTTGTACAAGAAAGCTGGGTATTCCAGTCTTCACGTACG
MpSACL (HLH)	Mp5g09710	cDNA	Forward Reverse	GGGGACAAGTTTGTACAAAAAAGCAGGCTACATGTCTCGCTCGAGCTGCAAAATG GGGGACCACCTTTGTACAAGAAAGCTGGGTATTCCAGTCTTCACGTACG
MpRSL1	Mp3g17930	cDNA	Forward Reverse	GGGGACAAGTTTGTACAAAAAAGCAGGCTTGATGAGCTCGAGAACGCTGACACT GGGGACCACCTTTGTACAAGAAAGCTGGGTAGAGTTGGTTGTCTGCTTGATTGG
MpLHW	Mp7g02370	GBLOCKS	Forward Reverse	GGGGACAAGTTTGTACAAAAAAGCAGGCTCAATGGCAATGGTGTCTGACAGCAG GGGGACCACCTTTGTACAAGAAAGCTGGGTCTCGGCTGTCACTTGGAGAGG
AtSAC51	At5g64340	Vera-Sirera et al. (2015)	Forward Reverse	- -
AtSACL3	At1G29950	GBLOCKS	Forward Reverse	GGGGACAAGTTTGTACAAAAAAGCAGGCTTGATGAGCAACAATCAGTTTCCTCACT GGGGACCACCTTTGTACAAGAAAGCTGGGTAGATTGGTTTGAGAAATGTCCAACG
AtRHD6	At1G66470	GBLOCKS	Forward Reverse	GGGGACAAGTTTGTACAAAAAAGCAGGCTTTATGGCACTCGTTAATGACCATCCCA GGGGACCACCTTTGTACAAGAAAGCTGGGTTTTAATTGGTGATCAGATTCGAATTCCTGC
AtRSL1	At5G37800	GBLOCKS	Forward Reverse	GGGGACAAGTTTGTACAAAAAAGCAGGCTTTATGTCACCTATTACGCAATTCGAATGA GGGGACCACCTTTGTACAAGAAAGCTGGGTTTTATTCTGCTATACCTTGTTCTCTAGTTGA
AtLHW	At2G27230	Vera-Sirera et al. (2015)	Forward Reverse	- -

Table 3. List of primers used for the generation of entry clones for Y2H and BiFC.

BiFC assays

For BiFC, the entry clones used for the Y2H assay were used to fuse the N-terminal or C-terminal ends to full proteins of SACL, LHW and RSL class I orthologs. SACL orthologs (MpSACL, AtSAC51 and AtSACL3) were cloned into pMDC43-YFN and the rest of the proteins (MpLHW, MpRSL1, AtRHD6, AtRSL1, and AtLHW) were cloned into an pMDC43-YFC (Belda-Palazón et al., 2012). The rest of the assay was performed as described in **Chapter 2**.



Generation of *M. polymorpha* transgenic lines

For the generation of *EF1::AtSACL3:citrine* lines, the entry clone containing AtSACL3 was fused with the pMpGWB108 plasmid (Ishizaki et al., 2015) through LR clonase II reaction (Gateway technology, Invitrogen). Successful pDEST clone was transformed into Tak-1 thalli as described in Ishizaki et al., (2008). Transformants were selected on ½ strength Gamborg media containing Hygromycin (Applichem, Epica S.L). Quantification of AtSACL3 and Mp1g08130 transcripts was performed from cDNA in a RT-qPCR, and the primers used for this analysis are listed on **Table 4**. PRI quantification was performed as described in **Chapter 1**.

Name	Gene	Direction	Sequence
AtSACL3	At1G29950	Forward	AGAAGAAGTCAGCACTGCTCGT
		Reverse	TGCCCGATAAACTCTGCTTCCT
-	Mp1g08130	Forward	CCACTCATGTTGTTGCTC
		Reverse	GCCGCATCTACTAGCCATGGTA

Table 4. List of primers used for RT-qPCR in *M. polymorpha*.

REFERENCES

- Ambrose, B. A., Lerner, D. R., Ciceri, P., Padilla, C. M., Yanofsky, M. F., & Schmidt, R. J.** (2000). Molecular and genetic analyses of the *silky1* gene reveal conservation in floral organ specification between eudicots and monocots. *Molecular Cell*, 5(3). [https://doi.org/10.1016/S1097-2765\(00\)80450-5](https://doi.org/10.1016/S1097-2765(00)80450-5)
- Aragón-Raygoza, A., Vasco, A., Bliou, I., Herrera-Estrella, L., & Cruz-Ramírez, A.** (2020). Development and cell cycle activity of the root apical meristem in the fern *Ceratopteris richardii*. *Genes*, 11(12). <https://doi.org/10.3390/genes11121455>
- Baima, S., Forte, V., Possenti, M., Peñalosa, A., Leoni, G., Salvi, S., Felici, B., Ruberti, I., & Morelli, G.** (2014). Negative feedback regulation of auxin signaling by ATHB8/ACL5-BUD2 transcription module. *Molecular Plant*, 7(6). <https://doi.org/10.1093/mp/ssu051>
- Baima, S., Nobili, F., Sessa, G., Lucchetti, S., Ruberti, I., & Morelli, G.** (1995). The expression of the *Athb-8* homeobox gene is restricted to provascular cells in *Arabidopsis thaliana*. *Development*, 121(12). <https://doi.org/10.1242/dev.121.12.4171>
- Belda-Palazón, B., Ruiz, L., Martí, E., Tárraga, S., Tiburcio, A. F., Culiáñez, F., Farràs, R., Carrasco, P., & Ferrando, A.** (2012). Aminopropyltransferases Involved in Polyamine



- Biosynthesis Localize Preferentially in the Nucleus of Plant Cells. *PLoS ONE*, 7(10).
<https://doi.org/10.1371/journal.pone.0046907>
- Bonacorsi, N. K., & Seago, J. L.** (2016). Root development and structure in seedlings of *Ginkgo biloba*. *American Journal of Botany*, 103(2). <https://doi.org/10.3732/ajb.1500312>
- Cartayrade, A., Bourgeois, G., Balz, J. P., & Carde, J. P.** (1990). The secretory apparatus of *Ginkgo biloba*: structure, differentiation and analysis of the secretory product. *Trees*, 4(4). <https://doi.org/10.1007/BF00225312>
- Catarino, B., Hetherington, A. J., Emms, D. M., Kelly, S., & Dolan, L.** (2016). The Stepwise Increase in the Number of Transcription Factor Families in the Precambrian Predated the Diversification of Plants on Land. *Molecular Biology and Evolution*, 33(11). <https://doi.org/10.1093/molbev/msw155>
- Clay, N. K., & Nelson, T.** (2005). *Arabidopsis* thickvein mutation affects vein thickness and organ vascularization, and resides in a provascular cell-specific spermine synthase involved in vein definition and in polar auxin transport. In *Plant Physiology* (Vol. 138, Issue 2). <https://doi.org/10.1104/pp.104.055756>
- Conway, S. J., & di Stilio, V. S.** (2020). An ontogenetic framework for functional studies in the model fern *Ceratopteris richardii*. *Developmental Biology*, 457(1). <https://doi.org/10.1016/j.ydbio.2019.08.017>
- de Rybel, B., Adibi, M., Breda, A. S., Wendrich, J. R., Smit, M. E., Novák, O., Yamaguchi, N., Yoshida, S., van Isterdael, G., Palovaara, J., Nijse, B., Boekschoten, M. v., Hooiveld, G., Beeckman, T., Wagner, D., Ljung, K., Fleck, C., & Weijers, D.** (2014). Integration of growth and patterning during vascular tissue formation in *Arabidopsis*. *Science*, 345(6197). <https://doi.org/10.1126/science.1255215>
- de Rybel, B., Möller, B., Yoshida, S., Grabowicz, I., Barbier de Reuille, P., Boeren, S., Smith, R. S., Borst, J. W., & Weijers, D.** (2013). A bHLH Complex Controls Embryonic Vascular Tissue Establishment and Indeterminate Growth in *Arabidopsis*. *Developmental Cell*, 24(4), 426–437. <https://doi.org/10.1016/j.devcel.2012.12.013>
- Dörken, V. M.** (2014). Morphology, anatomy and vasculature in leaves of *Ginkgo biloba* L. (Ginkgoaceae, Ginkgoales) under functional and evolutionary aspects. *Feddes Repertorium*, 124(2–3). <https://doi.org/10.1002/fedr.201400008>
- Floyd, S. K., & Bowman, J. L.** (2006). Distinct Developmental Mechanisms Reflect the Independent Origins of Leaves in Vascular Plants. *Current Biology*, 16(19). <https://doi.org/10.1016/j.cub.2006.07.067>



- Floyd, S. K., Ryan, J. G., Conway, S. J., Brenner, E., Burris, K. P., Burris, J. N., Chen, T., Edger, P. P., Graham, S. W., Leebens-Mack, J. H., Pires, J. C., Rothfels, C. J., Sigel, E. M., Stevenson, D. W., Neal Stewart, C., Wong, G. K. S., & Bowman, J. L.** (2014). Origin of a novel regulatory module by duplication and degeneration of an ancient plant transcription factor. *Molecular Phylogenetics and Evolution*, 81. <https://doi.org/10.1016/j.ympev.2014.06.017>
- Floyd, S. K., Zalewski, C. S., & Bowman, J. L.** (2006). Evolution of class III homeodomain-leucine zipper genes in streptophytes. *Genetics*, 173(1). <https://doi.org/10.1534/genetics.105.054239>
- Foster, A. S.** (1938). Structure and Growth of the Shoot Apex in Ginkgo Biloba. *Bulletin of the Torrey Botanical Club*, 65(8). <https://doi.org/10.2307/2480793>
- Fütterer, J., & Hohn, T.** (1992). Role of an upstream open reading frame in the translation of polycistronic mRNAs in plant cells. *Nucleic Acids Research*, 20(15), 3851–3857. <https://doi.org/10.1093/nar/20.15.3851>
- Gola, E. M.** (2014). Dichotomous branching: The plant form and integrity upon the apical meristem bifurcation. In *Frontiers in Plant Science* (Vol. 5, Issue JUN). <https://doi.org/10.3389/fpls.2014.00263>
- Gola, E. M., & Jernstedt, J. A.** (2016). Vascular structure contributes to shoot sectoriality in *Selaginella kraussiana*. *Acta Societatis Botanicorum Poloniae*, 85(3). <https://doi.org/10.5586/asbp.3515>
- Groff, P. A., & Kaplan, D. R.** (1988). The relation of root systems to shoot systems in vascular plants. *The Botanical Review*, 54(4). <https://doi.org/10.1007/BF02858417>
- Hara, N.** (1997). Morphology and Anatomy of Vegetative Organs in Ginkgo biloba. In *Ginkgo Biloba A Global Treasure* (pp. 3–15). Springer Japan. https://doi.org/10.1007/978-4-431-68416-9_1
- Harrison, C. J., Coriey, S. B., Moylan, E. C., Alexander, D. L., Scotland, R. W., & Langdale, J. A.** (2005). Independent recruitment of a conserved developmental mechanism during leaf evolution. *Nature*, 434(7032). <https://doi.org/10.1038/nature03410>
- Harrison, C. J., Rezvani, M., & Langdale, J. A.** (2007). Growth from two transient apical initials in the meristem of *Selaginella kraussiana*. *Development*, 134(5). <https://doi.org/10.1242/dev.001008>
- Hodin, J.** (2000). Plasticity and constraints in development and evolution. *Journal of Experimental Zoology*, 288(1), 1–20. [https://doi.org/10.1002/\(SICI\)1097-010X\(20000415\)288](https://doi.org/10.1002/(SICI)1097-010X(20000415)288)



- Hou, G., & Blancaflor, E. B.** (2018). Fern Root Development. In Annual Plant Reviews online (pp. 192–208). John Wiley & Sons, Ltd. <https://doi.org/10.1002/9781119312994.apr0403>
- Hou, G. C., & Hill, J. P.** (2002). Heteroblastic root development in *Ceratopteris richardii* (Parkeriaceae). International Journal of Plant Sciences, 163(3). <https://doi.org/10.1086/339156>
- Hou, G. C., & Hill, J. P.** (2004). Developmental anatomy of the fifth shoot-borne root in young sporophytes of *Ceratopteris richardii*. Planta, 219(2). <https://doi.org/10.1007/s00425-004-1225-6>
- Imai, A., Hanzawa, Y., Komura, M., Yamamoto, K. T., Komeda, Y., & Takahashi, T.** (2006). The dwarf phenotype of the *Arabidopsis* ac15 mutant is suppressed by a mutation in an upstream ORF of a bHLH gene. Development, 133(18). <https://doi.org/10.1242/dev.02535>
- Imaichi, R.** (2008). Meristem organization and organ diversity. In Biology and Evolution of Ferns and Lycophytes. <https://doi.org/10.1017/CBO9780511541827.004>
- Imaichi, R., & Kato, M.** (1989). Developmental anatomy of the shoot apical cell, rhizophore and root of *Selaginella uncinata*. The Botanical Magazine Tokyo, 102(3). <https://doi.org/10.1007/BF02488120>
- Imaichi, R., & Kato, M.** (1991). Developmental Study of Branched Rhizophores in Three *Selaginella* Species. American Journal of Botany, 78(12). <https://doi.org/10.2307/2444848>
- Ishizaki, K., Chiyoda, S., Yamato, K. T., & Kohchi, T.** (2008). Agrobacterium-mediated transformation of the haploid liverwort *Marchantia polymorpha* L., an emerging model for plant biology. Plant and Cell Physiology, 49(7). <https://doi.org/10.1093/pcp/pcn085>
- Ishizaki, K., Nishihama, R., Ueda, M., Inoue, K., Ishida, S., Nishimura, Y., Shikanai, T., & Kohchi, T.** (2015). Development of gateway binary vector series with four different selection markers for the liverwort *Marchantia polymorpha*. PLoS ONE, 10(9). <https://doi.org/10.1371/journal.pone.0138876>
- Takechi, J. I., Kuwashiro, Y., Niitsu, M., & Takahashi, T.** (2008). Thermospermine is Required for Stem Elongation in *Arabidopsis thaliana*. Plant and Cell Physiology, 49(9). <https://doi.org/10.1093/pcp/pcn109>
- Katayama, H., Iwamoto, K., Kariya, Y., Asakawa, T., Kan, T., Fukuda, H., & Ohashi-Ito, K.** (2015). A Negative Feedback Loop Controlling bHLH Complexes Is Involved in



- Vascular Cell Division and Differentiation in the Root Apical Meristem. *Current Biology*, 25(23), 3144–3150. <https://doi.org/10.1016/J.CUB.2015.10.051>
- Katoh, K., & Standley, D. M.** (2013). MAFFT multiple sequence alignment software version 7: Improvements in performance and usability. *Molecular Biology and Evolution*, 30(4). <https://doi.org/10.1093/molbev/mst010>
- Kozak, M.** (1987). Effects of intercistronic length on the efficiency of reinitiation by eucaryotic ribosomes. *Molecular and Cellular Biology*, 7(10). <https://doi.org/10.1128/mcb.7.10.3438-3445.1987>
- Kramer, E. M.** (2015). A stranger in a strange land: The utility and interpretation of heterologous expression. *Frontiers in Plant Science*, 6(September). <https://doi.org/10.3389/fpls.2015.00734>
- Kumar, S., Stecher, G., Li, M., Knyaz, C., & Tamura, K.** (2018). MEGA X: Molecular evolutionary genetics analysis across computing platforms. *Molecular Biology and Evolution*, 35(6). <https://doi.org/10.1093/molbev/msy096>
- Lemoine, F., Correia, D., Lefort, V., Doppelt-Azeroual, O., Mareuil, F., Cohen-Boulakia, S., & Gascuel, O.** (2019). NGPhylogeny.fr: New generation phylogenetic services for non-specialists. *Nucleic Acids Research*, 47(W1). <https://doi.org/10.1093/nar/gkz303>
- Lu, K. J., van't Wout Hofland, N., Mor, E., Mutte, S., Abrahams, P., Kato, H., Vandepoele, K., Weijers, D., & de Rybel, B.** (2020). Evolution of vascular plants through redeployment of ancient developmental regulators. *Proceedings of the National Academy of Sciences of the United States of America*, 117(1). <https://doi.org/10.1073/pnas.1912470117>
- Lu, P., & Jernstedt, J. A.** (1996). Rhizophore and root development in *Selaginella martensii*: Meristem transitions and identity. *International Journal of Plant Sciences*, 157(2). <https://doi.org/10.1086/297337>
- Milhinhos, A., Prestele, J., Bollhöner, B., Matos, A., Vera-Sirera, F., Rambla, J. L., Ljung, K., Carbonell, J., Blázquez, M. A., Tuominen, H., & Miguel, C. M.** (2013). Thermospermine levels are controlled by an auxin-dependent feedback loop mechanism in *Populus* xylem. *The Plant Journal*, 75(4), 685–698. <https://doi.org/10.1111/tpj.12231>
- Muñiz, L., Minguet, E. G., Singh, S. K., Pesquet, E., Vera-Sirera, F., Moreau-Courtois, C. L., Carbonell, J., Blázquez, M. A., & Tuominen, H.** (2008). ACAULIS5 controls *Arabidopsis* xylem specification through the prevention of premature cell death. *Development*, 135(15), 2573–2582. <https://doi.org/10.1242/dev.019349>



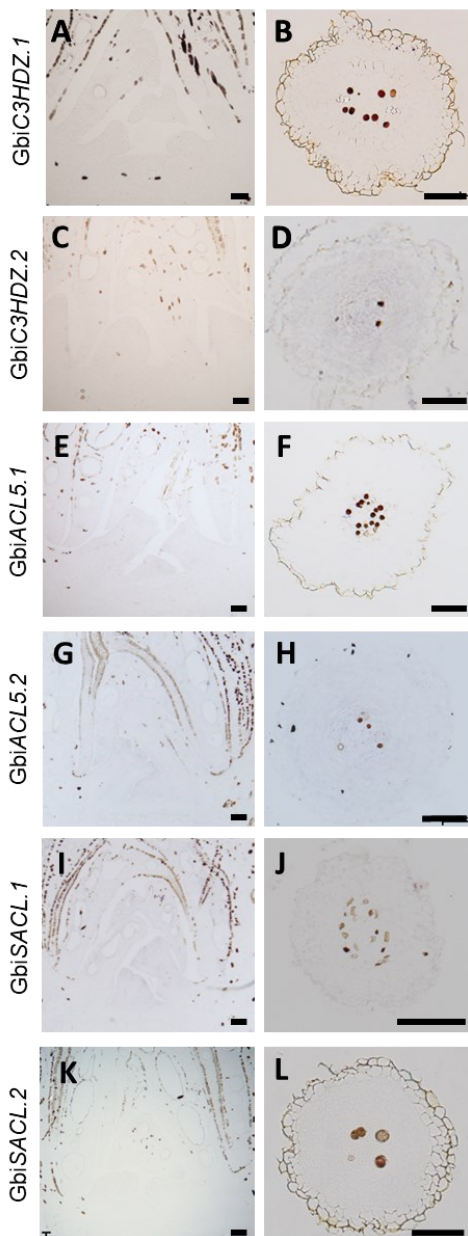
- Otreba, P., & Gola, E. M.** (2011). Specific intercalary growth of rhizophores and roots in *Selaginella kraussiana* (Selaginellaceae) is related to unique dichotomous branching. *Flora: Morphology, Distribution, Functional Ecology of Plants*, 206(3). <https://doi.org/10.1016/j.flora.2010.07.001>
- Pillai, A.** (1963). Root apical organization in gymnosperms—some cycads and *Ginkgo biloba*. *Proceedings / Indian Academy of Sciences*, 57(4), 211–222. <https://doi.org/10.1007/BF03053854>
- Pires, N., & Dolan, L.** (2010a). Origin and diversification of basic-helix-loop-helix proteins in plants. *Molecular Biology and Evolution*, 27(4), 862–874. <https://doi.org/10.1093/MOLBEV/MSP288>
- Pires, N., & Dolan, L.** (2010b). Early evolution of bHLH proteins in plants. *Plant Signaling and Behavior*, 5(7), 911–912. <https://doi.org/10.4161/psb.5.7.12100>
- Prigge, M. J., & Clark, S. E.** (2006b). Evolution of the class III HD-Zip gene family in land plants. *Evolution and Development*, 8(4), 350–361. <https://doi.org/10.1111/j.1525-142X.2006.00107.x>
- Soh, W. Y., Hong, S. S., & Cho, D. Y.** (1988). The ontogeny of the vascular cambium in *Ginkgo biloba* roots. *The Botanical Magazine Tokyo*, 101(1). <https://doi.org/10.1007/BF02488392>
- Vasco, A., Smalls, T. L., Graham, S. W., Cooper, E. D., Wong, G. K. S., Stevenson, D. W., Moran, R. C., & Ambrose, B. A.** (2016). Challenging the paradigms of leaf evolution: Class III HD-Zips in ferns and lycophytes. *New Phytologist*, 212(3). <https://doi.org/10.1111/nph.14075>
- Vera-Sirera, F., De Rybel, B., Úrbez, C., Kouklas, E., Pesquera, M., Álvarez-Mahecha, J. C., Minguet, E. G., Tuominen, H., Carbonell, J., Borst, J. W., Weijers, D., & Blázquez, M. A.** (2015). A bHLH-Based Feedback Loop Restricts Vascular Cell Proliferation in Plants. *Developmental Cell*, 35(4), 432–443. <https://doi.org/10.1016/j.devcel.2015.10.022>
- Vuosku, J., Muilu-Mäkelä, R., Avia, K., Suokas, M., Kestilä, J., Läärä, E., Häggman, H., Savolainen, O., & Sarjala, T.** (2019). Thermospermine Synthase (ACL5) and Diamine Oxidase (DAO) Expression Is Needed for Zygotic Embryogenesis and Vascular Development in Scots Pine. *Frontiers in Plant Science*, 10, 1600. <https://doi.org/10.3389/FPLS.2019.01600/BIBTEX>



- Wang, T., Zhang, N., & Du, L.** (2005). Isolation of RNA of high quality and yield from Ginkgo biloba leaves. *Biotechnology Letters*, 27(9). <https://doi.org/10.1007/s10529-005-3629-1>
- Winkler, J., Mylle, E., de Meyer, A., Pavie, B., Merchie, J., Grones, P., & van Damme, D.** (2021). Visualizing protein–protein interactions in plants by rapamycin-dependent delocalization. *Plant Cell*, 33(4). <https://doi.org/10.1093/plcell/koab004>
- Zumajo-Cardona, C., Little, D. P., Stevenson, D., & Ambrose, B. A.** (2021). Expression analyses in Ginkgo biloba provide new insights into the evolution and development of the seed. *Scientific Reports*, 11(1), 21995. <https://doi.org/10.1038/s41598-021-01483-0>



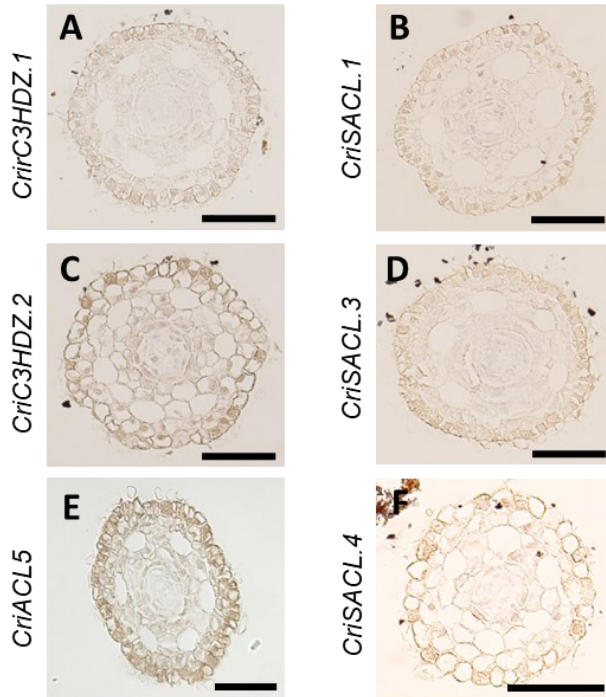
SUPPLEMENTAL FIGURE 1

***In situ* hybridizations with sense probes in *G. biloba* tissues.**

Longitudinal cross sections of vegetative long-shoot SAM (A, C, E, G, I, K) and cross sections of roots during primary development (B, D, F, H, J, L) using sense probes in *Ginkgo biloba*. Scale bars represent 500 μ m in shoot apical meristems, and 100 μ m in roots.



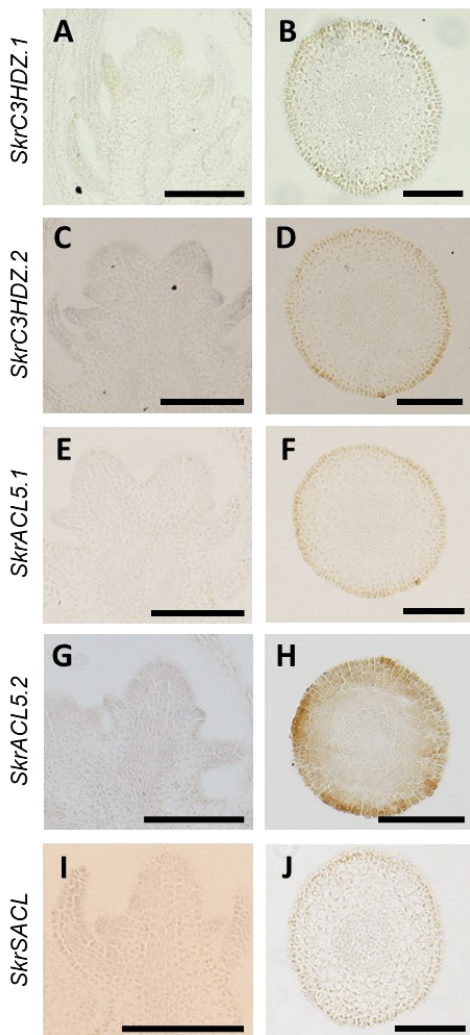
SUPPLEMENTAL FIGURE 2



In situ hybridization with sense probes in *Ceratopteris richardii* root. (A) *Cric3HDZ.1*, (B) *Cric3HDZ.2*, (C) *CriACL5*, (D) *CriSACL.1*, (E) *CriSACL.3* and (F) *CriSACL.4* in root cross sections. Scale bars represent 100µm



SUPPLEMENTAL FIGURE 3



In situ hybridizations with sense probes in *S. kraussiana* tissues. Longitudinal cross sections of shoot apical meristems (**A, C, E, G, I**) and cross sections of rhizophores during primary development (**B, D, F, H, J**) using sense probes in *S. kraussiana*. Scale bars represent 500µm.



GENERAL DISCUSSION





It has been less than a decade since the C3HDZ-ACL5-SACL module has been proposed as a regulatory mechanism that participates in vascular development through the TMO5/LHW heterodimer and cytokinin biosynthesis in *A. thaliana* (Katayama et al., 2015b; Vera-Sirera et al., 2015). Together, they create an incoherent feed-forward loop that is essential for the correct development of xylem tissues, with repercussions in the whole plant development (Baima et al., 1995, 2001, 2014; Katayama et al., 2015; Vera-Sirera et al., 2015). To date, there had been no studies about the existence of such module –or its functions– outside the angiosperm lineage (Milhinhos et al., 2013, 2020; Mo et al., 2015), which prevented any conclusion regarding the origin and evolutionary trajectory of the elements of the module in land plants.

Our results suggest a hypothetical model (**Figure 1**) by which the three main elements of the module, C3HDZ, ACL5 and SACL, were simultaneously present in the last common ancestor of land plants, where C3HDZ would already promote *ACL5* expression. Later in evolution, C3HDZ-ACL5 and SACL would have followed different lineage-dependent trajectories in bryophytes and in tracheophytes. In bryophytes, C3HDZ and ACL5 would regulate meristem-related processes, while SACL would have a different function. In tracheophytes, all three elements would have been recruited to vascular tissues, and a newly originated uORF in the 5'-leader sequence of SACL would have linked C3HDZ-ACL5 to SACL activity via Tspm-dependent translational regulation. In addition, SACL would have gained the capacity to interact with LHW, thereby converting the C3HDZ-ACL5-SACL module into a regulator of cambial activity. This model is supported in a wealth of observations, but it also has limitations. On one hand, it is based on a thorough study that has leveraged molecular genetic approaches in *M. polymorpha* providing functional information, as well as phylogenetic, *in silico* prediction, biochemical and cell biology analyses. On the other hand, it is limited by the lack of functional insight in other bryophytes (mosses, hornworts) and tracheophytes (at least lycophytes and ferns). What follows is a discussion on the evolutionary implications of each of the main aspects of our evolutionary model, with respect to vascular development and to the general principles that govern evo-devo.



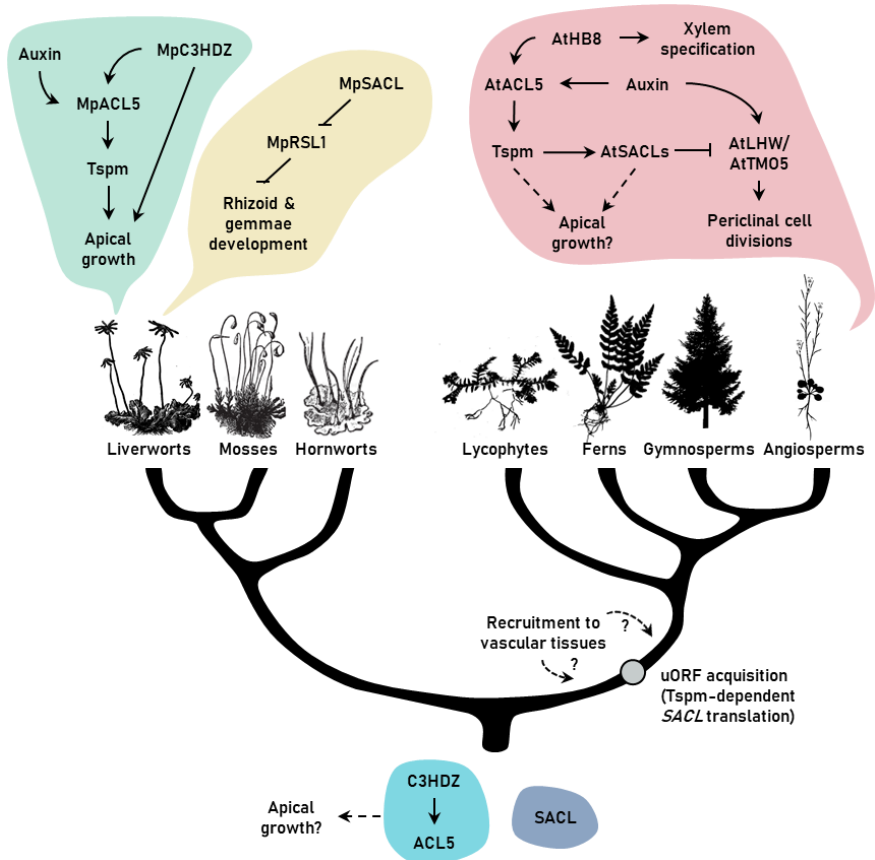


Figure 1. Hypothetical model of C3HDZ, ACL5 and SACL evolutionary trajectory in land plants. Summary of functional characterization in *A. thaliana* (Vera-Sirera et al., 2015; Katayama et al., 2015; Baima et al., 2014) and *M. polymorpha*, as well as the hypothetical intermediate states and key evolutionary events in bryophytes and tracheophytes. Phylogenetic relationships are based on the work of Harris B. et al., (2020).

The first highlight of the model is the ancient regulation of *ACL5* expression by auxin and C3HDZ. This observation is paradigmatic for the principle that the proteins encoded by ancient genes have been under severe functional constraints, and very few changes are to be expected in their biochemical properties even after hundreds of millions of years of divergence between orthologs (Carroll, 2008). A



long-standing discussion derived from this idea is how evolutionary innovations are then generated (Carroll, 2008; Doyle, 2012; True & Carroll, 2002). One example of this situation is the origin of the flower, whose master regulator is the TF *LEAFY* (*LFY*) (Blázquez et al., 1997; Molinero-Rosales et al., 1999; Schultz & Haughn, 1991; Weigel et al., 1992): it is present in all land plant lineages, but it regulates floral development in angiosperms, and non-reproductive apical growth in the rest of the plants (Plackett et al., 2018; Tanahashi et al., 2005). In this case, the innovation was associated to changes in the CRE bound by LFY, and the change of specificity in the LFY binding sites was possible thanks to an intermediate evolutionary state of LFY which could recognize both types of binding sites (Sayou et al., 2014). In the case of the functional innovations associated to C3HDZ-ACL5 (its participation in the regulation of vascular development in tracheophytes, vs in the regulation of apical meristem activity in bryophytes), the explanation does not lie in changes in the biochemical activities of C3HDZ or in ACL5, but in SACL, as discussed below.

The second key point of the model is the access of ACL5 to new downstream events coinciding with the emergence of a CRE in the 5' leader sequence of *SACL* transcripts that provides Tspm-dependent translation. The 5' leader sequences of *SACL* orthologs in bryophytes are generally long, and some of them contain uORFs that may inhibit the translation of the main ORF; however, those uORFs are not conserved in that lineage and at least the ones in *MpSACL* do not display regulation by Tspm.

The fact that ACL5 does not act through *SACL* in *M. polymorpha* opens an intriguing question. The only mechanism reported for the regulatory function of ACL5 –or the synthesis of Tspm– is the regulation of translation of *SACL* transcripts in *A. thaliana* (Cai et al., 2016; Imai et al., 2006; Ishitsuka et al., 2019; Vera-Sirera et al., 2015; Yamamoto & Takahashi, 2017). How does Tspm work in bryophytes then? Does this alternative mechanism also operate in tracheophytes, and can then be considered the “ancestral” mechanism? One possibility is that Tspm only acts as a translational regulator, through 5' leader sequences in genes other than *SACL*. In favor of this possibility, ribosome profiling of *A. thaliana* wild-type and *acl5* mutant seedlings shows translation defects in a few (but not many) genes different from the four



AtSACL paralogs (Y. Helariutta, personal communication). A second possibility is that Tspm acts through alternative signaling pathways or interferes with the biochemical properties of other macromolecules. In support of this possibility, other polyamines have been shown to ultimately regulate gene expression through diverse mechanisms. For instance, Spd participates in the post-translational modification of the translation elongation factor 5A (EIF5A) in eukaryotes, which is also crucial for the viability of the eukaryote organism (Chattopadhyay et al., 2008; Nishimura et al., 2012; Pagnussat et al., 2005; Park et al., 1997). For this process, Spd acts as a donor of an aminobutyl moiety that will be used to modify a lysine in the EIF5A in a process that is known as hypusination (Park et al., 1993), a step that is required for the correct post-translational activation of EIF5A (Park et al., 2010; Saini et al., 2009). Another example is in the translational regulation by polyamine homeostasis of the SAMDC enzyme, which participates in the polyamine biosynthetic pathway in animals and plants. In mammals, the *SAMDC* transcript contains a uORF that inhibits mORF translation in absence of Spd due to ribosome stalling (Dever & Ivanov, 2018). In plants, the translation of the *SAMDC* gene is dependent on the interplay between two uORFs in the plant *SAMDC* transcript, whose activity is regulated by Spd-induced frameshift (Hanfrey et al., 2005). In both animals and plants, these mechanisms are used to ultimately upregulate or repress *SAMDC* translation in low or high Spd, respectively.

The mechanism by which the regulatory uORF in *SACL* transcripts originated in the last common tracheophyten ancestor is difficult to establish, but it may be derived from one pre-existing uORF or initially recruited from a distant genome location. In any case, it is unclear whether the pressure to maintain the newly emerged uORF in the ancestral tracheophytes was an advantageous downregulation of translation or the fact that it was immediately a target for Tspm regulation. This latter case would have been necessarily paralleled by a second evolutionary event: the co-localization of Tspm and *SACL* transcripts.

In this regard, the third highlight is the spatial coincidence – or recruitment – of *C3HDZ*, *ACL5* and *SACL* transcripts in the same location, associated with the vascular tissues. In our analysis of a small number of representative species, the three



genes are co-expressed in the vasculature in all tracheophyte lineages. In the absence of functional evidence for a common action of the three genes outside angiosperms, we can only rely on expression analyses (and the presence of the novel uORF in SACL) to support our model. However, changes in the expression domains, which are a consequence of a high mutation rate in promoter regions upstream of gene bodies (Britten & Davidson, 1971; Carroll, 2008; King & Wilson, 1975; Monroe et al., 2022; Zuckerlandl & Pauling, 1965) are a recurrent strategy by which developmental innovations arise. One example is the multiple recruitment of *Class I Knotted-Like Homeobox (KNOX)* genes for leaf development in leaves from phylogenetically independent origins (Harrison et al., 2005; Tomescu, 2009; Vasco et al., 2013). A similar case is found in RSL class I orthologs, which were recruited for the development of analogous rooting structures in plants (see Glossary), such as rhizoids and other epidermal outgrowths in bryophytes and root hairs in tracheophytes (Honkanen et al., 2018; Jang et al., 2011; Menand et al., 2007; Proust et al., 2016). In animals, the Eyeless (Ey) protein and its ortholog, Paired box 6 (Pax6), were recruited independently for composite eye and camera-type eye development in fruit fly and mouse respectively (Halder et al., 1995).

One interesting observation is the expression of the *C3HDZ*, *ACL5* and *SACL* genes at the shoot apex of the examined tracheophytes (one lycophyte and one gymnosperm), in addition to their expression in the vasculature. It has been previously suggested that several genetic components that modulate SAM activity in angiosperms, like *SHOOTMERISTEMLESS (STM)*, *AINTEGUMENTA (ANT)*, *Class I knotted-like homeobox (KNOX)*, and even *C3HDZ* genes in *A. thaliana* have been co-opted for the regulation of the vascular cambium (Groover, 2005; Schrader et al., 2004; Spicer & Groover, 2010). Considering this, we can speculate that the C3HDZ-ACL5-SACL module initially emerged in the last common ancestor of tracheophytes as a regulator of SAM activity -derived from a putative function of C3HDZ and ACL5 in the meristem of the land plant ancestor. This ancestral function would be inferred from results obtained for C3HDZ in *P. patens* (Yip et al., 2016) and our own results with C3HDZ and ACL5 in *M. polymorpha*, but requires additional experimental



evidence in tracheophytes. Up to now, there has been no report of meristem-related functions for ACL5 or SACL in *A. thaliana*, based on the phenotype of the *acl5* mutants.

The fourth, and final, key event is the capacity of SACL proteins to establish preferential physical interaction with different sets of partners in tracheophytes and bryophytes. Our limited analysis of SACL interactions shows that MpSACL interacts with MpRSL1 but not MpLHW, while AtSACLs have developed the capacity to interact with AtLHW. Very likely, this differential capacity was reinforced by the spatial coincidence of AtSACL and AtLHW in the vasculature (De Rybel et al., 2013; Katayama et al., 2015b; Vera-Sirera et al., 2015), while *AtRSL class I* genes are expressed in the epidermis (Jang et al., 2011; Menand et al., 2007). In addition, we have shown that SACL orthologs underwent significant protein domain divergence, which most likely contributed to their differential interaction capacity with potential partners. The observation that a transcriptional regulator performs different functions in different species because of their interaction with different partners in each lineage is one more example of a rather general evolutionary strategy. For instance, a comparable situation in plants is found in the functional evolution of DELLA proteins. These proteins perform many lineage-specific functions, and this is due to two alternative mechanisms: (i) the establishment of particular interactions between DELLA and certain TFs in a species-specific manner; and (ii) diversification of the TF binding sites in different species, despite maintaining conserved DELLA-TF interactions (Briones-Moreno et al., 2023). The common theme is that the functional evolution of the transcriptional regulator (DELLA or SACL) in fact mirrors the evolution of its partners.

In summary, the main conclusion that can be drawn from comparing the divergent evolutionary trajectories of *C3HDZ*, *ACL5* and *SACL* genes in distant land plant lineages, is that a rewiring of gene regulatory networks coupled with functional divergence took place and facilitated the development of vascular tissues, which is one of the most important morphological innovations in land plant evolution.



REFERENCES

- Baima, S., Forte, V., Possenti, M., Peñalosa, A., Leoni, G., Salvi, S., Felici, B., Ruberti, I., & Morelli, G.** (2014). Negative feedback regulation of auxin signaling by ATHB8/ACL5-BUD2 transcription module. *Molecular Plant*, 7(6). <https://doi.org/10.1093/mp/ssu051>
- Baima, S., Nobili, F., Sessa, G., Lucchetti, S., Ruberti, I., & Morelli, G.** (1995). The expression of the Athb-8 homeobox gene is restricted to provascular cells in *Arabidopsis thaliana*. *Development*, 121(12). <https://doi.org/10.1242/dev.121.12.4171>
- Baima, S., Possenti, M., Matteucci, A., Wisman, E., Altamura, M. M., Ruberti, I., & Morelli, G.** (2001). The arabidopsis ATHB-8 HD-zip protein acts as a differentiation-promoting transcription factor of the vascular meristems. *Plant Physiology*, 126(2). <https://doi.org/10.1104/pp.126.2.643>
- Blázquez, M. A., Soowal, L. N., Lee, I., & Weigel, D.** (1997). LEAFY expression and flower initiation in *Arabidopsis*. *Development*, 124(19). <https://doi.org/10.1242/dev.124.19.3835>
- Briones-Moreno, A., Hernández-García, J., Vargas-Chávez, C., Blanco-Touriñán, N., Phokas, A., Úrbez, C., Cerdán, P. D., Coates, J. C., Alabadi, D., & Blázquez, M. A.** (2023). DELLA functions evolved by rewiring of associated transcriptional networks. *Nature Plants*. <https://doi.org/10.1038/s41477-023-01372-6>
- Cai, Q., Fukushima, H., Yamamoto, M., Ishii, N., Sakamoto, T., Kurata, T., Motose, H., & Takahashi, T.** (2016). The SAC51 family plays a central role in thermospermine responses in *Arabidopsis*. *Plant and Cell Physiology*, 57(8). <https://doi.org/10.1093/pccp/pcw113>
- Carroll, S. B.** (2008). Evo-Devo and an Expanding Evolutionary Synthesis: A Genetic Theory of Morphological Evolution. *Cell*, 134(1), 25–36. <https://doi.org/10.1016/j.cell.2008.06.030>
- Chattopadhyay, M. K., Myung, H. P., & Tabor, H.** (2008). Hypusine modification for growth is the major function of spermidine in *Saccharomyces cerevisiae* polyamine auxotrophs grown in limiting spermidine. *Proceedings of the National Academy of Sciences of the United States of America*, 105(18). <https://doi.org/10.1073/pnas.0710970105>
- De Rybel, B., Möller, B., Yoshida, S., Grabowicz, I., Barbier de Reuille, P., Boeren, S., Smith, R. S., Borst, J. W., & Weijers, D.** (2013). A bHLH Complex Controls Embryonic Vascular Tissue Establishment and Indeterminate Growth in *Arabidopsis*. *Developmental Cell*, 24(4), 426–437. <https://doi.org/10.1016/j.devcel.2012.12.013>



- Dever, T. E., & Ivanov, I. P.** (2018). Roles of polyamines in translation. In *Journal of Biological Chemistry* (Vol. 293, Issue 48). <https://doi.org/10.1074/jbc.TM118.003338>
- Doyle, J. A.** (2012). Phylogenetic Analyses and Morphological Innovations in Land Plants. In *The Evolution of Plant Form* (Vol. 45). <https://doi.org/10.1002/9781118305881.ch1>
- Groover, A. T.** (2005). What genes make a tree a tree? *Trends in Plant Science*, 10(5). <https://doi.org/10.1016/j.tplants.2005.03.001>
- Halder, G., Callaerts, P., & Gehring, W. J.** (1995). Induction of ectopic eyes by targeted expression of the eyeless gene in *Drosophila*. *Science*, 267(5205). <https://doi.org/10.1126/science.7892602>
- Hanfrey, C., Elliott, K. A., Franceschetti, M., Mayer, M. J., Illingworth, C., & Michael, A. J.** (2005). A dual upstream open reading frame-based autoregulatory circuit controlling polyamine-responsive translation. *Journal of Biological Chemistry*, 280(47). <https://doi.org/10.1074/jbc.M509340200>
- Harrison, C. J., Coriey, S. B., Moylan, E. C., Alexander, D. L., Scotland, R. W., & Langdale, J. A.** (2005). Independent recruitment of a conserved developmental mechanism during leaf evolution. *Nature*, 434(7032). <https://doi.org/10.1038/nature03410>
- Honkanen, S., Thamm, A., Arteaga-Vazquez, M. A., & Dolan, L.** (2018). Negative regulation of conserved RSL class I bHLH transcription factors evolved independently among land plants. *ELife*, 7. <https://doi.org/10.7554/eLife.38529>
- Imai, A., Hanzawa, Y., Komura, M., Yamamoto, K. T., Komeda, Y., & Takahashi, T.** (2006). The dwarf phenotype of the *Arabidopsis* ac15 mutant is suppressed by a mutation in an upstream ORF of a bHLH gene. *Development*, 133(18). <https://doi.org/10.1242/dev.02535>
- Ishitsuka, S., Yamamoto, M., Miyamoto, M., Kuwashiro, Y., Imai, A., Motose, H., & Takahashi, T.** (2019). Complexity and Conservation of Thermospermine-Responsive uORFs of SAC51 Family Genes in Angiosperms. *Frontiers in Plant Science*, 10. <https://doi.org/10.3389/FPLS.2019.00564>
- Jang, G., Yi, K., Pires, N. D., Menand, B., & Dolan, L.** (2011). RSL genes are sufficient for rhizoid system development in early diverging land plants. *Development*, 138(11). <https://doi.org/10.1242/dev.060582>
- Katayama, H., Iwamoto, K., Kariya, Y., Asakawa, T., Kan, T., Fukuda, H., & Ohashi-Ito, K.** (2015). A Negative Feedback Loop Controlling bHLH Complexes Is Involved in Vascular Cell Division and Differentiation in the Root Apical Meristem. *Current Biology*, 25(23), 3144–3150. <https://doi.org/10.1016/j.cub.2015.10.051>

- Menand, B., Yi, K., Jouannic, S., Hoffmann, L., Ryan, E., Linstead, P., Schaefer, D. G., & Dolan, L.** (2007). An ancient mechanism controls the development of cells with a rooting function in land plants. *Science*, *316*(5830). <https://doi.org/10.1126/science.1142618>
- Milhinhos, A., Bollhöner, B., Blázquez, M. A., Novák, O., Miguel, C. M., & Tuominen, H.** (2020). ACAULIS5 Is Required for Cytokinin Accumulation and Function During Secondary Growth of Populus Trees. *Frontiers in Plant Science*, *11*. <https://doi.org/10.3389/fpls.2020.601858>
- Milhinhos, A., Prestele, J., Bollhöner, B., Matos, A., Vera-Sirera, F., Rambla, J. L., Ljung, K., Carbonell, J., Blázquez, M. A., Tuominen, H., & Miguel, C. M.** (2013). Thermospermine levels are controlled by an auxin-dependent feedback loop mechanism in *Populus* xylem. *The Plant Journal*, *75*(4), 685–698. <https://doi.org/10.1111/tpj.12231>
- Mo, H., Wang, X., Zhang, Y., Yang, J., & Ma, Z.** (2015). Cotton ACAULIS5 is involved in stem elongation and the plant defense response to *Verticillium dahliae* through thermospermine alteration. *Plant Cell Reports*, *34*(11). <https://doi.org/10.1007/s00299-015-1844-3>
- Molinero-Rosales, N., Jamilena, M., Zurita, S., Gómez, P., Capel, J., & Lozano, R.** (1999). FALSIFLORA, the tomato orthologue of FLORICAULA and LEAFY, controls flowering time and floral meristem identity. *Plant Journal*, *20*(6). <https://doi.org/10.1046/j.1365-313X.1999.00641.x>
- Monroe, J. G., Srikant, T., Carbonell-Bejerano, P., Becker, C., Lensink, M., Exposito-Alonso, M., Klein, M., Hildebrandt, J., Neumann, M., Kliebenstein, D., Weng, M. L., Imbert, E., Ågren, J., Rutter, M. T., Fenster, C. B., & Weigel, D.** (2022). Mutation bias reflects natural selection in *Arabidopsis thaliana*. *Nature*, *602*(7895). <https://doi.org/10.1038/s41586-021-04269-6>
- Nishimura, K., Lee, S. B., Park, J. H., & Park, M. H.** (2012). Essential role of eIF5A-1 and deoxyhypusine synthase in mouse embryonic development. *Amino Acids*, *42*(2–3). <https://doi.org/10.1007/s00726-011-0986-z>
- Pagnussat, G. C., Yu, H. J., Ngo, Q. A., Rajani, S., Mayalagu, S., Johnson, C. S., Capron, A., Xie, L. F., Ye, D., & Sundaresan, V.** (2005). Genetic and molecular identification of genes required for female gametophyte development and function in *Arabidopsis*. *Development*, *132*(3). <https://doi.org/10.1242/dev.01595>
- Park, M. H., Lee, Y. B., & Joe, Y. A.** (1997). Hypusine is essential for eukaryotic cell proliferation. *NeuroSignals*, *6*(3). <https://doi.org/10.1159/000109117>



- Park, M. H., Nishimura, K., Zanelli, C. F., & Valentini, S. R.** (2010). Functional significance of eIF5A and its hypusine modification in eukaryotes. *Amino Acids*, 38(2). <https://doi.org/10.1007/s00726-009-0408-7>
- Park, M. H., Wolff, E. C., & Folk, J. E.** (1993). Hypusine: its post-translational formation in eukaryotic initiation factor 5A and its potential role in cellular regulation. *BioFactors (Oxford, England)*, 4(2).
- Plackett, A. R. G., Conway, S. J., Hazelton, K. D. H., Rabbinowitsch, E. H., Langdale, J. A., & di Stilio, V. S.** (2018). LEAFY maintains apical stem cell activity during shoot development in the fern *Ceratopteris richardii*. *eLife*, 7. <https://doi.org/10.7554/eLife.39625>
- Proust, H., Honkanen, S., Jones, V. A. S., Morieri, G., Prescott, H., Kelly, S., Ishizaki, K., Kohchi, T., & Dolan, L.** (2016). RSL Class i Genes Controlled the Development of Epidermal Structures in the Common Ancestor of Land Plants. *Current Biology*, 26(1). <https://doi.org/10.1016/j.cub.2015.11.042>
- Saini, P., Eyler, D. E., Green, R., & Dever, T. E.** (2009). Hypusine-containing protein eIF5A promotes translation elongation. *Nature*, 459(7243). <https://doi.org/10.1038/nature08034>
- Sayou, C., Monniaux, M., Nanao, M. H., Moyroud, E., Brockington, S. F., Thévenon, E., Chahtane, H., Warthmann, N., Melkonian, M., Zhang, Y., Wong, G. K. S., Weigel, D., Parcy, F., & Dumas, R.** (2014). A promiscuous intermediate underlies the evolution of LEAFY DNA binding specificity. *Science*, 343(6171). <https://doi.org/10.1126/science.1248229>
- Schrader, J., Nilsson, J., Mellerowicz, E., Berglund, A., Nilsson, P., Hertzberg, M., & Sandberg, G.** (2004). A high-resolution transcript profile across the wood-forming meristem of poplar identifies potential regulators of cambial stem cell identity. *Plant Cell*, 16(9). <https://doi.org/10.1105/tpc.104.024190>
- Schultz, E. A., & Haughn, G. W.** (1991). LEAFY, a homeotic gene that regulates inflorescence development in arabidopsis. *Plant Cell*, 3(8). <https://doi.org/10.1105/tpc.3.8.771>
- Spicer, R., & Groover, A.** (2010). Evolution of development of vascular cambia and secondary growth. In *New Phytologist* (Vol. 186, Issue 3). <https://doi.org/10.1111/j.1469-8137.2010.03236.x>
- Tanahashi, T., Sumikawa, N., Kato, M., & Hasebe, M.** (2005). Diversification of gene function: Homologs of the floral regulator FLO/LFY control the first zygotic cell division in the moss *Physcomitrella patens*. *Development*, 132(7). <https://doi.org/10.1242/dev.01709>

- Tomescu, A. M. F.** (2009). Megaphylls, microphylls and the evolution of leaf development. *Trends in Plant Science*, 14(1), 5–12. <https://doi.org/10.1016/j.tplants.2008.10.008>
- True, J. R., & Carroll, S. B.** (2002). Gene co-option in physiological and morphological evolution. In *Annual Review of Cell and Developmental Biology* (Vol. 18). <https://doi.org/10.1146/annurev.cellbio.18.020402.140619>
- Vasco, A., Moran, R. C., & Ambrose, B. A.** (2013). The evolution, morphology, and development of fern leaves. In *Frontiers in Plant Science* (Vol. 4, Issue SEP). <https://doi.org/10.3389/fpls.2013.00345>
- Vera-Sirera, F., De Rybel, B., Úrbez, C., Kouklas, E., Pesquera, M., Álvarez-Mahecha, J. C., Minguet, E. G., Tuominen, H., Carbonell, J., Borst, J. W., Weijers, D., & Blázquez, M. A.** (2015). A bHLH-Based Feedback Loop Restricts Vascular Cell Proliferation in Plants. *Developmental Cell*, 35(4), 432–443. <https://doi.org/10.1016/j.devcel.2015.10.022>
- Weigel, D., Alvarez, J., Smyth, D. R., Yanofsky, M. F., & Meyerowitz, E. M.** (1992). LEAFY controls floral meristem identity in Arabidopsis. *Cell*, 69(5). [https://doi.org/10.1016/0092-8674\(92\)90295-N](https://doi.org/10.1016/0092-8674(92)90295-N)
- Yamamoto, M., & Takahashi, T.** (2017). Thermospermine enhances translation of SAC51 and SACL1 in Arabidopsis. *Plant Signaling & Behavior*, 12(1), e1276685. <https://doi.org/10.1080/15592324.2016.1276685>
- Yip, H. K., Floyd, S. K., Sakakibara, K., & Bowman, J. L.** (2016). Class III HD-Zip activity coordinates leaf development in *Physcomitrella patens*. *Developmental Biology*, 419(1). <https://doi.org/10.1016/j.ydbio.2016.01.012>





CONCLUSIONS





1. The genetic regulation involving *C3HDZ* and *ACL5* genes predates the divergence of bryophytes and tracheophytes, while the Tspm-dependent translation of *SACL* transcripts occurred by acquisition of a CRE at the last tracheophyte common ancestor.
2. The association of the C3HDZ-ACL5-SACL module with vascular tissues occurred at the last tracheophyte common ancestor, probably derived from a previous expression in the apical meristem, and is conserved in extant tracheophyte lineages.
3. In *M. polymorpha*, MpC3HDZ and MpACL5 regulate apical growth, whereas MpSACL function in epidermal outgrowths is independent from MpC3HDZ and MpACL5.
4. SACL proteins have undergone divergent evolutionary trajectories in bryophytes and tracheophytes, that led to the regulation of disparate processes, like rooting structures and epidermal outgrowths, or periclinal cell divisions respectively.





ANNEXES



Conservation of Thermospermine Synthase Activity in Vascular and Non-vascular Plants

Anna Solé-Gil, Jorge Hernández-García, María Pilar López-Gresa, Miguel A. Blázquez and Javier Agustí*

Instituto de Biología Molecular y Celular de Plantas, Consejo Superior de Investigaciones Científicas – Universidad Politécnica de Valencia, Valencia, Spain

OPEN ACCESS

Edited by:
Rubén Alcázar,
University of Barcelona, Spain

Reviewed by:
Thomas Berberich,
Senckenberg Nature Research
Society, Germany
Toku Takahashi,
Okayama University, Japan

***Correspondence:**
Javier Agustí
jagusti@imicop.upv.es

Specialty section:
This article was submitted to
Plant Metabolism
and Chemodiversity,
a section of the journal
Frontiers in Plant Science

Received: 08 March 2019

Accepted: 02 May 2019

Published: 11 June 2019

Citation:
Solé-Gil A, Hernández-García J,
López-Gresa MP, Blázquez MA and
Agustí J (2019) Conservation
of Thermospermine Synthase Activity
in Vascular and Non-vascular Plants.
Front. Plant Sci. 10:663.
doi: 10.3389/fpls.2019.00663

In plants, the only confirmed function for thermospermine is regulating xylem cells maturation. However, genes putatively encoding thermospermine synthases have been identified in the genomes of both vascular and non-vascular plants. Here, we verify the activity of the thermospermine synthase genes and the presence of thermospermine in vascular and non-vascular land plants as well as in the aquatic plant *Chlamydomonas reinhardtii*. In addition, we provide information about differential content of thermospermine in diverse organs at different developmental stages in some vascular species that suggest that, although the major role of thermospermine in vascular plants is likely to be xylem development, other potential roles in development and/or responses to stress conditions could be associated to such polyamine. In summary, our results in vascular and non-vascular species indicate that the capacity to synthesize thermospermine is conserved throughout the entire plant kingdom.

Keywords: plants, polyamines, thermospermine, evolution, development

INTRODUCTION

Polyamines are positively charged aliphatic compounds with a widespread presence in all living organisms (Tabor and Tabor, 1984). The diamine putrescine (Put) and the triamine spermidine (Spd) are the most commonly found polyamines, while the tetra-amine spermine (Spm) is found in yeasts, most animals, seed plants and some bacteria (Pegg and Michael, 2010). Another tetra-amine, thermospermine (Tspm), has been detected in archaea, diatoms and plants, but not in animals or bacteria (Michael, 2016).

The ability to synthesize specific polyamines is clade-specific and is mainly the result of evolutionary adjustments in the polyamine biosynthesis pathway, reflected in the presence or absence of specific polyamine biosynthetic enzymes in given clades. Triamines and tetra-amines are mainly synthesized by a set of aminopropyl transferases, which are evolutionarily related to each other. It has been proposed that while Spm synthase (SPMS) genes in fungi and plants have likely emerged independently after duplication and neofunctionalization of Spd synthase (SPDS) genes (Minguel et al., 2008), the Tspm synthase (TSPMS) gene in plants was probably acquired through endosymbiosis of a cyanobacterium. However, it is arguable whether such gene originally encoded a TSPMS or an agmatine aminopropyl transferase (Pegg and Michael, 2010; Michael, 2016). All in all, the capacity to synthesize different polyamines in a given species is defined by (i) the presence or absence of specific polyamine biosynthetic enzymes and (ii) the degree of specificity



of the polyamine biosynthesis enzymes toward their substrates. For instance, it has been reported that an aminopropyl transferase from the archaea *Pyrobaculum aerophilum* displays its highest specificity *in vitro* toward norspermidine, resulting in norspermidine biosynthesis, but it is also able to synthesize Tspm from Spd (Knott et al., 2007). Similarly, the gymnosperm *Pinus sylvestris* lacks a specific SPMS gene, but the aminopropyl transferase encoded by *PSPDS* efficiently converts Put to Spd, as well as Spd to Spm (Vuosku et al., 2018). Both this flexibility in substrate recognition and the repeated independent generation of new aminopropyl transferases along evolution can be explained by the alteration of a few key residues in the active site of aminopropyl transferases that determine their characteristic substrate discrimination, as proposed through structural modeling and crystal structure comparisons of active sites (Wu et al., 2007; Minguet et al., 2008; Sekula and Dauter, 2018).

In plants, polyamines have been implicated in the response to stress and in the modulation of developmental processes (Chen et al., 2018). Correlations between specific endogenous levels of polyamines in plants under different stress conditions or during the progression of specific developmental processes have been extensively reported. In addition, the effects provoked by exogenous polyamines application have been largely documented. However, beyond such physiological reports, solid evidences for polyamines roles come from the analysis of loss of function mutants in polyamine metabolism genes. In this way, Put and Spd have been proved to be essential for life (Imai et al., 2004), while the tetra-amine Spm has been shown to be required for proper acclimation to salt, drought and heat stress (Yamaguchi et al., 2006, 2007; Sagor et al., 2013). Furthermore, both Spm and Tspm promote protection against bacterial pathogens (Gonzalez et al., 2011; Marina et al., 2013). However, the participation of Tspm could be a secondary effect of its primary function in vascular development (Vera-Sirera et al., 2010).

The most extensively studied role for a polyamine is that of Tspm in the regulation of xylem differentiation. The *Arabidopsis acaulis5* (*acl5*) mutant, impaired in TSPMS activity, displays stunted growth (Hanzawa et al., 1997, 2000) which has been associated to an increase in vascular cell proliferation, premature xylem cell death and miss-regulated lignin deposition (Clay and Nelson, 2005; Muniz et al., 2008). In *Arabidopsis*, the *ACL5* gene is specifically expressed in developing xylem cells (Clay and Nelson, 2005; Muniz et al., 2008), and the HD-ZIPIII transcription factor *AHB8* -which directs xylem differentiation and displays the same expression domain as *ACL5*- mediates its induction by auxin (Baïma et al., 2014). Auxin has been shown to promote cell proliferation by ensuring the formation of complexes between Target of Monopteros5 (TMO5) and Lonesome Highway (LHW), leading to the induction of cytokinin biosynthesis (De Rybel et al., 2013, 2014). Recent evidence suggests that Tspm is part of a negative feed-forward loop triggered by auxin that maintains proliferation of vascular cells within the correct range (Katayama et al., 2015; Vera-Sirera et al., 2015). The mechanism involves the promotion of translation of a small family of Suppressor of *ACL5* (SACL) transcriptional

regulators (Imai et al., 2006; Kakehi et al., 2008) which compete with TMO5 for the formation of inactive SACL-LHW complexes (Katayama et al., 2015; Vera-Sirera et al., 2015). This is not the only case in which polyamines have been implicated in translational regulation (Hanfrey et al., 2002, 2005).

Systematic sequencing of plant transcriptomes and genomes has revealed the presence of *ACL5* putative homologs in all plant lineages of vascular and non-vascular plants (including algae), raising the following questions: Do all putative *ACL5* genes across plant lineages encode enzymes with *bona-fide* TSPMS activity, even those present in non-vascular species? Is the expression of these genes associated to xylem development in all vascular plants? To start answering these questions, we have (i) examined the enzymatic activity of the *ACL5* homologs of several species in key plant lineages, (ii) searched for Tspm presence in vascular and non-vascular plants and (iii) studied the *ACL5* expression pattern in vegetative and reproductive organs of several seed-plant species at different developmental stages.

MATERIALS AND METHODS

Plant Material and Growth Conditions

Arabidopsis thaliana Columbia-0 (Col-0) plants were grown on MS media with sucrose (1%) under long-day conditions (16 h light, 8 h dark) at 22°C in a growth room. Samples for polyamine analysis and RNA extraction from Col-0 were taken after 15 days of growth. *P. abies* plant material was collected from adult trees that were identified in Catalonia (Spain) and frozen at -80°C until further analysis. *S. lepidophylla* plants were obtained from an external vendor, and hydrated before freezing the material at -80°C for further analysis. *P. patens* plant material was obtained from Jesús Vicente Carabajos's Lab (CBGP-Madrid, Spain) and grown in BCD medium + 1 mM Ca²⁺ under continuous light conditions in a growth room (Ashton and Cove, 1977). *M. polymorpha* Tak-1 plants were grown on 1/2 strength Gamborg's B5 medium for 15 days before tissue recollection under continuous light conditions in a growth room. *C. reinhardtii* plant material was obtained from Federico Valverde's Lab (IBVF-Sevilla, Spain).

Phylogenetic Analysis

Sequences used in this study were obtained by extensive BLAST analysis (tblastn) using the *Arabidopsis* thermospermine synthase (*ACL5*-AT5G19530), spermine synthase (*SPMS*-AT5G53120), and spermidine synthase 1 and 2 (*SPDS1*-AT1G23820, *SPDS2*-AT1G70310) genes as baits in the NCBI¹, Phytozome² and OneKP³ databases. All the sequences were managed using the Benchling tool⁴. Alignment of the sequences was done with using the MUSCLE algorithm (Siebers et al., 2017) included in the SeaView 4.6.4 GUI (Gouy et al., 2010), with 16 iterations, default clustering methods, gap open score

¹<http://www.ncbi.nlm.nih.gov>

²<http://www.phytozome.net>

³<http://db.engb.org/onekfp/>

⁴<https://benchling.com>



of -2.7 , and hydrophobicity multiplier of 1.2 , followed by manual curation. To select the best-fit model of amino acid substitution, the ProTest v3.4.2 (Darriba et al., 2011) was used on final multiple sequence alignment, together with AIC model for ranking. Maximum likelihood tree was produced with PhyML v3.1 (Guindon et al., 2010), using the best-scored model of amino acid substitution. Statistical significance was evaluated by bootstrap analysis of 1000 replicates. Phylogenetic tree graphical representations were initially generated using FigTree (version 1.4.3) software⁶, and final cartoons edited manually.

RNA Extraction and PCR Analysis

Total RNA was isolated from 200 mg of frozen powdered tissues using RNeasy plant mini kit (Qiagen) for *A. thaliana* and *M. polymorpha* tissues following the manufacturer's instructions. RNA from *C. reinhardtii*, *P. patens*, *S. lepidophylla* and *P. abies* was extracted by Trizol-Chloroform method as described (Siebers et al., 2017). cDNA synthesis was performed on 1 μ g DNase-treated RNA using PrimeScriptTM 1st strand cDNA synthesis kit (Takara). The resulting cDNA was used for PCR analysis with target gene-specific primers (Supplementary Table S2).

Cloning and Expression in Yeast

Coding sequence regions of thermospermine synthase genes from the selected species were obtained either from cDNA (*M. polymorpha*, *S. lepidophylla* and *A. thaliana*) or synthesized (Integrated DNA Technologies, IDT). The primers used for amplification are summarized in Supplementary Table S2. For plasmid construction, the CDS of the genes was cloned into pDONR207 through Gateway recombination (Invitrogen) and eventually into the destination vector pAG426GPD-ccdb-HA (a gift from Susan Lindquist; Addgene plasmid number 14252) for expression in yeast. The *A. thaliana* thermospermine synthase CDS was cloned into pCR8 through Golden Braid technology (Sarrion-Perdigones et al., 2011) and then shifted to Gateway technology to clone the CDS into the pDEST like the other species.

Yeast strain BY4741 (*MATa his3 leu2 met15 ura3*), kindly provided by Ramón Serrano's lab (IBMCP-Valencia, Spain), was grown on Synthetic Defined (SD) medium and transformed with the pAG426GPD containing the CDS of interest by LiAc/ssDNA/PEG. Selected transformants were grown on 50 mL liquid SD medium lacking Trp and Ura for 2 days, then harvested by centrifugation (about 200 mg of pellet) and frozen for further polyamine quantification.

Polyamine Quantification

Polyamine extraction from tissues and standards was done with a modification of a previously described method (Naka et al., 2010) as follows. About 1 g of plant samples in 3 replicates were frozen in liquid nitrogen and kept at -80°C until use. The tissue was ground with mortar and pestle (in the case of yeast pellets, the cells were broken with glass balls) and resuspended in 2.5 mL of 5% perchloric acid (PCA) in a 15-mL tube. At

this point 500 μL of the internal standard (diethylamine 1 mM, DEA) was added to the 5% PCA. The samples were kept on ice for 1 h and centrifuged at 4°C for 20 min at 15000 \times g. The whole supernatant was collected (between 2 and 3.5 mL) and transferred to a fresh 15 mL falcon tube. For each mL of supernatant, 0.66 mL of 2 M NaOH was added. Then, benzylation started with the addition of 10 μL of benzoyl chloride. After 1 min vortex, plant extracts were left at room temperature for 20 min. Then, for each mL of initial supernatant used, 1.33 mL of saturated NaCl solution was added. Two mL of diethyl ether was added, vortexed, and centrifuged at 3000 \times g for 1 min for the separation of the phases. The supernatant was transferred to a new pyrex vial and dried completely using N_2 . The remaining polyamines were resuspended in 130 μL methanol and filtered with a filter syringe (pore size 0.2 μm). Then, the filtrate was transferred to a plastic vial for HPLC analysis. Briefly, 30- μL aliquots were injected through a Waters 717plus autosampler into a 1525 Waters Binary HPLC pump equipped with a 996 Waters PDA detector and using a Luna C18(2) (Phenomenex) column (250 \times 4.6 mm, i.d. 5 μm). The column was equilibrated with 58% solvent A (acidic H_2O containing 10 mL acetic acid for each liter of distilled water) and 42% solvent B (acetonitrile). Elution was carried out at room temperature and for polyamine separation a 1 mL min^{-1} flow rate was used the isocratic gradient of 42% acetonitrile for 25 min. Then, the column was washed with 42–100% acetonitrile within 3 min and kept at 100% acetonitrile for 10 min. Eventually, the column was equilibrated with 42% acetonitrile for 17 min before the next injection. Detection of polyamines was performed at 254 nm.

Expression Analysis

Data for *TSPMS* gene expression in *A. thaliana*, *P. trichocarpa*, *M. truncatula*, *S. lycopersicum*, *Symphitum tuberosum*, *O. sativa*, *G. max*, *V. vinifera*, *B. distachyon*, *E. grandis*, *P. abies*, *Ananas comosus* and *P. patens* in different tissues was gathered from the Bio-Analytic Resource for Plant Biology (BAR⁶). Expression data was classified according to the organ tissue (stem, root, flower and leaf) and tissue age (mature or young). The total expression data per gene and species in the target organs was used to calculate the percentage of expression of the *TSPMS* gene in each organ. Heatmaps were drawn using the Matrix2png tool⁷.

RESULTS

Identification of Thermospermine Synthase Genes Across Plant Lineages

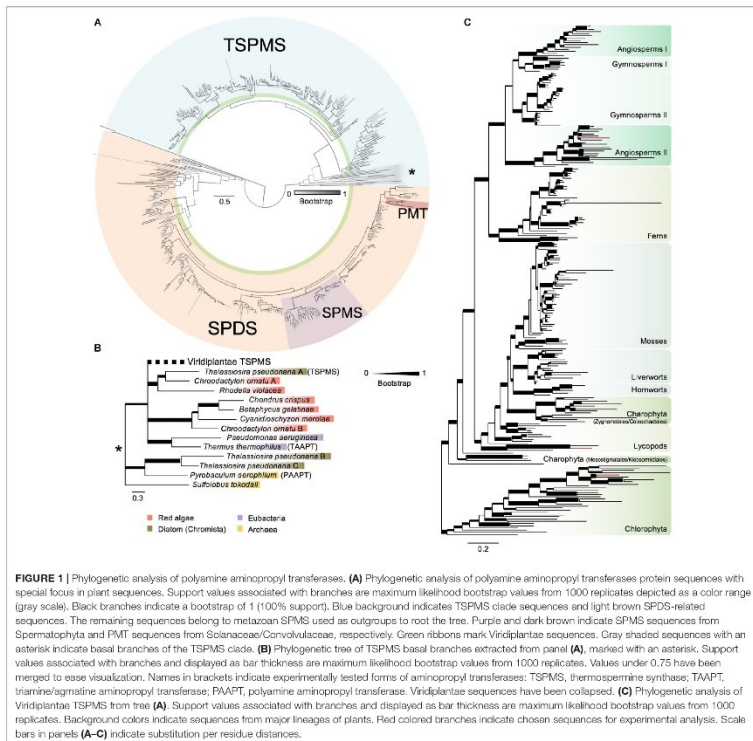
Polyamine biosynthesis enzymes display high degree of similarity (Ishimoto et al., 1998; Panicot et al., 2002; Teuber et al., 2007). Therefore, to guarantee accurate identification of putative *ACL5* orthologs, we screened the Phytosome and OneKP databases using as baits the Arabidopsis *ACL5* sequence, and also the

⁶<http://bar.toronto.ca>

⁷<https://matrix2png.msl.ubc.ca/>

⁸<http://tree.bio.ed.ac.uk/software/figtree/>





sequences of the two *Arabidopsis* genes encoding SPDS, and the single gene for SPMS (see Section “Materials and Methods” for details). We obtained 542 sequences covering every major plant lineages and included members of representative bacteria, archaea and other non-plant eukaryotic groups, which were aligned and used for the construction of a phylogenetic tree (Figure 1A and Supplementary Files S1–S3). This is the most extensive phylogenetic study of plant polyamine aminopropyl transferases done to date, and it not only confirms some of the previous evolutionary models (Hashimoto et al., 1998; Panicot et al., 2002; Teuber et al., 2007; Minguet et al., 2008), but also provides new details on certain key events.

First, our analysis expands the presence of *ACL5* homologs and *SPDS* genes to all plant lineages not previously studied, like charophytes and chlorophytes (Figure 1A). Second, the exclusive origin of *SPMS* genes in angiosperms, previously proposed based on only a few sequences (Minguet et al., 2008), is now set in the common ancestor of all Spermatophytes with more sequences from gymnosperms and their absence in multiple genomes of other land plants. Third, we find indications for a possible transfer of an additional SPDS of Holomycota origin to Setaphyta, based on the presence of extra copies in the genomes of the bryophyte *Sphagnum* and of several liverworts that unequivocally cluster with some sequences of that class



(Supplementary Files S1–S3). Fourth, as proposed in previous analyses (Minguet et al., 2008; Takano et al., 2012), our more extensive search still identifies *ACL5* orthologs only in plants, red algae, diatoms, archaea and bacteria (Figures 1A,B). The new data are compatible with the proposed model that TSPMS activity in Archaeplastida has a prokaryotic origin, while the common root with the Archaea *Sulfolobus* and *Pyrobaculum*, of two additional copies of *ACL5* orthologs in *Thalassiosira pseudonana* suggests a possible second event of horizontal gene transfer to Chromista (Figure 1B). And fourth, there are indications of an early *ACL5* duplication in Spermatophyta, followed by several species-specific losses of one of the copies within the angiosperms (some Brassicaceae like *Arabidopsis thaliana*, some Poaceae) (Figure 1C).

Thermospermine Is Synthesized Across All Plant Lineages

Our phylogenetic analyses identified at least one putative *ACL5* ortholog in all studied non-vascular plant species (Figure 1C). Since the only confirmed function for Tspm in plants is the regulation of xylem maturation dynamics (which, by definition, does not occur in non-vascular plants), we wondered whether the identified sequences encode enzymes displaying actual TSPMS activity. Therefore, we expressed the *ACL5* homologs of representative plant lineages in yeast, an organism that is unable to produce Tspm. Among the non-vascular plants, we tested *ACL5* homologs of a chlorophyte (*Chlamydomonas reinhardtii*), a liverwort (*Marchantia polymorpha*) and a moss (*Physcomitrella patens*) (Supplementary Table S1). As representative vascular plants we chose one lycophyte (*Selaginella lepidophylla*), and one gymnosperm (*Picea abies*), with the angiosperm *A. thaliana* as a control (Supplementary Table S1). As previously shown, HPLC analysis showed the presence of Put, Spd and Spm, but not Tspm, in the extracts of a wild-type yeast strain transformed with an empty plasmid (Figure 2A). In contrast, all the tested *ACL5* homologs allowed the production of Tspm in yeast (Figures 2B–G) demonstrating that these genes encode enzymes with TSPMS activity. This is in accordance with the previously reported partial complementation of the *Arabidopsis acL5* mutant by one of the *PpACL5* orthologs (Takahashi and Kakehi, 2010). The observed differences in Tspm production between the different *ACL5* genes suggest either species-specific variation in TSPMS activity kinetic parameters or in the variable capacity of yeast to express the different heterologous genes.

To check whether the presence of *ACL5* orthologs with TSPMS activity correlated with the ability of these species to synthesize Tspm *in vivo*, we examined the polyamine levels in samples of these plants grown in standard conditions (see Section “Materials and Methods”). As expected, all vascular and non-vascular species accumulated Put and Spd to different levels (Table 1). For instance, Put levels in the chlorophyte *C. reinhardtii* were between one and three orders of magnitude higher than in the land plants examined, while Spd levels were generally higher in the land plants than in *C. reinhardtii*, except for *P. patens*. On the other hand, Spm was detectable in *A. thaliana* and *P. abies*, in agreement with previous reports

for the occurrence of this tetraamine in seed plants (Gonzalez et al., 2011; Vuosku et al., 2018) and the presence of SPMS orthologs in this clade (Figure 1A). The detection of Spm in *S. lepidophylla* despite the absence of SPMS orthologs in lycophytes indicates that this tetra-amine might be synthesized by a less strict SPDS, as already suggested for *P. sylvestris* (Vuosku et al., 2018). With respect to Tspm, all the species tested were able to synthesize this polyamine at different levels, varying between 1.13 nM/g (fresh weight) in *C. reinhardtii* and 154 nM/g in *P. abies*. It is worth noting that, while previous reports show that Tspm tends to accumulate less than Spm in *Arabidopsis* (Naka et al., 2010; Rambla et al., 2010; Cai et al., 2016; Yoshimoto et al., 2016), in the species, tissues and conditions analyzed here, the two polyamines showed comparable levels. Although this result does not demonstrate that the *ACL5* orthologs identified in all the selected species are responsible for the Tspm synthesis shown here, this possibility is further supported by the observation that these genes are actually expressed in the same growth conditions as the ones used for Tspm quantification (Figure 3).

Differential *ACL5* Expression Dynamics in Vegetative and Reproductive Organs Throughout Development in Seed Plants

Tspm synthase activity has been associated to xylem development in *A. thaliana* (Muniz et al., 2008; Vera-Sirera et al., 2015), *Populus trichocarpa* (Milhinhos et al., 2013) and *P. sylvestris* (Vuosku et al., 2018). To investigate whether this association can be extended to other vascular plants and to point to additional potential roles in these species, we took advantage of the vast amount of publicly available transcriptomic data and examined the expression pattern of the *ACL5* orthologs in vegetative and reproductive organs of several vascular species at different developmental stages.

Although for some species we did not find data for stem or root, the available transcriptomic data shows that, for all studied species, *ACL5* transcripts tend to accumulate more in vegetative than in reproductive organs (Figure 4A). In the species for which transcriptomic data exists for both stem and root, *ACL5* expression is mostly higher in stems than in roots (7 out of 13 of the *ACL5* homologs), while only in two cases is the opposite behavior observed. In *Medicago truncatula*, where two *ACL5* paralogs exist, we found that one of them is more prominently accumulated in the stem, while the other one accumulates more in the root. Since our analyses are based on percentage of transcript accumulation across organs, in the species for which no transcriptomic data is available for stem tissue (i.e., *Solanum lycopersicum*), the proportion of transcript accumulation appears to be highly enriched in roots. For the same reason, in general, we regard the cases in which we found strong *ACL5* accumulation in flowers to the non-availability of expression data for stem or root (i.e., *Oryza sativa* or *Glycine max ACL5#4*). Only in the case of *Vitis vinifera* (where transcriptomic data was available for all tested organs) we found that one of the paralogs showed a (slight) preferential expression in flowers than in vegetative organs. In *P. trichocarpa*, where three paralogs exist, we found



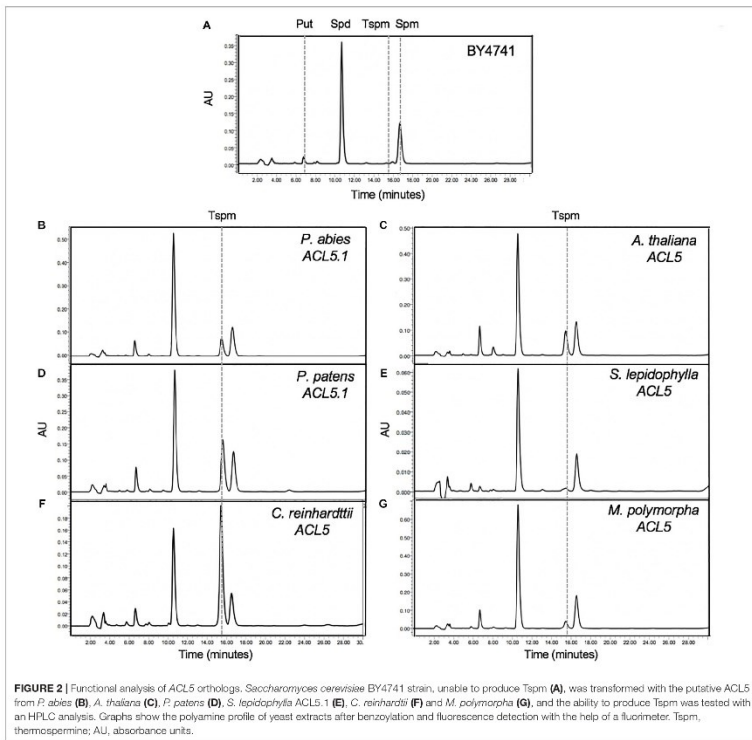
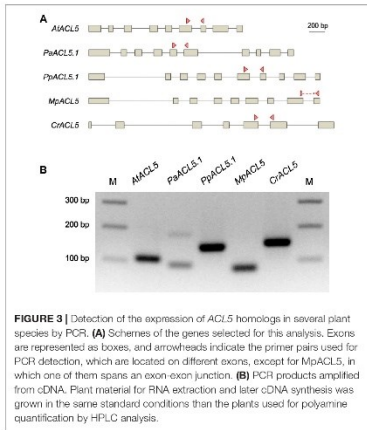


FIGURE 2 | Functional analysis of ACL5 orthologs. *Saccharomyces cerevisiae* BY4741 strain, unable to produce Tspm (A), was transformed with the putative ACL5 from *P. abies* (B), *A. thaliana* (C), *P. patens* (D), *S. lepidophylla* ACL5.1 (E), *C. reinhardtii* (F) and *M. polymorpha* (G), and the ability to produce Tspm was tested with an HPLC analysis. Graphs show the polyamine profile of yeast extracts after benzylation and fluorescence detection with the help of a fluorimeter. Tspm, thermospermine; AU, absorbance units.

TABLE 1 | Polyamine quantification in plant tissues.

	Polyamine concentration (nmol/g FW ± SE)			
	Putrescine	Spermidine	Spermine	Thermospermine
<i>A. thaliana</i>	10.76 ± 3.19	52.34 ± 15.48	2.14 ± 0.35	4.69 ± 1.77
<i>P. abies</i>	37.74 ± 5.31	131.09 ± 20.99	42.84 ± 12.39	154.06 ± 19.52
<i>S. lepidophylla</i>	77.59 ± 12.17	123.59 ± 24.80	1.21 ± 0.27	17.27 ± 3.75
<i>P. patens</i>	2.58 ± 0.54	19.87 ± 2.42	n.d.	10.7 ± 3.01
<i>M. polymorpha</i>	15.26 ± 5.05	53.88 ± 13.32	n.d.	1.37 ± 0.19
<i>C. reinhardtii</i>	1032.51 ± 16.62	27.44 ± 1.18	n.d.	1.13 ± 0.15

Polyamine quantification from *A. thaliana*, *P. abies*, *S. lepidophylla*, *P. patens*, *M. polymorpha*, and *C. reinhardtii* tissues. Polyamines were extracted and benzyolated from fresh tissues and measured with an HPLC analysis. Polyamine measurements were done in triplicates. FW, Fresh Weight; SE, Standard Error; n.d., not detected.

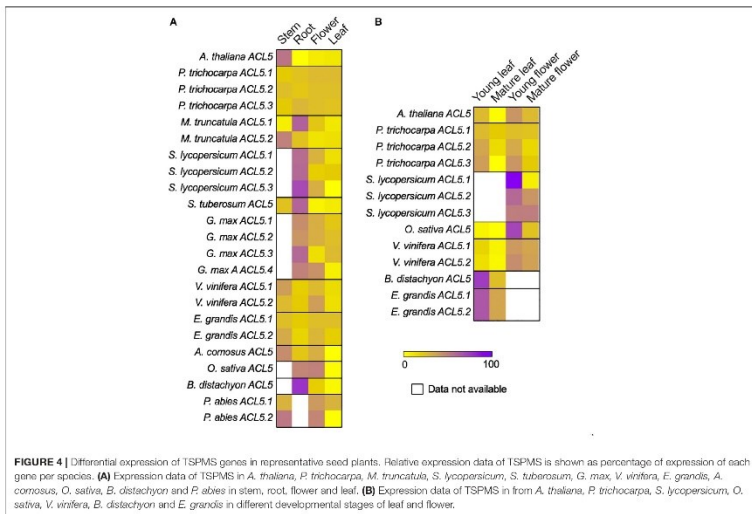


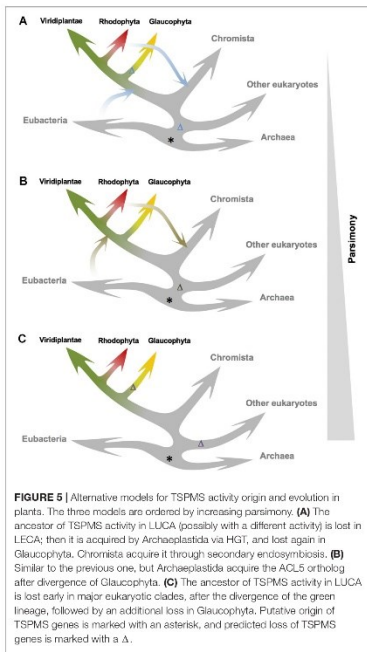
that none of them display preferential expression for any of the analyzed organs.

We also observed a marked preference of *ACL5* expression for young vs. mature organs (**Figure 4B**). In *A. thaliana*, *P. trichocarpa*, *O. sativa* and *V. vinifera*, this was visible in both flowers and leaves. There was no preferential expression between leaves and flowers except for the case of *V. vinifera*, in which both paralogs displayed higher preference for flowers than for leaves. For *S. lycopersicum*, we only found transcriptomes for young and mature flowers, while in *Brachypodium distachyon* and *Eucalyptus grandis*, we only found transcriptomes for young and mature leaves, and in all of them we found enriched *ACL5* expression in young organs. These results indicate a fairly widespread expression of *ACL5* homologs across organs, and mostly in young tissues with active vasculature development.

DISCUSSION

Our current knowledge about thermospermine is that its only confirmed function in plants is the coordination of xylem maturation. However, previous phylogenetic work reported the existence in the genomes of non-vascular plants of sequences clustering with TSPMS (Minguet et al., 2008;





Pegg and Michael, 2010), implying that Tspm might exist and, perhaps, play developmental and/or stress response-related roles also in such species. On one hand, as mentioned above, sequence similarity between all polyamine biosynthesis enzymes – especially those using putrescine or spermidine as substrates – has been extensively reported (Hashimoto et al., 1998; Panicot et al., 2002; Teuber et al., 2007). On the other hand, the sequencing of large numbers of genomes and transcriptomes of non-vascular plant species is relatively recent, and therefore previously published comparative analyses missed key clades in plant phylogeny.

It has been proposed that TSPMS had appeared in plants by endosymbiosis of a cyanobacterium (Minguet et al., 2008). Our data are compatible with three alternative hypotheses in this respect (Figure 5). The most parsimonious one is that TSPMS was already present before Eubacteria and Archaea and was lost in the major eukaryotic branch (Figure 5C). A second

loss would have occurred during the divergence of Glaucophyta, explaining the absence in such branch and the presence in the Chromista, Rhodophyta and Viridiplantae branches. A less parsimonious, but plausible possibility is that TSPMS was lost in the last eukaryotic common ancestor (LECA) and that it then was transferred either from Eubacteria or from Archaea (i) to Archaeplastida after Glaucophyta had diverged and (ii) to Chromista (Figure 5B). A third, less parsimonious hypothesis would postulate that TSPMS was lost in LECA and transferred either from Eubacteria or from Archaea to the early lineage of Archaeplastida and to Chromista (Figure 5A). TSPMS would have been lost again in Glaucophyta. However, phylogenetic positioning of TSPMS points to the horizontal transfer of TSPMS genes from Rhodophyta to diatoms (and possibly other algal groups originated during secondary chloroplast acquisition), thus excluding this latter hypothesis, which is also based in a very low sampling among Chromista representatives. Given that it is almost practically impossible to differentiate between the two remaining models, the hypothesis that contemplates only one loss and two reported horizontal transfers seems the most likely one (Figure 5B).

The identification of TSPMS activity in non-vascular plants clearly argues for possible functions of Tspm other than in xylem development. It has been proposed that Tspm might play a role in defense against stress conditions (Gonzalez et al., 2011; Marina et al., 2013), so it could also be the case that such activity is conserved across vascular and non-vascular plants and that developmental functions – either related with vascular development or with other, yet to be identified, processes – were only acquired in vascular plant lineages. In any case, further experimentation using mutant, overexpression and marker lines in emerging non-vascular model plant species such as *M. polymorpha* or *P. patens* might provide further information about what developmental and/or stress related processes might be controlled by this polyamine.

The *in silico* analyses of relative abundance of *ACL5* transcripts in different organs in representative seed-plant species presented here aimed at carrying out a first approach toward understanding whether, apart from coordinating xylem maturation, TSPM plays any other role in vascular plants. The higher prevalence of *ACL5* transcripts in vegetative than in reproductive organs and in young (presumably developing) than in mature organs argues for higher association of *ACL5* expression in organs developing more proportion of vascular tissues (vegetative) at early developmental stages, when vasculature is probably developing. However, the presence of *ACL5* transcripts in reproductive organs and in mature vegetative organs also argues for potential other (maybe less prominent) activities of TSPM in plants.

In summary, our work shows that Tspm exists in non-vascular plants and that there is a correlation between Tspm presence, TSPMS activity and *ACL5* expression throughout vascular and non-vascular plant lineages. Our results indicate that Tspm might play developmental and/or stress-related roles (apart from the described role in xylem development) not only in non-vascular but also in vascular plants. Future experimentation will shed new light on such intriguing topic.

DATA AVAILABILITY

All datasets generated for this study are included in the manuscript and/or the **Supplementary Files**.

AUTHOR CONTRIBUTIONS

AS-G, JH-G, MB, and JA conceived and designed the work. AS-G, JH-G, and MI-G performed all *in silico* and experimental analyses. JA and MB wrote the first draft of the manuscript, to which all authors contributed.

FUNDING

This work in the laboratories was funded by grants BFU2016-80621-P and BIO2016-79147-R of the Spanish Ministry of Economy, Industry and Competitiveness. AS-G and JH-G are recipients of Fellowships of the Spanish Ministry of Science, Innovation and Universities BES-2017-080387 and

of the Spanish Ministry of Education, Culture and Sport FPU15/01756, respectively. JA holds a Ramón y Cajal Contract RYC-2014-15752.

ACKNOWLEDGMENTS

We thank the members of the Hormone Signaling and Plasticity Lab at IBMCP (<http://plasticity.ibmcp.csic.es/>) for useful discussions and suggestions. We acknowledge Federico Valverde (IBVI-Sevilla, Spain), Jesús Vicente Carbajosa (CBGP-Madrid, Spain) and Ramón Serrano (IBMCP-Valencia, Spain) for sharing *C. reinhardtii*, *P. patens* and yeast materials, respectively.

SUPPLEMENTARY MATERIAL

The Supplementary Material for this article can be found online at: <https://www.frontiersin.org/articles/10.3389/fpls.2019.00663/full#supplementary-material>

REFERENCES

- Ashton, N. W., and Cove, D. J. (1977). The isolation and preliminary characterization of auxotrophic and analogic-resistant mutants of the moss, *Physcomitrella patens*. *Mol. Gen. Genet.* 154, 87–95.
- Baima, S., Forte, V., Possenti, M., Penolosa, A., Leoni, G., Sabi, S., et al. (2014). Negative feedback regulation of auxin signaling by ATHB8/ACL5-BUD2 transcription module. *Mol. Plant* 7, 1006–1025. doi: 10.1093/mp/psu051
- Cai, Q., Fukushima, H., Yamamoto, M., Ishii, N., Sakamoto, T., Kurata, T., et al. (2016). The SAC51 family plays a central role in thermospermine responses in *Arabidopsis*. *Plant Cell Physiol.* 57, 1583–1592. doi: 10.1093/pcp/pcw113
- Chen, D., Shao, Q., Yin, L., Younis, A., and Zheng, B. (2018). Polyamine function in plants: metabolism, regulation on development, and roles in abiotic stress responses. *Front. Plant Sci.* 9:1945. doi: 10.3389/fpls.2018.01945
- Clay, N. K., and Nelson, T. (2005). Arabidopsis thickvein mutation affects vein thickness and organ vascularization, and resides in a proline cell-specific spermine synthase involved in vein definition and in polar auxin transport. *Plant Physiol.* 138, 767–777. doi: 10.1104/pp.104.055756
- Darribas, D., Taboada, G. L., Doallo, R., and Posada, D. (2011). ProtTest 3: fast selection of best-fit models of protein evolution. *Bioinformatics* 27, 1164–1165. doi: 10.1093/bioinformatics/btr088
- De Rybel, B., Adibi, M., Treda, A. S., Wendrich, J. R., Smit, M. E., Novak, O., et al. (2014). Plant development. Integration of growth and patterning during vascular tissue formation in *Arabidopsis*. *Science* 345:125215. doi: 10.1126/science.1255215
- De Rybel, B., Moller, B., Yoshida, S., Grabowicz, I., Barbier de Reuille, P., Boerzen, S., et al. (2013). A bHLH complex controls embryonic vascular tissue establishment and indeterminate growth in *Arabidopsis*. *Dev. Cell* 24, 426–437. doi: 10.1016/j.devcel.2012.12.013
- Gonzalez, M. E., Marco, F., Minguet, E. G., Carrasco-Sorri, P., Blazquez, M. A., Carbonell, J., et al. (2011). Perturbation of spermine synthase gene expression and transcript profiling provide new insights on the role of the tetraamine spermine in *Arabidopsis* defense against *Pseudomonas viridiflava*. *Plant Physiol.* 156, 2266–2277. doi: 10.1104/pp.110.171413
- Gouy, M., Guindon, S., and Gascuel, O. (2010). SeaView version 4: a multiplatform graphical user interface for sequence alignment and phylogenetic tree building. *Mol. Biol. Evol.* 27, 221–224. doi: 10.1093/molbev/msp259
- Guindon, S., Dufayard, J. F., Lefort, V., Anisimova, M., Hordijk, W., and Gascuel, O. (2010). New algorithms and methods to estimate maximum-likelihood phylogenies: assessing the performance of PhyML 3.0. *Syst. Biol.* 59, 307–321. doi: 10.1093/sysbio/syq010
- Hanfrey, C., Elliott, K. A., Franceschetti, M., Mayer, M. J., Illingworth, C., and Michael, A. J. (2005). A dual upstream open reading frame-based autoregulatory circuit controlling polyamine-responsive translation. *J. Biol. Chem.* 280, 39229–39237. doi: 10.1074/jbc.M309340.200
- Hanfrey, C., Franceschetti, M., Mayer, M. J., Illingworth, C., and Michael, A. J. (2002). Abrogation of upstream open reading frame mediated translational control of a plant S-adenosylmethionine decarboxylase results in polyamine disruption and growth perturbations. *J. Biol. Chem.* 277, 44131–44139. doi: 10.1074/jbc.M206161.200
- Hanzawa, Y., Takahashi, T., and Komeda, Y. (1997). ACL5: an *Arabidopsis* gene required for internodal elongation after flowering. *Plant J.* 12, 863–874.
- Hanzawa, Y., Takahashi, T., Michael, A. J., Burtin, D., Long, D., Pineiro, M., et al. (2000). AGAULIS, an *Arabidopsis* gene required for stem elongation, encodes a spermine synthase. *EMBO J.* 19, 4248–4256. doi: 10.1093/emboj/19.16.4248
- Hashimoto, T., Tamaki, K., Suzuki, K., and Yamada, Y. (1998). Molecular cloning of plant spermidin synthases. *Plant Cell Physiol.* 39, 73–79.
- Imai, A., Hanzawa, Y., Komura, M., Yamamoto, K. T., Komeda, Y., and Takahashi, T. (2006). The dwarf phenotype of the *Arabidopsis* *acl5* mutant is suppressed by a mutation in an upstream ORF of a bHLH gene. *Development* 133, 3575–3585.
- Imai, A., Matsuyama, T., Hanzawa, Y., Akiyama, T., Tamaki, M., Saji, H., et al. (2004). Spermidine synthase genes are essential for survival of *Arabidopsis*. *Plant Physiol.* 135, 1565–1573. doi: 10.1104/pp.104.04.1699
- Kakehi, J. I., Kuwashiro, Y., Nitsua, M., and Takahashi, T. (2008). Thermospermine is required for stem elongation in *Arabidopsis thaliana*. *Plant Cell Physiol.* 49, 1342–1349. doi: 10.1093/pcp/pcn109
- Katayama, H., Iwamoto, K., Kariya, Y., Asakawa, T., Kan, T., Fukuda, H., et al. (2015). A negative feedback loop controlling bHLH complexes is involved in vascular cell division and differentiation in the root apical meristem. *Curr. Biol.* 25, 3144–3150. doi: 10.1016/j.cub.2015.10.051
- Knott, J. M., Romer, P., and Sumper, M. (2007). Putative spermine synthases from *Thalassiosira pseudonana* and *Arabidopsis thaliana* synthesize thermospermine rather than spermine. *FEBS Lett.* 581, 3081–3086.
- Marina, M., Sirena, F. V., Rambla, J. L., Gonzalez, M. E., Blazquez, M. A., Carbonell, J., et al. (2013). Thermospermine catabolism increases *Arabidopsis thaliana* resistance to *Pseudomonas viridiflava*. *J. Exp. Bot.* 64, 1393–1402. doi: 10.1093/jxb/ert012
- Michael, A. J. (2016). Polyamines in eukaryotes, bacteria, and archaea. *J. Biol. Chem.* 291, 14896–14903. doi: 10.1074/jbc.111.6.734780



- Milhinhos, A., Prestele, J., Bollhoner, B., Matos, A., Vera-Sirera, F., Rambla, J. L., et al. (2013). Thermospermine levels are controlled by an auxin-dependent feedback loop mechanism in populus xylem. *Plant J.* 75, 685–698. doi: 10.1111/tpj.12231
- Minguet, E. G., Vera-Sirera, F., Marina, A., Carbonell, J., and Blázquez, M. A. (2008). Evolutionary diversification in polyamine biosynthesis. *Mol. Biol. Evol.* 25, 2119–2128. doi: 10.1093/molbev/msn161
- Muniz, L., Minguet, E. G., Singh, S. K., Pesquet, E., Vera-Sirera, F., Moreau-Courtois, C. L., et al. (2008). ACAULIS5 controls *Arabidopsis* xylem specification through the prevention of premature cell death. *Development* 135, 2573–2582. doi: 10.1242/dev.019349
- Naka, Y., Watanabe, K., Sagor, G. H., Niitsu, M., Pillai, M. A., Kusano, T., et al. (2010). Quantitative analysis of plant polyamines including thermospermine during growth and salinity stress. *Plant Physiol. Biochem.* 48, 527–533. doi: 10.1016/j.plaphy.2010.01.013
- Panico, M., Minguet, E. G., Ferrando, A., Alcazar, R., Blázquez, M. A., Carbonell, J., et al. (2002). A polyamine metabolism involving aminopropyl transferase complexes in *Arabidopsis*. *Plant Cell* 14, 2539–2551.
- Pegg, A. E., and Michael, A. J. (2010). Spermine synthase. *Cell. Mol. Life Sci.* 67, 113–121. doi: 10.1007/s00018-009-0165-5
- Rambla, J. L., Vera-Sirera, F., Blázquez, M. A., Carbonell, J., and Granell, A. (2010). Quantitation of biogenic tetraamines in *Arabidopsis thaliana*. *Anal. Biochem.* 397, 208–211. doi: 10.1016/j.ab.2009.10.013
- Sagor, G. H., Berberich, T., Takahashi, Y., Niitsu, M., and Kusano, T. (2013). The polyamine spermine protects *Arabidopsis* from heat stress-induced damage by increasing expression of heat shock-related genes. *Transgenic Res.* 22, 595–605. doi: 10.1007/s11248-012-9666-3
- Sarrion-Perdigones, A., Falconi, E. E., Zandalinas, S. L., Juárez, P., Fernández del Carmen, A., Granell, A., et al. (2011). GoldenBraid: an iterative cloning system for standardized assembly of reusable genetic modules. *PLoS One* 6:e21622. doi: 10.1371/journal.pone.0021622
- Skula, B., and Dauter, Z. (2018). Crystal structure of thermospermine synthase from *Medicago truncatula* and substrate discriminatory features of plant aminopropyltransferases. *Biochem. J.* 475, 787–802. doi: 10.1042/bj20170900
- Siebers, T., Catarino, B., and Agustí, I. (2017). Identification and expression analyses of new potential regulators of xylem development and cambium activity in cassava (*Manihot esculenta*). *Planta* 245, 539–548. doi: 10.1007/s00425-016-2623-2
- Tabor, C. W., and Tabor, H. (1984). Polyamines. *Annu. Rev. Biochem.* 53, 749–790. doi: 10.1146/annurev.bi.53.070184.003533
- Takahashi, T., and Kakehi, J. (2010). Polyamines: ubiquitous polycations with unique roles in growth and stress responses. *Ann. Bot.* 105, 1–6. doi: 10.1093/aob/mcp259
- Takano, A., Kakehi, J., and Takahashi, T. (2012). Thermospermine is not a minor polyamine in the plant kingdom. *Plant Cell Physiol.* 53, 606–616. doi: 10.1093/pcp/pcs019
- Teuber, M., Azemi, M. E., Namjoo, F., Meier, A. C., Wodak, A., Brandt, W., et al. (2007). Putrescine N-methyltransferases—a structure-function analysis. *Plant Mol. Biol.* 63, 787–801. doi: 10.1007/s11103-006-9126-7
- Vera-Sirera, F., De Rybel, B., Urbez, C., Koukias, E., Pesquera, M., Alvarez-Mahecha, J. C., et al. (2015). A bHLH-based feedback loop restricts vascular cell proliferation in plants. *Dev. Cell* 35, 432–443. doi: 10.1016/j.devcel.2015.10.022
- Vera-Sirera, F., Minguet, E. G., Singh, S. K., Ljung, K., Tuominen, H., Blázquez, M. A., et al. (2010). Role of polyamines in plant vascular development. *Plant Physiol. Biochem.* 48, 534–539. doi: 10.1016/j.plaphy.2010.01.011
- Vuosku, J., Karppinen, K., Muilu-Makela, R., Kusano, T., Sagor, G. H. M., Avia, K., et al. (2018). Scots pine aminopropyltransferases shed new light on evolution of the polyamine biosynthesis pathway in seed plants. *Ann. Bot.* 121, 1243–1256. doi: 10.1093/aob/mcy012
- Wu, H., Min, J., Ikeguchi, Y., Zeng, H., Dong, A., Loppau, P., et al. (2007). Structure and mechanism of spermidine synthases. *Biochemistry* 46, 8331–8339. doi: 10.1021/bi602498k
- Yamaguchi, K., Takahashi, Y., Berberich, T., Imai, A., Miyazaki, A., Takahashi, T., et al. (2006). The polyamine spermine protects against high salt stress in *Arabidopsis thaliana*. *FEBS Lett.* 580, 6783–6788. doi: 10.1016/j.febslet.2006.10.078
- Yamaguchi, K., Takahashi, Y., Berberich, T., Imai, A., Takahashi, T., Michael, A. J., et al. (2007). A protective role for the polyamine spermine against drought stress in *Arabidopsis*. *Biochem. Biophys. Res. Commun.* 352, 486–490. doi: 10.1016/j.bbrc.2006.11.041
- Yoshimoto, K., Takamura, H., Kadota, I., Motose, H., and Takahashi, T. (2016). Chemical control of xylem differentiation by thermospermine, xylemin and auxin. *Sci. Rep.* 6:21487. doi: 10.1038/srep21487

Conflict of Interest Statement: The authors declare that the research was conducted in the absence of any commercial or financial relationships that could be construed as a potential conflict of interest.

Copyright © 2019 Solé-Gil, Hernández-García, López-Gresa, Blázquez and Agustí. This is an open-access article distributed under the terms of the Creative Commons Attribution License (CC BY). The use, distribution or reproduction in other forums is permitted, provided the original author(s) and the copyright owner(s) are credited and that the original publication in this journal is cited, in accordance with accepted academic practice. No use, distribution or reproduction is permitted which does not comply with these terms.





